

Synthesis, characterization and applications of polymer based conjugate materials for infectious diseases of poverty

by

Lesego Lovius Tshweu

**Submitted in partial fulfillment of the requirements for the
PhD Degree in Chemistry
in the Faculty of Natural & Agricultural Sciences**

University of Pretoria

December, 2018

Summary

Title:

Synthesis, characterization and applications of polymer based conjugate materials for infectious diseases of poverty

By:

Lesego Lovius Tshweu

Supervisor:

Dr Lynne A. Pilcher

Co-supervisors:

Dr Mohammed Balogun

Department:

Department of Chemistry

Degree:

PhD

The major disease burden for the majority of the world's population is due to infectious diseases. The most prevalent are HIV/AIDS, tuberculosis, lower respiratory tract infections, diarrhoeal diseases and malaria. In particular, malaria and tuberculosis have not benefited much from new technological developments in disease management. Most of the drugs used are several decades old and have significant toxicity profiles which impact patient compliance. New potential drugs being discovered stumble on the road to the clinic because of solubility issues. Many just end up being shelved. It is estimated that over 70% of new chemical entities have poor solubility issues. On the other hand, HIV/AIDS remains a major health problem worldwide, as currently there is no cure available. Chronic intake of highly active antiretroviral treatment (HAART) is compulsory to control HIV infection and any non-adherence leads to a quick increase in the viral load. Poor targeting ability of antiretrovirals (ARVs) to latent sites of infection is the main reason for the relapse.

Nanomedicines have significantly improved the clinical management of deadly diseases like cancer. Conventional drugs show improved pharmacological indices when designed as nanomedicines. It improves solubility, absorption, clinical performance, and reduces the amount of drug needed to achieve the desired therapeutic effect. The resultant effect is improved solubility and reduced toxicity. The most common method to design nanomedicines is through physical entrapment or encapsulation in polymeric carriers. Today, however, modern delivery systems are being designed by chemical synthesis. Either the drugs are chemically linked to the polymeric carriers or the polymers are chemically derivatized to be more efficient at encapsulating the active agents. In this project, we report on our attempts to chemically modify polymers with active drugs to synthesize smart macromolecular pro-drugs or produce more efficient drug encapsulation systems.

The work presented in this project is outlined in the following six chapters.

Chapter 1 contains the literature review of the major infectious diseases; namely HIV/AIDS, tuberculosis and malaria; what has been done to increase patient compliance or success of available drugs i.e (to reduce the viral load or attempted to cure the virus with the ARVs in the field of HIV/AIDS, or administration of combination therapy in anti-tuberculosis/malarial field to minimize drug resistance and increase therapeutic success). The use of nanomedicine to ameliorate problems associated with treatment regime for infectious diseases is discussed. Methods for nanoencapsulation or inclusion of the existing drugs within the approved materials is described in detail. A concise general introduction to polymer therapeutics is discussed, followed by a review of polymers that are normally used in polymer-drug conjugation; highlighting advantages and disadvantages of each. Finally a clinical perspective on the use of polymer-drug conjugation for infectious diseases is outlined.

Chapter 2 introduces the problems associated with the current ARVs used in the treatment of HIV/AIDS and emphasizes the need to target latent sites of infection using aptamer technology. Aptamers were subsequently conjugated to polyethylene glycol (PEG) using carbodiimide chemistry. The TZM-bl neutralization assay and *in vitro* stability in human breast milk studies showed that aptamers maintained their binding integrity after pegylation and were more stable than the parent aptamers. Finally the conjugated aptamers were nanoencapsulated into poly(epsilon-caprolactone) [PCL] nanoparticles using a double emulsion method. Nanoparticles of less than 150 nm were

produced with a higher surface charge, showing that the nanoparticles were stable. The *in vitro* binding assay using electrochemical methods showed that the nanoparticles coated with PEGylated RNA aptamers had higher affinity and specificity to HIV-1 gp 120. The overall results demonstrated that these nanoparticles could be used in HIV drug delivery applications to help minimize changes associated with ARVs.

Chapter 3 describes nanomedicinal formulations of the anti-TB drug moxifloxacin (Mox). Mox is a relatively hydrophilic drug. The target pathological site where the *Mycobacterium tuberculosis* resides is a lipid dense granuloma in the lungs. Hence, a large dose will have to be administered to deliver an adequate therapeutic dose i.e. 400 mg is required for Mox. Mox was covalently conjugated into PEG via a releasable amide bond. Similarly a hybrid system was formed by nanoencapsulating the PEG-Mox conjugate into PCL nanoparticles using double emulsion method. The system constitutes the PCL, which is envisaged to increase the hydrophobicity of the PEG-Mox conjugate. PEG-Mox conjugates and PCL-Mox nanoparticles were found to be hemocompatible, inducing only minimal hemolysis. Mox was more toxic than the PEG-Mox conjugate and PCL-Mox nanoparticles. *In vitro* stability in human plasma showed that PCL-Mox nanoparticles were stable for over 72 hrs. Data obtained emphasizes that PCL nanoparticles could be used as a drug delivery system to minimize the high toxicity of TB drugs

Chapter 4 establishes the conjugation of the hydrophobic drug, lumefantrine [Lumf] to water soluble polymers. Lumf is insoluble in water with an octanol-water partition coefficient (\log_p) of 8.34. As a result a series of Lumf prodrug conjugates were synthesized using two different polymers (polyethylene glycol and p-NAM-stat-p-AA). Average particle size below 200 nm was achieved and PDI values were always below 0.2, which is an indication of the relatively homogeneous size distribution achieved with carbodiimide chemistry. We have for the first time, by applying the polymer therapeutics techniques, synthesized a polymer-drug conjugate of Lumf which has increased the solubility of the drug more than 10^3 times.

Chapter 5 gives the conclusions of the experimental chapters.

Through the three different experimental chapters, we have demonstrated that polymer based drug conjugates can be used to address different issues: (1) drug delivery through coating nanoparticles with appropriate aptamers, (2) drug toxicity through encapsulation of a toxic drug in a

hemocompatible nanoparticle and (3) greatly improved aqueous solubility of a hydrophobic drug. Furthermore, while there has been much excellent work using polymer based drug conjugates in cancer, we have explored the approach to tackle different problems related to three different infectious diseases of poverty, namely HIV, TB and malaria.

Declaration

I declare that the thesis/dissertation, which I hereby submit for the degree PhD (Chemistry) at the University of Pretoria, is my own work and has not previously been submitted by me for a degree at this or any other tertiary institution.

Signature.....

Date.....

Plagiarism Declaration

1. I understand what plagiarism is and am aware of the University's policy in this regard.
2. I declare that this (eg essay, report, project, assignment, dissertation, thesis, etc) is my own original work. Where other people's work has been used (either from a printed source, Internet or any other source), this has been properly acknowledged and referenced in accordance with departmental requirements.
3. I have not used work previously produced by another student or any other person to hand in as my own.
4. I have not allowed, and will not allow, anyone to copy my work with the intention of passing it off as his or her own work.

SIGNATURE.....

Acknowledgements

My project would never have been so exciting and enormously successfully without the very useful advice from many people at the CSIR. I will always keep in my heart, all the moments we had in the lab and individual contribution to people who contributed to this wonderful experience.

I would like to thank my supervisor, Dr Lynne Pilcher (UP). No expression can do justice to the appreciation I felt for the constant guidance, assistance, kindness and nonstop encouragement throughout my project. She was not only my supervisor but also a great mentor.

I am thankful to my co-supervisor, Dr Mohammed Balogun (CSIR), contributions throughout the study and his genuine guidance.

I would like to extend my special appreciation to Dr Avashnee Chetty (Our research group leader), and Dr Mamoeletsi Mosia (Competency manager) for granting the opportunity.

Finally, I would like to thank my parents, family and friends for their unconditional love, encouragement, patience throughout my study. Thank you so much, you are the best

Table of Contents

Summary	I
Declaration	V
Plagiarism Declaration	VI
Acknowledgements	VII
Table of Contents	VIII
List of Figures	XI
List of Schemes	XIII
List of Tables	XIV
Abbreviations	XV
1 Chapter One: Polymer therapeutics for poverty related diseases: Promises or fallacy	1
1.1 Introduction	1
1.2 Scope of the thesis	5
1.3 HIV/AIDS	6
1.3.1 Current chemotherapy in HIV/AIDS therapy and challenges	8
1.4 TB	14
1.4.1 Current chemotherapy in TB therapy and challenges	15
1.5 Malaria	19
1.5.1 Current chemotherapy in malaria therapy and challenges	21
1.6 Application of nanomedicine in infectious diseases	24
1.6.1 Encapsulation	25
1.6.1.1 Solvent evaporation method	27
1.6.1.2 Spray drying method	28
1.6.2 Polymer therapeutics	30
1.6.2.1 Polymer-drug conjugation	34
1.6.2.2 Selection of linkers	37
1.6.2.3 Carbodiimide crosslinking chemistry	38
1.6.2.4 Selection of polymers	40
1.6.3 Poly (ethylene glycol)	42
1.6.3.1 PEG–HIV drug conjugates	43
1.6.4 Chitosan	48
1.6.4.1 Chitosan–HIV agent conjugates	50

1.6.5	Poly glutamic acid.....	51
1.6.5.1	PGA-Malaria conjugates.....	52
1.6.6	Dextran.....	54
1.6.6.1	Dextran–HIV agent conjugates.....	55
1.6.7	Cyclodextrins.....	57
1.6.8	N-(2-hydroxypropyl)methacrylamide (HPMA) copolymers.....	57
1.6.9	Alginate.....	58
1.7	Clinical Perspective for infectious diseases.....	58
1.8	Characterization of nanomedicinal drugs.....	61
1.8.1	Dynamic light scattering.....	61
1.8.2	X-ray diffraction.....	63
1.8.3	Thermogravimetric analysis.....	64
1.8.4	Electrophoresis.....	65
1.9	Significance of the review.....	66
1.10	Hypothesis.....	66
1.11	Aims.....	66
2	Chapter Two: PEGylated aptamers coated onto the surface of poly(epsilon-caprolactone) nanoparticles for HIV/AIDS applications: Synthesis and characterisation.....	68
2.1	Introduction.....	68
2.1.1	Poly (epsilon-caprolactone).....	70
2.2	Results and Discussion.....	71
2.2.1	Preparation and characterisation of PEGylated aptamers.....	71
2.2.2	Stability of RNA aptamers and PEGylated RNA aptamers in human breast milk.....	76
2.2.3	Preparation and characterization of PCL NPs coated with PEGylated RNA aptamers.	80
2.2.4	<i>In vitro</i> binding assay using electrochemical techniques.....	83
2.3	Conclusions.....	89
3	Chapter Three: Synthesis and characterization of PEG-MOX conjugate encapsulated into PCL nanoparticles for anti-TB application.....	91
3.1	Introduction.....	91
3.1.1	Cell wall components.....	93
3.1.1.1	Peptidoglycan.....	93

3.1.1.2	Arabinogalactan	93
3.1.1.3	Mycolic acids	94
3.2	Results and discussions	94
3.2.1	NMR analysis	95
3.2.2	Particle size, zeta potential, morphology and encapsulation efficiency.....	100
3.2.3	Attenuated total reflectance/Fourier transform-infrared spectroscopy (ATR-FTIR).	102
3.2.4	X-ray diffraction (XRD) analysis.....	104
3.2.5	Thermogravimetric Analysis (TGA) studies.....	105
3.2.6	Hemolysis study	107
3.2.7	Cytotoxicity	108
3.2.8	Plasma stability studies	109
3.3	Conclusions	111
4	Chapter Four: Synthesis and characterization of polymer based lumefantrine conjugates for anti-malarial application	112
4.1	Introduction	112
4.2	Results and Discussion	116
4.2.1	Synthesis and characterization of novel lumefantrine conjugates	116
4.2.1.1	Lumf-Succ conjugate	117
4.2.1.2	Synthesis and characterisation of PEG-NH ₂	122
4.2.1.3	Conjugation of Lumf-Succ to PEG.....	124
4.2.1.4	Conjugation of Lumf to p-NAM- <i>stat</i> -p-AA	132
4.2.2	Solubility studies	136
4.3	Conclusion	137
5	Chapter Five: Conclusion	139
6	Chapter Six: Experimental	143
6.1	Experimental for Chapters Two	143
6.2	Experimental for Chapter Three	148
6.3	Experimental for Chapter Four.....	153
	References	158

List of Figures

Figure 1.1: Global death picture of the top 10 disease burden, statistics adapted from the World Health Organisation (A) 2000, (B) 2015 (WHO 2016).	3
Figure 1.2: The top 10 causes of deaths in 2015, (A) low-income countries and (B) high income countries (WHO 2016).	5
Figure 1.3: HIV replication cycle and targets for antiretroviral therapy (Pietrucha, 2015).	8
Figure 1.4: <i>M. tuberculosis</i> A. bacilli B. colonies growing on solid medium (Todar, 2009)	15
Figure 1.5: The life cycle of malaria parasites in human host and anopheles mosquito vector (White, 2004).	20
Figure 1.6: Schematic representations of main components for the mini spray dryer B-290 (Büchi Labortechnik AG, 2002). 1. Two-fluid nozzle, with compressed air to disperse the emulsion or liquid into fine droplets, 2. Electric heating, 3. Spray chamber for drying the fine droplets to powder, 4. Cyclone for collection, 5. Outlet filter to eliminate fine particles, 6. Aspirator for producing the flow	29
Figure 1.7: Ringsdorf's model for polymer- drug conjugate systems (Pasut and Veronese, 2007)..	35
Figure 1.8: Schematic representation of a polymer-drug conjugates designed for lysosomotropic and endosomotropic delivery (Duncan, 2003).	38
Figure 1.9: ¹ H NMR Spectra of AZT (a), AZT Succinyl ester(b), mPEG (750) -AZT (c), mPEG (2kDa) -AZT (d), mPEG (5kDa) -AZT (e), and mPEG (10 kDa) -AZT(f). (Li et al., 2012)	45
Figure 1.10: Confocal laser scanning microscopy images of rat intestines (duodenum and jejunum) after administration of fluorescein isothiocyanate (FITC)-labeled CS administration. Taken after 30 minutes. (Chae et al. 2005).	50
Figure 1.11: The <i>in vivo</i> imaging studies in mouse. A and C presents mouse 1 inoculated with PGA labelled green and Gal-BSA labelled red. Panel E displays a combined image of A and C. Image B, D, and F represents mouse 2 inoculated with PGA-TriGalNAc labelled green and Gal-BSA labelled red. Panel F displays a combined image of B and D. Note, image E shows excretion of PGA in the bladder and F demonstrate co-localization of Gal-BSA and PGA-TriGalNAc in the liver. (Tomiya et al., 2013).	53
Figure 1.12: Schematic diagram of the basic principle of DLS.	62
Figure 2.1: Confirmation of conjugation of RNA aptamers to PEG:(A) M = molecular marker, Apt = RNA aptamer, 1 = PEGylated RNA aptamers (not purified), 2 = O-(2-Aminoethyl) PEG. (B) 1 = RNA aptamers + O-(2-Aminoethyl) PEG (reaction carried-out in the absence of coupling reagents), 2 = PEGylated RNA aptamers (EDAC/imidazole) and 3 = PEGylated RNA aptamers (EDAC/sulfo-NHS).	74

Figure 2.2. Inhibition of HIV-1 infection with parent and PEGylated RNA aptamers. Pink squares show the HIV-1 inhibitory curve of the parent aptamer. The PEGylated RNA aptamer prepared using EDAC/imidazole and EDAC/Sulfo-NHS anti-viral activities are shown with red triangles and purple squares; respectively. PEG alone, used as a control, is shown by the blue curve. (Data represent mean± SD, n = 3) 76

Figure 2.3: Stability of RNA aptamers and PEGylated aptamers in breast milk. (A) RNA aptamers in breast milk, (B) RNA aptamers in PBS (7.4) and (C) stability studies of RNA aptamers PEGylated aptamers in human breast milk. Apt = RNA aptamers and PEG-Apt = PEGylated aptamers..... 79

Figure 2.4: Preparation of PCL nanoparticles coated with PEGylated RNA aptamers using double emulsion method. 82

Figure 2.5: Particle size and particle size distribution of the NPs. (A) PCL nanoparticles, (B) PCL coated nanoparticles. (Data represent mean± SD, n = 3) 83

Figure 2.6: Gradual deposition of monolayers to the bare Au electrode. 85

Figure 2.7: CV results obtained at the scan rate 20 mV/s. Overlay plot of CV spectra of bare Au and SAM-modified Au electrodes 87

Figure 2.8: Overlay plot of Impedance spectra of bare Au and SAM-modified Au electrodes..... 89

Figure 3.1: Schematic representation of the mycobacterial cell wall (Brennan and Crick, 2007)... 93

Figure 3.2: Proton NMR spectra of (A) Mox (D₂O)..... 97

Figure 3.3: Proton NMR spectra of PEG (D₂O) 98

Figure 3.4: Proton NMR spectra of PEG-Mox conjugate (CDCl₃) 99

Figure 3.5: (A): Average particle size of PEG-Mox conjugate, PCL nanoparticles and PCL-Mox nanoparticles. (B) SEM image of PCL nanoparticles or PCL-Mox nanoparticles 101

Figure 3.6: FTIR spectra of Mox, PEG and PEG-Mox conjugate 103

Figure 3.7: FTIR spectra of Mox, PCL, PCL nanoparticles, and PCL-Mox nanoparticles. 104

Figure 3.8: X-ray diffraction patterns of Mox, PCL, PCL nanoparticles and PCL-Mox nanoparticles. X-axis represent 2 theta (degree). 105

Figure 3.9: TGA thermograms of (A) Polymer conjugates, (B) Polymer nanoparticles. 106

Figure 3.10: *In vitro* erythrocytes lysis with Mox, PEG-Mox conjugate, PCL(PEG-MOX) NPs = PCL-Mox nanoparticles and PCL nanoparticles incubated with human RBCs suspension for 4 hrs at 37 °C. Data represent mean ± SD, n = 3. 108

Figure 3.11: *In vitro* cell viability of Mox, PEG-Mox conjugate and PCL-Mox nanoparticles measured by MTT assay. NPs = nanoparticles. Data represent mean ± SD, n = 3..... 109

Figure 3.12: The <i>in vitro</i> stability of PCL-Mox nanoparticles in human plasma.	111
Figure 4.1: Proton NMR of Lumf (500 MHz, CDCl ₃).....	118
Figure 4.2: Proton NMR of Lumf-Succ conjugates (500 MHz, CDCl ₃).	121
Figure 4.3: FTIR of A) Lumf, B) Lumf-Succ, C) PEG-OH and D) PEG-O-Succ-Lumf	121
Figure 4.4: Mass spectrometry A) Lumf and B) Lumf-Succ conjugate.	122
Figure 4.5 Proton NMR of PEG (600 MHz, D ₂ O), Lumf (600 MHz, CDCl ₃), Lumf-Succ conjugates (600 MHz, CDCl ₃) and PEG-Succ-Lumf conjugate (600 MHz, CDCl ₃).....	129
Figure 4.6: FTIR of A) Lumf, B) Lumf-Succ, C) PEG-OH and D) PEG-NH-Succ-Lumf	130
Figure 4.7: Average particle size distribution of PEG-Succ-conjugate (A) and p-NAM- <i>stat</i> -p-AA-Lumf conjugate (B).	132
Figure 4.8: ¹ H NMR of p-NAM- <i>stat</i> -p-AA-Lumf conjugate showing corresponding peaks to both Lumf and p-NAM- <i>stat</i> -p-AA (500 MHz, CDCl ₃).	134
Figure 4.9: FTIR of A) Lumf, B) p-NAM- <i>stat</i> -p-AA, C) p-NAM- <i>stat</i> -p-AA-Lumf conjugate.....	136
Figure 4.10: Solubility studies of the polymer-Lumf conjugate in PBS buffer (pH 7.5) (A) PEG-NH-Succ-Lumf. 1a = 1 mg/mL, 1b = 2 mg/mL, 1c = 3 mg/mL, 1d = 4 mg/mL and (B) p-NAM- <i>stat</i> -p-AA-Lumf: 2a = 1 mg/mL, 2b = 2 mg/mL, 2c = 3 mg/mL, 2d = 4 mg/mL.	137

List of Schemes*

Scheme 1.1: Schematic representation of double emulsion method (w/o/w).....	28
Scheme 1.2: <i>N</i> -(2-hydroxypropyl) methacrylamide (HPMA) copolymer-doxorubicin conjugates. PK1= HPMA-DOX, PK2= (HPMA-DOX-Gal). Gal- galactosamine (to promote liver targeting). DOX (doxorubicin). Glycyl Phenylalanyl Leucyl Glycine (GFLG).	37
Scheme 1.3: 1-ethyl-3-(3-dimethylaminopropyl) carbodiimide hydrochloride (EDAC) and <i>N</i> -Hydroxysulfosuccinimide sodium salt (sulfo-NHS) reacts with carboxylic acids to produce an active-sulfo-NHS ester intermediate. The activated acid can be coupled with a primary amine containing molecule forming an amide bond. An isourea is released as by-product. (Hermanson, 2008).....	40
Scheme 1.4: Synthetic route of mPEG-AZT conjugates using DCC and DMAP as coupling reagents. (Li et al., 2012).....	44
Scheme 1.5: Scheme to synthesize SQV-based prodrug (i) 3 equivalence of Fmoc-Cys(S-Trt)-COOH in CH ₂ Cl ₂ with DIPC/DMAP; (ii) 20% piperidine in CH ₂ Cl ₂ ; (iii) TFA/CH ₂ Cl ₂ (1:1); (iv) 2 equivalence of biotin-PEG-NHS in CH ₂ Cl ₂ with DIEA; (v) 2 equivalence of Fmoc-PEG-NHS in CH ₂ Cl ₂ with DIEA; (vi) 2 equivalence of 2,2'-dithiodipyridine in DMSO; (vii) 2 equivalence of R.I.CK-Tat9 in DMSO; (viii) 2 equiv of R.I.CK(stearate)-Tat9 in DMSO. (Gunaseelan et al.,2004)	47
Scheme 1.6: Scheme to synthesize CS- <i>O</i> -isopropyl-5'- <i>O</i> -d4T monophosphate conjugate. (Yang et al. 2010).....	51
Scheme 1.7: Structure of PGA-PQ-TriGalNAc, labeled with SFX.	54
Scheme 1.8: Scheme to synthesize 4- <i>N</i> -(4,4'-Dimethoxytrityl)-5'- <i>O</i> -(succinate)-2',3'-dideoxy-3'-thiacytidine (4- <i>N</i> -(4,4'-Dimethoxytrityl) lamivudine succinate, 5). (i) <i>tert</i> -Butyldimethylsilyl chloride, imidazole, dry <i>N,N</i> dimethylformamide; (ii) 4,4'-dimethoxytrityl chloride, pyridine; (iii) <i>tert</i> -butylammonium fluoride, molecular sieves (4 Å); (iv) succinic anhydride, DMF, pyridine, 4-Dimethylaminopyridine (DMAP); (v) Acetic acid (80%).	56
Scheme 1.9: Scheme to synthesize 3TCS–Dextran (3TCSD, 8). (i) dextran 25 kDa, <i>N,N'</i> -diisopropylcarbodiimide, DMAP, dry dimethyl sulfoxide (DMSO), <i>N,N'</i> -diisopropylethylamine; (ii) Acetic acid (80%).	57

* Only Schemes from Chapter 1 are listed.

List of Tables

Table 1.1: Representation of nucleoside reverse transcriptase inhibitors currently used to treat HIV/AIDS	10
Table 1.2: Representation of non-nucleoside reverse transcriptase inhibitors currently used to treat HIV/AIDS	11
Table 1.3: Representation of protease inhibitors currently used to treat HIV/AIDS	12
Table 1.4: Representation of Viral fusion/entry and Integrase inhibitors currently used to treat HIV/AIDS	13
Table 1.5: Physico-chemical properties of current anti-TB drugs.....	17
Table 1.6: WHO recommended artemisinin combination therapy.....	22
Table 1.7: Encapsulation vs polymer therapeutics	26
Table 1.8: Examples of polymer therapeutics products on the market or in clinical development (Hare et al., 2017)(Duncan, 2003).....	31
Table 1.9: Schematic illustration of polymers and oligomers used in the production of polymer-drug conjugation.	41
Table 3.1: Properties of PEG-Mox conjugates, PCL nanoparticles and PCL-Mox nanoparticles (data represent mean \pm SD, n = 3).....	100
Table 4.1: Antimalarial drugs based on chemical structure.	114
Table 4.2: TLC of Lumf-Succ prodrugs and Lumf-succinic acid conjugate after silica gel purification	120
Table 4.3: Functional groups reactivity organized approximately in decreasing ability to leave (Smith and March, 2006)	123
Table 4.4: TLC analysis and purified PEG-Succ-Lumf conjugate in aqueous solution.....	127
Table 4.5: Mean particle size, PDI, zeta potential (ZP, mV) and drug loading of the conjugates (data represent mean \pm SD, n = 3).....	131
Table 4.6: TLC analysis and purified p-NAM- <i>stat</i> -p-AA-Lumf in aqueous solution.....	133
Table 4.7: Solubility studies of the polymer-Lumf conjugate in PBS buffer.....	137

Abbreviations

°C	degree Celsius
µm	micrometre
AIDS	acquired immune deficiency syndrome
aq	aqueous
atm	atmosphere
ACT	Artemisinin combination therapy
ARVs	Antiretroviral
Au	gold
Au—S	gold-thiolate
BBB	blood-brain barrier
BCS	Biopharmaceutical Classification System
C	concentration
CMC	1-cyclohexyl-3-(2-morpholinoethyl) carbodiimide
ddd H ₂ O	double distilled deionized water
DCC	dicyclohexyl carbodiimide
DCM	dichloromethane
DHA	dihydroartemisinin
DIC	diisopropyl carbodiimide
DMF	dimethyl formamide
DMAP	4-(dimethylamino)-pyridine
EDAC	1-ethyl-3-(3-dimethylaminopropyl)carbodiimide hydrochloride
EIS	electrochemical impedance spectroscopy
EPR	enhanced permeability and retention
eV	electron volts

h	hour(s)
HAART	highly active antiretroviral treatment
HIV	human immunodeficiency virus
HPLC	high performance liquid chromatography
HPMA	N-(2-Hydroxypropyl)methacrylamide
IR	infra red
I.V	Intravenously
KE	kinetic energy
K_d	affinity constant
KHz	kilohertz
LRTIs	lower respiratory tract infections
\log_p	octanol-water partition coefficient
m	multiplet
<i>M.tb</i>	<i>Mycobacterium tuberculosis</i>
MA(s)	mycolic acid(s)
MACA	mercaptoacetic acid
MDR	multi-drug resistant (TB)
min	minute(s)
mM	millimolar
mol. eq.	molar equivalent
Mox	moxifloxacin
N(E)	number of electrons per second
nm	nanometer
NMR	nuclear magnetic resonance
NNRTIs	non-nucleoside reverse transcriptase inhibitors

NRTIs/nRTIs	nucleoside/nucleotide reverse transcriptase inhibitors
PIs	protease inhibitors
ppm	parts per million
r.t.	room temperature
s	second(s)
s	singlet
SAM	self assembled monolayer
S _N 2	substitution nucleophilic bimolecular
SEM	scanning electron microscopy
t	triplet
TB	tuberculosis
TEM	transmission electron microscope
TLC	thin layer chromatography
US-FDA	United State Food and Drug Administration
UV	ultraviolet
WHO	World Health Organization
XDR	extensively drug resistant (TB)
Z	impedance

1 Chapter One:

Polymer therapeutics for poverty related diseases: Promises or fallacy

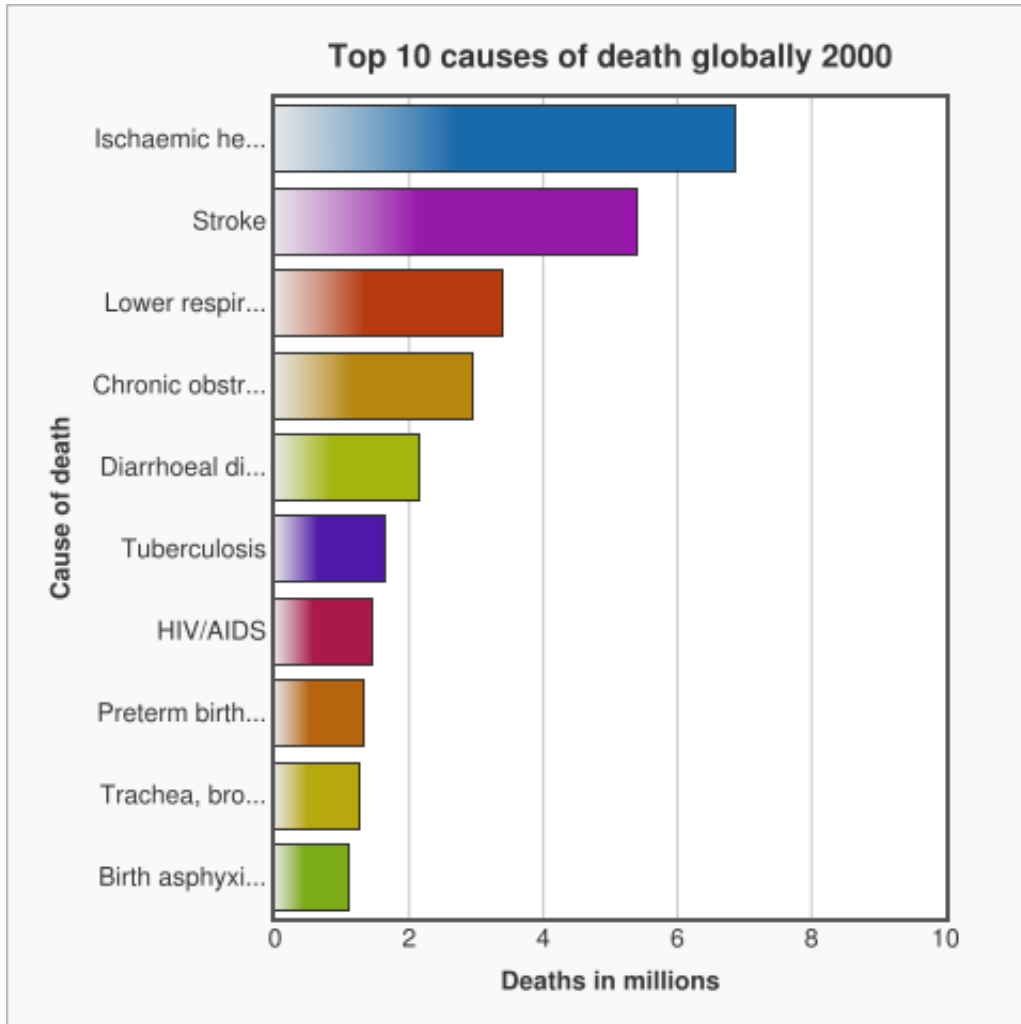
1.1 Introduction

According to the World Health Organization (WHO) an infectious disease is “caused by pathogenic microorganisms, such as bacteria, viruses, parasites or fungi which can be spread, directly or indirectly, from one person to another”.

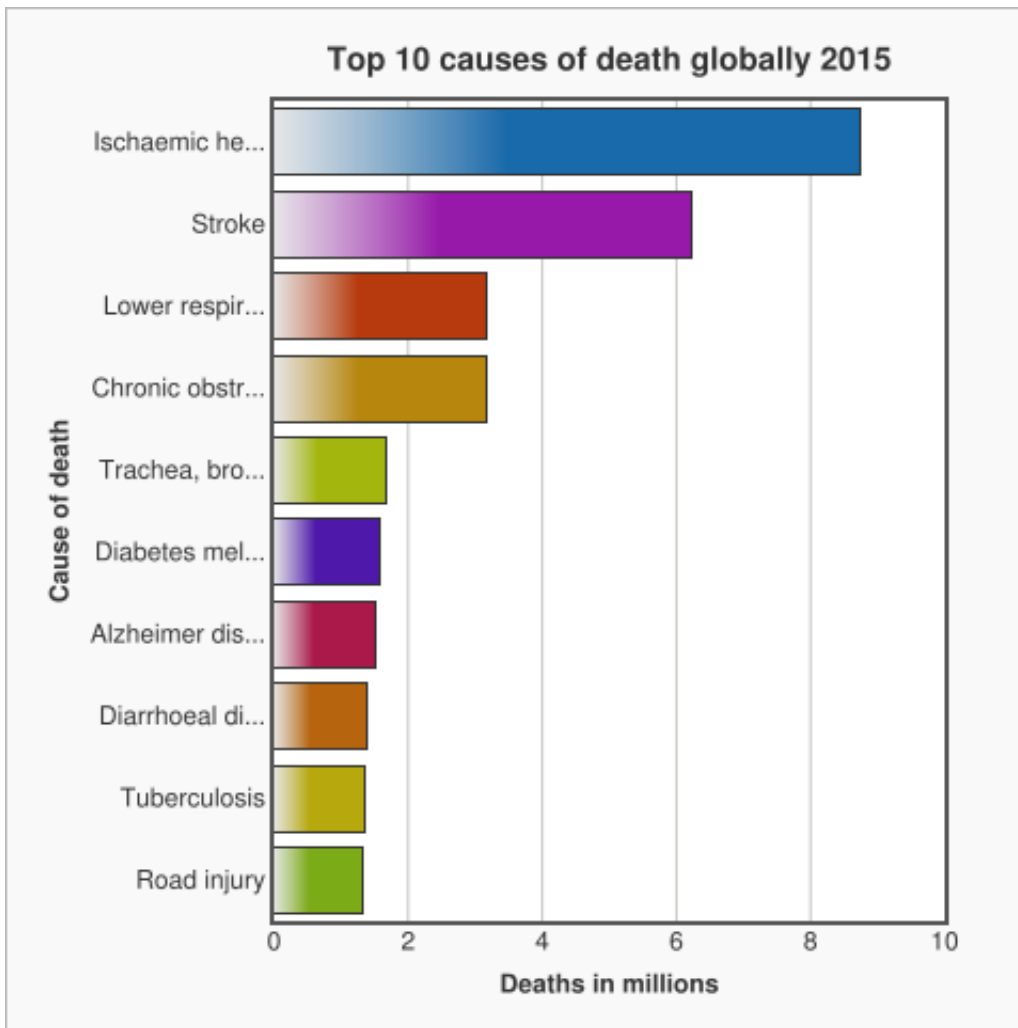
Infectious diseases have been around for as long as human history extends and some pathogens are believed to have co-evolved with humans (Hershkovitz et al., 2008)(Hirsh et al., 2004). Reports of isolation of *Mycobacterium tuberculosis* (*M.tb*) from the excavations of prehistoric remains attest to this fact (Baker et al., 2015). Infectious diseases have also had significant impacts on the course of history itself (Byerly, 2017)(Beaumier et al., 2013)(Taubenberger and Morens, 2006). The Great Smallpox Epidemic of 1775 to 1782 caused mass deaths among both the British and American armies during the American war of independence. This and many other infectious disease epidemics are believed to have killed more American soldiers than enemy troops have. In World War I, the disease typhus killed up to 3 million people, a very significant figure considering that the total death of the entire conflict is estimated at 17 million. At the close of the war in 1918, a global influenza pandemic killed as many as 40 million people out of a total infected case of 500 million, which was a third of the global population. In the Second World War, the entire divisions of the United States (U. S) military were crippled by outbreaks of malaria infections on the eastern front. Around the same time, allied armies in Africa and the Middle East suffered greatly from diarrheal diseases and malaria (Mackie, 1946). The great French general Napoleon Bonaparte is believed to have feared his army being decimated by infectious diseases more than by enemy troops.

According to the WHO, of the total recorded deaths in 2015, about 54% were due to only 10 causes [Figure 1.1] (WHO 2016). Three of these were infectious diseases—lower respiratory tract infections (LRTIs, 3.2 million), diarrhoeal diseases (1.4 million) and tuberculosis (TB)

(1.4 million)—which made up a tenth of the total global deaths. This is an improvement on the global death picture as it was at the turn of the century when there were four infectious diseases in the top 10 causes of deaths, contributing 8.7 million deaths compared to 6 million in 2015.



(A)

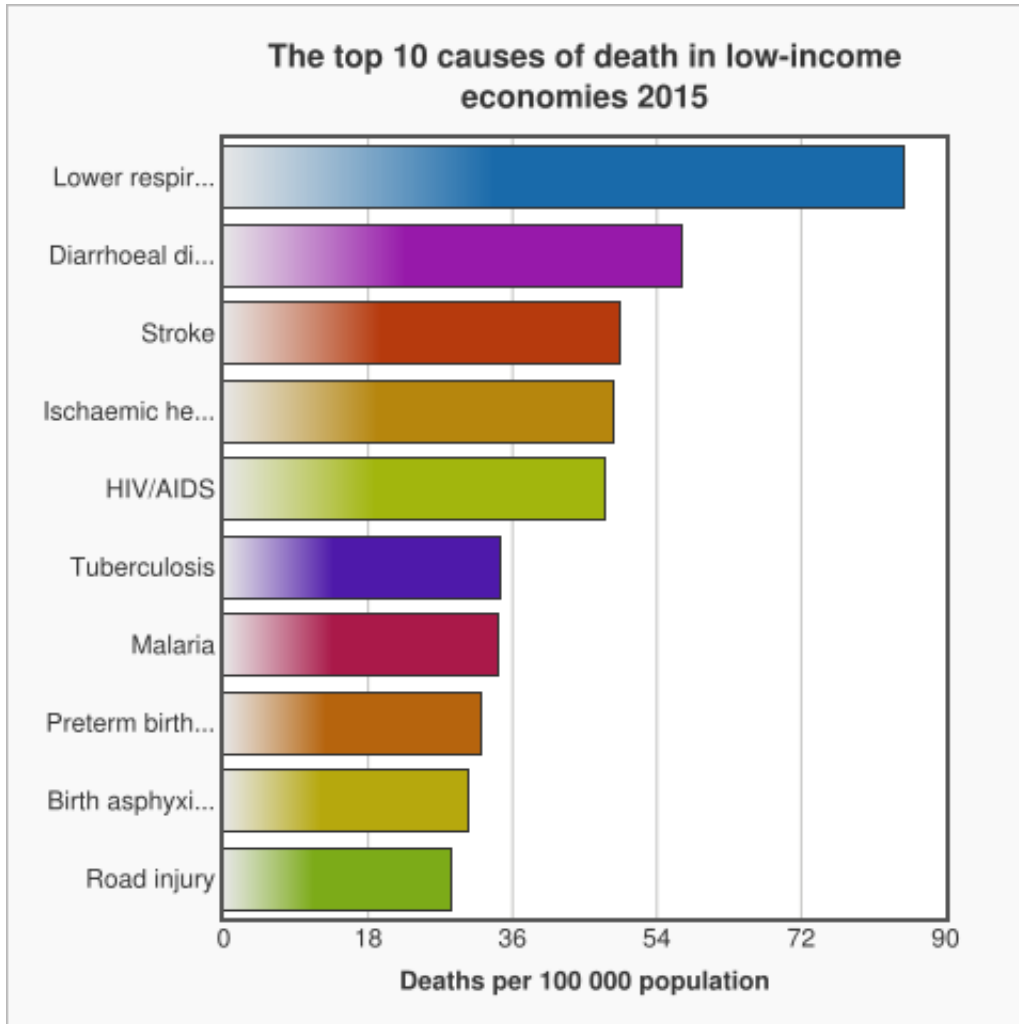


(B)

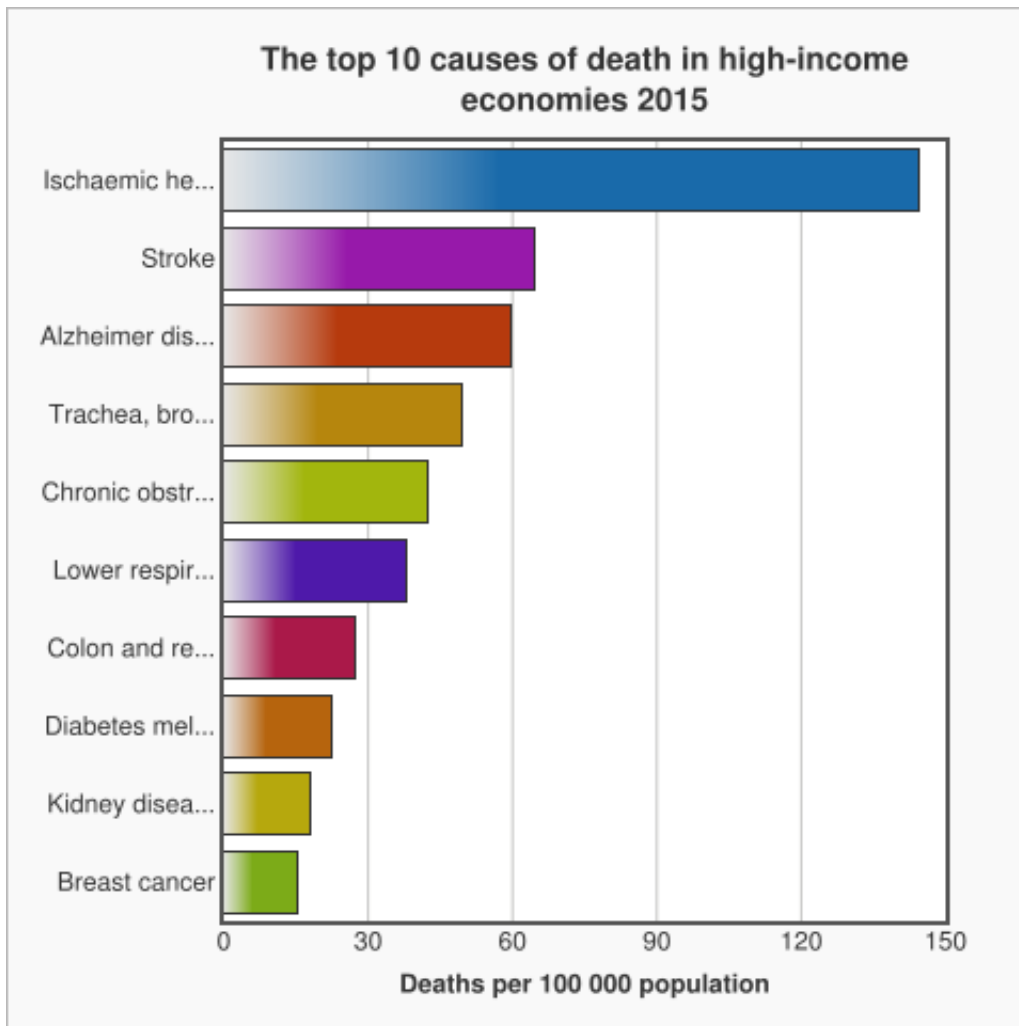
Figure 1.1: Global death picture of the top 10 disease burden, statistics adapted from the World Health Organisation (A) 2000, (B) 2015 (WHO 2016).

The picture is different when looked at from an economic angle. There were five infectious diseases in the top 10 causes of deaths in low-income countries in 2015 compared to only one in high income countries (WHO 2016). The single infectious disease, LRTIs, in the top 10 of the high-income countries caused 38.2 deaths per 100 000 of the population which pales in comparison to the 258.7 deaths caused by the five diseases— LRTIs, diarrhoeal diseases, human immunodeficiency virus associated/acquired immune deficiency syndrome

(HIV/AIDS), TB and malaria—which made the top 10 in low-income countries for the same population size [Figure 1.2]. The conclusion is that after millennia of laying siege to the human population, infectious diseases continue to exert an enormous burden, especially on the most vulnerable communities.



(A)



B)

Figure 1.2: The top 10 causes of deaths in 2015, (A) low-income countries and (B) high income countries (WHO 2016).

1.2 Scope of the thesis

LRTIs and diarrhoeal diseases are groupings of diseases with similar sites of infections and symptoms but different causative agents (Tregoning and Schwarze, 2010). LRTIs affect the lungs, bronchi and trachea (Tregoning and Schwarze, 2010)(Mizgerd, 2008). Infected individuals present with pneumonia and bronchitis. Infection could be caused by a bacterium, virus or parasitic protozoan. The most notable LRTI diseases are influenzas and pneumonia

(Tregoning and Schwarze, 2010)(BiscevicTokic et al., 2013). LRTIs cannot be classified as infectious diseases of poverty because they occur across all economic strata (WHO 2016). For this reason, they fall outside the scope of this review.

Diarrhoeal diseases are classified by the WHO as poverty related diseases (PRDs) and are indeed, most often, caused by poor sanitation which is inherent to a state of poverty (WHO, 2017). Diarrhoea is caused by infectious organisms like bacteria, viruses, protozoans and helminths (WHO, 2017)(Keusch et al., 2006). Although antibiotics are used to treat bloody diarrhoea, treatment is mostly supportive with the use of electrolyte replacement therapy to reverse dehydration (WHO, 2017). Because of the multiple causative agents and treatment not being specifically defined against the cause of the disease, diarrhoeal diseases fall outside the scope of this review.

Of the diseases that have a specific causative organism and a defined treatment regimen, HIV/AIDS, TB and malaria feature almost exclusively in the main causes of deaths in low-income countries. They are officially classified as diseases of poverty (Stevens, 2004). These three diseases fall under the scope of this thesis because they have specific causative organisms and defined treatment regimens.

1.3 HIV/AIDS

HIV falls into the retroviridae family and is classified as a Lentivirus (Seitz, 2016)(das Neves et al., 2010) (Wong et al., 2010)(Simon et al., 2010). Simian immunodeficiency virus (SIV), the immunodeficiency infections of primates are also classified to the genus Lentivirus (Seitz, 2016)(Williams and Burdo, 2009)(Montefiori, 2005). Lentiviruses often cause immunodeficiency in their host by killing the differentiation 4 positive (CD4+) T lymphocytes (CD4⁺ T-cell) (Gupta and Jain, 2010)(Simon et al., 2010)(Clapham and McKnight, 2002). By doing so it permits life threatening opportunistic infectious diseases like TB and malaria to succeed (Wong et al., 2010)(Rao et al., 2009). There are two major classes of HIV that can cause AIDS, HIV-1 and HIV-2 (Seitz, 2016)(Gupta and Jain, 2010)(das Neves et al., 2010)(Wong et al., 2010). These two viruses are closely related; differing in their biological origin and in some accessory genes (Gupta and Jain, 2010). HIV-

1 and HIV 2 originates from simian immunodeficiency virus from Central African chimpanzees (SIVcpz) and West African sooty mangabeys (SIVsm); respectively (Cohen et al., 2008)(Apetrei et al., 2004)(Santiago et al., 2005). HIV-2 is less dangerous than HIV-1, and it is known for its slower progression to AIDS (Wong et al., 2010)(de Silva et al., 2008).

HIV can be seen as a biological nanostructure that has a diameter of around 100 to 150 nm (Seitz, 2016)(das Neves et al., 2010), spherical in shape as shown in **Figure 1.3**. It is composed of nucleocapsid and genetic material in the form of ribonucleic acid (RNA) containing three structural genes, reserved from the human cell when the new virus is formed (das Neves et al., 2010). The virus outer viral envelope consist of two glycoproteins i.e gp120 and gp41, which are predisposed for identifying the CD4 receptor and the CCR5 or CXCR4 co-receptors of the host cell membrane (Mallipeddi and Rohan, 2010). In addition to the viral core, HIV has six regulatory genes: transactivator protein (Tat) and RNA splicing-regulator (Rev) are essential for the commencement of HIV replication, the other regulatory proteins negative regulating factor (Nef), viral infectivity factor (Vif), virus protein r (Vpr) and virus protein unique (Vpu) have an influence on virus budding, viral replication, and pathogenesis (Seitz, 2016)(Sauter et al., 2012). Infection with HIV occurs by sexual contact with an infected partner, needles and from mother to child from an infected individual during pregnancy or breast feeding (Mallipeddi and Rohan, 2010)(Coovadia and Rollins, 1999). Once inside the human body, the virus can go through the human cell in three important mechanisms (Rao et al., 2009)(Gallo et al., 2003);

- Binding of the HIV surface gp 120 to the CD4 receptor situated on the cell membrane.
- Interaction of the gp 120 protein and CD4 complex with a co- receptor
- Binding of the virus-cell membrane to the CD4 mediated by the trans-membrane gp 41 protein

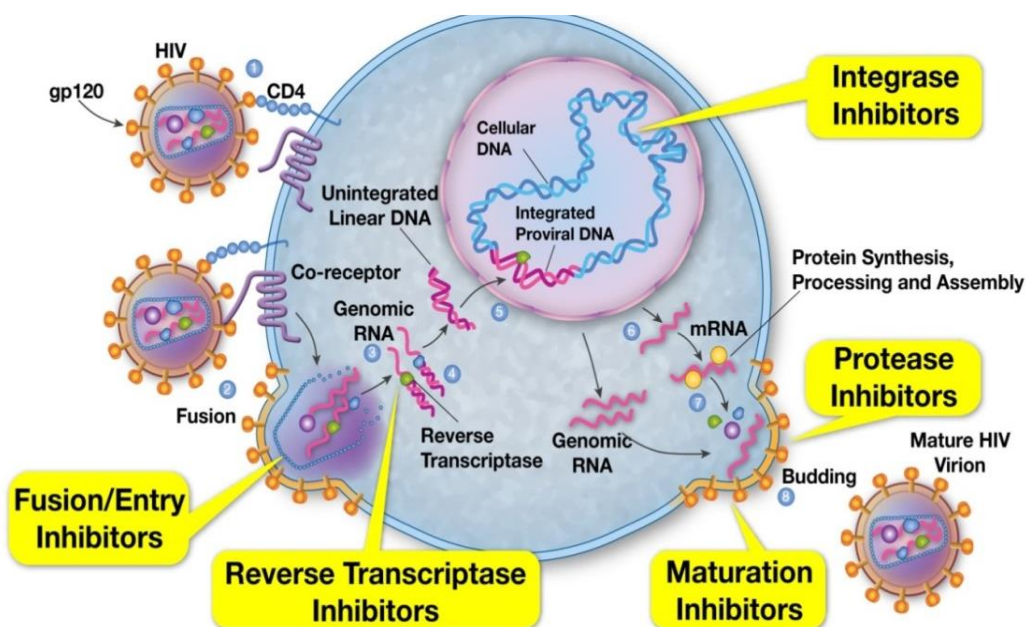


Figure 1.3: HIV replication cycle and targets for antiretroviral therapy (Pietrucha, 2015).

After binding with the human cell, two viral enzymes namely reverse transcriptase (RT) and integrase are discharged into the cytol of the host cell (Tian et al., 2018)(das Neves et al., 2010). The RT enzyme then transcribe the single stranded RNA into double stranded deoxyribonucleic acid (DNA), followed by assimilation of the viral DNA into the host genome causing the development of a provirus (Nermut and Fassati, 2003).

1.3.1 Current chemotherapy in HIV/AIDS therapy and challenges

The identification of HIV as the primary cause of AIDS, launched an intensive research campaign to find active agents that can target various steps in the HIV replication cycle (Esté and Cihlar, 2010)(Broder, 2010)(De Clercq, 2010). The first active agent to be used as an anti-HIV drug, zidovudine, received the United State Food and Drug Administration (US-FDA) approval in 1987, demonstrating a significant clinical proof-of-concept that HIV virus might be treated with chemotherapy (Broder, 2010)(Esté and Cihlar, 2010). Today there are more than 25 anti-HIV drugs known as the antiretrovirals (ARVs) therapy some of which are also available in a fixed dose combination (FDC). These drugs fall into six mechanistic classes and are categorized as (Esté and Cihlar, 2010): nucleoside/nucleotide reverse

transcriptase inhibitors (NRTIs/nRTIs, **Table 1.1**), non-nucleoside reverse transcriptase inhibitors (NNRTIs, **Table 1.2**), protease inhibitors (PIs, **Table 1.3**), integrase inhibitors, entry/fusion inhibitors (FIs, **Table 1.4**) and chemokine receptor antagonists (CRAs, **Table 1.4**)

The highly active antiretroviral treatment (HAART), which is the current clinical therapy for HIV/AIDS, consists of at least three ARVs from different mechanistic classes (Mallipeddi and Rohan, 2010). It is considered as one of the most important advances in the field of HIV/AIDS (Sharma and Garg, 2010). HAART has dramatically changed the clinical course of HIV/AIDS infection by suppressing the virus, and has led to a great improvement by extending the life of the HIV/AIDS infected patients (Sosnik et al., 2009). In this context, it has turned HIV/AIDS from a deadly disease to a controllable chronic condition (Delaney, 2006).

HAART is a lifetime obligation that is only used to control the viral load of the infected patients; any non-adherence leads to rebound of viral replication (Sharma and Garg, 2010)(Richman et al., 2009). According to epidemiological studies, deviation levels below 95% tend to diminish the chances of therapeutic success approximately to 50% (Shah, 2007). Unfortunately even good compliance to HAART regime does not lead to complete eradication of the virus in the body, and as a result HIV/AIDS is incurable (Mamo et al., 2010). Most ARVs are administered orally and some undergo extensive first pass metabolism and gastrointestinal (GI) degradation, which all leads to low bioavailability (Sosnik et al., 2009). Another significant challenge with HAART today is the development of multi-drug resistance (MDR) against ARV agents established throughout the course of therapy (Gupta and Jain, 2010). To overcome the factor of drug resistance, US-FDA-approved drugs, e.g. etravirine, are to be used with other ARVs in patients who have developed resistance. However, due to their recent approval, their long-term side effects are unknown. Thus over the coming year's clinical experience will probably show their biopharmaceutical weaknesses and disadvantages (Sosnik et al., 2009). More importantly, HIV primarily resides in the anatomical (i.e. the central nervous system, lymphatic system, liver etc) and cellular reservoirs (i.e. CD4+ T lymphocytes and macrophages/monocytes) of the human body,

which is the main problem as the ARVs cannot reach these places in therapeutic concentrations. In addition, administration of HAART regimen in high doses contributes to poor patient compliance because of the undesirable side-effects experienced by the patients. Therapeutic success relies not only on the affordability to medications but more importantly on the patient compliance.

Table 1.1: Representation of nucleoside reverse transcriptase inhibitors currently used to treat HIV/AIDS

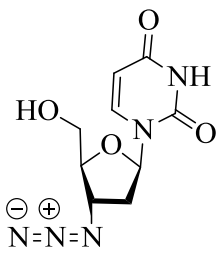
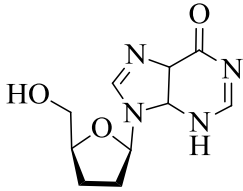
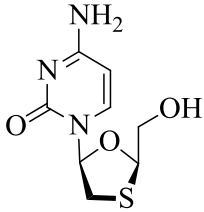
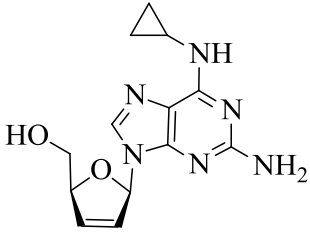
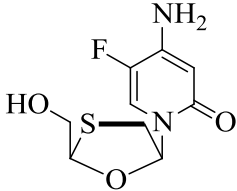
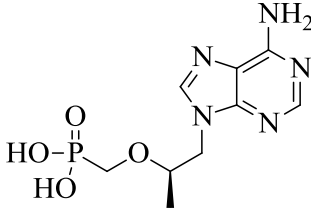
 <p>Zidovudine</p>	 <p>Didanosine</p>
 <p>Lamivudine</p>	 <p>Abacavir</p>
 <p>Emtricitabine</p>	 <p>Tenofovir</p>

Table 1.2: Representation of non-nucleoside reverse transcriptase inhibitors currently used to treat HIV/AIDS

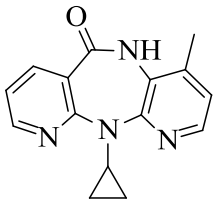
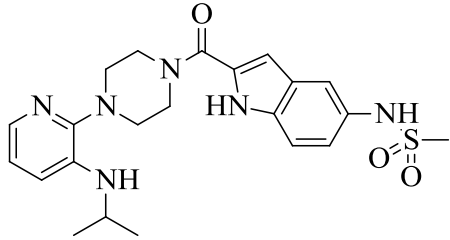
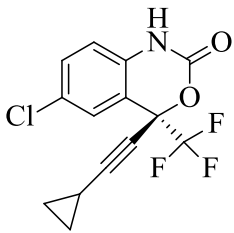
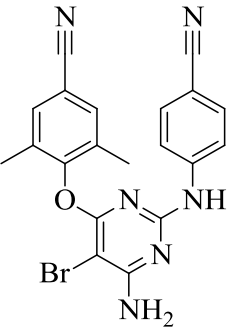
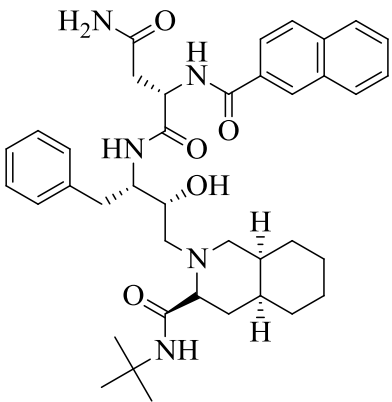
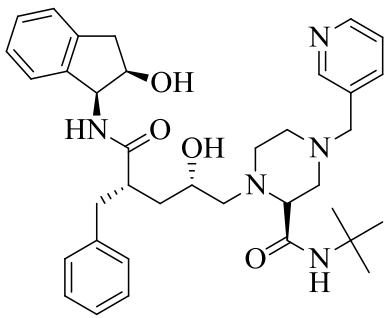
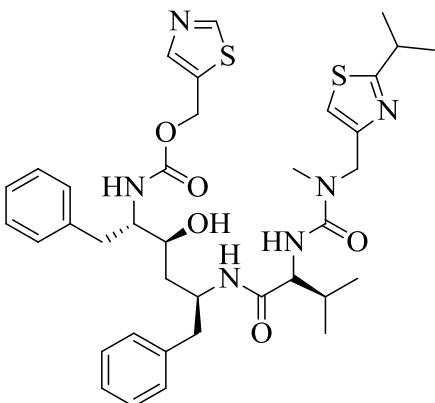
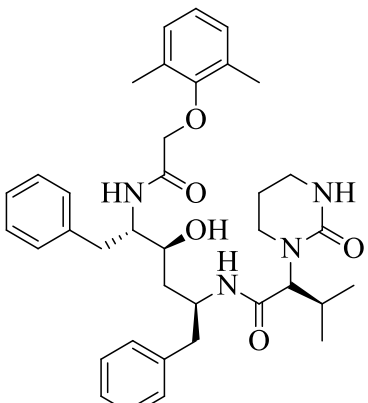
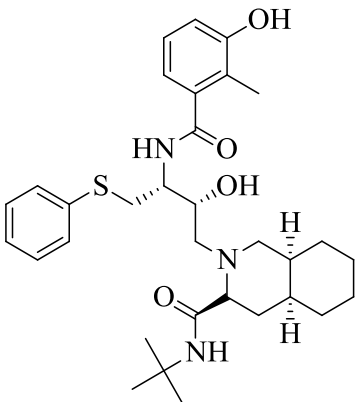
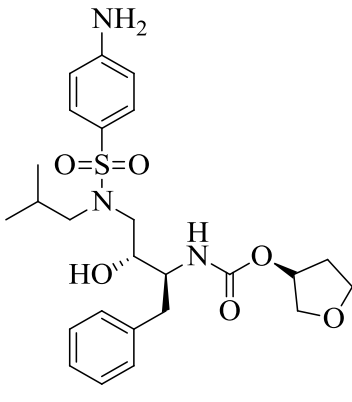
 <p>Nevirapine</p>	 <p>Delavirdine</p>
 <p>Efavirenz</p>	 <p>Etravirine</p>

Table 1.3: Representation of protease inhibitors currently used to treat HIV/AIDS

 <p>The structure of Saquinavir features a central bicyclic core (a decalin system) with a tert-butylamino group and a hydroxyl group. It is substituted with a benzyl group, a hydroxyl group, and a side chain containing a hydroxyl group, a benzyl group, and a dihydroquinoline ring system with a primary amide group.</p> <p>Saquinavir</p>	 <p>The structure of Indinavir consists of a bicyclic core with a hydroxyl group and a piperazine ring. It is substituted with a benzyl group, a hydroxyl group, and a side chain containing a hydroxyl group, a benzyl group, and a piperazine ring with a tert-butylamino group and a pyridine ring.</p> <p>Indinavir</p>
 <p>The structure of Ritonavir features a central bicyclic core with a tert-butylamino group and a hydroxyl group. It is substituted with a benzyl group, a hydroxyl group, and a side chain containing a hydroxyl group, a benzyl group, and a thiazole ring system.</p> <p>Ritonavir</p>	 <p>The structure of Lopinavir consists of a bicyclic core with a hydroxyl group and a piperazine ring. It is substituted with a benzyl group, a hydroxyl group, and a side chain containing a hydroxyl group, a benzyl group, and a piperazine ring with a tert-butylamino group and a pyridine ring.</p> <p>Lopinavir</p>
 <p>The structure of Nelfinavir features a central bicyclic core with a tert-butylamino group and a hydroxyl group. It is substituted with a benzyl group, a hydroxyl group, and a side chain containing a hydroxyl group, a benzyl group, and a piperazine ring with a tert-butylamino group and a pyridine ring.</p> <p>Nelfinavir</p>	 <p>The structure of Amprenavir consists of a bicyclic core with a hydroxyl group and a piperazine ring. It is substituted with a benzyl group, a hydroxyl group, and a side chain containing a hydroxyl group, a benzyl group, and a piperazine ring with a tert-butylamino group and a pyridine ring.</p> <p>Amprenavir</p>

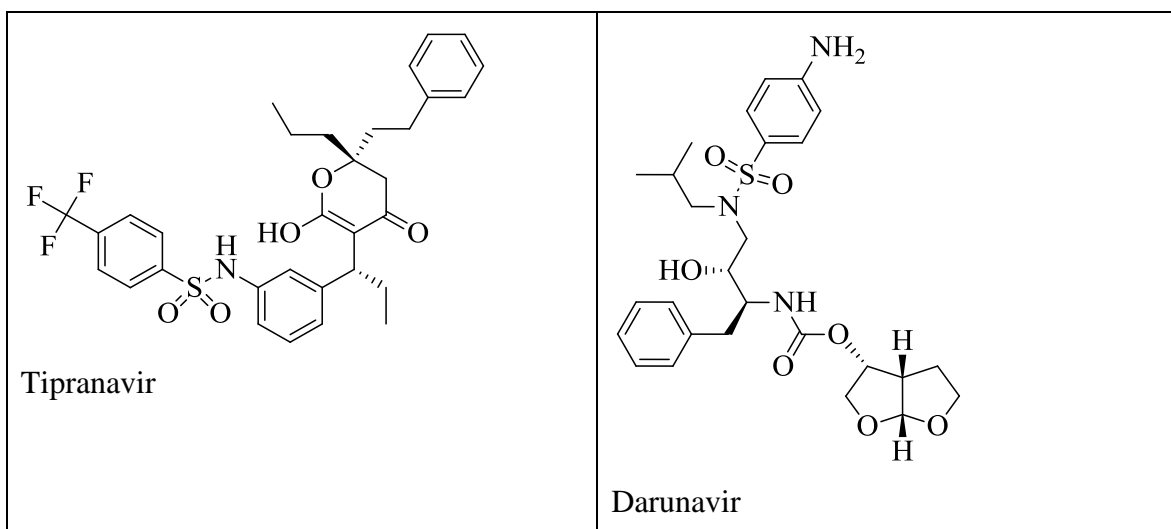
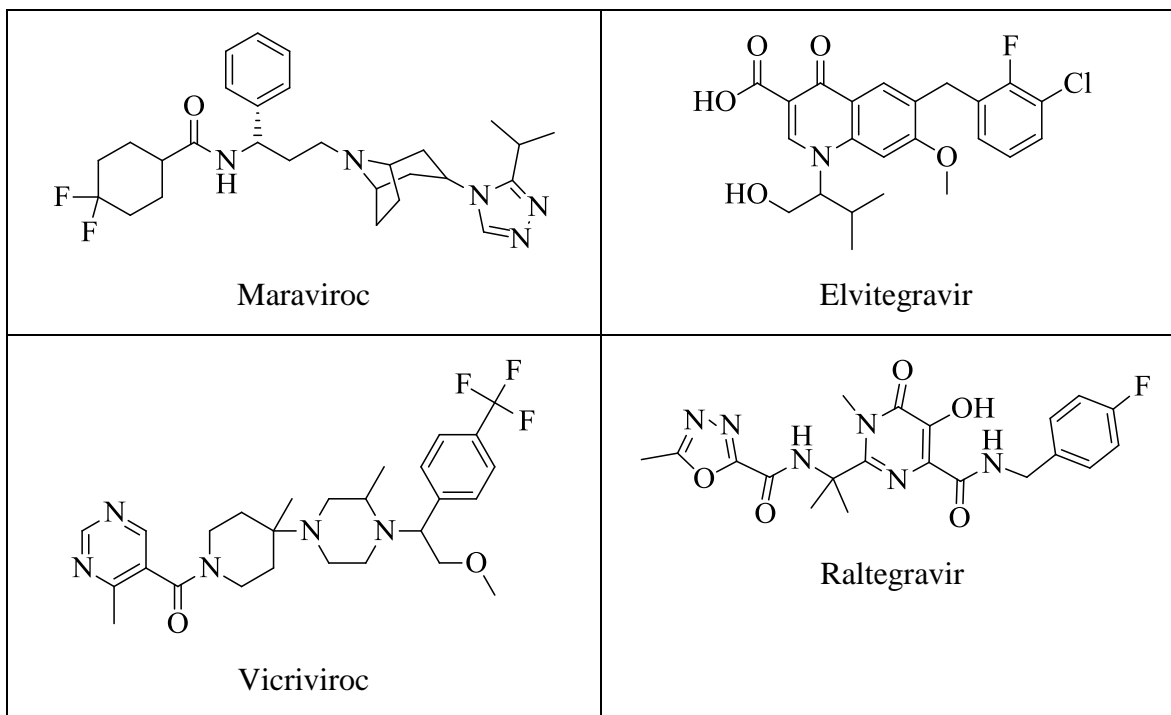


Table 1.4: Representation of Viral fusion/entry and Integrase inhibitors currently used to treat HIV/AIDS



1.4 TB

TB is one of the oldest infections of man and it usually attacks the lungs. However, it can infect virtually any part of the human body. A person infected with TB does not automatically feel ill – and such conditions are referred to as “latent” or silent infections (Matteelli et al., 2017). A collapse of the immune system causes TB to become “active”. Symptoms include cough that last for more than two weeks, loss of appetite and weight loss, fever and coughing up blood. Co-infection with other pathogens might also generate development to TB. This has incentivized the recent reappearance of TB as a co-epidemic with HIV/AIDS (Tiberi et al., 2017)(Deffur et al., 2013)(Diedrich and Flynn, 2011). People living with HIV are up to 50 to 60% more likely to develop TB (Tiberi et al., 2017)(Diedrich et al., 2016). Conversely, HIV-negative patients have 6 to 10% chance to grow the bacteria and, in most of the occasion, because of the revival of a pre-existing infection (Tiberi et al., 2017)(Schluger, 2005). Another aspect of the resurgence of TB is the evolution of drug-resistant strains (Diedrich et al., 2016)(Manjelievskaia et al., 2015). The strains are formed by inadequate and inconsistent treatment practices that allow the bacteria to evolve mechanisms of avoiding the effects of the drugs. The multidrug-resistant (MDR) strains are much more costly and difficult to treat and are often fatal (Manjelievskaia et al., 2015).

TB is caused by *Mycobacterium tuberculosis* (*M.tb*). It is a rod-shaped obligate aerobe of 2-4 µm in length and 0.2-0.5 µm in width [Figure 1.4] (Todar, 2009). It survives best in a physiologic pH of 7.4. TB infection is normally actuated by inhalation of aerosol droplets containing *Mtb* to the respiratory system (Fogel, 2015)(Smith, 2003). Once inhaled, the *Mtb* are phagocytosed and reside within alveolar macrophages and dendritic cells (Queval et al., 2017)(Sasindran and Torrelles, 2011). Macrophages, as phagocytes, ingest and try to kill *Mtb*, while the bacteria tries to destabilize macrophages using different strategies (reviewed by Ehrt & Schnappinger 2009) so as to multiply, disseminate and escape to infect a new host cell. The bacilli that escape the killing by macrophages increase exponentially. After 3 to 8 weeks of infection, the bacterium kills the host cells and result in the destruction of macrophages and spreads to the regional lymph nodes in the lungs by lymphatic circulation (Smith, 2003). Dissemination of the bacilli to other organs such as the spleen, liver, kidneys

and CNS takes place 3 months after infection. At this period, acute TB meningitis can occasionally cause death.

A



B



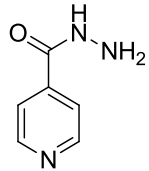
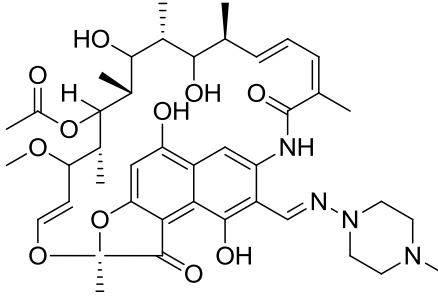
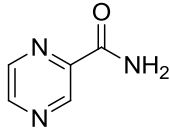
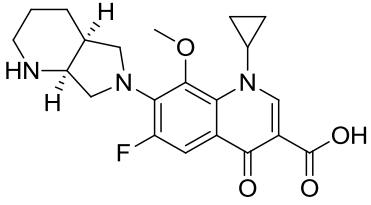
Figure 1.4: *M. tuberculosis* A. bacilli B. colonies growing on solid medium (Todar, 2009)

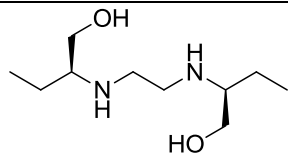
1.4.1 Current chemotherapy in TB therapy and challenges

The main priorities of anti-TB drugs include rapid killing of actively growing bacilli, sterilization of infected host tissues to avoid clinical relapse and preclusion of developed drug resistance (Shin and Kwon, 2015). The current recommended treatment requires at least 6 months duration and attains cure rates of >95% when taken under supervision (Zumla et al., 2013). It consists of combination therapy of isoniazid (INH), rifampicin (RIF) and pyrazinamide (PYZ). During the first 2 months, these three drugs are taken orally together with ethambutol (ETB) or streptomycin (SM) (Sosnik et al., 2010). The last 4 months comprises solely of INH and RIF. Any patient non-adherence results in resurgence of the bacteria and more importantly multi-drug resistance (Sosnik et al., 2010). Drug resistance to RIF and INH is the most shared type of resistance among *Mtb* isolates (Seifert et al., 2015). MDR-TB is treated with PYZ for 9 to 12 months to assure therapeutic success (Mukherjee et al., 2004)(Smith, 2003). PYZ is administered together with second-line drugs such as capreomycin, fluoroquinolones, ethionamide, p-aminosalicylic acid, prothio-namide and cycloserine (Mpagama et al., 2013) (Sosnik et al., 2010)(Mukherjee et al., 2004). These treatment is more expensive and less active than the first-line drugs. Toxicity is still a problem

and most of the drugs used to treat TB are antibiotics with significant aqueous solubility, hence the prolonged treatment [**Table 1.5**]. The logP of these drugs are mainly below 0. Thus this is a contrary to a cell wall that has a highly hydrophobic linked skeleton (discussed in **Chapter three**).

Table 1.5: Physico-chemical properties of current anti-TB drugs.

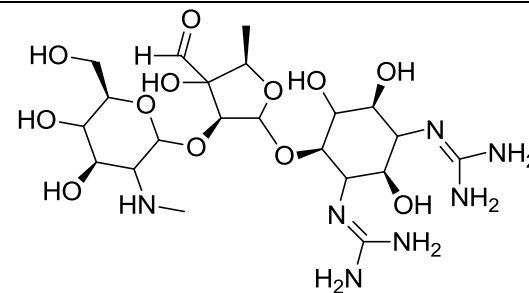
 <p>Isoniazid (INH)</p> <p>Aqueous solubility (mg/mL) = 125</p> <p>LogP = -0.70</p>	 <p>Rifampicin</p> <p>Aqueous solubility (mg/mL) = 1-2</p> <p>LogP = 2.70</p>
 <p>Pyrazinamide</p> <p>Aqueous solubility (mg/mL) = 14</p> <p>LogP = -0.60</p>	 <p>Moxifloxacin (Mox)</p> <p>Aqueous solubility (mg/mL) = N/A</p> <p>LogP = 2.90</p>



Ethambutol

Aqueous solubility (mg/mL) = 100

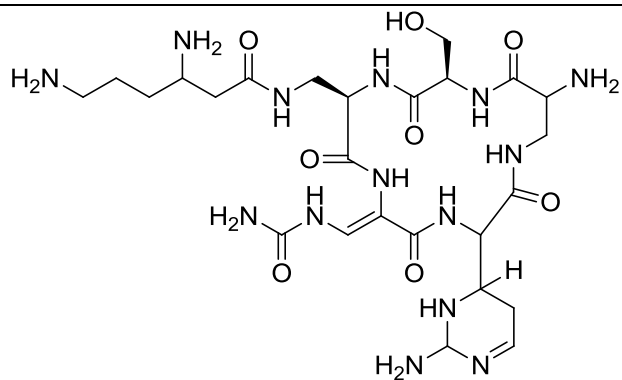
LogP = -0.30



Streptomycin

Aqueous solubility (mg/mL) = > 20

LogP = -6.40



Capreomycin

Aqueous solubility (mg/mL) = Soluble in water

LogP = -9.61

1.5 Malaria

Malaria is an acute infection caused by apicomplex protozoan parasite of the *Plasmodium* genus that are transferred to human through the bites of infected mosquitoes of the *Anopheles* genus (Gazzinelli et al., 2014)(Santos-Magalhães and Mosqueira, 2010)(White, 2004) [Figure 1.5]. *Plasmodium* sporozoites are injected into the skin by female mosquitoes seeking a blood meal to nurture their eggs (Orfano et al., 2016)(Aly et al., 2010) (Gazzinelli et al., 2014). Sporozoites efficiently enter the bloodstream and travel to the liver (Kumar et al., 2016)(Antoniana U Krettli and Miller, 2001). The liver stage does not result in the manifestation of the disease but leads to a 10,000-fold boosting of parasite numbers (Gazzinelli et al., 2014)(Aly et al., 2010), and eventually invade the hepatocytes by undergoing asexual replication (Gazzinelli et al., 2014). Thousands of exoerythrocytic merozoites resulting from hepatocytes rapidly invade red blood cells (RBCs) and initiate a series of asexual multiplication cycles (Soulard et al., 2015) (Gazzinelli et al., 2014).

Four species of malaria are prevalent in tropical and subtropical regions. These are *P. falciparum*, *P. vivax*, *P. malariae* and *P. ovale* (Santos-Magalhães and Mosqueira, 2010). The *P. falciparum* is the most dangerous of the four malaria parasites; the most effective malaria parasite and the most difficult to control (Bousema and Drakeley, 2011)(Santos-Magalhães and Mosqueira, 2010). It is mostly prevalent in the African continent and is responsible for most morbidity and mortality (WHO, 2015) (Bousema and Drakeley, 2011)(Santos-Magalhães and Mosqueira, 2010). The remaining malaria parasites contribute significantly to its morbidity. There were an estimated 214 million malaria cases in 2015 (Mischlinger et al., 2016) (WHO, 2016)(WHO 2015). Approximately 88% of these episodes occurred in African regions. The number of malaria deaths globally diminished from 839 000 in 2000, to 438 000 in 2015, a decline of 48%. Most deaths were in the African regions (90%) (WHO, 2016)(WHO 2015). Though substantial progress has been made in reducing the mortality rate in African regions, the report also says that there were about 292 000 deaths in children under the age of 5 in 2015 (Mischlinger et al., 2016). The disturbing fact is that malaria remains a main killer of minors, taking the life of a juvenile every 2 minutes

(Mischlinger et al., 2016). Pregnant women are also at higher risk for clinical malaria than non-pregnant women.

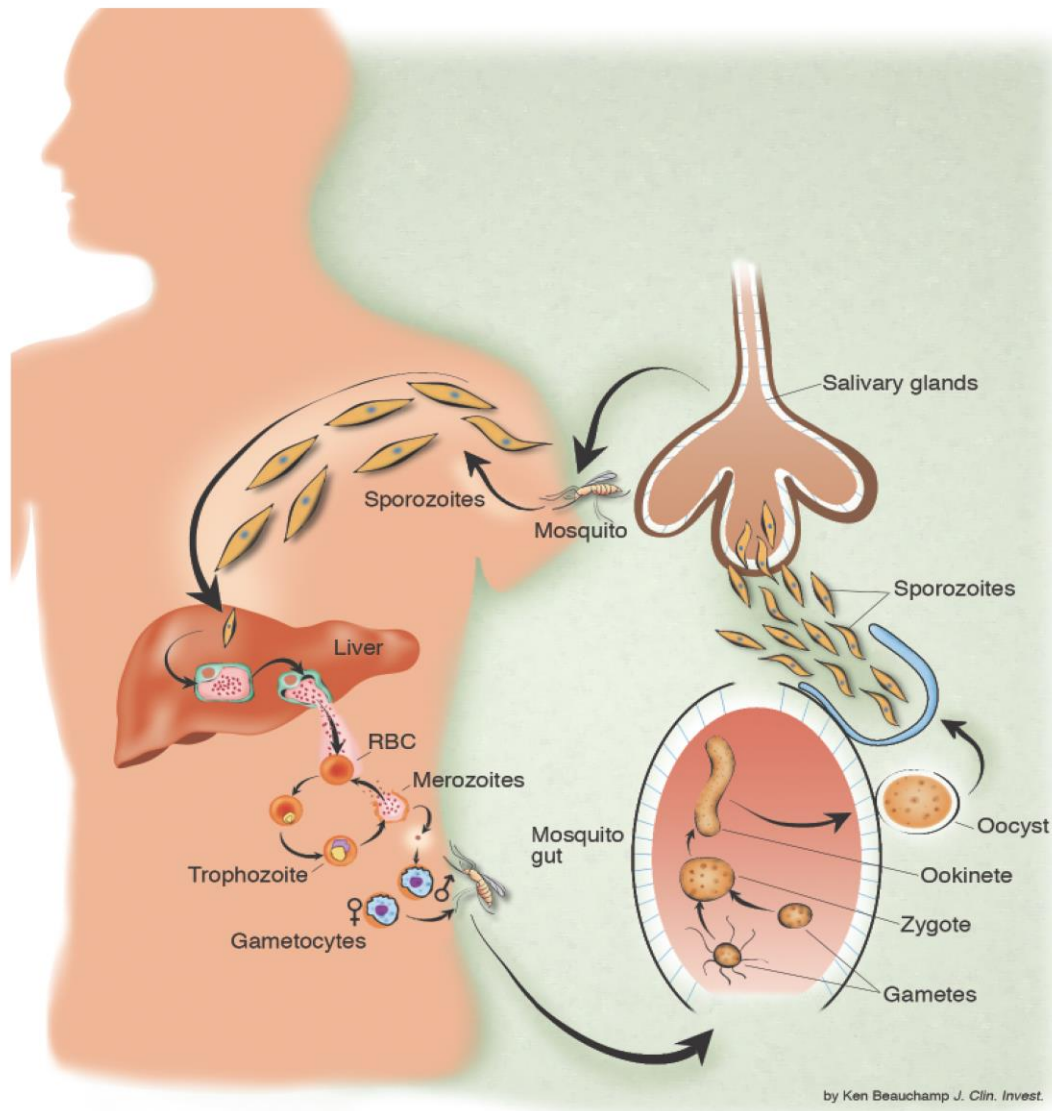


Figure 1.5: The life cycle of malaria parasites in human host and anopheles mosquito vector (White, 2004).

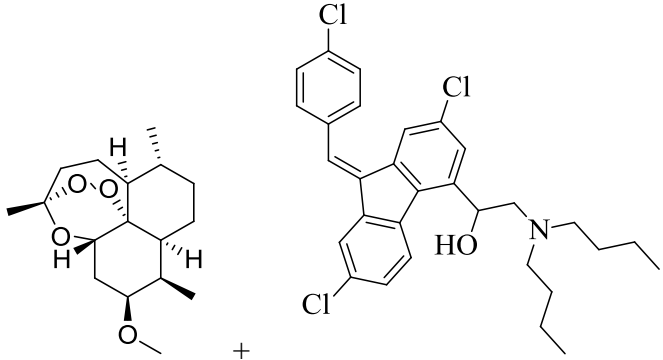
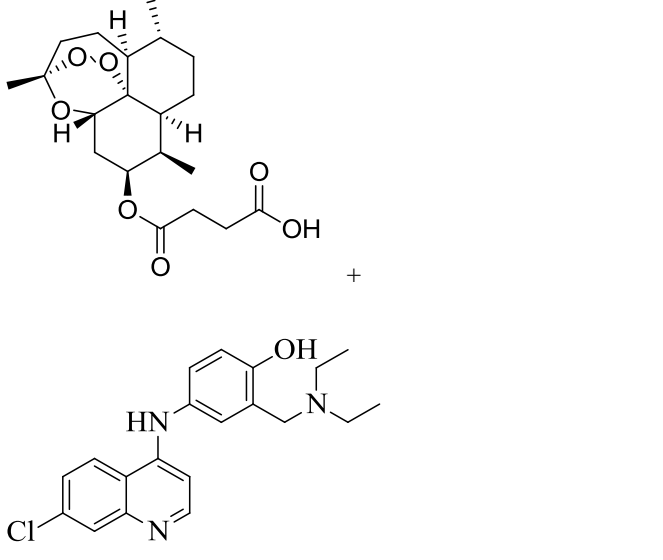
1.5.1 Current chemotherapy in malaria therapy and challenges

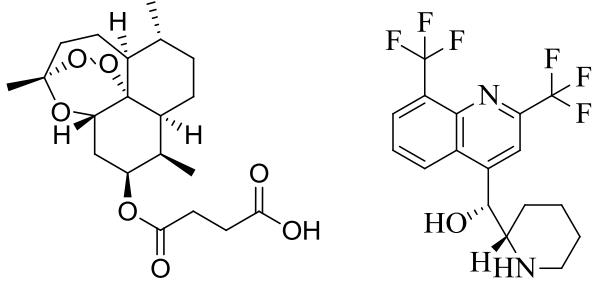
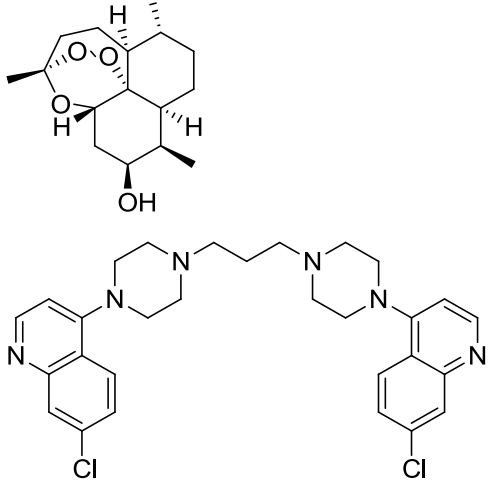
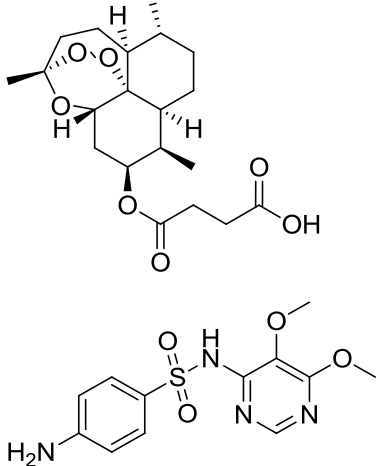
Artemisinin combination therapy (ACT) is used for the treatment and prevention of uncomplicated *P. falciparum* malaria (WHO, 2016). The combination therapy is based on the administration of an artemisinin-based drug with another agent, often an aryl-alcohol chemical class of drugs. This concept of combining artemisinins with a long acting partner drug ensures that residual parasites that may have remained after dihydroartemisinin (DHA, more potent active metabolite of artemisinin derivatives) has been cleared from the body are eliminated, thus minimizing reactivation of the parasite. The artemisinins produce faster clearance of parasitaemia than conventional antimalarial drugs by reducing parasite numbers 100- to 1000-fold per asexual cycle of the parasite. Different forms of ACT's are available on the market [Table 1.6]. Examples include artesunate + amodiaquine, artesunate + sulfadoxine/pyrimethamine, artesunate + mefloquine, and artemether + lumefantrine. These compounds are administered orally once or twice daily for 3 days. Coartem (artemether [20 mg] + lumefantrine [120 mg]) is widely used in African regions and is administered orally twice daily for the period of 3 days. Complicated or severe *P. falciparum* malaria is treated with injectable artesunate for at least 24 hours and followed by a complete 3 day course of Coartem.

According to World Malaria report (2015), 15 million of the 28 million pregnant women in danger did not get a single dose of Intermittent preventive treatment of malaria (IPTp) and between 68 and 80 million of the 92 million kids with malaria did not obtain ACT (WHO, 2016). Thus in spite of spectacular advances in malaria intervention coverage, lots of people still do not obtain the facilities they need. While the economic costs pose challenges, most anti-malarial drugs suffer from solubility and biocompatibility issues. Another significant problem that is growing exponentially is the development and spread of drug resistance. Resistance to artemisinins has now been reported in 5 countries namely Cambodia, Laos Peoples Democratic Republic, Myanmar, Thailand and Vietnam (WHO, 2016). Artemisinin-based drugs are an important element of treatments for multidrug resistance *P. falciparum* malaria. Resistance has now been established to all the antimalarial drug classes (Cui et al.,

2015)(White, 2004). If we lose ACT's through the development of multi-drug resistance strains, we may be faced with incurable disease in Africa.

Table 1.6: WHO recommended artemisinin combination therapy.

Combination therapy	Chemical family
 <p style="text-align: center;">Artemether+lumefantrine</p>	Sesquiterpene lactones+ Amino-alcohols
 <p style="text-align: center;">Artesunate+amodiaquine</p>	Sesquiterpene lactones+4-Aminoquinolines

 <p>Artesunate+mefloquine</p>	<p>Sesquiterpene lactones+Amino-alcohols</p>
 <p>Dihydroartemisinin+piperazine</p>	<p>Sesquiterpene lactones+4- Aminoquinolines</p>
 <p>Artesunate+Sulfadoxine-Pyrimethamine</p>	<p>Sesquiterpene lactones+ Sulfonamides and sulfones- Diaminopyrimidine</p>

1.6 Application of nanomedicine in infectious diseases

Nanomedicine is a relatively emerging field that offers therapeutic formulations with a size range of 1 nm to 10^3 nm (Smolkova et al., 2017)(Mamo et al., 2010). The field is distinct as it exceptionally concentrates on medically related, patient-centric nanotechnologies. It has seen applications in several areas of health care including diagnostics, biological imaging, and disease treatment (Smolkova et al., 2017)(Semete et al., 2010)(Duncan, 2005). The overall goal of nanomedicine is exactly the same as that of medicine; to diagnose as accurately and as early as possible and to treat as effectively as possible without any detrimental effects (Riehemann et al., 2009). The significance of this size range is that ‘nanomedicinal’ structures larger than 1 μ m will find difficulty traversing biological barriers like the GI wall while structures smaller than 1 nm may experience clearance not much different from the native bioactive compounds (Longmire et al., 2008)(Choi et al., 2007).

The use of nanotechnology for medicinal platforms is continuously transforming medical science in many areas of disease management (Shi et al., 2017). Cancer victims have been the main inheritors of this revolution to date, with substantial developments in the last few decades (Mamo et al., 2010)(Duncan & Gaspar 2011). Several advanced delivery systems for cancer therapy are either under evaluations or FDA approved (Dakwar et al., 2017)(Hare et al., 2017). This remarkable accomplishments have been due to the exceptional features that nanomedicine presents on drug delivery systems (Smolkova et al., 2017). Applying nanomedicine, targeted delivery of active ingredients to specific compartments and better delivery of poorly water-soluble drugs has become probable (Mamo et al., 2010)(Duncan & Gaspar 2011)(Duncan et al., 2006).

Nanomedicines often involve the use of polymeric carriers whose attractive physicochemical properties mask the unfavourable characteristics of the bioactive agent (Mishra et al., 2010). Traditionally, nanomedicines have been designed by encapsulating active drugs into polymeric nanoparticles. With no chemical interaction between the drug payload and the carrying vehicle drug loading is practical. Recently, chemical modification of the drug by conjugating to a polymeric carrier is gaining momentum in the field. Polymer therapeutics

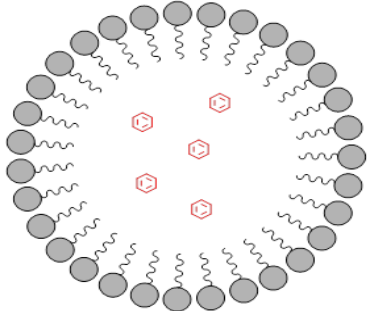
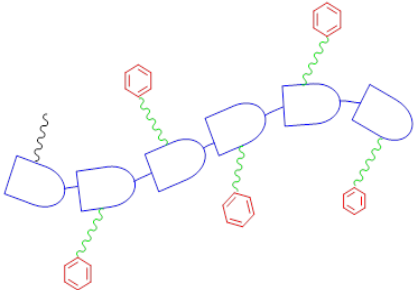
offers a powerful technological solution to the high toxicity and poor pharmacokinetics of drugs (Duncan, 2017)(Duncan and Gaspar, 2011)(Duncan and Vicent, 2013). The two techniques are compared in **Table 1.7**.

1.6.1 Encapsulation

Encapsulation is a process of enclosing one substance (a solid, liquid and gas) within another material, which in turn protects them from the external environment (Ghosh, 2006). The substance that is encapsulated into another material is usually called the core material, an active ingredient or internal phase (Poshadri and Kuna, 2010). The material encapsulating the core is mainly referred to as the membrane, shell or wall material (Ghosh, 2006)(Poshadri and Kuna, 2010)(Jyothi et al., 2010). If the material being encapsulated results in a size less than 1 μm , the process is called nano-encapsulation, conversely above 1 μm the process is referred to as micro-encapsulation. Substances that are usually encapsulated include drugs, foods, oils and sensitive materials (Jyothi et al., 2010). Many researchers use polymers to form the shell (Rao and Geckeler, 2011). The choice of the polymer depends on the physicochemical properties of the core, process of encapsulation, and the desired properties of the final product (Soppimath et al., 2001). Some advantages of encapsulation include (Jyothi et al., 2010):

- to protect the sensitive material (e.g. drug) from the external environment
- to obtain the controlled release of the drug as the polymer degrades
- to make handling of the material much easier and
- to avoid side effects like gastric irritation of the drug

Table 1.7: Encapsulation vs polymer therapeutics

Encapsulation	Polymer therapeutics
	
<ul style="list-style-type: none"> • The bioactive ingredient is physically entrapped into biodegradable and biocompatible polymers. Hydrophilic and hydrophobic polymers are normally used in the process. • Any bioactive ingredient could be encapsulated. • Encapsulation using polymeric materials can be designed for both oral and intravenous (I.V) administration. • No chemical bonds. • Solubility is mainly increased by encapsulating bioactive ingredients into micelles. • i.e Nanoparticles are not water soluble but can be dispersed in aqueous medium thus increasing dissolution rate of the encapsulated material. 	<ul style="list-style-type: none"> • The bioactive ingredient is covalently linked to a biocompatible water soluble polymer such as polysaccharides or synthetic polymers i.e only polymers with attachment point such as hydroxyls (-OH), amino (-NH₂), carboxylic (-COOH), and thiols (-SH). • Bioactive ingredient with conjugable functional groups like hydroxyls (-OH), amino (-NH₂), carboxylic (-COOH), and thiols (-SH) offer facile conjugating points to polymers. • Polymer drug conjugates are normally administered intravenous (I.V) • Chemical bond normally used includes amide and esters • Solubility is mainly increased by converting active drugs to pro-drugs by conjugating them to water-soluble polymeric carriers

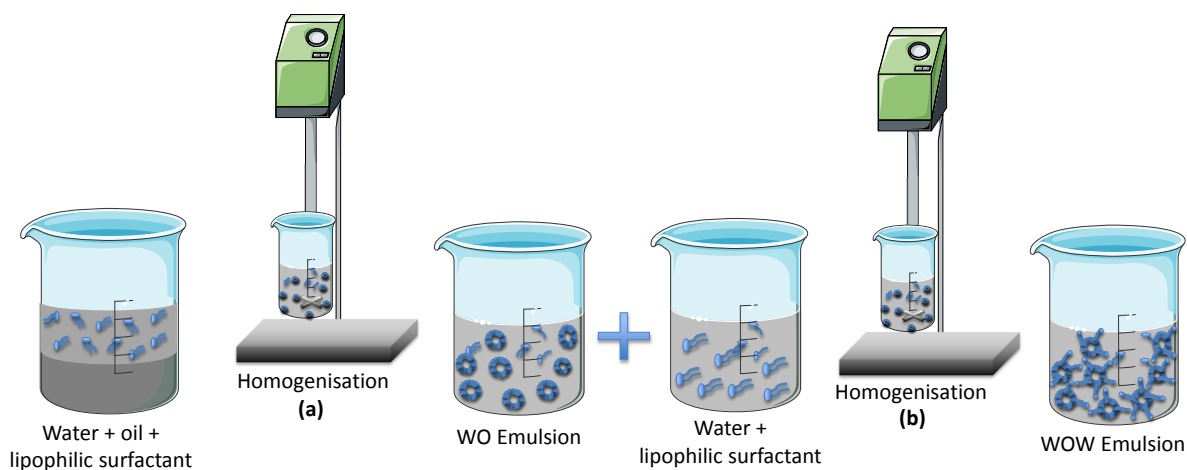
Encapsulation using polymeric materials can be achieved by dispersion of the preformed polymers into suitable solvents (Rao and Geckeler, 2011)(Pinto Reis et al., 2006)(Soppimath et al., 2001). The previously studied method includes polymerization of monomers. However the key downsides of the polymerization techniques are the existence of residual by-products that impart toxicity to the final product. Also drug release or physicochemical properties can be hampered due to cross interactions of the active ingredient with the activated monomers and H^+ ions that results during polymerization that requires washing of the final product (Pinto Reis et al., 2006). As a result dispersion of the preformed polymer into a suitable solvent is preferred over polymerization methods, and these include: solvent evaporation, nanoprecipitation, salting-out, dialysis and supercritical fluid technology (Rao and Geckeler, 2011).

Details of the methods are covered in the review papers by Rao & Geckeler 2011 and Soppimath et al. 2001. Each synthetic method has its own advantages and disadvantages. For the present review the solvent evaporation method is discussed below as a method of choice, since it was used in this project. It allows various polymers and solvents to be used, and both hydrophilic and hydrophobic drugs can be encapsulated using the method.

1.6.1.1 Solvent evaporation method

Solvent evaporation has been extensively used in the preparation of nanoparticles using various polymers (Jain, 2000). Two main strategies can be used for the preparation of emulsions, namely single emulsion i.e. oil-in-water (o/w) and double emulsion i.e. water-in-oil-in-water (w/o/w) (Rao and Geckeler, 2011)(Pinto Reis et al., 2006)(Soppimath et al., 2001). In these two strategies, the polymer is dissolved in a suitable organic solvent, such as dichloromethane (DCM), chloroform or ethyl acetate etc. The resultant solution is then emulsified in an aqueous continuous phase containing stabilizers followed by homogenization (at high speed or pressure) or ultrasonication to form o/w emulsion. The detailed procedure for w/o/w method is presented in **Scheme 1.1**, in which the resulting solution from the first step (o/w) is transferred into another aqueous phase containing

surfactants, followed by homogenization to obtain w/o/w emulsion. The resulting emulsion is normally fed in to the spray-dryer to obtain a dry pellet or powder.



Scheme 1.1: Schematic representation of double emulsion method (w/o/w).

1.6.1.2 Spray drying method

Spray drying is the conversion of liquid mixture such as an emulsion, suspension or dispersion to a dry powder (Patel et al., 2015)(Guterres et al., 2009)(Büchi Labortechnik AG, 2002). This is achieved by atomizing (spraying) the fluid and passing it through a hot drying gas causing the solvent to evaporate quickly, giving a powder with particles of a relatively uniform size (Sollohub & Cal 2010)(Büchi Labortechnik AG, 2002). It is a well-established method with a wide range of applications in a number of industries e.g. food, cosmetic and pharmaceutical industries. A typical spray drying process consists of three steps involving; 1) atomization of the liquid (emulsion, suspension or dispersion), 2) drying of the liquid and 3) particle collection (Büchi Labortechnik AG, 2002). Initially, the liquid feed is directed through an atomizer device that put the feed in contact with the hot drying gas, and produces fine droplets into the drying chamber (Manu et al., 2012)(Sollohub & Cal 2010). Atomizers may vary depending on the applications, and this includes rotary atomizers, hydraulic nozzles, pneumatic nozzles and ultrasonic nozzles. The hot drying gas is normally the

atmospheric air, but other gases like nitrogen or inert gases can be used, however these gases are normally avoided as they are expensive and require installation (Sollohub & Cal 2010). In general the contact time of the hot drying gas and spray droplet is only a few seconds, as a result the dried particle never reaches the temperature of the drying air (Manu et al., 2012). This property allows spray drying to be suitable process for thermally sensitive substances (Manu et al., 2012)(Sollohub & Cal 2010). The final product is discharged from the hot drying chamber and recovered from the cyclone or filter bag **Figure 1.6** presents the main components of a spray dryer.

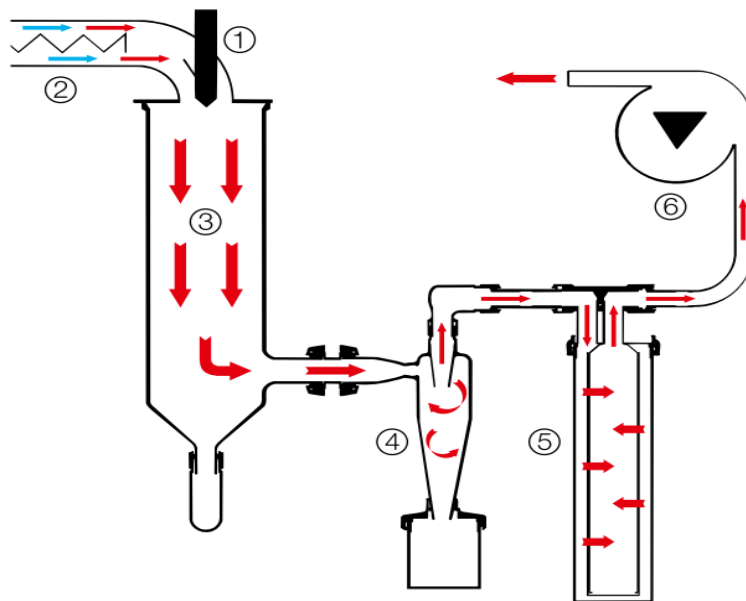


Figure 1.6: Schematic representations of main components for the mini spray dryer B-290 (Büchi Labortechnik AG, 2002). 1. Two-fluid nozzle, with compressed air to disperse the emulsion or liquid into fine droplets, 2. Electric heating, 3. Spray chamber for drying the fine droplets to powder, 4. Cyclone for collection, 5. Outlet filter to eliminate fine particles, 6. Aspirator for producing the flow

1.6.2 Polymer therapeutics

Polymer therapeutics is a multidisciplinary field that covers a wide spectrum of nanoscale technologies like polymer-protein conjugates, polymer-drug conjugates, polymeric micelles and supramolecular drug delivery systems (DDS) (Li and Mahato, 2017)(Sanchis et al., 2010) (Duncan, 2003). The shared uniqueness of the group is that the bioactive ingredient is not encapsulated, but covalently linked to a biocompatible water soluble polymer such as polysaccharides or synthetic polymers (Duncan et al., 2006)(Duncan, 2003). There is substantial hope that these nanomedicinal platforms, invented with the understanding of the physiopathology of diseased tissue using innovative polymer chemistry and precision engineering at a molecular level, will unleash the full therapeutic potential of medicine (Duncan, 2003). Decades ago polymer therapeutics was classified by many as a peculiarity explored by a minority who desired to work at the interface of the biological sciences and polymer chemistry (Duncan, 2003). The first commercialized products were based on polymer-protein conjugates using poly(ethylene glycol) [PEG] in the early 1990s (Markovsky et al., 2012)(Pasut and Veronese, 2009) (Fuertges and Abuchowski, 1990). Today more than five systems are on the market [**Table 1.8**], and many are in clinical trials for cancer treatment using polymer-drug conjugation. These polymer-drug conjugations have mainly been employed successfully in cancer treatment; giving us a greater interpretation of the possibilities linked with their clinical improvement. This sets the stage to develop other polymer-drug conjugations based on infectious diseases. The focus of this review will be to review polymers normally used for polymer-drug conjugation (as the main focus of this thesis), highlighting advantages and disadvantages of each. Other possible polymers that might be used for infectious diseases are also discussed.

Table 1.8: Examples of polymer therapeutics products on the market or in clinical development (Hare et al., 2017)(Duncan, 2003).

Product	Description/drug	Application	Phase
Zinostatin Simalmer®	SMANCS ^a	Hepatocellular carcinoma (local administration via hepatic artery infusion)	Approved
CRLX101 (cyclodextrin adamantane) /Cerulean	Camptothecin	Renal cancer, Small cell lung cancer, Ovarian cancer	Phase II
Adagen	PEG-adenosine deaminase	Severe combined immunodeficiency syndrome	Approved
Oncaspar™ (PEG)/Baxalta	Asparaginase	Acute lymphoblastic leukaemia	Approved
Oncaspar®	PEG-asparaginase	Acute lymphocytic leukaemia	Approved
Opaxio™ (Polyglycerol adipate)/CTI Biopharma		Ovarian cancer	Phase III maintenance

PEGIntron®	PEG-Interferon alpha 2b	Hepatitis C	Approved
NKTR102 (PEG)/Nektar		Metastatic breast cancer	Phase III
PEGASYS®	PEG-Interferon alpha 2a	Hepatitis C	Approved
CRLX101 (nanoparticle)/Cerulean		Renal cell carcinoma (3rd/4th line)	Phase II
Neulasta™	PEG-Human-GCSF	Chemotherapy-induced neutopenia	Approved
AP 5346 (Hydroxypropylmethacrylate)/ProLindac™		Ovarian cancer	Phase II
Cimzia®	PEG-anti-TNF Fab	Crohn's disease; arthritis	Approved
CriPec™ docetaxel (nanoparticle)/Cristal Therapeutics		Solid tumours	Phase I

Somavert[®]	PEG-HGH antagonist	Acromegaly	Approved
-----------------------------	-----------------------	------------	----------

^a Styrene maleic anhydride (SMA)-neocarzinostatin (NCS)

1.6.2.1 Polymer-drug conjugation

The perfect concept for polymer-drug conjugation was first proposed by Helmut Ringsdorf in 1975 [Figure 1.7] (Ringsdorf, 1975). The ideal model consists primarily of an active drug, conjugated to a macromolecule through a bioresponsive linker. Good strategies are however required to design such effective polymer-drug conjugates. The polymer, whose function is to transport the conjugate to the preferred sanctuaries, must protect the drug against degradation and reduce clearance by the kidneys (Yurkovetskiy and Fram, 2009)(Duncan, 2003). The bioresponsive linker must ensure stability during conjugate transport and be able to release the drug at the required rate on arrival at the target site (Larson and Ghandehari, 2012). The goal of the linker goes further than simply tying up the drug and the polymer and ensuring stability; it can also be active by causing drug release under specific conditions (Sanchis et al., 2010). The Ringdorf model also includes addition of a targeting moiety or ligand at the polymer backbone to boost the therapeutic index. For example, aptamers, antibodies and sugar ligands are normally used to target disease-related antigens or receptors (Mercier et al., 2017)(Duncan and Vicent, 2013)(Duncan and Gaspar, 2011). These approaches have significantly improved the clinical management of deadly diseases like cancer. Conventional drugs show improved pharmacological indices when covalently bound to a biocompatible polymer. It improves solubility, absorption, clinical performance, and reduces the amount of drug needed to achieve a desired therapeutic effect. The resultant effect is improved solubility with enhanced bioavailability and reduced toxicity. This is of importance considering that nearly 40 to 70% of drugs in development show poor bioavailability due to low aqueous solubility (Kalepu and Nekkanti, 2015). The field of polymer-drug conjugation opens new prospects for active drugs which have been unsuccessful in early clinical evaluations due to their high toxicity and inappropriate hydrophobic properties.

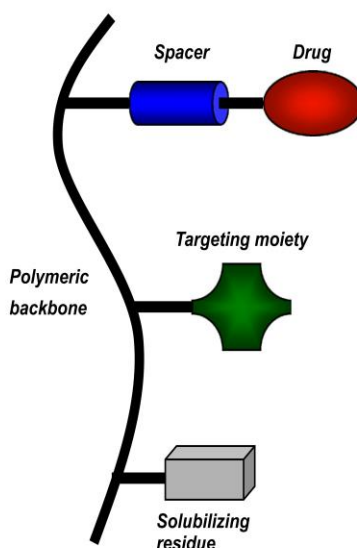
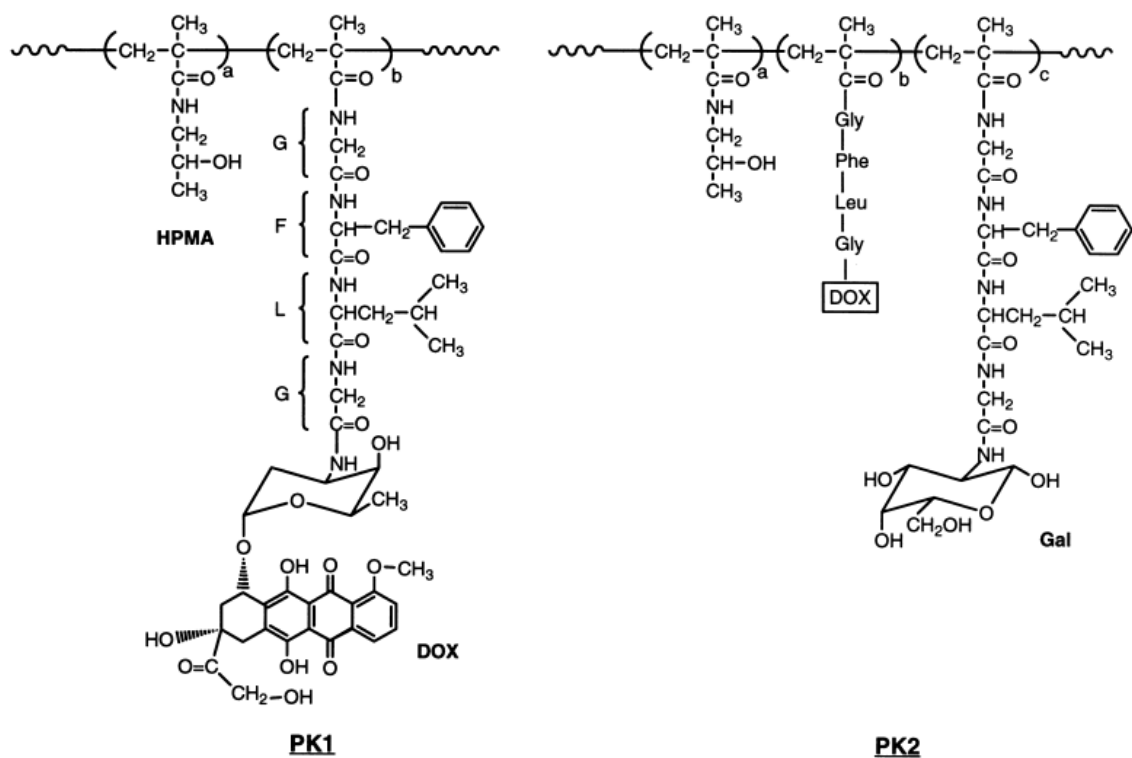


Figure 1.7: Ringsdorf's model for polymer- drug conjugate systems (Pasut and Veronese, 2007).

Following the Ringdorf model; originally, it was thought that targeting ligands would be a requirement for tumour selectivity in cancer research. However, studies based on polymer-anticancer-drug conjugates targeting tumour cells has been limited due to the awareness that sustained plasma circulation of the conjugates itself led to a significant passive tumour targeting by the 'enhanced permeability and retention' (EPR) effect (Duncan, 2003). The EPR effect is the phenomena by which particular molecular sizes tend to accumulate more in tumor tissues than they do in normal tissues (Kobayashi et al., 2014). This landmark discovery was first proposed by Maeda in the 1980s (Maeda et al., 2013)(Maeda, 2001). Early studies using poly(styrene-co-maleic acid)-neocarzinostatin conjugates (SMANCS), showed that the conjugate could more favorably distribute to the tumour sites and remain there for sustained periods of time than free neocarzinostatin solution (Maeda, 2001). This favorable accumulation of conjugate to tumour sites was attributed to the presence of leaks in the tumour blood vessels due to the poor lymphatic drainage in the tissue (Hare et al., 2017)(Maeda, 2001). In another study; Duncan *et al.*, 1992 synthesized two polymer-anticancer-drug conjugates; namely N-(2-Hydroxypropyl) methacrylamide copolymer-doxorubicin conjugate (HPMA-DOX, PK1) and the other HPMA-DOX containing

galactosamine (HPMA-DOX-Gal, PK2) [**Scheme 1.2**]. In all the conjugates DOX was attached to the polymer backbone via biodegradable Gly-Phe-Leu-Gly peptidyl linker. HPMA copolymer had molecular weight (Mw) of approximately 20 000 Da and DOX content of 7 wt%. PK2 had Gal content of approximately 4 mol%. Gal was attached to promote liver targeting (Duncan et al., 2001). PK2 is the only polymer-anticancer conjugate containing a targeting moiety to be evaluated clinically (Chytil et al., 2018)(Duncan, 2003). When both the conjugates were administered intravenously (I.V.) *in vitro* by rat liver and rat lysosomal enzymes, degradation was observed. In another study, the two conjugates were administered either by I.V. (single dose, 13–100 mg DOX/kg) or intraperitoneally (i.p.) at doses 2.5–50 mg DOX/kg (triplicate doses) to mice infected with L1210 leukaemia; all conjugates presented good antitumour activity. Activity of the conjugates was tested against a range of solid tumour models and showed better increase in survival time than the free drug. Even though PK2 did minimize tumour burden related to liver metastases it did not perform better than PK1 or free DOX. However conjugation greatly decreases all characteristics of DOX-related toxicity



Scheme 1.2: *N*-(2-hydroxypropyl) methacrylamide (HPMA) copolymer-doxorubicin conjugates. PK1= HPMA-DOX, PK2= (HPMA-DOX-Gal). Gal- galactosamine (to promote liver targeting). DOX (doxorubicin). Glycyl Phenylalanyl Leucyl Glycine (GFLG).

1.6.2.2 Selection of linkers

Polymer-drug conjugates are designed to enhance or improve therapeutic properties of drugs. The release of the drug from the polymeric carrier is an important function which allows the efficacy and safety of their use. When the conjugates reach the ideal site, the covalently attached drug is released through a mechanism so that the active ingredient can have their pharmacological properties (Duncan, 2003). A commonly used method relies on an intracellular drug release. Endocytosis is anticipated to internalized the conjugates into the cell followed by the endosomal and lysosomal pathways as shown in **Figure 1.8** (Duncan, 2003). The presence of enzymes and protons in these compartments generates an acidic intravesicular environment – typical pH 6.5–4.0– to allow the design of linkers to be decomposed intracellularly. HPMA-DOX conjugate (PK1) described above contains

tetrapeptide linker namely Glycyl Phenylalanyl Leucyl Glycine. The linker is degraded by lysosomal thiol-dependent protease cathepsin B upon endocytic uptake of the conjugate from the tumour interstitium. This linker was observed to be stable in the circulation. Other types of linkers can be design to suite specific application, for example hydazone, acetal, disulfide bridges, acid and enzymatically cleavable linkers have also been used. For general oview on this linkers the reader is advised to see Leriche et al., 2012.

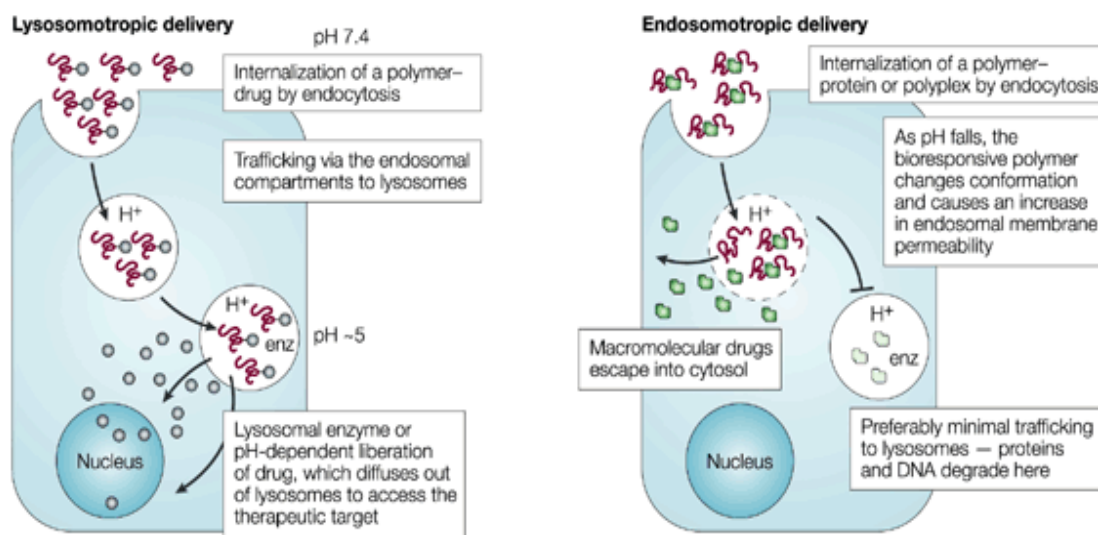


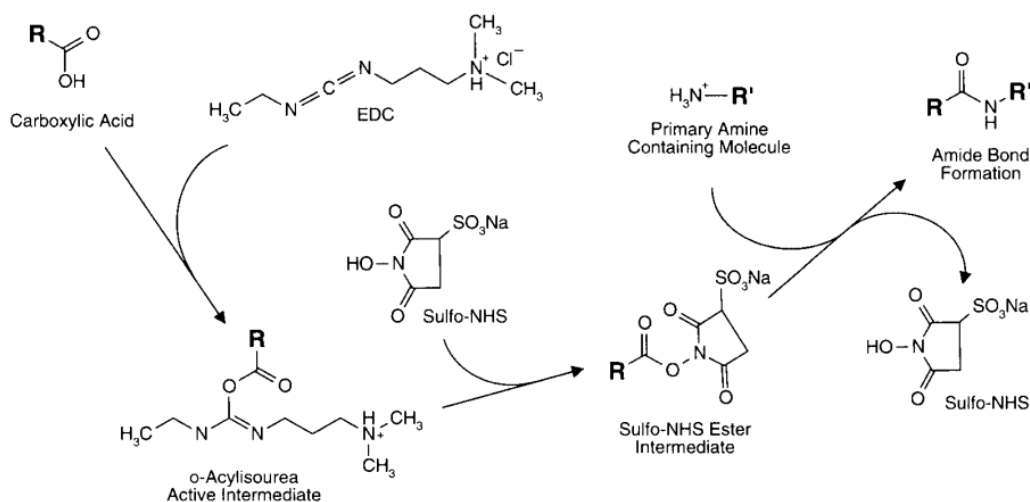
Figure 1.8: Schematic representation of a polymer-drug conjugates designed for lysosomal and endosomal delivery (Duncan, 2003).

1.6.2.3 Carbodiimide crosslinking chemistry

Carbodiimides are classified as unsaturated compounds containing an allene structure [RN=C=NR'] (Nakajima and Ikada, 1995)(Williams and Ibrahim, 1981). The molecule has two centres of reactivity; the central carbon atom is electrophilic and the terminal nitrogens electron rich. In polymer therapeutics, they are used to facilitate the conjugation between the polymer and the active ingredient by forming a bond containing no additional chemical structures (Hermanson, 2008)(Khandare and Minko, 2006). Carbodiimide can initiate the formation of three types of bonds: an amide linkage prepared by the condensation of a primary amine with a carboxylic acid, a phosphoramidate linkage prepared between an

organic phosphate group reacting with a primary amine, and a secondary or tertiary amine linkage prepared by the reductive amination of a primary or secondary amine with an aldehyde group (Hermanson, 2008). All of the chemical reactions are fairly efficient depending on the active functional groups on the carbodiimide reagents and the reactive groups present on the molecule to be derivatised. Also the reaction media plays a vital role.

The carbodiimide reagents are either water-soluble or water-insoluble (Hermanson, 2008). The water-soluble ones comprise 1-ethyl-3-(3-dimethylaminopropyl)carbodiimide hydrochloride (EDAC) and 1-cyclohexyl-3-(2-morpholinoethyl)carbodiimide (CMC) and water insoluble ones comprise of dicyclohexyl carbodiimide (DCC) and diisopropyl carbodiimide (DIC) (Hermanson, 2008). EDAC is the most common choice for biochemical conjugations. Both the reagent and the by-product formed (isourea) are water-soluble and may be removed easily by dialysis or gel filtration (Everaerts et al., 2008)(Hermanson, 2008). Frequently EDAC is used in combination with *N*-Hydroxysulfosuccinimide sodium salt or *N*-hydroxysuccinimide (sulfo-NHS/NHS) to increase the solubility and stability of the active intermediate, which eventually reacts with the attacking nucleophiles [**Scheme 1.3**]. Nucleophiles such as amine, sulfhydryl and hydroxyl groups may attack the active species and form the amide, thiol ester and ester linkages; respectively (Hermanson, 2008). However, thiol esters and esters are unstable in aqueous environment compared with the amide linkages because of the competition with the water molecules. To ameliorate the problem, reactions are usually carried out under dry conditions in organic solvents (Hermanson, 2008).



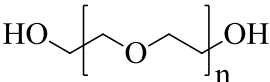
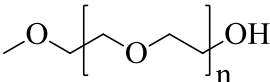
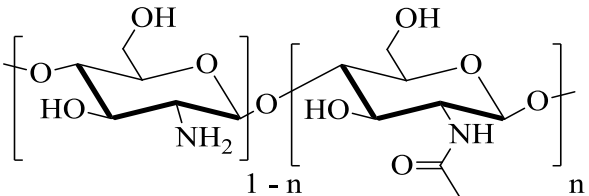
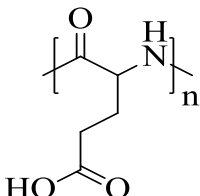
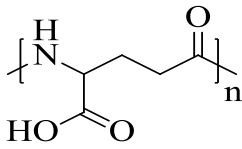
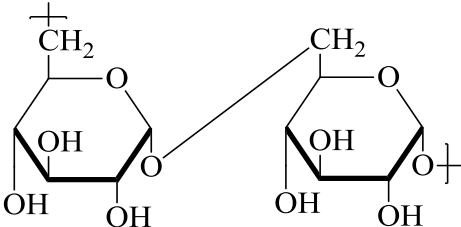
Scheme 1.3: 1-ethyl-3-(3-dimethylaminopropyl) carbodiimide hydrochloride (EDAC) and *N*-Hydroxysulfosuccinimide sodium salt (sulfo-NHS) reacts with carboxylic acids to produce an active- sulfo-NHS ester intermediate. The activated acid can be coupled with a primary amine containing molecule forming an amide bond. An isourea is released as a by-product. (Hermanson, 2008)

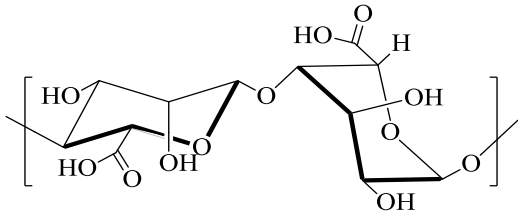
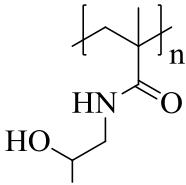
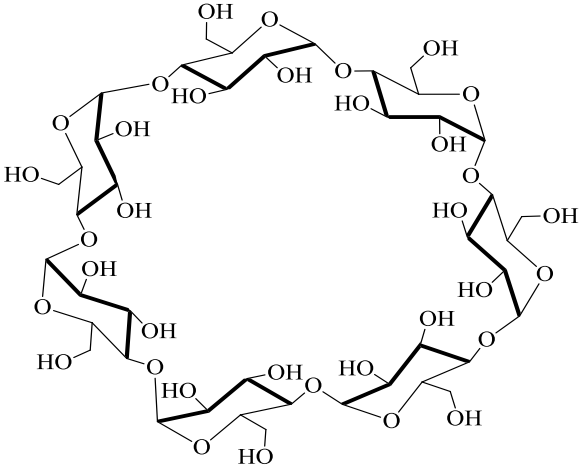
1.6.2.4 Selection of polymers

A wide variety of natural and synthetic polymers are available in the market for use in polymer-drug conjugation applications [Table 1.9]. The essential criterion for polymer-drug conjugation is that the polymer must be non-toxic and non-immunogenic (Duncan, 2003). The Mw must be large enough to evade rapid elimination via kidney ultrafiltration and adequately low to avoid unwanted accumulation in the body (Duncan et al., 2001). Polymeric structures have a significant effect on the physio-chemical preoperties, pharmacodynamics and pharmacokinetics of the conjugated drug (Markovsky et al., 2012). For example, properties of a polymer such as Mw, polydispersity index (PDI), apparent electric charge i.e. zeta potential and its density, hydrophilicity and biological stability, define the drug solubility and bioavailability (Markovsky et al., 2012).

The polymer, the drug and the linker should contain functional group(s) which can promote covalent linkage (Ulbrich et al., 2016)(Khandare and Minko, 2006). Functional groups such as carboxylic acids (-COOH), organic phosphate groups (-PO₄), amines (-NH₂), sulfhydryl (-SH) and hydroxyl groups (-OH) are mostly used. For successful chemical conjugation, appropriate methods, processes, and reagents are vital since some polymers/drugs may experience various structural changes with solvents and coupling agents (Khandare and Minko, 2006). As a result carbodiimide chemistry is often preferred.

Table 1.9: Schematic illustration of some polymers and oligomers used in the production of polymer-drug conjugation.

 <p>Poly(ethylene glycol) [PEG]</p>	 <p>Methoxy poly(ethylene glycol) [m-PEG]</p>
 <p>Chitosan (CS)</p>	 <p>Alpha Poly glutamic acid (α-PGA)</p>
 <p>Gamma Poly glutamic acid (γ-PGA)</p>	 <p>Dextran</p>

 <p>Alginate</p>	 <p><i>N</i>-[2-hydroxypropyl]methacrylamide (HPMA)</p>
 <p>Beta-Cyclodextrin (β-CD)</p>	

1.6.3 Poly (ethylene glycol)

PEG is one of the first biopolymers to be established in a clinical platform as shown in [Table 1.8]. The polymer is comprised of repeating units of ethylene oxide (Li et al. 2013)(Roberts et al., 2002), and readily available in a number of molecular weights. Each ethylene oxide has a Mw of 44 Da (Bailon et al., 1998)(Li et al. 2013). In its most common form, PEG is a linear polyether terminated with hydroxyl groups suitable for bioconjugation applications [Table 1.9] (Roberts et al., 2002). It is a biocompatible, non-ionic polymer and presents an outstanding pharmacokinetics and biodistribution profile. The *in vivo* studies showed great durability in the blood stream and little cumulation by the mononuclear phagocyte system organs (Kopeček, 2013). These fascinating properties make PEG a polymer of choice for

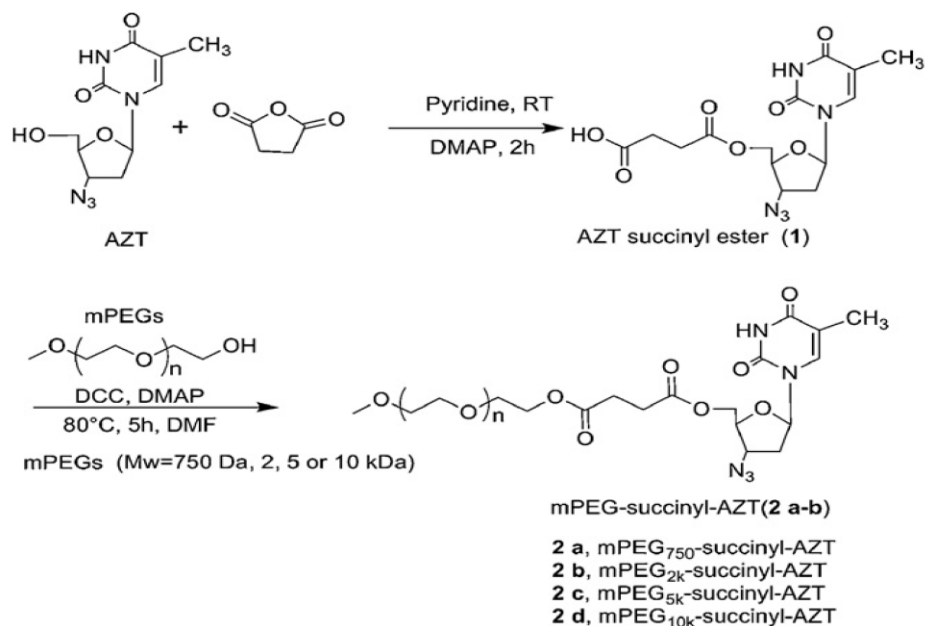
pharmaceutical applications. For example; the polymer is also used across the field of nanomedicine to increase blood circulation of polymeric nanoparticles.

Protein PEGylation has been successful in clinical applications, mainly using monomethoxy poly(ethylene glycol) (mPEG–OH). However having only one or two terminal functional groups, the polymer presents a crucial limit for conjugation with low molecular weight drugs and other biological components (Banerjee et al., 2012)(Larson and Ghandehari, 2012). The inherently low drug loading had for many years prohibited the advance of PEG-drug conjugates (Larson and Ghandehari, 2012). In a strategy to overcome these restrictions, branched PEGs terminated with hydroxyl or amino groups have been investigated. However, these modified forms of PEGs are more expensive and the polymer is non-biodegradable.

1.6.3.1 PEG–HIV drug conjugates

NRTIs are the first class of ARVs that were approved for the treatment of HIV infection (Arts and Hazuda, 2012)(De Clercq, 2009)(Balint, 2001). Most NRTIs require phosphorylation by intracellular activation to become NRTIs-triphosphates (Kallianpur & Hulgan 2009)(Anderson et al., 2004). Once activated, these active agents compete with the RT enzyme; an enzyme that HIV virus needs to transcribe the single stranded RNA into double strand DNA. Li and co-workers developed a strategy to conjugate 3'-azido-3'-deoxythymidine (AZT, zidovudine) onto mPEG [**Scheme 1.4**] (Li et al., 2012). In the synthetic process, AZT was firstly succinylated to introduce a carboxylic functional group by reacting with succinic anhydride in pyridine base. Different Mw forms of mPEG i.e. 750 Da, 2 kDa, 5 kDa and 10 kDa were conjugated respectively with succinylated AZT using DCC and 4-Dimethylaminopyridine (DMAP) as coupling reagents. The ¹H NMR spectra confirmed the formation of the new ester linkage between COOH group of succinylated AZT and OH group of mPEGs [**Figure 1.9**]. The *in vitro* release studies showed that the Mw of mPEG was a clear factor influencing the release of the drug. All the mPEG-AZT conjugates displayed improved stability over the free AZT, as the free AZT was completely released within the first two hours in all controls but the conjugates were not. The mPEG-AZT conjugates with lower Mw were hydrolysed more quickly than those with high Mw. The anti-

HIV activity and cytotoxicity in MT-4 cells followed the same array; mPEG (750Da)-AZT demonstrated good inhibition to wild-type viruses (strains IIIB and ROD) with half maximal effective concentration (EC_{50}) values of 0.11 and 0.090 mol/L, respectively, and showed no cytotoxicity up to 110 mol/L. The group further investigated the oral pharmacokinetics of the mPEG-AZT conjugates in rats. Findings showed that the conjugates separately displayed ~ 2.3-fold (750 Da), 2.1-fold (2 kDa), 2.1-fold (5 kDa) and 1.6-fold (10 kDa) longer half-life than free AZT.



Scheme 1.4: Synthetic route of mPEG-AZT conjugates using DCC and DMAP as coupling reagents. (Li et al., 2012)

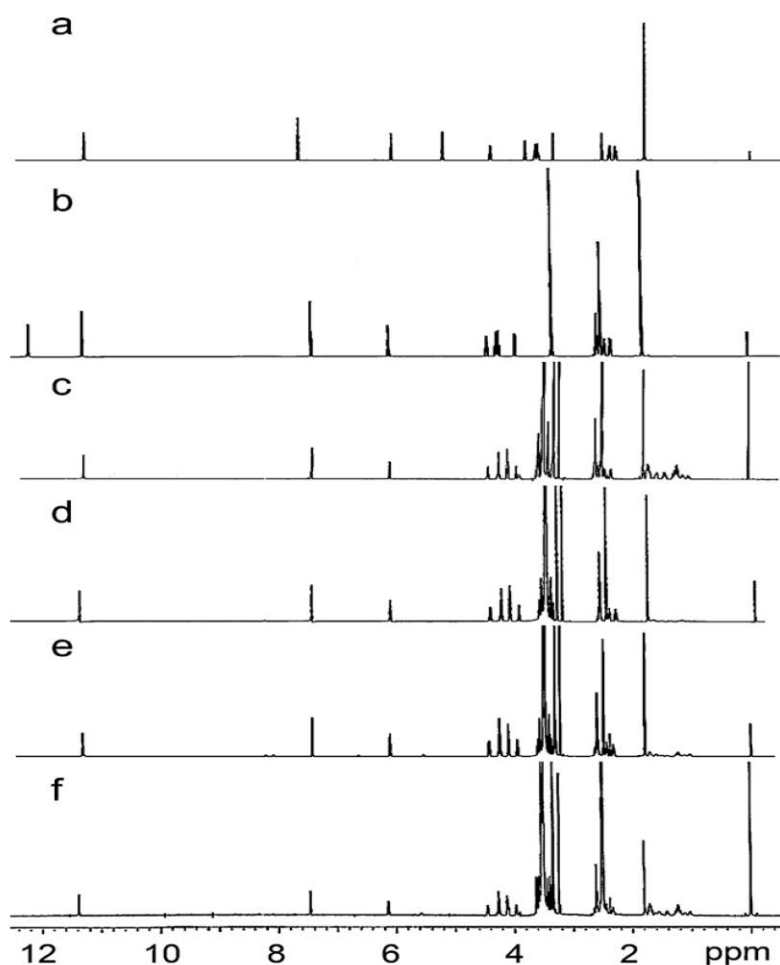
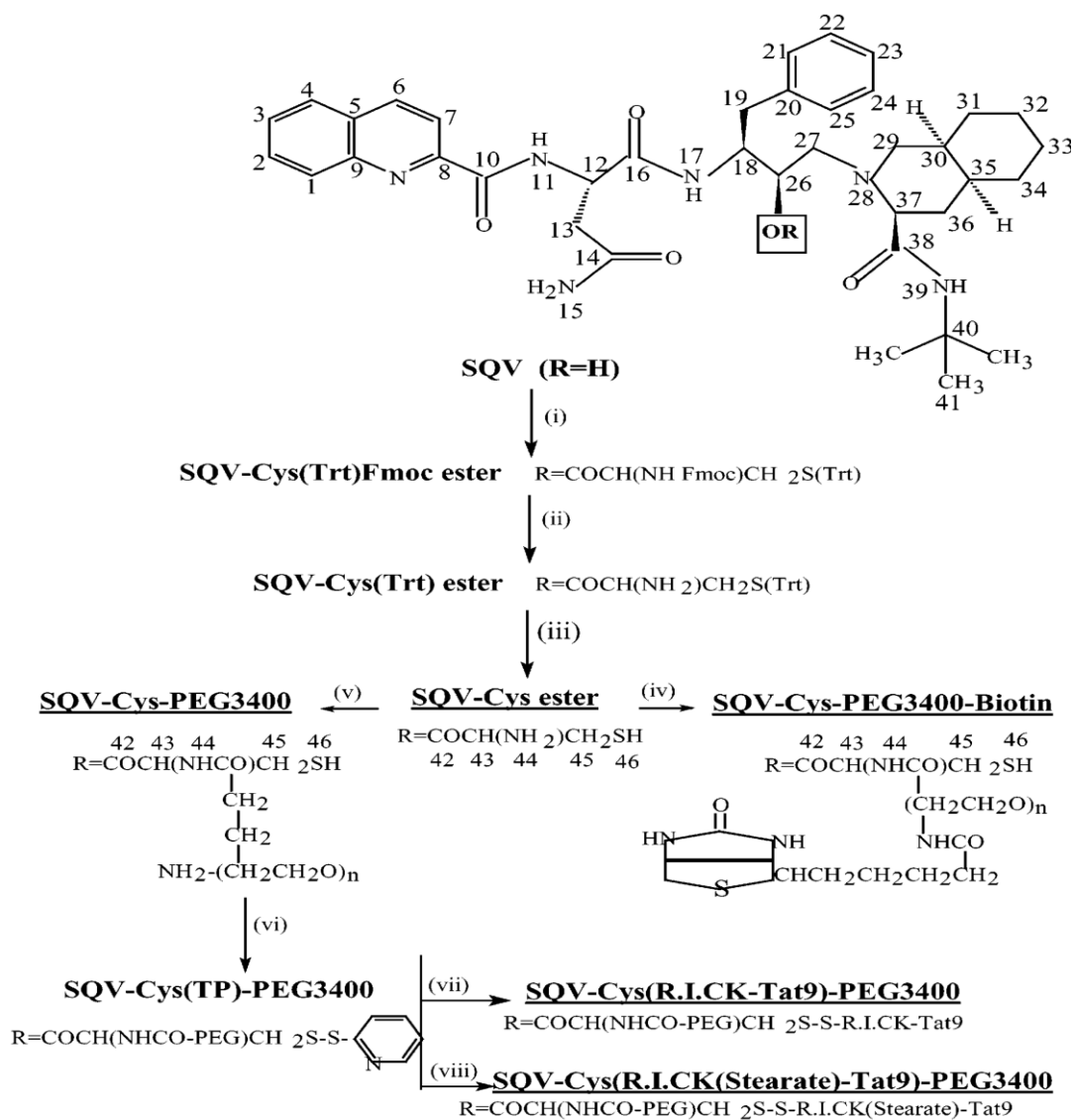


Figure 1.9: ^1H NMR Spectra of AZT (a), AZT Succinyl ester(b), mPEG (750) -AZT (c), mPEG (2kDa) -AZT (d), mPEG (5kDa) -AZT (e), and mPEG (10 kDa) -AZT(f). (Li et al., 2012)

Therapeutic use of anti-HIV protease inhibitors has been limited due to poor aqueous solubility and low or variable oral bioavailability of the approved drugs (Lv et al., 2015). This is the case of Saquinavir (SQV), the first HIV-protease inhibitor to be approved by the FDA (Lv et al., 2015)(Washington et al., 2000). The oral bioavailability of SQV in clinical formulation is only 4% or variable due to its metabolism by cytochrome P450, 3A4 and to the membrane transporters namely the P-glycoprotein (P-gp) (Vyas et al., 2008)(Buss et al., 2001). In a strategy to increase aqueous solubility and intracellular delivery of SQV, Gunaseelan and co-workers (2004) prepared a series of PEG-based prodrug conjugates of the

SQV [**Scheme 1.5**]. The formulations included SQV–cysteine–PEG(3400), SQV–cysteine–PEG(3400)–biotin, SQV–cysteine (R.I.CK-Tat9) [a cationic retro-inverso-cysteine-lysine-Tat nonapeptide]–PEG(3400), and SQV–cysteine(R.I.CK(stearate)-Tat9)–PEG(3400). In all formulations, SQV hydroxyl group was covalently linked to cysteine carboxylic acid group using *N,N'*-Diisopropylcarbodiimide (DIPC) and DMAP as coupling reagent to form a releasable ester bond. A more stable amide bond was formed between cysteine and the polymers using amino group of the linker. The targeting moieties namely the cationic peptides, R.I.CK-Tat9 and R.I.CK(stearate)-Tat9 were successfully bound to the cysteine via disulfide bonds. The *in vitro* studies in non-infected MT-2 cells showed a reduced toxicity of the synthesized prodrug conjugates compared to free SQV. The *in vitro* findings with HIV infected MT-2 cells indicated that PEG-SQV conjugate presented a 60-fold lower activity compared to SQV. However anti-HIV activity was restored with the addition of biotin (SQV–cysteine–PEG(3400)–biotin) in the reaction recipe. Enhanced cellular uptake was even observed more when biotin was replaced by R.I.CK-Tat9 peptides. These targeting ligands have been proven to enhance membrane penetration and influence an inhibitory effect by binding or interacting with HIV receptors. The group suggested that the lower cellular uptake in the case of SQV–cysteine–PEG(3400) could be attributed to slow cleavage of the ester bonds.



Scheme 1.5: Scheme to synthesize SQV-based prodrug (i) 3 equivalence of Fmoc-Cys(S-Trt)-COOH in CH_2Cl_2 with DIPC/DMAP; (ii) 20% piperidine in CH_2Cl_2 ; (iii) TFA/ CH_2Cl_2 (1:1); (iv) 2 equivalence of biotin-PEG-NHS in CH_2Cl_2 with DIEA; (v) 2 equivalence of Fmoc-PEG-NHS in CH_2Cl_2 with DIEA; (vi) 2 equivalence of 2,2'-dithiodipyridine in DMSO; (vii) 2 equivalence of R.I.CK-Tat9 in DMSO; (viii) 2 equiv of R.I.CK(stearate)-Tat9 in DMSO. (Gunaseelan et al.,2004)

1.6.4 Chitosan

Chitosan (CS) is a linear natural cationic polysaccharide obtained from the deacetylation of chitin, the second most abundant polysaccharide after cellulose [Table 1.9] (Daniel Elieh-Ali-Komi, 2017)(Goy et al., 2009). When the degree of acetylated amine groups is reduced to 40-35%, the resultant co-polymer, *N*-acetylglucosamine and glucosamine; becomes soluble in dilute aqueous acidic solutions and is then referred to as CS (Rodrigues et al., 2012)(Goy et al., 2009)(Rinaudo, 2006). It is soluble in aqueous acidic media below its pKa (~6.3), because the primary amino group on the C-2 position of the D-glucosamine repeat unit is protonated into the soluble protonated form NH_3^+ at a lower pH (Rodrigues et al., 2012)(Kurita, 2006). The degree of deacetylation (DD) and Mw strongly affects its solubility at neutral pH and the physicochemical and biological properties of CS (Goy et al., 2009)(Nwe et al., 2009)(Thanou et al., 2001). When compared to other FDA approved biodegradable polymers, CS is the only one displaying a cationic character with mucoadhesive properties (Rodrigues et al., 2012)(Jayakumar et al., 2010).

Chitosan is biocompatible and biodegrades into non-toxic amino sugars under normal physiological conditions (Liu et al., 2016)(Cheung et al., 2015). Typical applications include wound dressing (Jayakumar et al., 2010), films, scaffolds for tissue and bone engineering, slimming and antimicrobial properties (Goy et al., 2009). The primary hydroxyls at the C6 and C3 positions and the amine groups at the C2 position on the polymer backbone render special properties that make CS very useful for polymer-drug conjugation applications (Goy et al., 2009). Also across the field of nanomedicine, CS is widely used to facilitate paracellular transport since it is able to open the tight intersections of intestinal epithelium (Patel et al., 2014)(Sung et al., 2012).

Although CS has been established as an attractive biopolymer for drug delivery systems, applications are slightly restricted due to CS being water-insoluble at neutral pH. The disadvantages were recently muted by the use of low-Mw CS (LMwCS). LMwCS present good properties such as better water solubility at neutral pH, minor toxicity, and a narrower

molecular weight distribution compared with the traditional high-Mw CS (HMwCS) (Markovsky et al., 2012).

Chae et al. (2005) investigated the effect of CS's Mw on the permeability through the differentiated Caco-2 cell layer (*in vitro*) and intestinal absorption patterns after oral administration (*in vivo*) of water-soluble CS. Five different Mw were compared i.e. 3.8 kDa, 7.5 kDa, 13 kDa, 22 kDa, and 230 kDa. Findings showed that the absorption of CS through the Caco-2 cell layer was dependent on the Mw. The fastest permeation was observed with the LMwCS i.e. 3.8 kDa. As the Mw increased, the penetration rates decreased. Compared with the HMwCS (230 kDa), more than 23-times-enhanced transport was observed with LMwCS 3.8 kDa by 120-min treatment. The *in vivo* studies followed the same pattern. Plasma CS concentrations, calculated on the basis of fluorescence intensity, reached the maximum level at 30 min after administration and decreased continuously [**Figure 1.10**]. The maximum plasma CS concentrations (C max) of 20.23, 9.30, 5.86, and 4.32 Ag/mL were observed by oral administration of CS 3.8 kDa, 7.5 kDa, 13 kDa, and 22 kDa, respectively. In the case of HMwCS 230 kDa, plasma CS levels were maintained at baseline with negligible C max value (less than 0.5 Ag/mL) because of poor absorption. According to the AUC data, LMwCS 3.8 kDa showed an enhanced absorption 25 times higher than HMwCS 230 kDa.

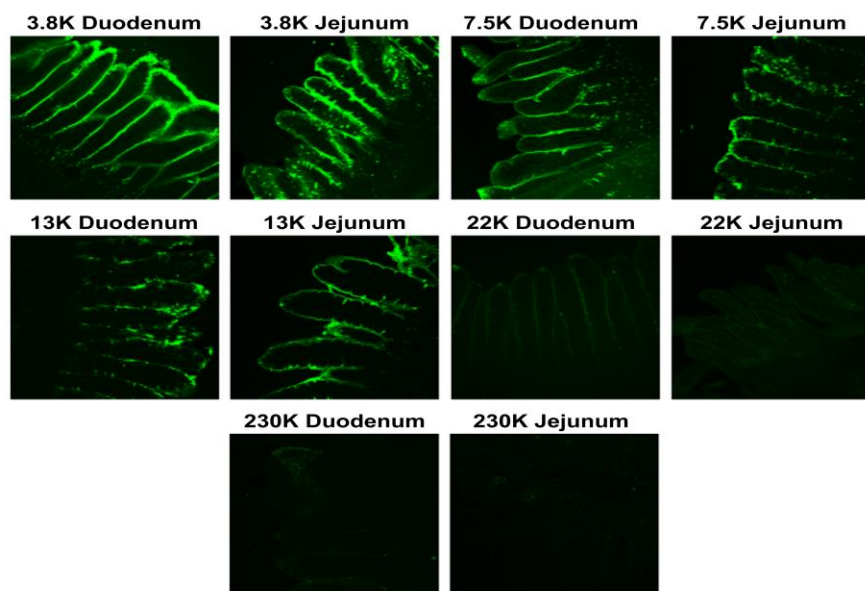
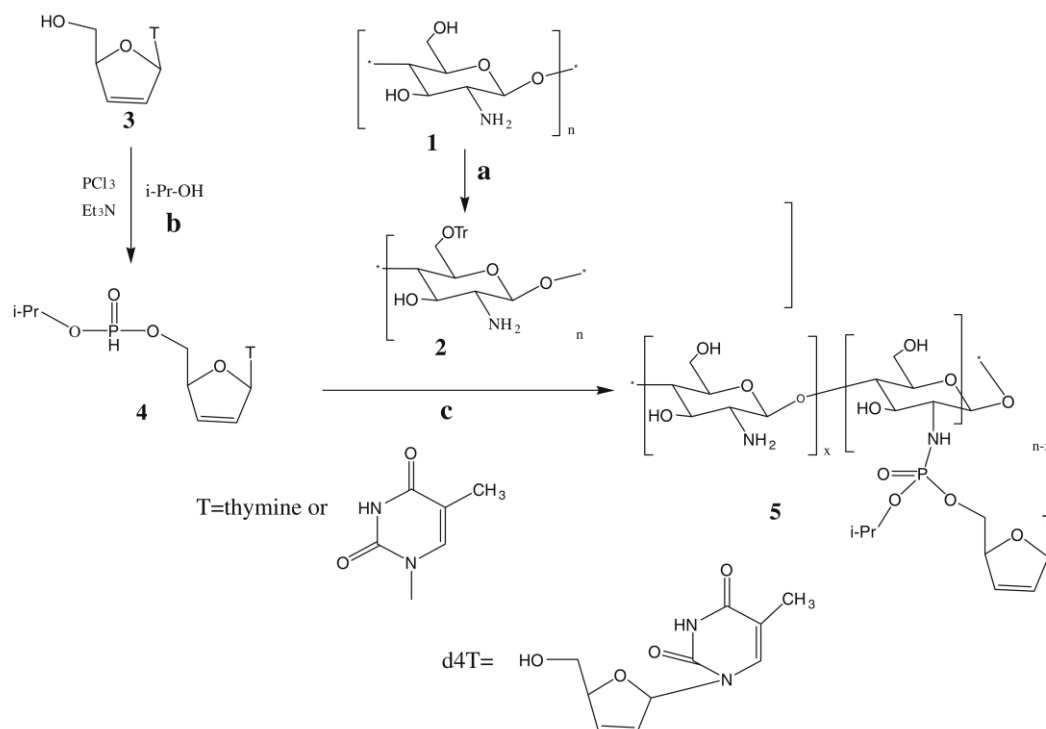


Figure 1.10: Confocal laser scanning microscopy images of rat intestines (duodenum and jejunum) after administration of fluorescein isothiocyanate (FITC)-labeled CS administration. Taken after 30 minutes. (Chae et al. 2005)

1.6.4.1 Chitosan–HIV agent conjugates

ARV drugs tend to degrade in the stomach which reduces the bioavailability of the drug. This degradation could be reduced by the formation of polymer-drug conjugates. Yang et al. 2010 investigated a novel approach to improve the antiviral efficacy of NRTIs and reduce their side effects by creating a nanosized NRTI monophosphate-polymer conjugate using stavudine (d4T) as a model drug [Scheme 1.6]. d4T was conjugated to CS using phosphoramidate linkage between glucosamine and the nucleoside's monophosphate. The prepared CS-O-isopropyl-5'-O-d4T monophosphate conjugate were further ionically crosslinked with tripolyphosphate (TPP) to form CS-O-isopropyl-5'-O-d4T monophosphate conjugate nanoparticles. The anti-viral activity and cytotoxicity of the CS-O-isopropyl-5'-O-d4T monophosphate conjugate evaluated in MT4 cell line displayed remarkable anti-viral effect and low cytotoxicity. The *in vitro* drug release studies at pH 1.1 and pH 7.4 suggested that both the CS-O-isopropyl-5'-O-d4T monophosphate conjugate and its nanoparticles preferred to release d4T 5'-O-isopropyl monophosphate than free d4T for prolonged periods,

which resulted in an enhancement of anti-HIV selectivity for the polymeric conjugate relative to the free d4T due to a bypassing of the metabolic bottleneck of mono-phosphorylation. Furthermore, the authors suggested that the cross-linked conjugate could prevent the conjugated drug from leaking out of the nanoparticles before entering the target viral reservoirs.



Scheme 1.6: Scheme to synthesize CS-O-isopropyl-5'-O-d4T monophosphate conjugate. (Yang et al. 2010)

1.6.5 Poly glutamic acid

Poly glutamic acid (PGA) is a polyamide composed solely of glutamic acid units (Luo et al., 2016)(Bajaj and Singhal, 2011). It exists in two isoforms namely, α -PGA and γ -PGA depending on the attachment of the carboxy group (Ogunleye et al., 2015)(Bajaj and Singhal, 2011) [Table 1.9]. It is biodegradable, biocompatible, non-toxic and non-immunogenic (Khalil et al., 2017). Due to these benefits, PGA has found various industrial applications

such as in polymer-drug conjugation, tissue engineering, curable biological adhesives, cosmetics and agriculture. In polymer-drug conjugation applications, it is able to increase the water solubility of hydrophobic drugs, and since it is a multivalent polymer, it can allow the conjugation of more than one compound within the polymer backbone (Eldar-Boock et al., 2017)(Eldar-Boock et al., 2011)(Singer, 2005). It undergoes hydrolysis upon implantation into the body, forming glutamic acid and enters the normal citric acid cycle (Ogunleye et al., 2015). The products are eventually eliminated from the body without causing any harm. However, a big obstacle in its application for infectious diseases is the rather high cost and it is produced in small quantities (Bajaj and Singhal, 2011).

1.6.5.1 PGA-Malaria conjugates

Primaquine (PQ) is an 8-aminoquinoline, a class of drugs known for their effective treatment of malaria that can prevent relapse by targeting *Plasmodium* at the liver stages (Graves et al. 2018). Although it is the only drug approved for liver stages, it is also known for haemolytic toxicity especially in glucose-6-phosphate dehydrogenase (G6PD) deficient patients. Tomiya and co-workers (2013) conjugated synthetic trivalent glyco-ligand (TriGalNAc) to γ -PGA for the hepatocyte asialoglycoprotein receptor (ASGP-R) (Tomiya et al., 2013). The *in vivo* distribution after intravenous (i.v) administration in mice showed that PGA-TriGalNAc was transported to the liver over 20 to 80 minutes [**Figure 1.11**]. Conversely, most of γ -PGA was found to accumulate in the bladder over the same period of time. A minimum amount of the polymer was also found in the liver. The group further conjugated PQ to PGA-TriGalNAc, labelled with 6-[Fluorescein-5(6)-carboxamido]-hexanoic acid, succinimidyl ester [5(6)-SFX]. About 33% and 4% of glutamic acids were conjugated with PQ and TriGalNAc; respectively. Only 1% of SFX was coupled to the conjugate [**Scheme 1.7**]. Binding and uptake studies conducted in rat hepatocytes at 0 °C indicated that nearly 250 ng per million cells of the PGA-PQ-TriGalNAc conjugate bound to 1 million cells, and when the conjugate was incubated at 37 °C only 2 μ g per million cells were taken up over 7h. Moreover after 7 h of incubation in rat hepatocytes, gel filtration analysis indicated enzymatic digestion of the PGA-PQ-TriGalNAc conjugate, suggesting that the conjugate was degraded by lysosomes and endosomes. The authors concluded that the TriGalNAc ligand can assist as a good liver

targeting device and also this could substantially decrease haemolytic toxicity in G6PD deficient patients.

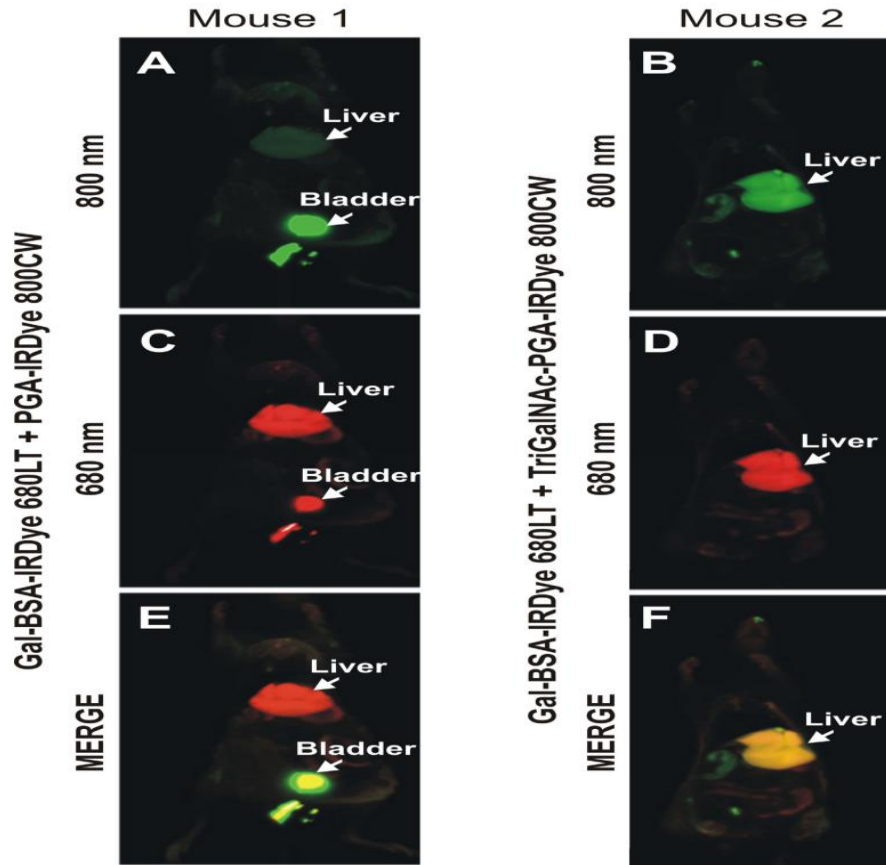
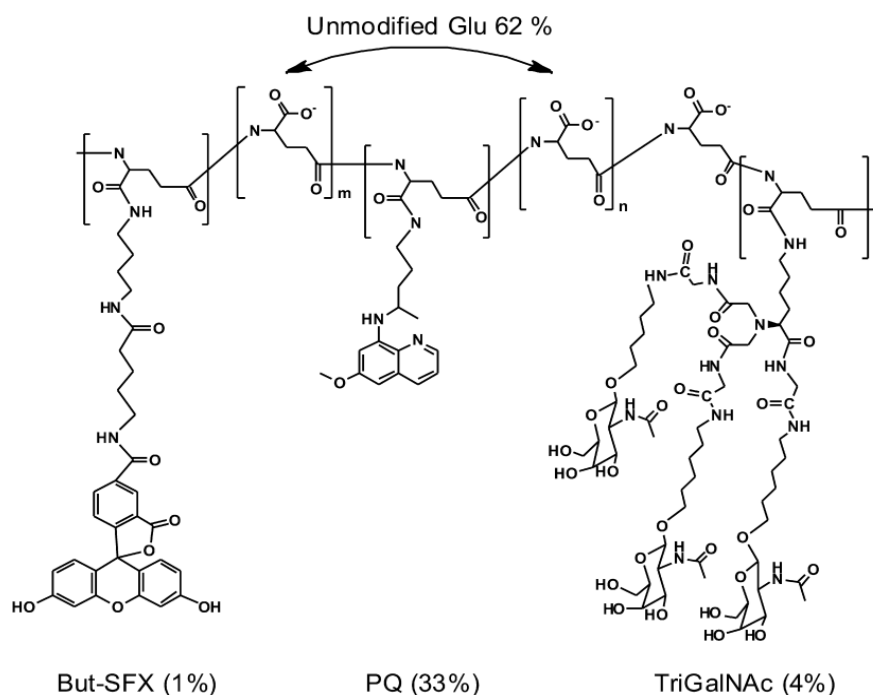


Figure 1.11: The *in vivo* imaging studies in mouse. A and C presents mouse 1 inoculated with PGA labelled green and Gal-BSA labelled red. Panel E displays a combined image of A and C. Image B, D, and F represents mouse 2 inoculated with PGA-TriGalNAc labelled green and Gal-BSA labelled red. Panel F displays a combined image of B and D. Note, image E shows excretion of PGA in the bladder and F demonstrate co-localization of Gal-BSA and PGA-TriGalNAc in the liver. (Tomiya et al., 2013)



Scheme 1.7: Structure of PGA-PQ-TriGalNAc, labeled with SFX.

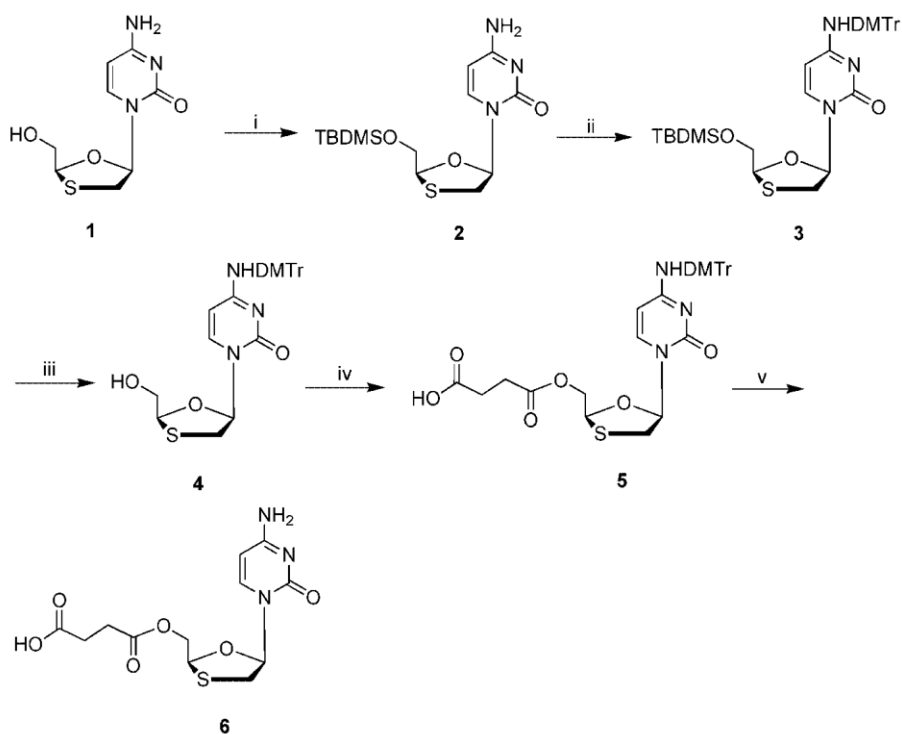
1.6.6 Dextran

Dextran is a naturally occurring polysaccharide composed solely of glucose (Mehvar, 2000)(Santos and Teixeira, 2000)(Mehvar et al., 1994) [Table 1.9]. The biopolymer consist mainly of linear 1,6-glycosidic linkages with some degree of branching via 1,3- linkages (Mehvar, 2000)(Santos and Teixeira, 2000). The degree of branching may differ from 0.5 to 60% depending on the source of the polymer. It is produced by dextransucrase, an extracellular enzyme extruded/produced by lactic acid bacteria viz., *Leuconostoc* or *Streptococcus* (Khandare and Minko, 2006). The chemical properties can be modified to match certain applications, as a result dextrans have prolific usage in food, fine chemicals, cosmetics and agricultural industries (Mehvar, 2000). For drug delivery applications, the biopolymer possesses multiple primary and secondary hydroxyl groups and therefore can be easily conjugated with drugs by direct conjugation or by incorporation of a linker (Khandare and Minko, 2006). The approved dextran for clinical usage is dextran 40 kDa and dextran 70 kDa, with MW ranging from 10 90 kDa and 20 to 200 kDa; respectively (Mehvar, 2000).

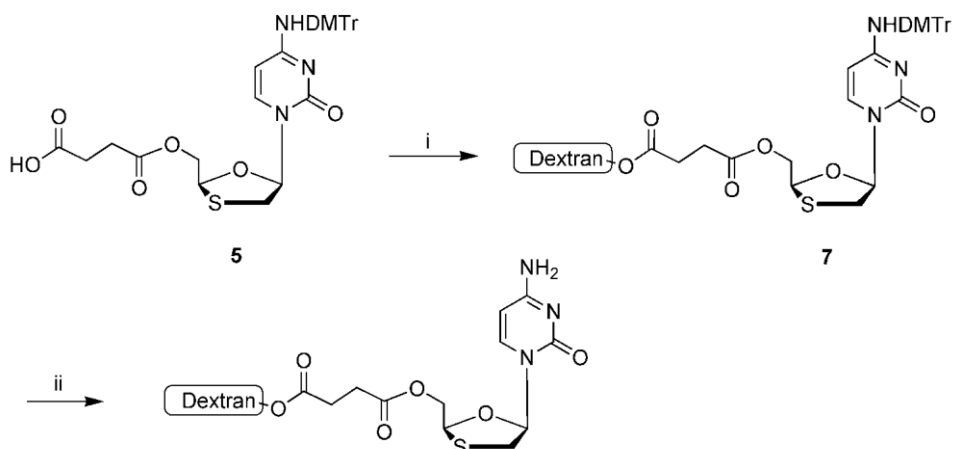
Due to its high water solubility, biocompatibility and biodegradability, it has been extensively studied as a delivery vehicle for anti-cancer drugs to the tumor tissue. However, after oral administration the polymer is not significantly absorbed. Consequently, most of the potential applications of dextrans as a delivery vehicle are through injections (Khandare and Minko, 2006). Moreover studies have shown that the distribution and elimination of dextrans are dependent on Mw.

1.6.6.1 Dextran–HIV agent conjugates

Taking advantage of the *in vivo* biodistribution of dextran, Chimalakonda et al., 2007; synthesized and characterized a conjugate of lamivudine (3TC) with 25 kDa dextran. The conjugate was intended for selective delivery to the liver. 3TC was conjugated to dextran using a succinate linker in two major steps by synthesis of 5'-O-succinate ester of the drug [**Scheme 1.8**], followed by the reaction of the ester conjugate with dextran [**Scheme 1.9**]. The synthetic approach afforded a degree of substitution of 6.5 mg of 3TC in 100 mg of 3TCSD powder. The *in vitro* studies showed that the conjugate was relatively stable in plasma and in buffers. The conjugate was able to release 3TC only in the presence of rat liver lysosomes (*in vitro* studies). *In vivo* studies in rats showed that while conjugation of 3TC to dextran resulted in 40- and 7-fold decreases in the clearance and volume of distribution of the drug, respectively. The accumulation of the dextran-3TC conjugate in the liver was 50-fold higher than that of the unconjugated 3TC.



Scheme 1.8: Scheme to synthesize 4-*N*-(4,4'-Dimethoxytrityl)-5'-*O*-(succinate)-2',3'-dideoxy-3'-thiacytidine (4-*N*-(4,4'-Dimethoxytrityl) lamivudine succinate, 5). (i) *tert*-Butyldimethylsilyl chloride, imidazole, dry *N,N*dimethylformamide; (ii) 4,4'-dimethoxytrityl chloride, pyridine; (iii) *tert*-butylammonium fluoride, molecular sieves (4 Å); (iv) succinic anhydride, DMF, pyridine, 4-Dimethylaminopyridine (DMAP); (v) Acetic acid (80%).



Scheme 1.9: Scheme to synthesize 3TCS–Dextran (3TCS-D, 8). (i) dextran 25 kDa, *N,N'*-diisopropylcarbodiimide, DMAP, dry dimethyl sulfoxide (DMSO), *N,N'*-diisopropylethylamine; (ii) Acetic acid (80%).

1.6.7 Cyclodextrins

Cyclodextrins are cyclic oligosaccharides of α -D glucopyranose components produced from starch (Grumezescu et al., 2016)(Roy et al., 2016) [Table 1.9]. These types of oligosaccharides normally have the hydrophobic cavity and the hydrophilic outer surface. Currently the marked class of cyclodextrins include, α -cyclodextrins, β -cyclodextrins and γ -cyclodextrins containing 6, 7 and 8 (α -1,4)- linked α -D glucopyranose units and their derivatives. Their main use in the pharmaceutical standpoint, arises from their ability to form complexes with drugs, improvement of the aqueous solubility of biopharmaceutical classification system (BCS) class 2 or 4 materials, and their ability to increase the bioavailability and the stability of many drugs.

1.6.8 N-(2-hydroxypropyl)methacrylamide (HPMA) copolymers

HPMA copolymers were first synthesized by Kopeček and co-workers in the early 1970s with the first polymerization of HPMA [Table 1.9] (Duncan, 2009)(Duncan and Vicent, 2010)(Kopeček and Kopečková, 2010). *N*-substituted methacrylamide is usually preferred because the substitution of the α -carbon and the presence of the *N*-substituted amide bond

ensure hydrolytic stability of the side-chains (Kopeček and Kopečková, 2010). Primarily; HPMA homopolymer was exploited as a blood plasma expander. The copolymer being biocompatible and hydrophilic increases the water solubility of the drugs. In 1994; HPMA copolymer-doxorubicin entered clinical assessment as the first polymer-drug conjugate. The HPMA copolymer evaluated clinically was synthesized using free radical polymerization (Duncan, 2009) from the comonomers HPMA and methacryloylated-peptidyl-nitrophenylester. Drugs and other active agent have generally been conjugated to these polymeric intermediates using an aminolysis reaction (Duncan, 2009).

1.6.9 Alginate

Alginate biopolymers are a family of linear unbranched polysaccharides extracted primarily from marine brown algae (Pawar and Edgar, 2012)(Li et al., 2008) [Table 1.9]. Alginate comprises of (1→4) linked β -D-mannuronic and α -L-guluronic acid residues, arranged in a pattern of blocks along the chain (Pawar and Edgar, 2012). The composition, degree of β -D-mannuronic and α -L-guluronic acid residues, and the average molecular weight of the polymer strongly determine the physicochemical properties of the alginates. It is an anionic polymer, and has been found to be non-toxic, non-immunogenic and possesses mucoadhesive properties.

1.7 Clinical Perspective for infectious diseases

Over the past 10 years a major investment by researches, funders and the WHO has led to a resurgence of activity into new drug development and evaluation. However, due to new challenges such as the emergence of drug resistance, infectious diseases continue to pose a threat in the medical sector. Emergence of drug resistance poses a dynamic challenge as there has been no new and improved drug approved by FDA over the last few decades to fight against these new strains. Given the present drug approval rates; up to 95% of drugs fail clinical trials (Duncan and Vicent, 2013). Thus it is difficult to predict the future in medicinal development for infectious diseases. Vaccines can prevent the spread of infections and in some cases eliminate some diseases from global communities (McClean, 1998).

Unfortunately, there are several challenges in the identification of effective antigens, and the necessary level and type of activation of the immune system to promote long term protection.

Polymer-drug conjugation, on the other hand, presents new prospects to conquer challenges related with conventional drug therapies and has therefore attracted enormous interest in the treatment of diseases. For polymer-drug conjugates, IV administration is convenient as the water soluble conjugate enters the bloodstream immediately and is spread all over the body within seconds (Markovsky et al., 2012). However, for chronic diseases like HIV/AIDS or TB this route of administration presents a major obstacle as it can decrease patient compliance. The oral route is therefore the best way to increase patient adherence. For the last quarter of the 20th Century, polymer therapeutics are amongst the most successful first generation nanomedicines compared to other advanced drug delivery systems for oral delivery (Duncan and Vicent, 2013).

Naloxegol (NKTR-118), a PEGylated derivative of the opioid antagonist naloxone is an orally-administered conjugate currently in clinical trials (Al-Huniti et al., 2016)(Gursahani et al., 2010). It relieves opioid-induced constipation by acting at the peripheral opioid receptors without reversing centrally mediated analgesia (Gursahani et al., 2010). Despite the barriers, the free “naked” drug is usually subjected to degradation before absorption can take place i.e in an acidic environment in the stomach; tightly-bound intestinal epithelial cells (enterocytes) and degradation by liver enzymes (Markovsky et al., 2012). The PEG-naloxol conjugate altered the distribution and metabolism of naloxone by changing its pharmacokinetics. Bioavailability was increased due to minimizing the first-past effect i.e preventing degradation by the liver. Furthermore, the conjugate showed a reduced uptake rate by the brain. Chitosan is also used to increase the oral bioavailability of small molecules. As discussed in **Section 1.6.4**, chitosan is the only cationic polymer with mucoadhesive properties approved by FDA. It is able to open the tight junction of the intestinal epithelium to promote paracellular delivery. Lee and co-workers synthesized an orally administered conjugate of paclitaxel and docetaxel by conjugating to low molecular weight CS (E. Lee et al., 2009)(Lee et al., 2008). Both are extremely active anti-cancer drugs from the taxane family that show poor aqueous solubility. As a result these are usually solubilized in

appropriate vehicles containing ethanol, cremophor EL and tween 80/ethanol/ saline (Taxotere®) (Lee et al., 2008). However; these formulations (I.V) often causes acute adverse side effects; examples include rash, chest pain, tachycardia and hypotension (Weiss et al., 1990). The low molecular weight CS-paclitaxel or docetaxel conjugate system showed increased water solubility of the parent drugs. Enhanced bioavailability and ability to bypass cytochrome P450 enzymes were observed (E. Lee et al., 2009)(Lee et al., 2008). Also due to mucoadhesive properties of the polymer, a sustained retention of the polymer-drug conjugate in the GI tract was reported.

Translation of polymer-drug conjugation technology to infectious diseases poses many hurdles. Unlike most of cancer tumours where delivery can be achieved by the EPR effect, most infectious diseases require intracellular targeting and efficient absorption to the site of infection. The blood-brain barrier (BBB) is a compactly controlled and selectively permeable barrier, which restricts the passage of many substances, thereby hindering drug delivery (in efficient concentrations) from the blood to the brain (Kumar Pandey et al., 2016). Hence, some infectious diseases such as HIV is able to establish latency in the brain where there is no exposure to ARV drugs. As also emphasized in **Table 1.7** not all drugs are amenable to conjugation which implies the need for alternative methods or technologies for their delivery. Efavirenz, (belonging to the NNRTIs); is a highly potent HIV/AIDS drug currently used in sub-Saharan Africa. The drug does not have special groups to enable coupling to a polymer as shown in **Table 1.2**. Thus delivering this drug effectively would require combining traditional nanoencapsulation with polymer therapeutics. The polymer can be functionalized with targeting ligands after successful nanoencapsulation. Kataoka and colleagues have synthesized and characterized self-assembling micelles (NK911;42 nm in diameter) by means of block copolymers of PEG (Mw 5000 Da)-poly(aspartic acid) that also contain the conjugation of anti-cancer drug; doxorubicin, bound to the polymer (45%) as well as free drug (Osada et al., 2009)(Duncan and Gaspar, 2011). This type of system can be employed to extend the application of nanomedicine to infectious diseases. For examples if the drug does not have functional groups amenable to conjugation, the polymer can be chemically modified with active drugs to produce smart macromolecular pro-drugs or produce more

efficient drug encapsulation systems. These will be relevant for delivering anti-TB drugs which are highly hydrophilic (discussed in **Chapter 3**). Elimination of *M.tb* remains challenging due to the lipid barriers surrounding the bacteria that prevent antibiotics from reaching sites of infection. The layer protecting the pathogen is characterized by highly lipophilic chains. Thus coating the polymer-drug conjugates with hydrophobic polymers might improve delivery of anti-TB drugs.

1.8 Characterization of nanomedicinal drugs

Drug delivery system using nanomedicine significantly influence the behaviour of the drug in the body. This is due to the fact that nanomedicinal drugs have distinctive physico-chemical properties in terms of size, surface properties, stability, and solubility. However before they are tested *in vitro*, *in vivo* or clinically, a strict characterization of these systems is needed to ensure safety and quality, and to allow the rational development of nanomedicines. Methods frequently used to analyse the structural characteristics of polymer-drug conjugates are dynamic light scattering (DLS), zeta potential, ultraviolet–visible spectrophotometry (UV–Vis), nuclear magnetic resonance spectroscopy (NMR), X-ray diffraction (XRD), thermal studies (e.g thermogravimetric analysis), gel electrophoresis (for biological molecules), transmission electron microscopy (TEM) and scanning electron microscopy (SEM). The information generated from these analytical methods is important to guide the development of a potential nanomedicinal system. Using these analytical tools in combination to corroborate the results could possibly provide necessary information to predict or understand biodistribution and pharmacokinetics of nanomedicine, and can also lead to new ideas to advance the drug delivery systems (Manaia et al., 2017). Dynamic light scattering, zeta potential, X-ray diffraction, gel electrophoresis and thermal techniques are discussed below

1.8.1 Dynamic light scattering

Dynamic light scattering (DLS) is a method that is developed to measure the particle size of biomolecules in solution (Stetefeld et al., 2016)(Nobbmann et al., 2007)(Malvern Instruments, 2011)[**Figure 1.12**]. DLS is fairly fast, taking only minutes for a measurement

(Stetefeld et al., 2016). Typical applications are proteins, polymers, micelles, polymer conjugates, emulsions, colloids and nanoparticles.

DLS measures the Brownian motion due to the fluctuations of the scattering intensity and relates this to the size of the particles (Nobbmann et al., 2007). Brownian motion is the random movement of particles in a fluid, as a result of continuous bombardment from solvent molecules that surround them. A laser beam is directed through a sample and the fluctuations of the scattered intensity are measured at a known angle (θ) by means of a photon detector (Nobbmann et al., 2007)(Malvern Instruments, 2011). The correlator is used to analyse the statistics of the scattering signal, and the resulting correlation function is inverted to determine a size distribution.

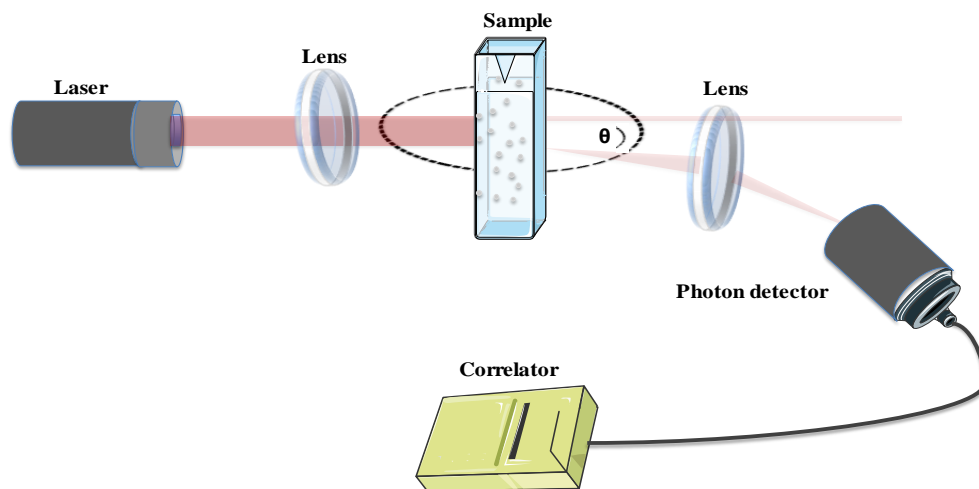


Figure 1.12: Schematic diagram of the basic principle of DLS.

The wave vector determines the length scale over which molecular motions are detected and it is given by

$$q = 2\pi n \sin(\theta/2) / \lambda$$

Equation 1.1

where n is the refractive index, λ is the wavelength of the radiation, and θ is the scattering angle. The correlation function

$$G(\tau) = \int \frac{I(t)I(t+\tau)}{[I(t)]^2} dt \quad \text{Equation 1.2}$$

is collected over the period of the measurement of the intensity $I(t)$ as a function of time, and under ideal conditions is expected to show a single exponential decay

$$G(\tau) = 1 + \beta \exp(-Dq^2\tau) \quad \text{Equation 1.3}$$

where the decay rate Dq^2 contains the diffusion coefficient D of the particles. The fitting parameter β is correlated to the ratio of coherent signal to incoherent noise. The size of the particle is determined from the translational diffusion coefficient by utilising the Stokes-Einstein equation;

$$D = \frac{k_B T}{3\pi\eta d_H} \quad \text{Equation 1.4}$$

Where D is the translational diffusion coefficient, $d(H)$ is the hydrodynamic diameter, k is the Boltzmann's constant, T is the absolute temperature and η is the viscosity of the buffer. The exponential model illustrated in equation 3.3 produces an overall average particle size. In practise, DLS works without precise knowledge of the sample concentration. The only prerequisite is that sufficient light must be scattered to attain adequate statistical accuracy of the correlation function.

DLS was used throughout the experimental chapters to ensure that all the developed polymer-drug conjugates or nano-carriers have particle sizes ranging from 1 to 1000 nm. Particle size distribution (described as polydispersity index, PDI) was obtained using DLS. PDI is an important factor since it could predict the homogeneity of nanoparticles or polymer-drug conjugates. Zeta potential or surface charge was also measured using DLS.

1.8.2 X-ray diffraction

X-ray diffraction (XRD) is a non-destructive method that gives data on structural phases and crystallinity of the material (Bunaciu et al., 2015). It is widely used for pharmaceuticals to determine whether a resultant material has a crystalline or amorphous nature. Amorphous solid drugs, characterized by having no long-range ordered molecular packing, show useful

properties such as higher solubility and dissolution rate than the crystalline form (Yu, 2001). XRD is also important to classify the crystalline phases of impurities in drug synthesis processes. Amorphous and crystalline materials are observed by broad and sharp diffraction peaks, respectively (Manaia et al., 2017),

X-rays are electromagnetic radiation with photon energies typically ranging from 100 eV to 100 keV. XRD is built on constructive interference of monochromatic X-rays from a crystalline material (Bunaciu et al., 2015). These X-rays are produced in a cathode ray tube by raising a temperature in a filament to generate monochromatic radiation. Monochromatic radiations (electrons) are then accelerated towards the material by applying a voltage. Unique X-ray spectra are generated when electrons have adequate energy to displace inner shell electrons of the targeted material. When conditions satisfy Bragg's law, the interaction of the incident rays with the material generates constructive interference and a diffracted ray, and the following equation applies:

$$n\lambda = 2d \sin\theta$$

Equation 1.5

where n is the order of diffraction, λ is the wavelength of the X-rays, d is the interplaner spacing producing the diffraction, and θ is the diffraction angle.

1.8.3 Thermogravimetric analysis

Thermogravimetric analysis (TGA) is a technique of thermal analysis which measures physical and chemical changes of the material as a function of temperature (or time) at a constant heating rate in a controlled atmosphere (PerkinElmer, 2010). TGA curves are distinctive for a particular material since the physiochemical reactions depend on the molecular structure. The process happens over certain temperature ranges and at rates that are functions of the chemical reactions within the characterized material. Loss of weight is a result of chemical degradation leading to the generation and release of volatile products. A gain in weight may occur upon reaction with the atmosphere such as in oxidation reactions. TGA can quantify loss of solvent or water, oxidation and decomposition during an experiment (PerkinElmer, 2010). The data generated from TGA represents the kinetics and

thermodynamics of the physicochemical reactions revealing intermediates in the process and giving information on the final degradation products. A TGA consists of a sample pan that resides in a furnace. The furnace is cooled or heated and the changes in mass are recorded during the test while the purge gas controls the sample environment. The purge gas may be reactive or inert.

1.8.4 Electrophoresis

Electrophoresis is a standard technique used to identify, purify and separate proteins and nucleic acids (Hellman and Fried, 2007). Biological molecules generally contain negative or positive electrical charges in their structural network. When these molecules are placed under an electric field of field strength E , electrostatic attraction occurs since they will spontaneously move near the electrode of opposite charge (Reddy and Raju, 2012). Depending on the molecular weight, physical characteristics of the biological molecule and on experimental conditions, different molecules will migrate towards the electrode at individual rates. The displacement of the biological molecule in an electric field is determined using the variables described by:

$$v = E \cdot q / f$$

Equation 1.6

Where v is the velocity of the movement, q is the total charge on the molecule and f is the frictional coefficient (Adamson and Reynolds, 1997). The total charge is measured by the number of negative and positive charges in the molecule. While the frictional coefficient is determined by the frictional resistance the molecule poses to move towards the electrode. The frictional coefficient strongly depends on factors such as molecular weight, porosity and viscosity of the gel in which the experiment is performed. Agarose and polyacrylamide gels are normally utilized since they are porous in nature (Stellwagen, 2010). Polyacrylamide gels can resolve higher quantities of proteins and nucleic acids without major loss in resolution than agarose gels (Barril and Nates, 2012). The pore size of the polyacrylamide gels can be managed easily by altering the concentrations of the monomers (Barril and Nates, 2012). Moreover, nucleic acids retained from polyacrylamide gels are very pure. In chapter 2 a polyacrylamide gel was used to confirm the conjugation of RNA aptamers to PEG.

1.9 Significance of the review

In particular, malaria and TB have not benefited much from new technological development in disease management. Most of the drugs used are several decades old and have significant toxicity profiles which impact poor patient adherence. New and potent drugs being discovered stumble on the road to the clinic because of solubility issues. Poor solubility is an ongoing challenge in pharmaceutical growth, as results many just end up being shelved. It is estimated that over 40% to 70% of new chemical entities have poor solubility. Thus the search for new chemical entities and advanced delivery actions are the major driving force in polymer therapeutics.

The review is relevant since literature available on the FDA approved drugs for infectious diseases conjugated to water-soluble biocompatible and biodegradable polymers is limited, particularly that deals with the conjugation of anti-malarial and anti-TB drugs. Most work involving these drugs is mainly based on encapsulation.

1.10 Hypothesis

The conjugation of an active ingredient to polymers offers a powerful technological solution to drugs with high toxicity and poor pharmacokinetics. The polymer conjugation can be applied to protect the conjugated drugs from enzymatic degradation. The stability could be increased and also hydrophilic polymers tend to increase solubility of poorly water soluble drugs. Combining this technology with traditional nanoencapsulation techniques will produce optimized materials that could be used for oral administration to treat infectious diseases.

1.11 Aims and objectives

This project has three experimental chapters. Each chapter was designed to solve problems associated with HIV/AIDS, TB and malaria.

The aims and primary objectives for each chapter of this project are to:

1. Conjugate RNA aptamers to polyethylene glycol (PEG) using carbodiimide chemistry.
2. Encapsulate PEGylated RNA aptamers into poly(epsilon-caprolactone) [PCL] nanoparticles using a double emulsion method for the treatment of HIV/AIDS.
 - Compare the stability of aptamers and conjugated aptamers using human breast milk.
 - Characterize PCL nanoparticles by physical and electrochemical analytical techniques
3. Develop of a hybrid nanoparticle drug delivery system by encapsulating a polymer-drug conjugate of Mox in a nanoparticle hydrophobic carrier for the treatment of TB
 - Characterize PCL nanoparticles or polymer-drug conjugate by analytical techniques
4. Conjugate a hydrophobic drug, lumefantrine to water soluble polymers for the treatment of malaria.
 - Characterize polymer-lumefantrine conjugate by analytical techniques

2 Chapter Two: PEGylated aptamers coated onto the surface of poly(epsilon- caprolactone) nanoparticles for HIV/AIDS applications: Synthesis and characterisation

2.1 Introduction

HIV/AIDS remains a major health problem worldwide, as currently there is no cure available (Jacob et al., 2017)(Giacalone et al., 2015)(Sosnik et al., 2009). The burden of the disease includes the demanding drug-regimen compliance (Jacob et al., 2017)(Sharma and Garg, 2010)(WHO. 2014). Chronic intake of HAART is compulsory to control HIV infection and any non-adherence leads to a quick increase in the viral load (Richman et al., 2009)(Sharma and Garg, 2010)(Sosnik et al., 2009). Poor targeting ability of ARVs to latent sites of infection is the main reason for the relapse (Shi et al., 2016)(Varatharajan and Thomas, 2009). Short residence time and low concentration of ARV drugs at certain sanctuaries (viral reservoir sites) such as lymphatic system, macrophages, lymphocyte and central nervous system is another major drawback (Mallipeddi and Rohan, 2010). To ameliorate the challenges, ARVs are usually administered in higher doses, which in turn results in advanced toxicity (L. Tshweu et al., 2013). For a chronic treatment, even adequate toxicity may lead to poor patient compliance (Sharma and Garg, 2010).

Aptamers are a class of nucleic acid-based ligands, such as ribonucleic acid (RNA) and single-strand deoxyribonucleic acid (ssDNA) that bind to target molecules with high specificity and affinity (Alexandre et al., 2016)(Dey et al., 2005)(Tan et al., 2011)(Song et al., 2012)(Zhou and Rossi, 2010). They are known to be non-toxic and non-immunogenic in clinical applications (Alexandre et al., 2016)(Mokhtarzadeh et al., 2016), which makes them prominent molecules for targeting diseases either for prevention or as therapeutics (Bouchard et al., 2010). Aptamers can be synthesised *in vitro* via systematic evolution of ligands by exponential enrichment (SELEX) against any given biological agent that is expressed in

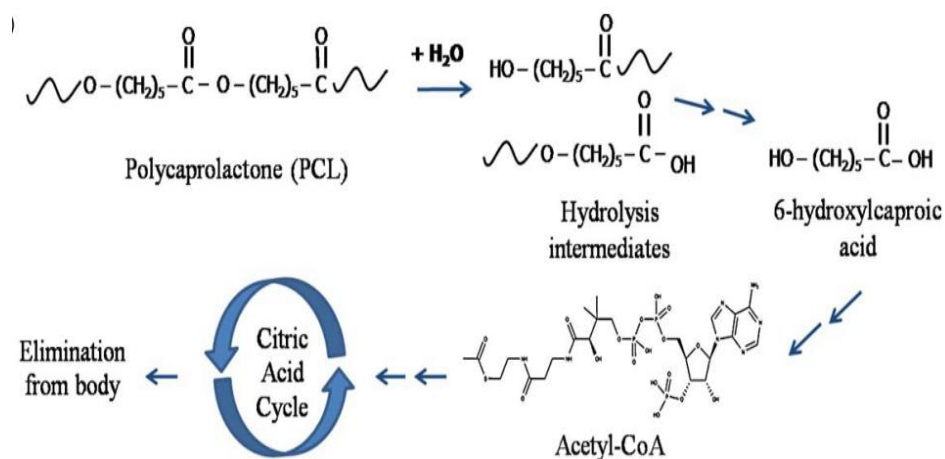
diseased cells (Mokhtarzadeh et al., 2016). Macugen[®] is an aptamer-based therapeutic compound already on the market approved by FDA for the treatment of age-related macular degeneration (Duncan and Gaspar, 2011)(Levy-Nissenbaum et al., 2008)(Ng et al., 2006). Many aptamers, targeting specific cell surface receptors, have been used against different proteins, nucleic acids, and pathologies by various researchers around the world (Li et al., 2015)(Guo et al., 2011)(Sun et al., 2014)(Hovanessian et al., 2010)(Barbas et al., 2010)(Lee et al., 2005). In the case of HIV-1, our group isolated novel RNA aptamers that prevent HIV-1 entry by binding to the core conserved residues on gp120 and other viral surface molecules required for entry (Khati et al., 2003)(Mufhandu et al., 2012)(London et al., 2015). London et al. 2015 synthesized RNA aptamers namely CSIR1.1, CSIR1.4, CSIR1.5 and CSIR1.6, containing 2'-fluoro-substitution to enhance stability of the aptamers. Findings showed that CSIR1.1, CSIR1.4, CSIR1.5 and CSIR1.6, bound to gp120 with affinity constant (K_d) of 16.1 ± 5.5 nM; 33 ± 14 nM; 195 ± 81 nM and 60 ± 39 nM, respectively. These values are all superior to those of antibodies, whose K_d s are in the micromolar to millimolar range (Li et al., 2015)(Tan et al., 2011). In addition aptamers can be produced much cheaper and faster than antibodies and their production allows for easier and controllable modification to accomplish different therapeutic and diagnostic purposes (Tan et al., 2011). Though 2'-F-RNA aptamers are highly stable and can withstand a wide range of temperatures, pHs (4–9) and organic solvents without loss of activity (Ruscito and DeRosa, 2016)(Sun et al., 2014)(Kong and Byun, 2013), these molecules can be degraded easily by nucleases (Levy-Nissenbaum et al., 2008). As a result, poly (ethylene glycol) (PEG) was selected to stabilize the aptamer CSIR1.1. PEG is a biocompatible polymer that has been utilized extensively in the field of nanomedicine (Pasut and Veronese, 2009)(Guo et al., 2011). It is FDA approved and the chemical structure of the polymer presents terminal groups that can be easily conjugated to biological molecules (Pasut and Veronese, 2009). The stability of free aptamers and PEGylated-aptamers were compared *in vitro* using human breast milk. Previously our team produced poly(epsilon-caprolactone)[PCL] nanoparticles using double emulsion method (L. Tshweu et al. 2013). The synthesized PCL nanoparticles had no targeting ligands. Thus, we envisaged that when PEGylated-aptamers are coated onto the surface of PCL nanoparticles, these HIV-1 targeting ligands would still achieve active binding to HIV-1. In this study, we

proposed to use *in vitro* electrochemical impedance spectroscopy to elucidate the binding of these aptamer modified PCL nanoparticles to gp120 protein

2.1.1 Poly (epsilon-caprolactone)

Synthetic polyesters are among the most used in the drug delivery application, as encapsulation agents, controlled drug release and site specific delivery. These include polylactic acid (PLA), poly-glycolic acid (PGA), poly (D,L lactide-co-glycolide) (PLGA) and PCL etc (Soppimath et al., 2001). The advantage of using these polymers is that they are biocompatible, biodegradable and US-FDA-approved materials.

PCL has found various biomedical applications such as in drug delivery, suture and scaffold in tissue engineering (Woodruff and Hutmacher, 2010). PCL is a hydrophobic polyester. It undergoes hydrolysis upon implantation into the body, forming 6-hydroxylcaproic acid that is converted into acetyl-CoA and enters the normal citric acid cycle. The products are eventually eliminated from the body without causing any harm as shown in **Scheme 2.1** (Woodruff and Hutmacher, 2010). Furthermore it is cheaper and degrades slower when compared to other polyesters. For these reasons, PCL was selected as a polymer of choice in the present project.

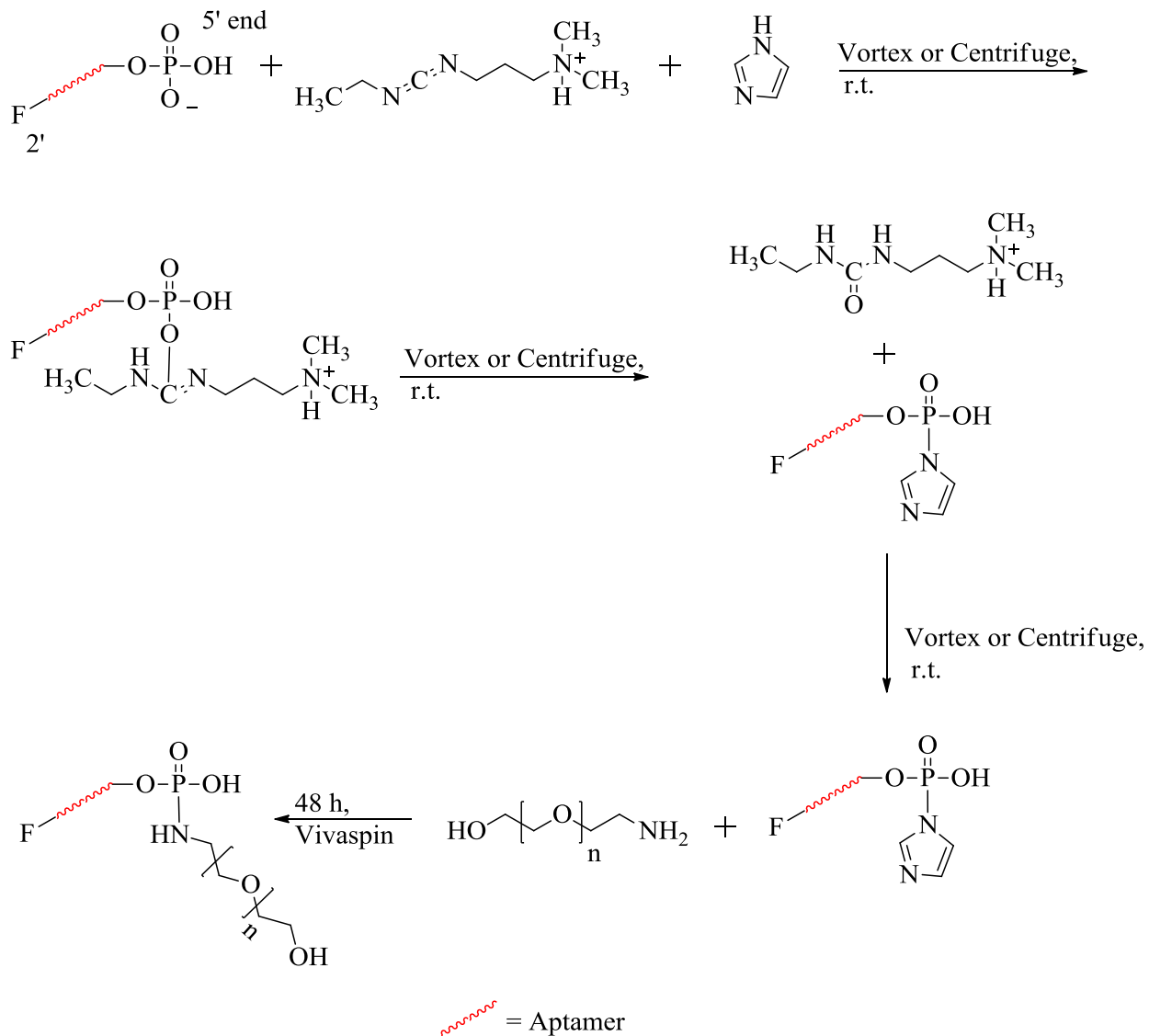


Scheme 2.1: Hydrolysis of polycaprolactone polymer (Woodruff and Hutmacher, 2010)

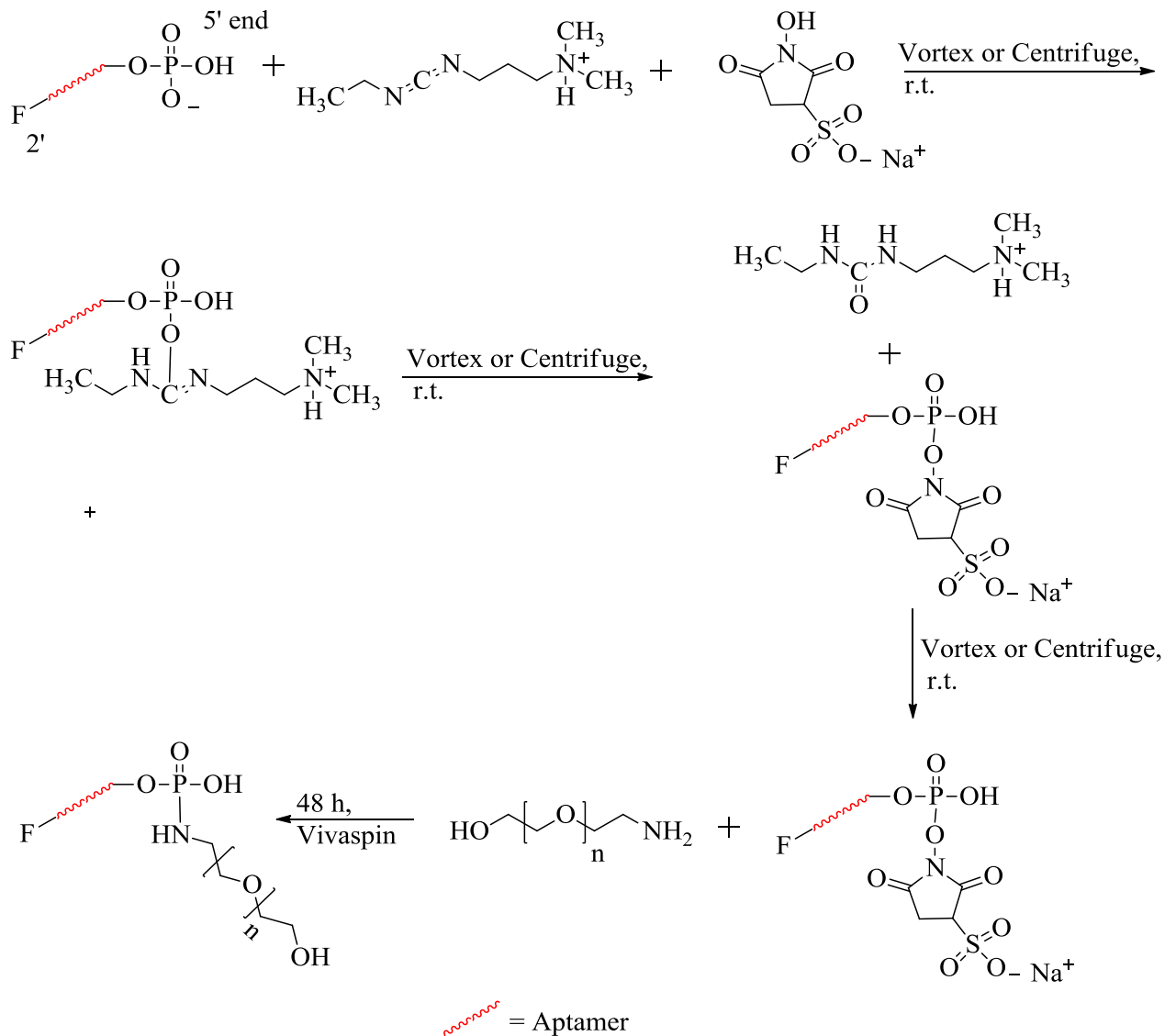
2.2 Results and Discussion

2.2.1 Preparation and characterisation of PEGylated aptamers

In this study RNA aptamers binding to HIV-1 gp 120 were used as the targeting moieties to functionalize the surface of biodegradable and biocompatible PCL nanoparticles for anti-HIV applications. RNA aptamers were conjugated to O-(2-Aminoethyl) PEG using EDAC/imidazole [**Scheme 2.1**] (or EDAC/Sulfo-NHS) chemistry (Ghosh et al., 1990)(Ghosh et al., 1989)(Chu et al., 1986)(Chu et al., 1983). Taking the advantage of the uncapped 5' phosphate group of the RNA aptamers (**CSIR 1.1**), the water soluble carbodiimide EDAC activates the phosphate group to a highly reactive phosphodiester intermediate. A second reactive intermediate, a phosphorimidazole, was created from phosphodiester intermediate by adding imidazole to the reaction. The formation of a phosphorimidazole intermediate provides better reactivity towards amine nucleophiles than EDAC phosphodieters, since the latter has a short half-life in aqueous media due to competition with water molecules (i.e. hydrolysis) (Chu et al., 1986)(Chu et al., 1983)(Kirby and Younas, 1970). The free amine of the O-(2-Aminoethyl) PEG was reacted with the phosphorimidazole intermediate, creating a phosphoramidate linkage with a loss of the imidazole leaving group (Chu et al., 1986)(Chu et al., 1983). The same reaction was repeated with Sulfo-NHS instead of imidazole and yielded the same product [**Scheme 2.2**].



Scheme 2.2



Scheme 2.3

Urea gel electrophoresis was used to confirm the conjugation of RNA aptamers to O-(2-Aminoethyl) PEG [Figure 2.1]. The polymer did not depict any band on the urea gel [Figure 2.1A, 2]. Free RNA aptamers had a clear migration on the urea gel [Figure 2.1A, Apt], corresponding to molecular weight between 100 and 150 base pairs (bps). In the presence of EDAC/imidazole or EDAC/sulfo-NHS, RNA aptamer was efficiently conjugated to O-(2-Aminoethyl) PEG polymer [Figure 2.1B, 2&3]. The formation of the PEGylated RNA

aptamers was confirmed by the band observed below the original band of the free RNA aptamers from the baseline. This was not surprising because the molecular weight of RNA aptamer was 10 times higher than that of the polymer. The RNA aptamer was incubated with PEG without the coupling reagent and as expected there was no conjugation [Figure 2.1B, 1]; this was confirmed by the fact that its migration in the urea gel was the same as the original RNA aptamer. Moreover before washing, PEGylated RNA aptamers showed the smearing effect indicating the presence of unmodified RNA aptamers and excess imidazole [Figure 2.1A, 1]. This was expected because imidazole contains protons. These protons were causing smearing since the RNA aptamers bears a negative charge because of the phosphodiester linkage.

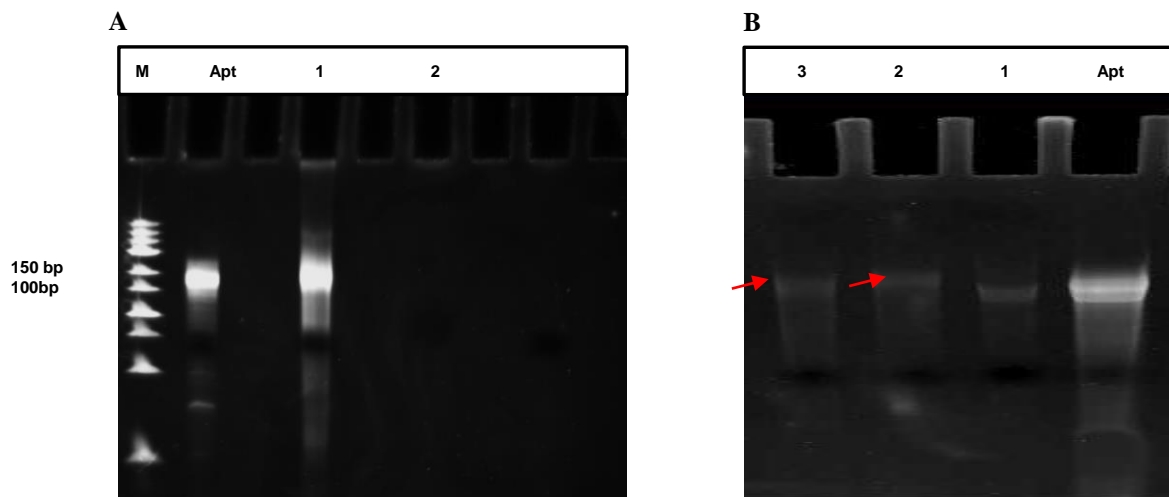


Figure 2.1: Confirmation of conjugation of RNA aptamers to PEG via urea polyacrylamide gel electrophoresis: (A) M = molecular marker, Apt = RNA aptamer, 1 = PEGylated RNA aptamers (not purified), 2 = O-(2-Aminoethyl) PEG. (B) 1 = RNA aptamers + O-(2-Aminoethyl) PEG (reaction carried-out in the absence of coupling reagents), 2 = PEGylated RNA aptamers (EDAC/imidazole) and 3 = PEGylated RNA aptamers (EDAC/sulfo-NHS).

To confirm that PEGylation did not affect the aptamer ability to bind HIV-1, the TZM-bl neutralization assay was performed with the parent and PEGylated RNA aptamers. The pseudovirus neutralisation assay that was used measures the neutralisation of HIV-1 as a function of the reduction in Tat-regulated luciferase reporter gene after a single round of

infection in TZM-bl cells (Montefiori et al., 2007). TZM-bl cells which are CXCR4-positive HeLa cell clone are engineered by retroviral transduction to express CD4 and CCR5 co-receptors to mimic cells in the human body (Platt et al., 1998). The cell line was also engineered with HIV-1-based vector to contain reporter genes regulated by HIV long-terminal repeat sequences (Montefiori et al., 2007). The reporter genes are Tat-responsive for firefly luciferase and *E. coli* β -galactosidase (Wei et al., 2002), as such, the engineering of these cells makes them susceptible for infection by HIV-1, SIV and SHIV (Montefiori et al., 2007)(Platt et al., 1998). We used the idea here that if PEGylation had no effect on the RNA aptamers' ability to bind HIV-1 gp120 the parent RNA aptamer and its derivatives should inhibit the virus with similar potency. As shown in **Figure 2.2** all aptamers neutralized HIV-1 infection of TZM-bl cells with IC_{50} ranging from 2 to 3 nM suggesting that PEGylation did not affect the aptamer ability to interact with the virus.

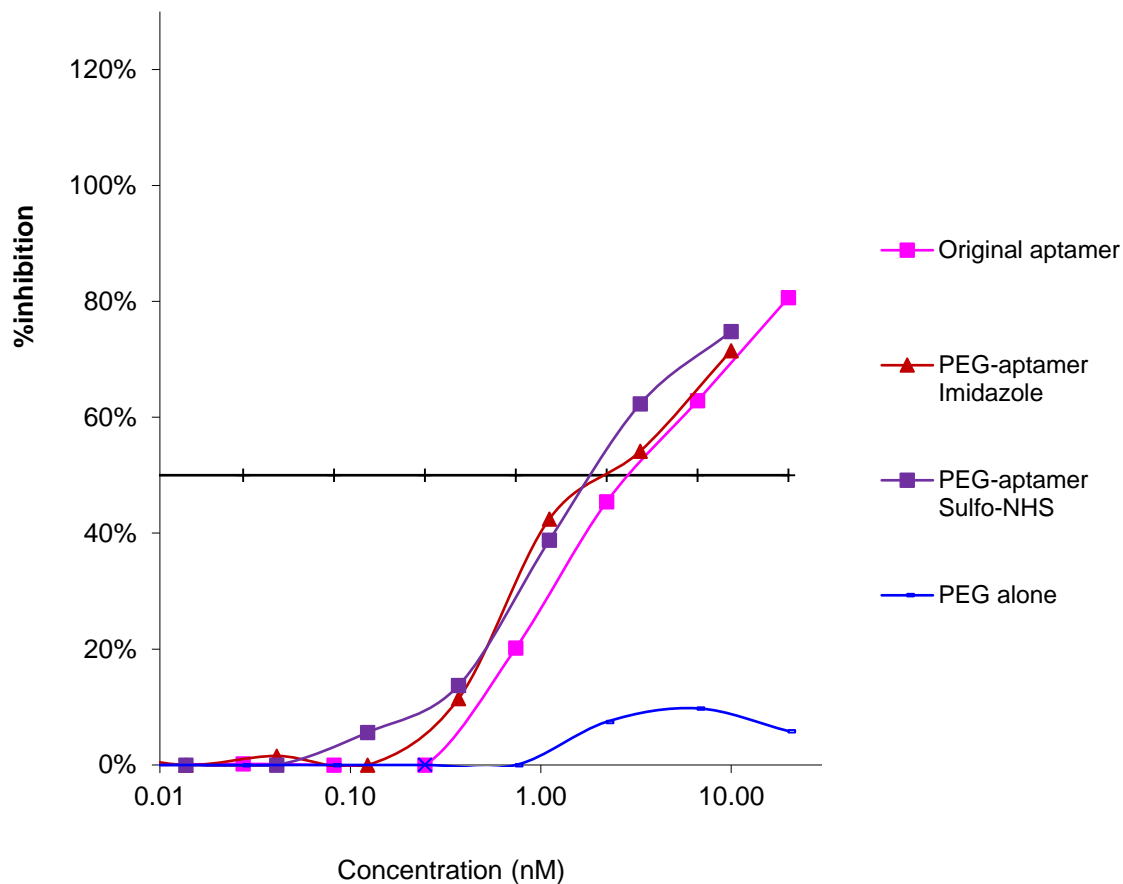


Figure 2.2. Inhibition of HIV-1 infection with parent and PEGylated RNA aptamers. Data depict mean 50% inhibitory concentration (IC_{50}) of the respective aptamers. Pink squares show the HIV-1 inhibitory curve of the parent aptamer. The PEGylated RNA aptamer prepared using EDAC/imidazole and EDAC/Sulfo-NHS anti-viral activities are shown with red triangles and purple squares; respectively. PEG alone, used as a control, is shown by the blue curve.

2.2.2 Stability of RNA aptamers and PEGylated RNA aptamers in human breast milk

HIV-1 entry commences with the attachment of the virions to the cell surface facilitated by an interaction of extracellular domain of gp 120 and cellular receptors. The CD4 receptor and CCR5 or CXCR4 co-receptors are major receptors for the virus. Therefore, obstructing HIV-1 entry into the host cells appears to be the ideal strategy for preventing the infection of cells.

RNA aptamers used in this study have been shown previously *in vitro* to prevent HIV-1 entry, without cytotoxicity, by binding to core conserved residues on gp120. However, the stability of aptamers (RNA or DNA) is a key property of any application that aims to use these nucleic acids. Nucleases and enzymes are known to degrade any foreign nucleic acids that enter's the body. Even when RNA aptamers are stabilised (e.g., by 2-O-methyl or 2-fluoro modifications), degradation and clearance is unavoidable.

Breastmilk was used to compare the stability of parent aptamers and PEGylated aptamers. Lactoferrin is an active nuclease generated by mucosal epithelial cells in several mammalian species including humans, goats and cows (González-Chávez et al., 2009). This multifunctional glycoprotein is present in several mucosal secretions like saliva, tears, semen, vaginal fluids, gastrointestinal fluids and most highly in milk (Farnaud and Evans, 2003)(González-Chávez et al., 2009)(Van der Strate et al., 2001). Lactoferrin is an 80 kDa glycosylated protein, consisting of 692 amino acids (Van der Strate et al., 2001). It is classified as a transferrin protein and the inhibitor of carbonic anhydrase, whose function is to transport ions in the blood serum(González-Chávez et al., 2009). Due to its antimicrobial properties against bacteria, fungi and several viruses, lactoferrin is also an important component of the non-specific immune system. Another essential property of lactoferrin is that it has DNase, RNase, ATPase and phosphatase activity. As a result it is capable of binding to and hydrolysing polyanions such as DNA, RNA, polysaccharides and heparin etc. Thus RNA aptamers can be degraded easily by lactoferin. Therefore; measuring the stability of the PEGylated aptamers in the breastmilk will provide a good indication of resistance to degradation.

Figure 2.3 shows urea-gel electrophoresis images. From the urea-gel image, we could observe that the free RNA aptamers started to degrade from time 0 (**Figure 2.3 A**). These results are in agreement with the literature. Babina et al. 2005 studied hydrolyses of nucleoside 5-triphosphate using human milk. Using different methods, including in-gel ATPase activity assay, it was shown that hydrolysis of ATP and nucleotide's is an inherent nature of lactoferrin. Findings also demonstrated that lactoferrin is the major ATPase of human milk. The results corroborate with our findings. **Figure 2.3 B** displays the incubation

of aptamers in a PBS buffer (pH 7.4) which lacks the nuclease enzymes. There was no degradation across the time studied.

PEGylated RNA aptamer was still stable in breast milk from time 0 until 30 minutes (**Figure 2.3, C**). Slight degradation was observed after 1 hour of incubation. The reduced degradation as compared to the parent aptamer can be described by increased mechanical and thermal stability of the PEGylated aptamer, and the resistance towards degradation by nucleases is caused by the ‘shielding’ effects of the PEG polymer over sites on the RNA aptamer that are vulnerable to degradation. These effects have been mainly observed in the PEGylation of proteins. According to literature PEGylating increases proteolytic resistance (Lawrence et al., 2014). These results further confirmed the conjugation of PEG to RNA aptamers. Babina et al. 2005 also demonstrated that the ATP-hydrolyzing center of the lactoferrin protein is located at the C-terminal domain and that contact between this center and ATP increases the oligonucleotide-hydrolyzing activity of the binding. This interaction in our study was minimised due to the newly phosphoramidate linkage between the aptamers and the polymer.

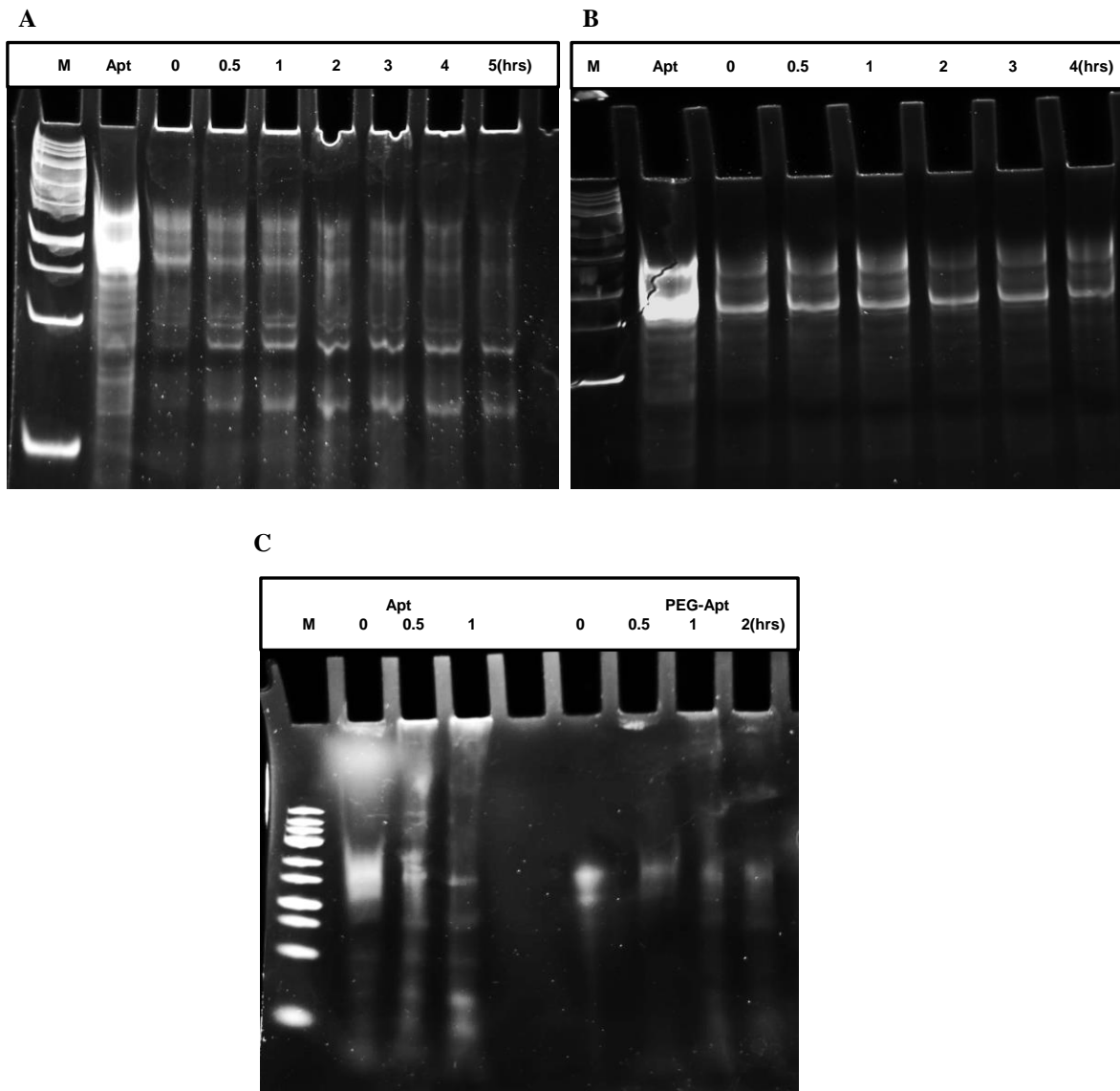


Figure 2.3: Stability of RNA aptamers and PEGylated aptamers in breast milk via urea polyacrylamide gel electrophoresis. (A) RNA aptamers in breast milk, (B) RNA aptamers in PBS (7.4) and (C) stability studies of RNA aptamers PEGylated aptamers in human breast milk. Apt = RNA aptamers and PEG-Apt = PEGylated aptamers.

2.2.3 Preparation and characterization of PCL NPs coated with PEGylated RNA aptamers.

PEGylated RNA aptamers were successfully coated to the surface of PCL nanoparticles using the double emulsion technique as shown in **Figure 2.4**. Under the optimized conditions, the mean particle size of the prepared PCL nanoparticles was 76.2 ± 0.9 nm with PDI of 0.14 ± 0.01 [**Figure 2.5**]. Coating PEGylated RNA aptamers to the surface of the PCL nanoparticles resulted in a slight increase of the mean particle size (112.0 ± 1.0 nm, PDI = 0.13 ± 0.01). However both the prepared PCL/coated nanoparticles had PDI less than 0.2, an indication of homogeneous nanoparticles. Zeta potential was observed to be -17.4 ± 2.7 mV for PCL nanoparticles and found to increase to -46.2 ± 3.0 mV probably due to phosphodiester bonds present in PEGylated RNA aptamers (Guo et al., 2011)(Cheng et al., 2007)(Farokhzad et al., 2006). The zeta potential is described as the surface charge of the nanoparticles relative to the dispersing medium. High net surface charge compared to the dispersing medium is preferred to prevent agglomeration or aggregation. Similar ionic charges on the nanoparticles will facilitate repulsive force, thus it will automatically prevent natural attractive forces such as hydrogen bonding and van der Waals interactions.

Particle size and surface charge (zeta potential) are the key factors of the clearance kinetics and biodistribution of nanoparticles (Storm et al., 1995). The nanoparticles offer many unique rewards compared to microparticles. The sub-micron size allows higher intracellular up-take when compared to microparticles. This was demonstrated in that 100 nm size nanoparticles exhibited 2.5 fold better up-take compared to 1 μ m and 6 fold higher up-takes when compared to 10 μ m particles in Caco-2 cell line (Desai et al., 1997). The overall size of the PEGylated aptamer-PCL nanoparticles were less than 150 nm, suggesting that they could bind efficiently to the HIV-1 gp 120 *in vivo*. Other researchers have shown that the sub-micron particles can cross the blood-brain-barrier (BBB) of the central nervous system (CNS), which is one place where current ARVs cannot reach appropriately (Rao et al., 2009).

Surface charge of nanoparticles is one of the factors that tends to affect the up-take and targeting of the nanoparticles (A. L. Z. Lee et al., 2009)(Sarmiento et al., 2011)(Singh and W., 2009). It has been shown that the probabilities of the nanoparticle to escape the endo-lysosomes mode of uptake depend on the surface charge. Nanoparticles that show transition in their surface charge from anionic (pH 7) to cationic in the acidic endosomal environment (pH 4-5) are found to escape the endosomal compartment whereas the nanoparticles which remain negatively charged at pH 4, were mostly retained in the endosomal compartment. The obtained negatively charged PCL nanoparticles are preferred, since they may diminish the nonspecific interaction with the negatively charged PEGylated RNA aptamers, thus preserving conformation and binding characteristics of RNA aptamers (Guo et al., 2011)(Farokhzad et al., 2006).

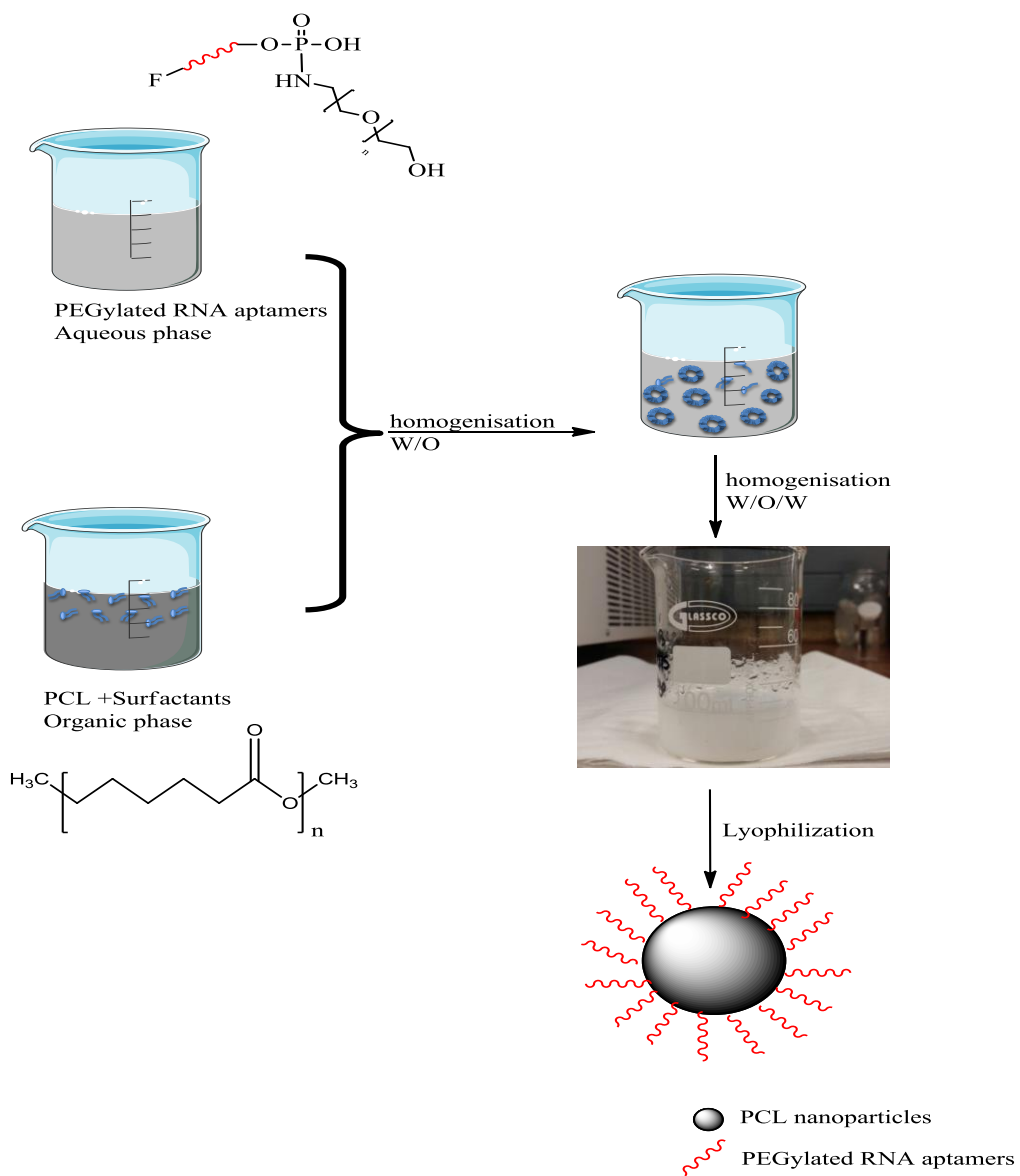
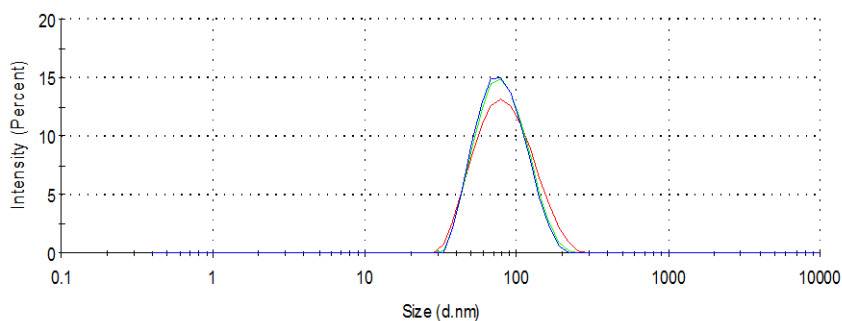
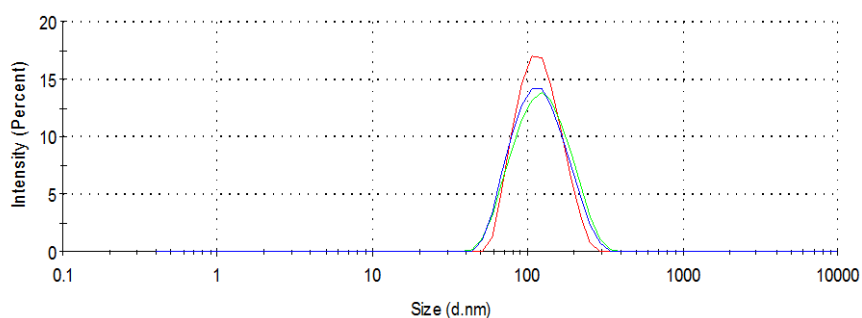


Figure 2.4: Preparation of PCL nanoparticles coated with PEGylated RNA aptamers using double emulsion method.



(A)



(B)

Figure 2.5: Particle size and particle size distribution of the NPs. (A) PCL nanoparticles, (B) PCL coated nanoparticles. (Data represent mean \pm SD, n = 3)

2.2.4 *In vitro* binding assay using electrochemical techniques

Cyclic voltammetry (CV) and electrochemical impedance spectroscopy (EIS) are two electrochemical techniques used to investigate changes on the electrode surface. These techniques have gained extensive appreciation in literature for characterization of monolayers deposited onto solid substrates particularly in areas such as optics, corrosion protection, microelectronics and electrochemical sensors (Geng et al., 2008)(Rodgers and Amemiya, 2007)(Retna Raj and Ohsaka, 2002)(Zhao et al., 2006). More recently the techniques were used for the first time to elucidate the binding antibodies to mycolic acid antigens for distinguishing between TB positive and negative human sera (Mathebula et al.,

2009). In the experimental results discussed in this section, the binding of PCL nanoparticles coated with PEGylated RNA aptamers to HIV-1 gp 120 was investigated by these two methods. They were developed to monitor the extent to which each substrate permitted electron transport between a redox probe solution $[\text{Fe}(\text{CN})_6]^{3-}/[\text{Fe}(\text{CN})_6]^{4-}$ and the core gold (Au) electrode.

The bare Au electrode was properly washed before every experiment. The washing process is a laborious procedure that involves physical, chemical, and electrochemical cleaning. Details of this protocol are outlined in **Chapter 6**. As reported by Diao et al. 2000 voltammogram or impedance of different samples is not precisely the same even under the same experimental conditions probably due to the surface states of the bare Au electrode that may differ from sample to sample. To diminish such uncertainties, in this work, one Au electrode was utilized throughout.

HIV-1 gp 120 proteins do not contain sulfur in its molecular structure for integration onto Au electrode as a self-assembled monolayer (SAM). As a result, mercaptoacetic acid (MACA) was applied for self-assembly on the bare Au electrode surface to form monolayers through the stable Au-thiolate bond. MACA is known to form quasi-crystalline SAMs relatively rapidly and their electrochemical behaviors are well studied (Geng et al., 2008). SAMs developed by the adsorption of thiols onto Au are widely used. The specificity and strength of the Au-sulfur interface permits the introduction of many significant terminal functional groups to be incorporated (Folkers et al., 1992). The free carboxylic acid group on the newly formed SAMs was used to introduce HIV-1 gp 120. The water soluble carbodiimide EDAC was used to form active ester functionalities with the monolayer of MACA on the Au electrode in the presence of sulfo-NHS. The active esters on the SAMs were replaced by amines of the HIV-1 gp 120 protein by forming the stable amide bond. The specificity and affinity of PCL nanoparticles coated with PEGylated RNA aptamers on HIV-1 gp 120 on the electrode was compared with PCL nanoparticles. A SAM of MACA is also investigated as a comparative standard to help understand the electrochemical performance of HIV-1 gp 120 SAM on the Au electrode.

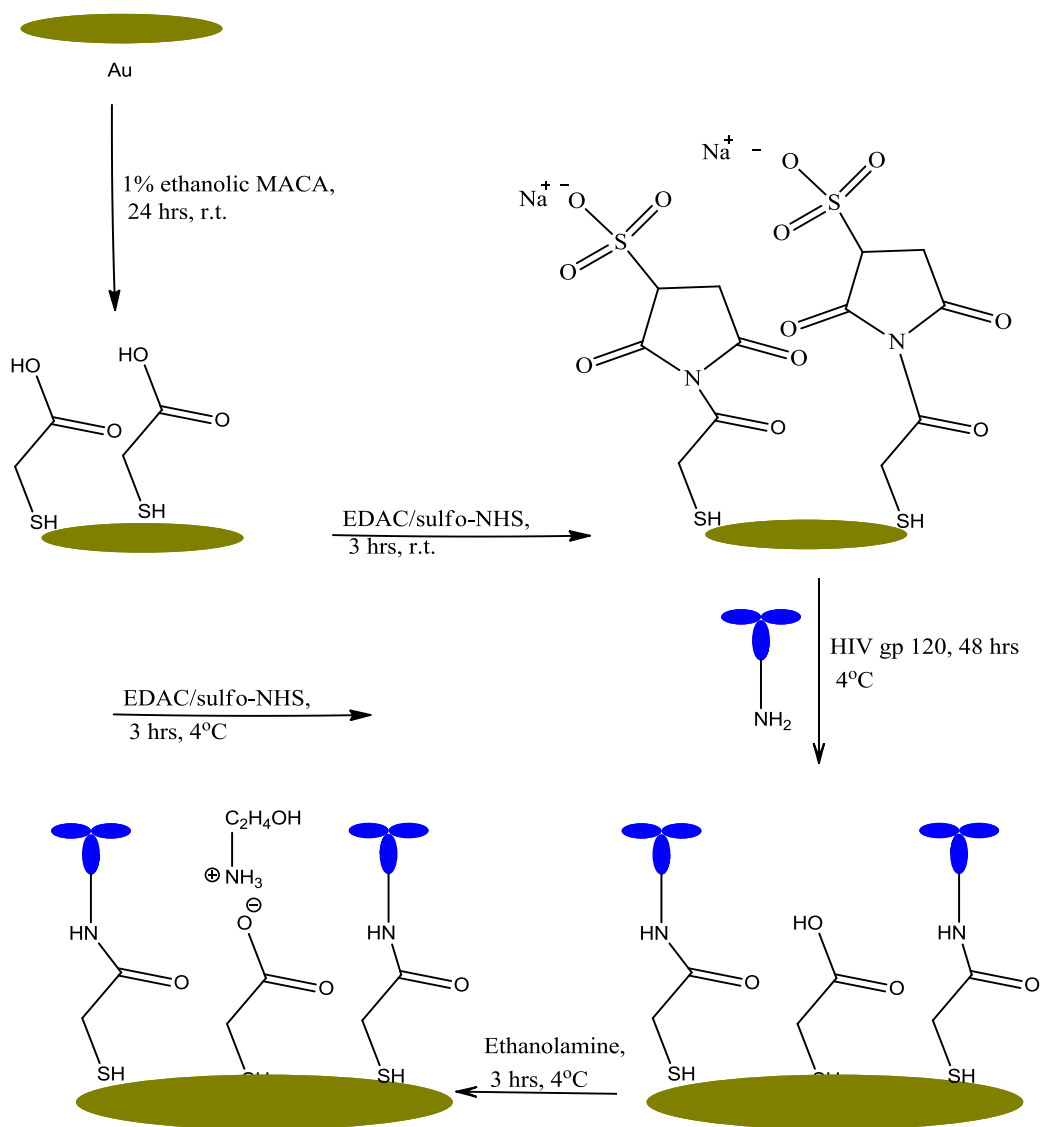


Figure 2.6: Gradual deposition of monolayers to the bare Au electrode.

Figure 2.7 depicts an overlay plot of the cyclic voltammograms of the Au electrode before and after it was immobilised with MACA and HIV-1 gp 120 monolayers. CV is most valuable for evaluating changes happening on the electrode as continuous fabrication steps modify the Au surface. The redox probe $[\text{Fe}(\text{CN})_6]^{3-}/[\text{Fe}(\text{CN})_6]^{4-}$ reveals a reversible process in all the experiments. When the bare gold was incubated in a 1% ethanolic solution of MACA for 24 h, a decrease in responsive current was observed. The redox probe showed moderate penetration of the SAM indicating that ions can move through the short chain thiols

on the electrode surface (Su and Li, 2004). After activating the terminal carboxylate groups of the MACA, the redox peak increased similar to the results of Su and Li. The positively/ neutrally charged NHS ester attracted the negative redox probe to the electrode surface (Geng et al. 2008), thus resulting in an increase in current response. After incubating HIV-1 gp 120 proteins to MACA monolayers for 48 hrs, the redox peak was decreased due to thickness developed at the electrode interface. The longer incubation period for the HIV-1 gp 120 was chosen because a lower concentration was used and because it was anticipated that the HIV-1 gp 120 chains would not readily pack into a neat array as the MACA due to their nature to adopt folded conformations. Before elucidating the binding of PCL nanoparticles coated with PEGylated RNA aptamers to HIV-1 gp 120, the electrode was immersed in 1.5 mg/mL PBS solution of ethanolamine for 4 hrs to block the unreacted and nonspecific binding sites by salt formation (RCOO^- and R-NH_3^+). The CV plot of Au system gave a shape symbolic of the formation of a SAM. Evidence of resistance to electron transfer caused by SAM fabrication of the Au surface is seen in the change in the peak-to-peak separation. As expected the nanoparticles coated with aptamers presented higher affinity or binding to the HIV-1 gp 120 when compared with the non-coated nanoparticles. This result suggests that PEGylated RNA aptamers were on the surface of the PCL nanoparticles. PEGylated RNA aptamers displays higher degree of hydrophilicity and PCL is a hydrophobic polymer. In the formation of the nanoparticles employing double emulsion technique, hydrophobic polymers usually form the core. The surface charge of the nanoparticles also decreased from -17.4 ± 2.7 mV to -46.2 ± 3.0 mV, suggesting that aptamers were sticking out from the nanoparticles. In the CV experiments presented above the ramping potential was 25 mV and it was repeated for 20 cycles. The SAM remained stable during the ramping process. It maintained its stability even when the ramping potential was doubled to 50 mV for 20 cycles.

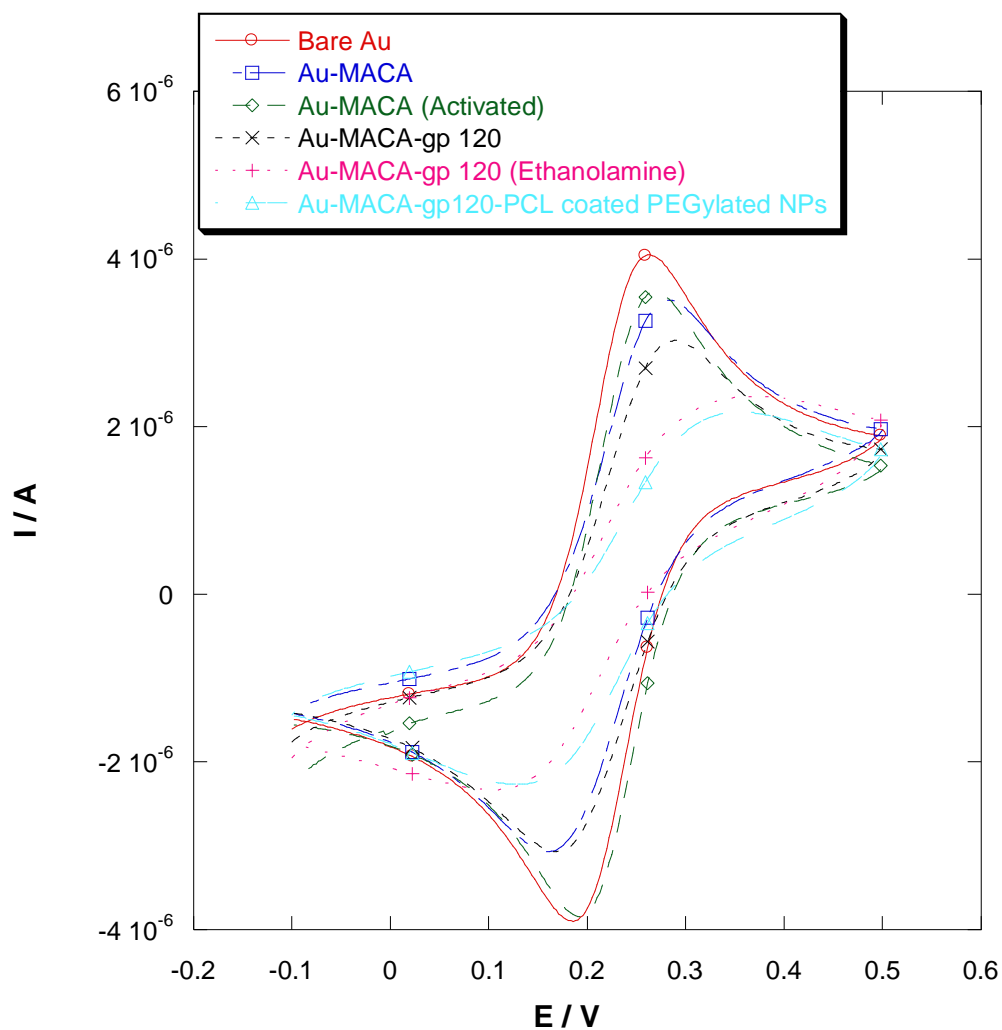


Figure 2.7: CV results obtained at the scan rate 20 mV/s. Overlay plot of CV spectra of bare Au and SAM-modified Au electrodes

EIS was also utilised to characterize the HIV-1 gp 120-Au system in relation to a bare Au and MACA-Au electrodes and determine their permissivity to single-electron transfer between the $[\text{Fe}(\text{CN})_6]^{3-}/[\text{Fe}(\text{CN})_6]^{4-}$ redox probe and Au. It offers supportive information of

the electron transfer kinetics and more detail about the actual surface-solution interface occurring during electrochemical reactions. Electro-transfer resistance is given as impedance, Z , in the alternating current EIS method. In the Nyquist plots of the Au and SAM-modified Au electrode systems investigated here, the real impedance (Z') is compared to an imaginary ($-Z''$) impedance. An alternating perturbing potential of 5 mV was applied between 10 mHz and 10 kHz at the formal potential of $E_{1/2} = 209$ mV.

Figure 2.8 displays the Nyquist plots of the gradual installation of monolayers to the bare Au electrode. A linear profile at nearly 45° angle to the horizontal axis was observed with the bare Au. This was expected as it depicts homogeneous diffusion across the unmodified Au surface. This result clearly displays an unimpeded transfer of charge between the redox probe solution and the Au. Immobilizing MACA on to the Au surface resulted in the evolution of the plot to characteristic semicircular shapes at high frequencies [**Figure 2.6**]. This is an indication of resistance of the charge transfer process. The increased resistance to electron transfer is due to the development of SAM on the Au surface. The HIV-1 gp 120 SAM plot followed a semicircular path at high frequency which then turns linear at lower frequencies. More increased resistance was also observed when ethanolamine was introduced to the surface. As expected PCL nanoparticles coated with PEGylated aptamers caused more resistance to electron transfer compared PCL nanoparticles. PCL nanoparticles resistance to electron transfer was almost comparable to when ethanolamine was immobilised to the surface. This results shows that the used aptamers had high affinity for the HIV-1 gp 120 protein.

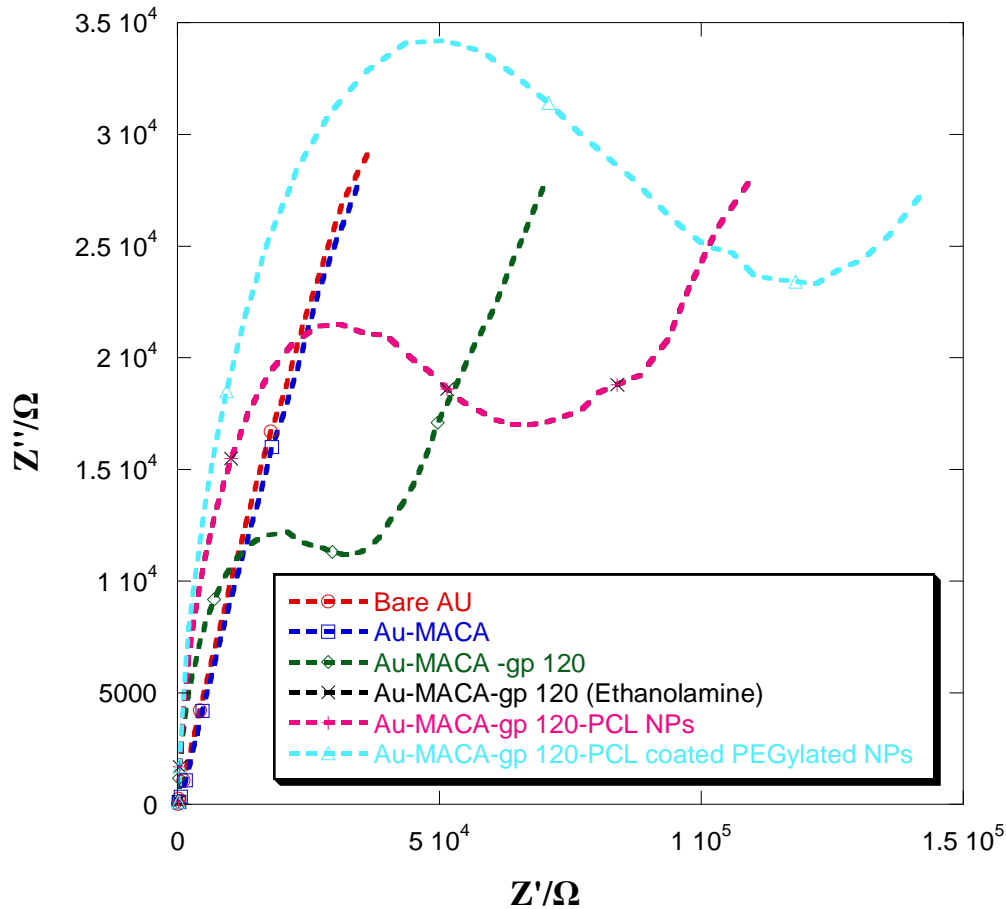


Figure 2.8: Overlay plot of Impedance spectra of bare Au and SAM-modified Au electrodes.

2.3 Conclusions

The RNA aptamers were successfully conjugated to O-(2-Aminoethyl) PEG using carbodiimide chemistry. The conjugation was confirmed by urea gel electrophoresis. PEGylated RNA aptamers showed better stability in a human breast milk than the parent aptamers. To confirm that PEGylation did not affect the aptamer ability to bind HIV-1, the TZM-bl neutralization assay was performed with the parent and PEGylated RNA aptamers.

Results showed that aptamers maintained their binding integrity *in vitro* after pegylation. Under the optimized conditions, aptamers were coated on to the surface of PCL nanoparticles using double emulsion technique. Nanoparticles of less than 150 nm were produced with a higher surface charge, showing that the nanoparticles were stable. The obtained negatively charged nanoparticles are preferred, since they may diminish the nonspecific interaction with the negatively charged PEGylated RNA aptamers, thus preserving conformation and binding characteristics (Guo et al., 2011)(Farokhzad et al., 2006). The CV and EIS experiments showed that the mercaptoacetic acid (MACA) monolayers were stable when subjected to an electrical potential. The strong attraction of gold for thiol made the functionalization of MACA convenient for immobilization of the gp 120 protein on MACA SAM. The *In vitro* binding assay showed that the nanoparticles coated with PEGylated RNA aptamers had higher affinity and specificity to HIV-1 gp 120. The overall results demonstrate that these nanoparticles could be used in HIV drug delivery applications to help minimize challenges associated with the ARVs.

3 Chapter Three:

Synthesis and characterization of PEG-MOX conjugate encapsulated into PCL nanoparticles for anti-TB application

3.1 Introduction

Major infectious diseases such as TB and malaria have not benefited much from new technological development in disease management (Zumla et al., 2013). In 2015, 10.4 million and 214 million cases of TB and malaria were recorded; respectively (WHO 2015). TB claimed 1.8 million deaths and 438 000 deaths resulted from malaria in 2015. The sub-Saharan Africa accounts for the highest morbidity and mortality. These regions continue to be the major victims of infectious diseases, even though signs of decline in the case of new infections have been observed due to awareness and treatment programmes. However, most of the drugs used are several decades old and have significant toxicity profiles which impact poor patient adherence. Thus the search for new chemical entities and advanced delivery actions are the major driving force in nanomedicine.

Nanomedicinal formulations have improved the pharmacological potentials of many drugs especially in cancer chemotherapy (Duncan, 2017)(Bobo et al., 2016)(Bertrand et al., 2015)(Venditto and Szoka, 2013)(Duncan and Vicent, 2013)(Duncan and Gaspar, 2011) (Pasut and Veronese, 2009). One major formulation method is the encapsulation of drugs in polymeric nanocarriers (Bobo et al., 2016)(Woodruff and Hutmacher, 2010)(Katata et al., 2012). The first commercially available nanoparticle drug delivery system, ABRAXANE[®], for breast cancer application was approved by FDA in January 2005 (Pillai and Ceballos-Coronel, 2013)(Ma and Mumper, 2013)(Miele et al., 2009). This drug delivery system is based on albumin-bound (nab[®]) paclitaxel, showed better and faster rate of shrinking tumors in 460 patients with metastatic breast cancer, almost double compared with solvent-based taxol[®] (Miele et al., 2009). A newer method is the covalent conjugation of drugs to polymeric carriers (Duncan, 2017)(Liechty et al. 2010)(Larson and Ghandehari, 2012)(Duncan, 2003)(Markovsky et al., 2012)(Pasut and Veronese, 2009). The anticancer drug paclitaxel has been conjugated to the

polymer polyglutamic acid (PGA; 40, 000 g mol⁻¹) through the 2' position to form an ester bond to the γ -carboxylic acid of the polymer (Duncan, 2003). The conjugate contains 37 wt% of paclitaxel and the polymer backbone is cleaved by cathepsin B to release the drug. In early clinical trials, a significant number of patients have shown partial responses or stable disease. The PGA-Paclitaxel conjugate (Opaxio[®]) is now under clinical evaluation.

In the present work we made nanomedicinal formulations of the anti-TB drug moxifloxacin (Mox). Mox is recommended by the WHO as a second-line drug for treating multidrug-resistant TB (MDR-TB) (WHO & Global Tuberculosis Programme 2016). Patients receiving this drug have a strain of *M.tb* resistant to isoniazid and rifampicin (Espinal, 2003). Treatment of MDR-TB could be as long as two years and many side effects, including hearing loss, are common (Caminero, 2006)(WHO & Global Tuberculosis Programme 2016). Failure of patient compliance to the second-line treatment regimen could lead to a more serious form of TB which is resistant to all available anti-TB antibiotics (Matteelli et al., 2014).

Mox is a relatively hydrophilic drug. The target pathological site where the *M.tb* resides is a lipid dense granuloma in the lungs [**Figure 3.1**]. The cell wall membrane is a peptidoglycan layer covalently attached to arabinogalactans (Brennan and Crick, 2007)(Chatterjee, 1997)(McNeil et al., 1990). The arabinogalactans are in turn covalently attached to the mycolic acids (Brennan, 2003). This intricate covalently linked skeleton forms an almost impenetrable cell wall fortress around the mycobacterium. Hence, a large dose will have to be administered to deliver an adequate therapeutic dose i.e. 400 mg is required for Mox. Also contrary to lipid dense granuloma surrounding *M.tb*, most anti-TB antibiotics are hydrophilic [**Table 1.5**]. This means that it will be very difficult for the drug to penetrate into this tissue region. Hence the objective of the study was to conjugate Mox onto poly(ethylene glycol) [PEG] to sterically protect the drug from degradation and to decrease toxicity to human cells. Hybrid system was formed by nanoencapsulating the PEG-Mox conjugate into poly(epsilon-caprolactone) [PCL] nanoparticles. The system constitutes the PCL, which is envisaged to increase the hydrophobicity of the PEG-Mox conjugate. The produced nanomedicinal formulations of Mox were investigated for its physico-chemical and toxicity profiles.

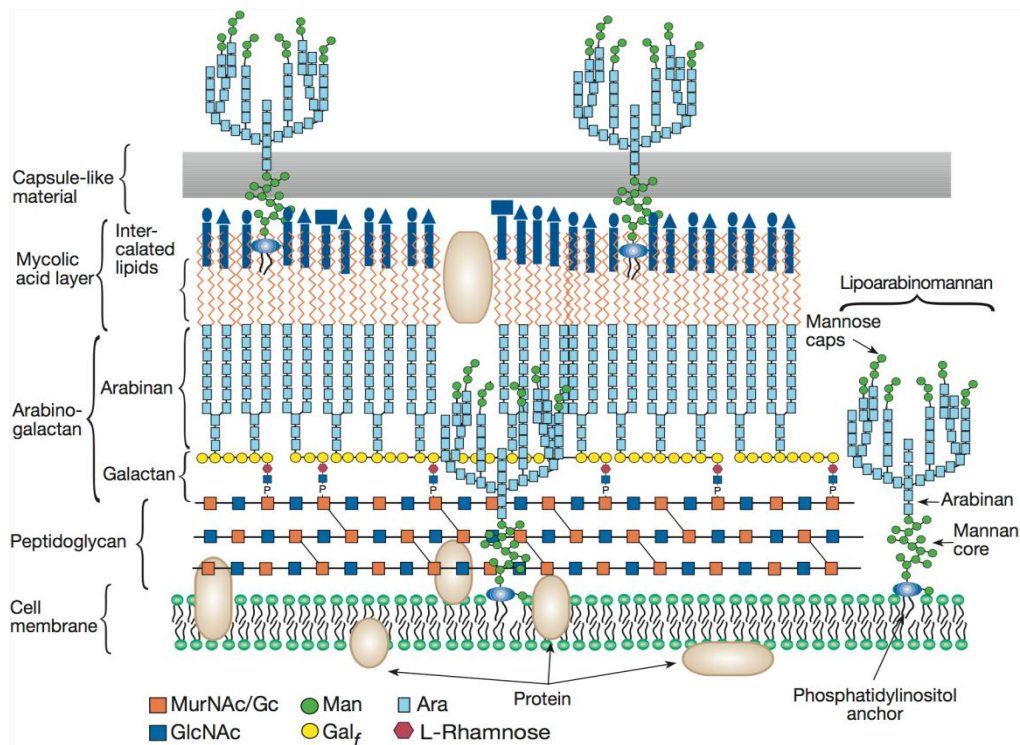


Figure 3.1: Schematic representation of the mycobacterial cell wall (Brennan and Crick, 2007).

3.1.1 Cell wall components

3.1.1.1 Peptidoglycan

The peptidoglycan component of the cell wall is a polysaccharide chain composed of alternating units of *N*-acetylglucosamine and *N*-glycolylmuramic acid units (Chatterjee, 1997). These units are crosslinked by L-alanyl-D-isoglutaminyl-meso-diaminopimelyl-D-alanine peptide chains linked to the lactoyl groups of muramic acid residues. While the peptidoglycan, Alay, is common in most plasma membrane of most bacteria. The mycobacterial peptidoglycan differs since the muramic acid residues are *N*-glycolylated with glycolic acid rather than *N*-acetylated (Azuma et al, 1969). Also the cross-linkages contain a percentage of bonds between two residues of diaminopimelic acid as well as between diaminopimelic acid and D-alanine. Peptidoglycan is known to protect the *Mycobacterium* from degradation (Chatterjee, 1997).

3.1.1.2 Arabinogalactan

Arabinogalactan is a distinctive polysaccharide consisting of linear galactan chains composed of alternating D-galactofuranoses and D-arabinofuranoses (Besra and Brennan,

1997)(Chatterjee, 1997). The D-galactofuranoses and D-arabinofuranoses are extremely rare in nature. The non-reducing termini of arabinan constitute a branched hexaarabinofuranosyl structure. Arabinogalactan is attached through mycobacterial peptidoglycan structure through a phosphodiester linkage between C6 of muramic acid residues (10-12%) and a disaccharide linker unit attached to the non-reducing terminus of the galactan.

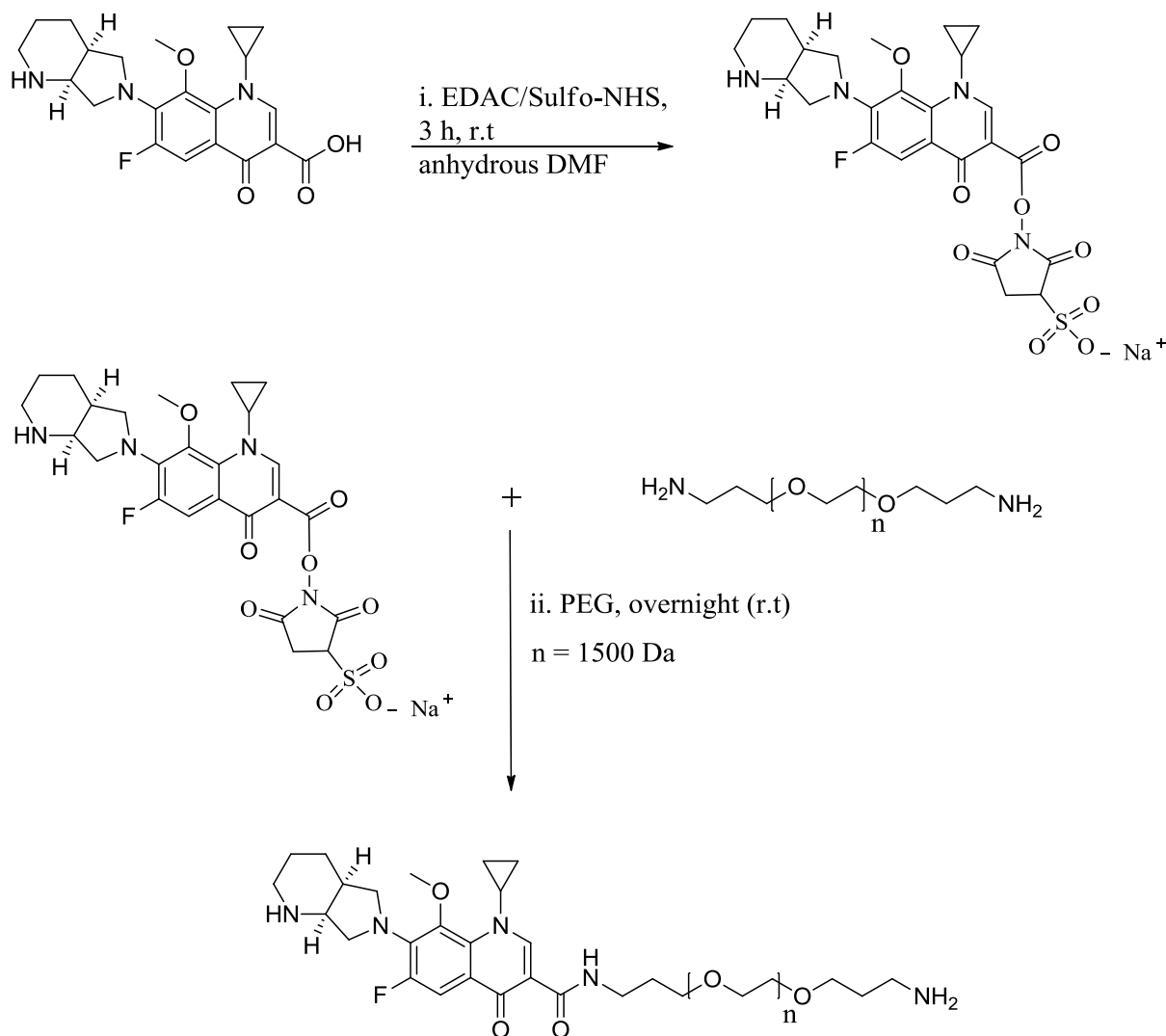
3.1.1.3 Mycolic acids

Mycolic acids are high molecular weight α -branched β -hydroxylated fatty acids (Besra and Brennan, 1997)(Barry 3rd et al., 1998). They contain 70 to 90 carbon atoms and occur either as tetramycolylpentaarabinofuranosyl clusters on the arabinan portion of mycolylarabinogalactan or as extractable lipids, mainly as trehalose 6,6'-dimycolate. Mycolic acids are major and specific lipid components of the mycobacterial cell envelope, constituting more than 50% by weight of the mass of the cell-wall core (Brennan and Crick, 2007). They act together through powerful cumulative hydrophobic interactions to form a lipid shell surrounding the organisms. This hydrophobically-linked skeleton affords a three dimensional matrix, low permeability of the cell wall, and unquestionably accountable for the notorious “lipid complex” and consequent endogenous resistance to many drugs (Jarlier et al., 1991) (Brennan and Crick, 2007).

3.2 Results and discussions

PEGylation, the conjugation of small molecules to PEG, has become a well-established prodrug delivery system (Li et al. 2013)(Banerjee et al., 2012). Such prodrug conjugations are primarily developed to increase half-life due to reduced kidney clearance, protect the drug against enzymatic degradation and minimise toxicity due to biocompatibility of the polymer (Pasut and Veronese, 2009)(Kopeček, 2013). PEGylation is also known to enhance water solubility of the respective drugs, particularly relevant for drugs with low aqueous solubility (Markovsky et al., 2012)(Pasut and Veronese, 2009)(Larson and Ghandehari, 2012). In this study, Mox was covalently conjugated to the terminal NH_2 groups of linear PEG-amine using carbodiimide chemistry (Khandare and Minko, 2006)(Tukulula et al., 2015). In the synthesis of PEG-Mox conjugate [Scheme 3.1], the active carboxylic acid group of Mox dissolved in DMF was activated using EDAC/Sulfo-NHS as coupling reagent. After 3 hours of activation, Mox-succinimide was added dropwise to a solution of PEG- NH_2 and left overnight to yield a

golden yellow crude solution. DMF was removed under reduced pressure and the crude compound was precipitated from cold ether. The pellet was washed several times with cold ether, re-dissolved in PBS buffer (pH 7.4) and freeze-dried to obtain the PEG-Mox conjugate as a yellowish powder.



Scheme 3.1: Synthesis of PEG-Mox conjugates using carbodiimide chemistry.

3.2.1 NMR analysis

PEG-Mox conjugate was readily synthesized via two steps as illustrated in **Scheme 3.1**. Conjugation of Mox to the PEG was confirmed by ¹HNMR. ¹HNMR spectrum of Mox shows distinctive aromatic protons as singlet at 8.71 ppm and 3J coupling (between F and H) resulting

in a doublet at 7.27 ppm [Figure 3.2]. A multiplet at 1.24 to 0.90 ppm corresponding to $-\text{CH}_2$ of cyclopropane. Piperazine protons were observed as a multiplet at 3.92 to 3.64 ppm and 3.36 to 1.78 ppm. A singlet at 3.53 ppm was due to methoxy group, thus confirming the identity of Mox (Sadeek et al., 2011a). The characteristic methylene protons of PEG backbone as a multiplet were observed at 3.61 ppm [Figure 3.3]. A triplet at 2.97 ppm and 2.71 ppm were attributed to the methylene protons next to the ether and NH_2 groups; respectively. The triplet of triplet appeared at 1.69 ppm [see Figure 3.3]. The typical signals of both the Mox and PEG were observed in the spectrum of the product (PEG-Mox conjugate); using CDCl_3 as the solvent [Figure 3.4]. Mox is completely insoluble in chloroform. However the conjugate was completely soluble due to the inherent properties of PEG polymer. PEGs are readily soluble in polar and non-polar solvents. The broadening of the signals further confirmed the successful conjugation of Mox to PEG.

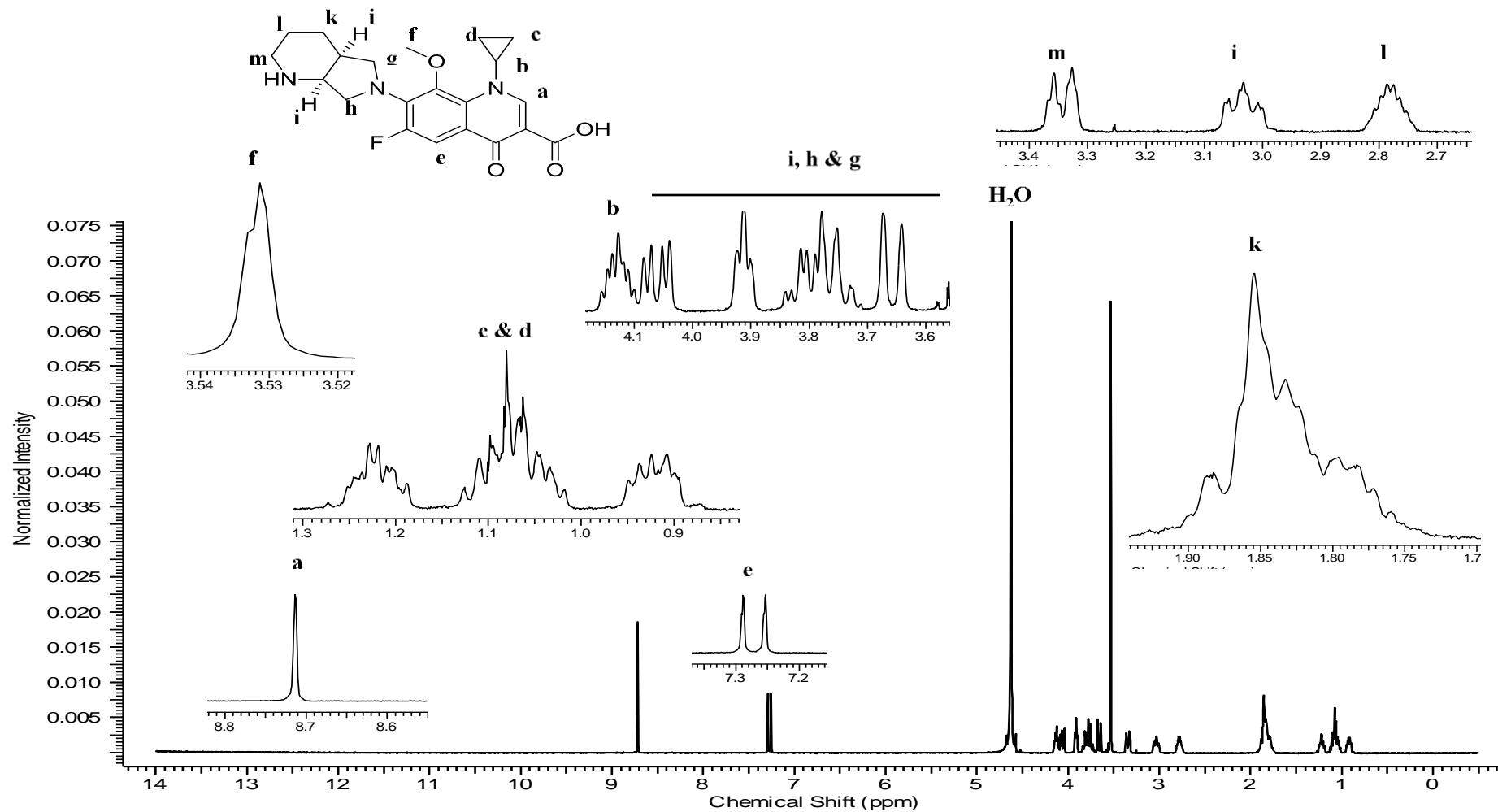


Figure 3.2: Proton NMR spectra of (A) Mox (D₂O).

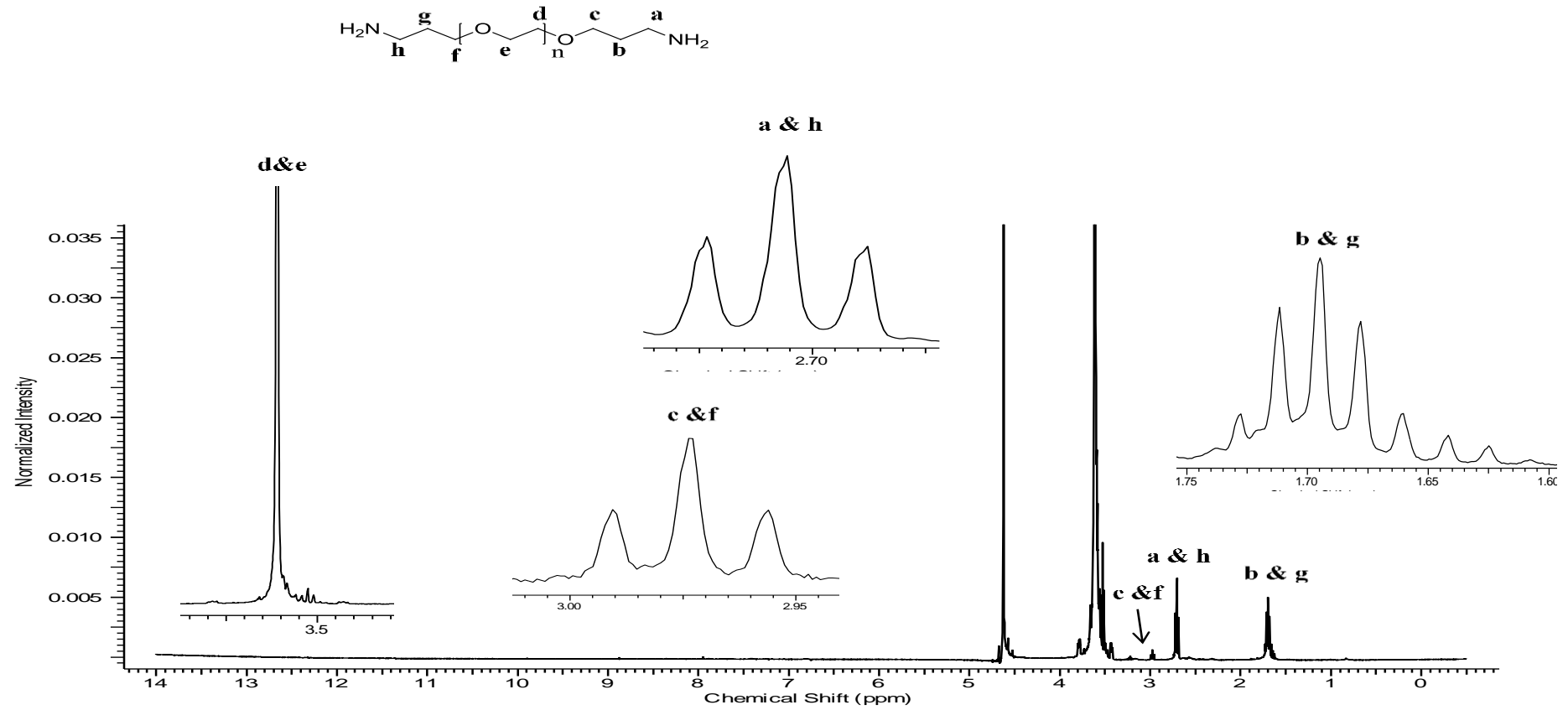


Figure 3.3: Proton NMR spectra of PEG (D₂O)

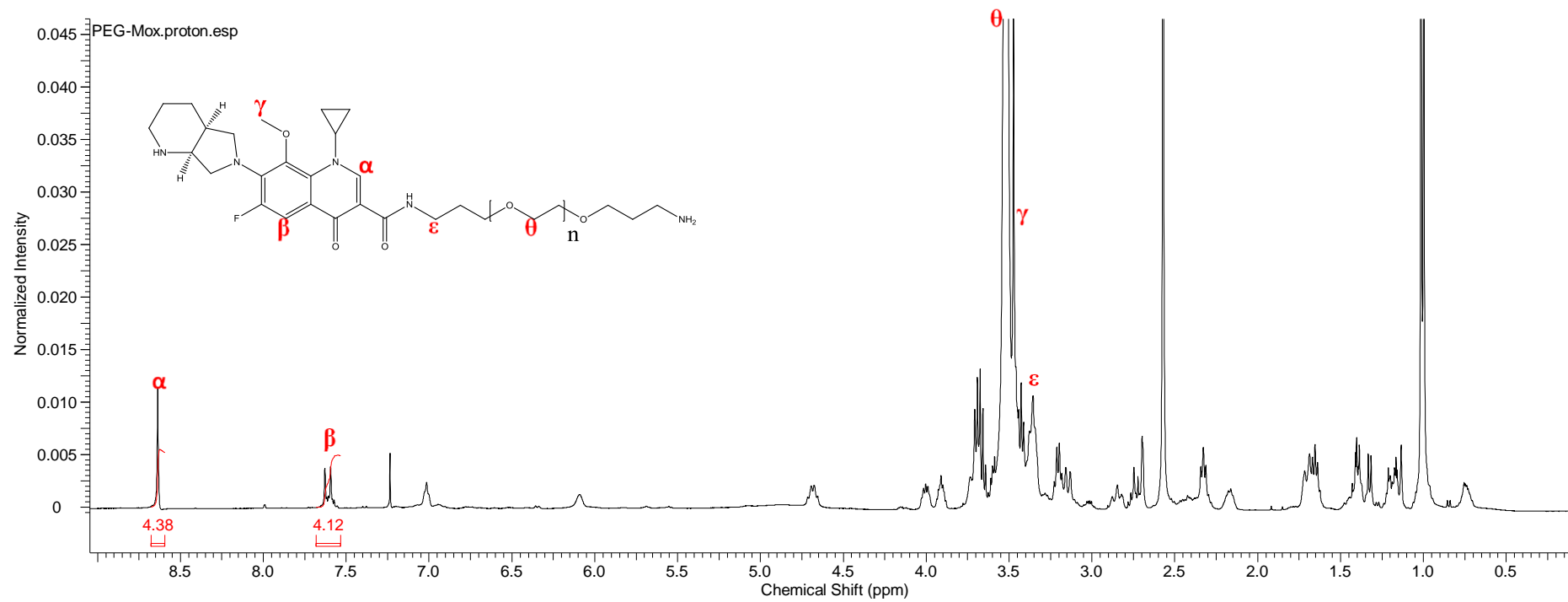


Figure 3.4: Proton NMR spectra of PEG-Mox conjugate (CDCl₃).

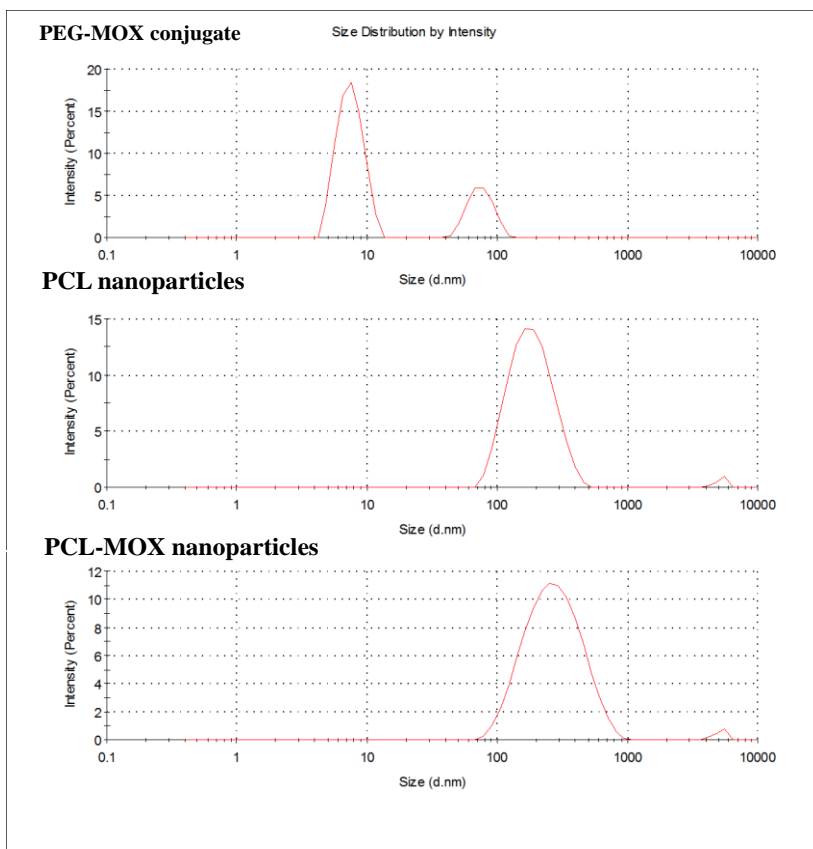
3.2.2 Particle size, zeta potential, morphology and encapsulation efficiency

In order to increase the hydrophobicity, PEG-Mox conjugate was further nanoencapsulated into PCL nanoparticles using double emulsion spray-drying technique (L Tshweu *et al.*, 2013). **Table 3.1** presents the average particle size, PDI and zeta potential of the synthesised polymer conjugate and nanoparticles. PEG-Mox conjugate showed distributions of two average particle sizes of 8 nm and 76 nm [**Figure 3.5**]. The PDI was observed to be 0.19. PCL nanoparticles displayed spherical particles with an average particle size of 174 ± 10 nm and PDI of 0.22 ± 0.02 [**Figure 3.5**]. Encapsulation of PEG-Mox conjugate into PCL nanoparticles increased the particle size to 242 ± 4 nm (Spherical in shape). Irrespective of the influence of the PEG-Mox conjugate on the average particle size of the nanoparticles, PDI of 0.24 ± 0.01 was obtained, signifying homogeneous size distribution (Katata *et al.*, 2012). The %EE was found to be 60%, similar results were obtained by Mahor *et al.* 2016, when Mox (not conjugated) was encapsulated into gelatin nanoparticles. Zeta potential is a critical factor to examine the long-term stability of the nanoparticles. High values of zeta potential (± 13 mV) prevents particle agglomeration due to electrostatic repulsion (Das *et al.*, 2011). The overall nanoparticles displayed zeta potential of more than -20 mV.

Table 3.1: Properties of PEG-Mox conjugates, PCL nanoparticles and PCL-Mox nanoparticles (data represent mean \pm SD, n = 3).

Formulation	Particle size (nm)	PDI	Zeta potential (mV)
PEG-Mox conjugate	8 ± 4 & 76 ± 10	0.19 ± 0.04	N/A
PCL nanoparticles	174 ± 10	0.22 ± 0.02	-20 ± 0.4
PCL-Mox nanoparticles	242 ± 4	0.24 ± 0.01	-23 ± 0.9

(A)



(B)

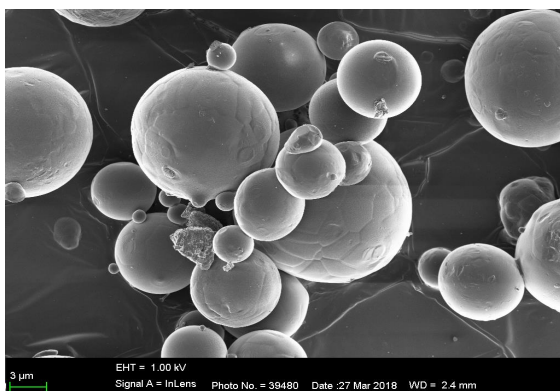


Figure 3.5: (A): Average particle size of PEG-Mox conjugate, PCL nanoparticles and PCL-Mox nanoparticles. (B) SEM image of PCL-Mox nanoparticles.

3.2.3 Attenuated total reflectance/Fourier transform-infrared spectroscopy (ATR-FTIR)

ATR-FTIR spectra of PEG, PCL, Mox, PEG-Mox conjugate and PCL-Mox nanoparticles are presented in **Figure 3.6** and **Figure 3.7**. The conjugation of Mox to PEG was further confirmed by the formation of the amide bond around 1779.9 cm^{-1} [**Figure 3.6**]. The ATR-FTIR analysis of PCL, PCL nanoparticles and PCL-Mox nanoparticles showed the characteristic peak of the PCL polymer at around 1722.4 cm^{-1} and 1728.4 cm^{-1} due to the C=O stretching vibration [**Figure 3.7**]. The obtained results were in agreement with the literature (Persenaire et al., 2001)(Wu, 2005)(Sahoo et al., 2010). Spectra of pure Mox presented functional bands at 1704.7 cm^{-1} due to carboxylic acid C=O stretching vibration, C-H bonding for the substituted benzene at 1875 cm^{-1} , stretching at 1621.6 cm^{-1} , 1514.6 cm^{-1} and 1453.4 cm^{-1} due to aromatic C=C, and C-N banding at 1320 cm^{-1} (Mahor et al., 2016). Weak distinctive functional bands of Mox or PEG-Mox conjugate were also found in the spectra of PCL-Mox nanoparticles, suggesting that most of the Mox conjugates were nanoencapsulated into the nanoparticles. Slight shifts in the functional bands originate from the fact that Mox was amorphized during the processing (see XRD results).

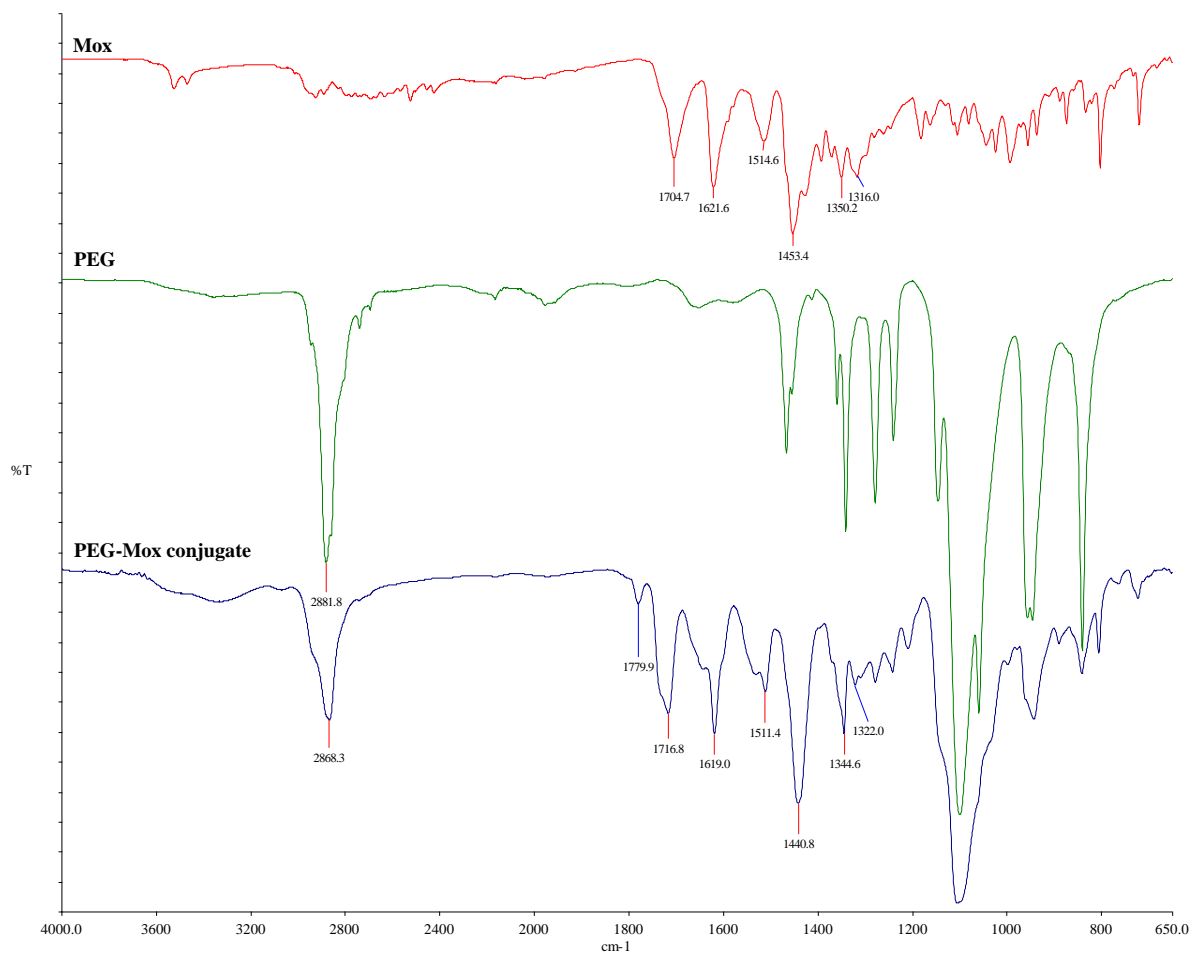


Figure 3.6: FTIR spectra of Mox, PEG and PEG-Mox conjugate



Figure 3.7: FTIR spectra of Mox, PCL, PCL nanoparticles, and PCL-Mox nanoparticles.

3.2.4 X-ray diffraction (XRD) analysis

XRD spectroscopy was used to evaluate the crystallinity and amorphousness of the synthesised nanoparticles [Figure 3.8]. PCL showed two sharp peaks at about 21.3° and 23.9°, as reported by Wu 2005. The peaks are triggered by scattering from crystalline region and the hump due the amorphous region (Young and Lovell, 1991). The diffractogram of Mox showed multiple peaks, an indication of crystalline material. XRD patterns of all the synthesised nanoparticles (PCL nanoparticles and PCL-Mox nanoparticles) presented a broad hump and the lack of any sharp peaks over the entire 2 theta. The results showed that the spray-dried nanoparticles were amorphous. Drug molecules on the surface are less constrained in their thermal movement and weakly bound than molecules within the crystal lattice, thus leading to a decrease of the crystallinity due to higher surface area of the

produced nanoparticles (Schmidt et al., 1998). These results together with the complementary average particle size, %EE, SEM and ATR-FTIR stress the benefit of the double emulsion spray-drying method for the synthesis of amorphous nanoparticles without changing chemical integrity of the materials.

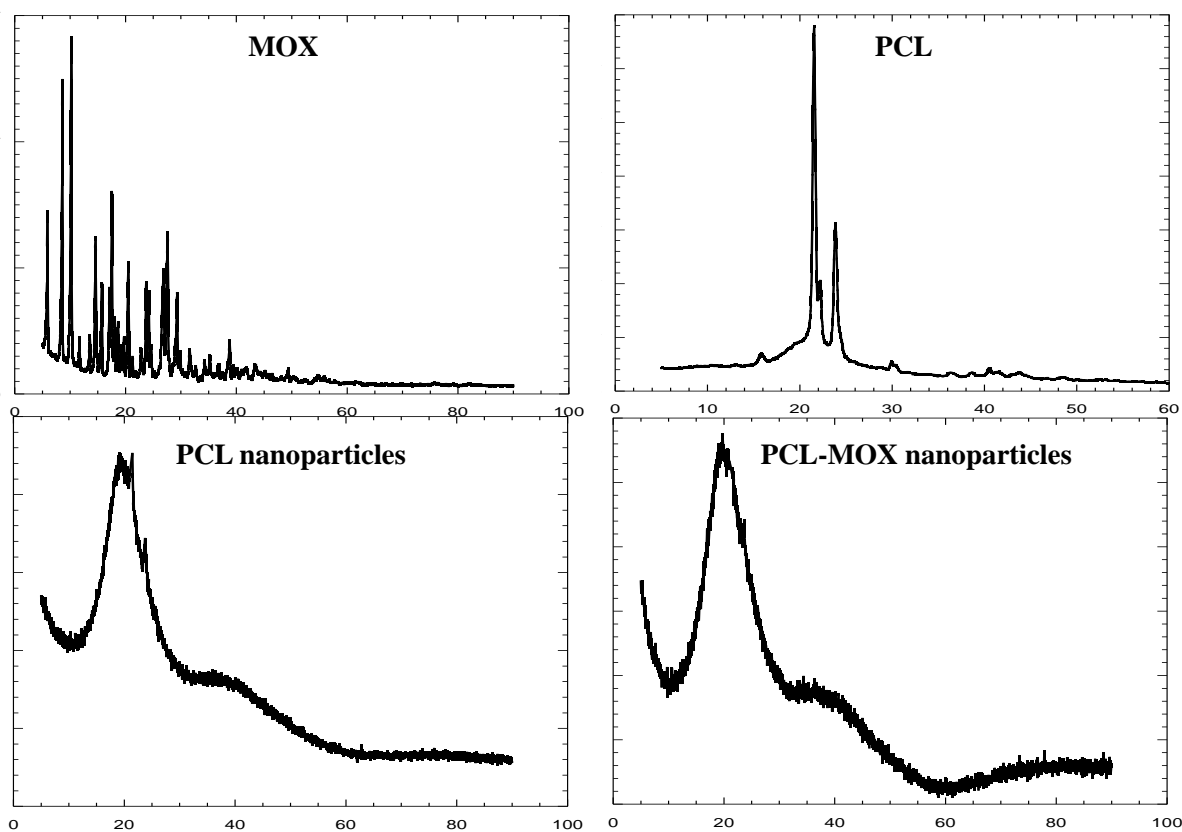


Figure 3.8: X-ray diffraction patterns of Mox, PCL, PCL nanoparticles and PCL-Mox nanoparticles. X-axis represent 2 theta (degree).

3.2.5 Thermogravimetric Analysis (TGA) studies

Figure 3.9 presents the TGA thermograms of the PEG, Mox, PEG-Mox conjugate, PCL, PCL nanoparticles and PCL-Mox nanoparticles. All the samples showed an initial weight loss of about 3% to 6% attributed to the loss of water or moisture. PEG-NH₂ underwent rapid decomposition from 320 to 430 °C with weight loss of about 89% attributed to the loss of the

capped regions and oxidized products of ethylene glycol (Guan et al., 2009). Mox decomposition occurred in several stages following a similar trend of decay as reported by Sadeek et al. 2011. Apart from the initial loss in moisture, the first degradation occurred from 230 to 350 °C, the second from 350 to 500 °C and final decomposition occurring from 500 to 700 °C contributing to a total weight loss of 83% (Sadeek et al., 2011a)(Sadeek et al., 2011b). PEG-Mox conjugate followed a similar route of decomposition compared to Mox. Decomposition from 210 to 400 °C was gradual in comparison to the drastic weight loss from 400 to 435 °C and a plateaued decomposition from 435 to 700 °C

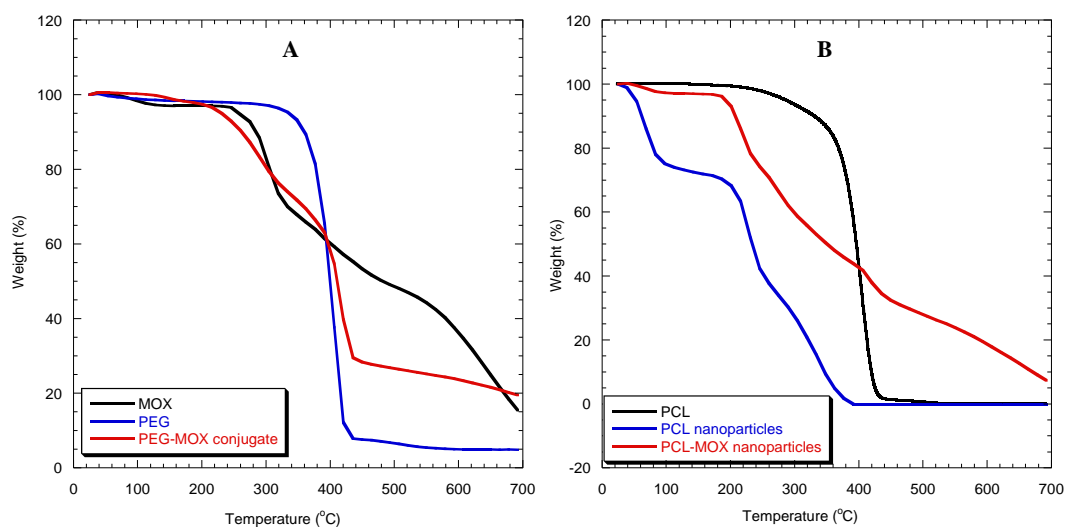


Figure 3.9: TGA thermograms of (A) Polymer conjugates, (B) Polymer nanoparticles.

TGA curve of pure PCL showed that polymer was thermally stable until 136.27 °C. The weight loss of PCL polymer occurred in 3 steps at temperature of 345.09 °C, 428.64 °C and 509.48 °C with a weight loss of 12.24%, 84.28% and 2.89%, respectively, attributed to thermal decomposition. Both the PCL nanoparticles and PCL-Mox nanoparticles showed low thermal stability when compared to the pure PCL polymer. This may be due to the fact that the nanoparticles have a greater superficial area, since they are more reactive than the polymer; consequently the thermal decomposition tends to occur much faster (Mainardes et al., 2006). The residual moisture of the PCL nanoparticle and PCL-Mox nanoparticles was

ranging from 4.28 to 4.26%; respectively. The results obtained are in agreement with the reported values of spray-dried particles, which range from 2% to 15% (Li et al., 2010)(Arpagaus et al., 2010).

3.2.6 Hemolysis study

Red blood cells (RBCs), nature's long circulating delivery vehicles (Hu et al., 2011) represent the most vital cellular essential of the blood (>99%) and play a significant part in drug delivery of nanoparticles (Pan et al., 2016)(Muzykantov, 2011). RBCs resistance to mechanical stress is one of the key physiological features that contribute to RBC longevity in the bloodstream. Hemodynamic stress can cause mechanical damage to RBCs, resulting in rupture of the cell's membrane which leads to hemolysis (Pan et al., 2016). **Figure 3.10** presents the percentage hemolysis of Mox, PEG-Mox conjugate, PCL-Mox nanoparticles and PCL nanoparticles against the RBCs evaluated by the hemolysis assay. The conjugates, nanoparticles and controls, PBS (negative control) and 1% Triton-100 (positive control), a detergent that disrupts cell membranes, was incubated with human RBCs suspension at 37 °C for 30 min; respectively. Hemolysis of the erythrocytes was determined by Abbotta Kinetic Spectrophotometer at $\lambda = 540$ nm based on haemoglobin release. PBS displayed no spontaneous erythrocytes lysis after incubation with the RBCs. As a result it was assumed that incubation with 1% Triton-100 will yield 100% erythrocytes lysis. As expected Mox exhibited dose-dependent haemolytic properties, and the haemolytic tendency significantly increased with the concentration. For example, at the concentration of 1 mg/mL, 0.5 mg/mL and 0.25 mg/mL, the percentage hemolysis induced by Mox were 89.0 ± 3.1 , 85.2 ± 1.9 and 54.9 ± 2.5 ; respectively. However, that induced by PEG-Mox conjugate and PCL-Mox nanoparticles were 16.2 ± 0.5 , 13.5 ± 0.2 , 9.4 ± 0.1 and 21.7 ± 1.5 , 14.3 ± 0.2 and 9.7 ± 0.2 ; respectively. These results show that PEG-Mox conjugate and PCL-Mox nanoparticles were found to be hemocompatible, inducing only minimal hemolysis as compared to free Mox. As expected PCL nanoparticles were hemocompatible across the tested concentrations, showing that PCL is a biocompatible polymer (Woodruff and Hutmacher, 2010) [**Figure 3.10**]

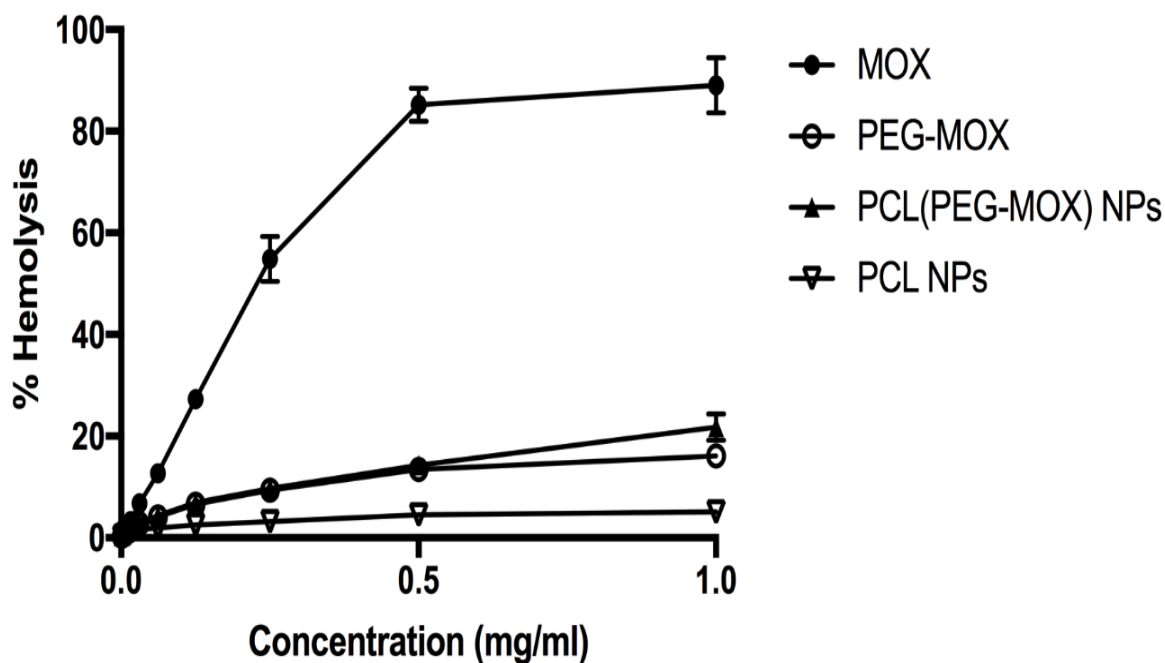


Figure 3.10: *In vitro* erythrocytes lysis with Mox, PEG-Mox conjugate, PCL(PEG-MOX) NPs = PCL-Mox nanoparticles and PCL nanoparticles incubated with human RBCs suspension for 4 hrs at 37 °C. Data represent mean \pm SD, n = 3.

3.2.7 Cytotoxicity

The *in vitro* cytotoxicity of Mox, PEG-Mox conjugate and PCL-Mox nanoparticles against MDBK cell lines were assessed by MTT assay. The MTT assays are primarily used to provide critical information about the toxicological profile of new chemical entities and help to avoid the unwanted exposure of animals to toxic materials. In the present study MDBK cell lines were used as they have definite cell junction, polarity and a rapid growth rate (Trif et al., 2015). In several studies MDBK cell lines have been utilised as an alternative model to Caco-2 cells (Lai et al., 2008).

Figure 3.11 presents the cytotoxicity of the studied materials. MTT assay results showed that Mox exhibited observable toxicity than PEG-Mox conjugate and PCL-Mox nanoparticles in the range of tested concentrations. It is also apparent that at the highest concentration tested i.e 1 mg/ mL, PEG-Mox conjugate and PCL-Mox nanoparticles induced cytotoxicity of less

than 50%, while the free Mox presented cytotoxicity of 96.22%. This finding further supports the hemolysis studies. PCL nanoparticles did not show any sign of hemolysis, thus it was expected that PCL-Mox nanoparticles will exhibit lower toxicity than the free Mox. These results further support that Mox was conjugated to PEG. PEG is known to lower toxicity of small molecules.

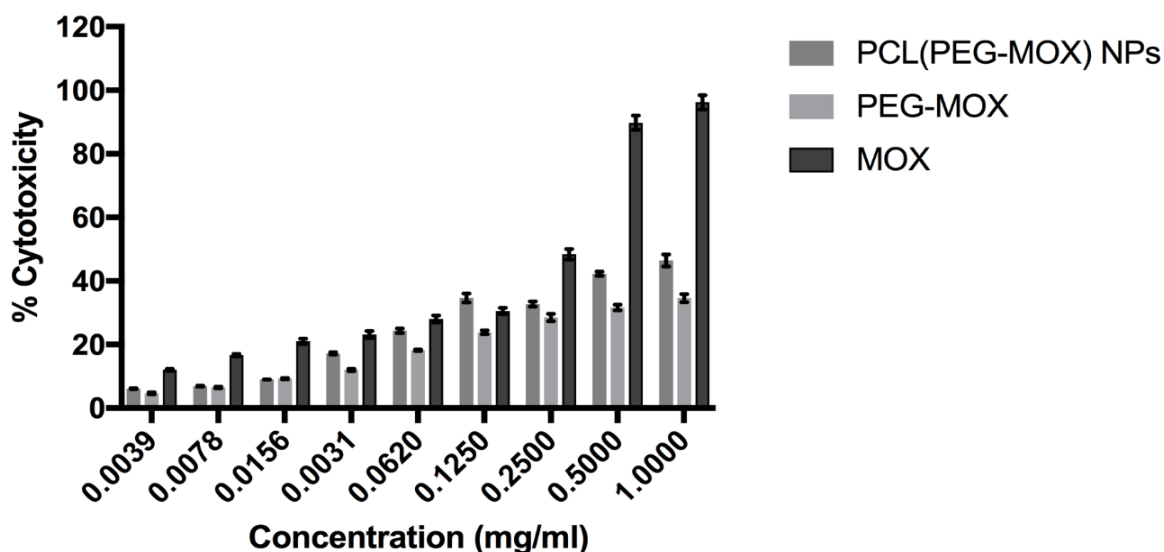


Figure 3.11: *In vitro* cell viability of Mox, PEG-Mox conjugate and PCL-Mox nanoparticles measured by MTT assay. NPs = nanoparticles. Data represent mean \pm SD, n = 3.

3.2.8 Plasma stability studies

The stability of therapeutic compound in plasma is important for maintaining adequate drug concentration as slight metabolism can change bioavailability of the drug (Hartman, 2003). Therapeutic compounds with functional groups such as esters, amide, carbamides, lactams and sulphonamides are susceptible to hydrolysis due to enzymes present in plasma (Rehman et al., 2016)(Konsoula & Jung. 2009)(Di et al. 2005). Unstable compounds tend to display rapid clearance and short half-life resulting in poor *in vivo* performance (Di et al. 2005).

Figure 3.12 presents *in vitro* stability of PCL-Mox nanoparticles in human plasma. Plasma stability was explored at a concentration of 1 mg/mL, 3 mg/mL and 5 mg/mL. As expected, the release of Mox from the PCL-Mox nanoparticles in the presence of plasma was slower than PEG-Mox. This is due to the fact that before double emulsion spray-drying was carried out; Mox was firstly conjugated to PEG via a stable amide bond. PEG-Mox conjugate was then nanoencapsulated to form a hybrid system consisting of hydrophobic PCL nanoparticles onto the surface. The release of Mox is therefore not only governed by diffusion from the nanoparticles but also the cleavage of the amide bond between the drug and the PEG. The hydrolysis of amides is slower than that of the esters such that amides are typically excreted in the urine unchanged (Hartman, 2003). However in the case of PEG-Mox conjugate, PEG is capable of sterically preventing the approach of destabilizing plasma components towards the surface of the PCL-Mox nanoparticles, thus reducing their specific interaction with the plasma membrane and increasing the circulation of Mox in the system (Heiati et al., 1998). It is worth mentioning that most of the release was due to PEG-Mox conjugate on the surface of the nanoparticles since only 60% was nanoencapsulated (see **section 3.2**). Our results are in agreement with the literature (Letchford et al., 2009)(Heiati et al., 1998).

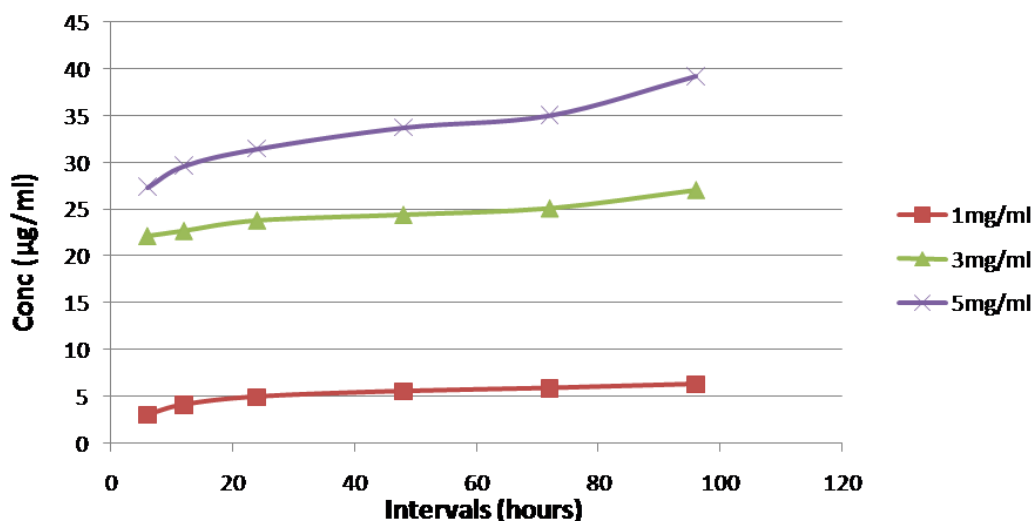


Figure 3.12: The *in vitro* stability of PCL-Mox nanoparticles in human plasma.

3.3 Conclusions

Mox was covalently conjugated into PEG via a releasable amide bond. This is the first study that illustrated the inclusion of such polymer-drug conjugate into PCL nanoparticles with improved physico-chemical properties of the drug. Compared to free Mox, PEG-Mox conjugates and PCL-Mox nanoparticles were found to be hemocompatible, inducing only minimal hemolysis. PCL nanoparticles were hemocompatible across the tested concentrations, showing that the polymer is biocompatible, biodegradable and non-toxic. *In vitro* cell viability by MTT assay complemented the hemolysis assay. Mox was more toxic than PEG-Mox conjugate and PCL-Mox nanoparticles. *In vitro* stability in human plasma showed that PCL-Mox nanoparticles were stable for over 72 hrs. The nanoparticles were stable due to PEG. PEG is known to increase blood circulation of the conjugates/nanoparticles. Data obtained emphasises that PCL nanoparticles could be used as a drug delivery system to minimise the high toxicity of TB drugs. PCL is readily available at a relatively low cost (Woodruff and Hutmacher, 2010). It would facilitate the nanoencapsulation of other anti-TB drugs in the same nanoparticles that would simplify drug administration by oral route and increases patient adherence. Studies are underway to examine the pharmacokinetic profile of the produced PCL-Mox nanoparticles.

4 Chapter Four:

Synthesis and characterization of polymer based lumefantrine conjugates for anti-malarial application

4.1 Introduction

Malaria continues to be one of the deadliest infectious diseases. Historically, it has afflicted virtually every region of the globe but today its greatest morbidity and mortality are largely limited to tropical regions (Mischlinger et al., 2016)(Gazzinelli et al., 2014)(Santos-Magalhães and Mosqueira, 2010)(Antoniana U Krettli and Miller, 2001)(WHO 2005). According to the WHO data, over 90% of clinical malaria cases occur in Africa and the majority of these cases are paediatric (Mischlinger et al., 2016)(WHO 2015).

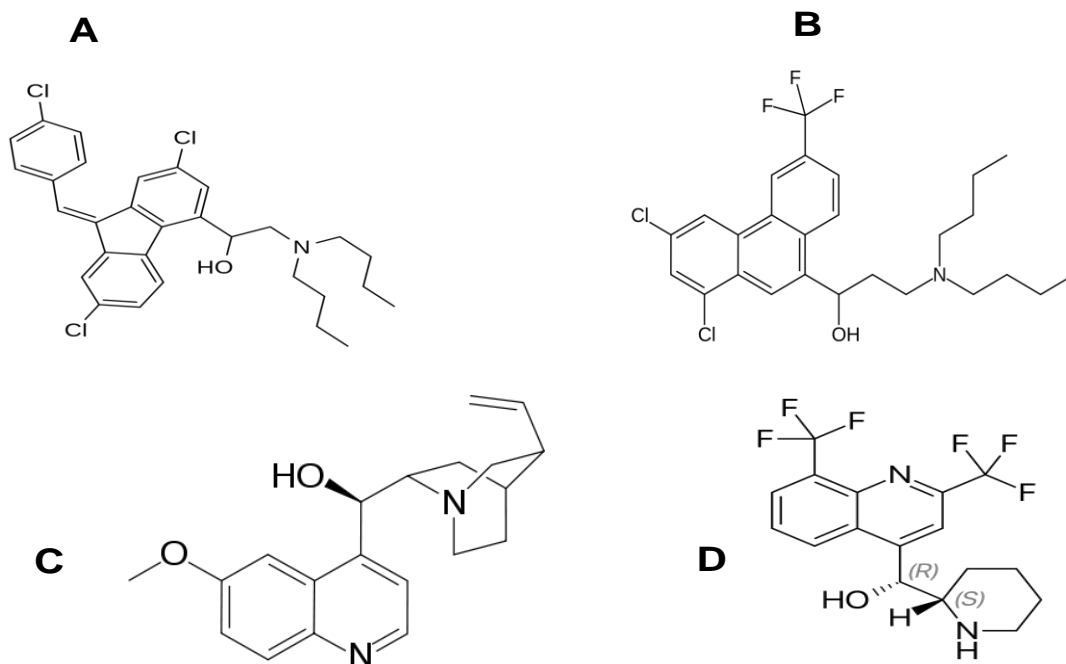
For centuries malaria has been a curable disease (WHO 2005)(Antoniana U Krettli and Miller, 2001). The chemotherapy of malaria has seen several generations of treatment regimens (Souto, 2012)[**Table 4.1**]. Each generation has terminated with the development of resistance by the *Plasmodium* parasite (Souto, 2012)(Santos-Magalhães and Mosqueira, 2010) (WHO, 2010)(Talisuna et al., 2004). The current WHO-approved treatment is Artemisinin Combination Therapy (ACT) (Mischlinger et al., 2016)(WHO 2015)(Alessandro, 2009)(Nosten and White, 2007). The combination therapy is based on the administration of an artemisinin-based drug with another agent, often an aryl-alcohol chemical class of drugs (Mischlinger et al., 2016)(Cui & Su 2009)(Santos-Magalhães and Mosqueira, 2010).

Artemisinin and its derivatives provide rapid relief of clinical symptoms but must be co-administered with a slower acting agent when treating uncomplicated malaria (WHO 2015)(Ramharter et al., 2008)(Koram et al., 2005). The most widely used co-drug is lumefantrine [Lumf] (Souto, 2012) (Santos-Magalhães and Mosqueira, 2010)(Krudsood et al., 2003)(Van Vugt et al., 1999). It acts for several days clearing remnants of parasites in the blood (Santos-Magalhães and Mosqueira, 2010)(Makanga and Krudsood, 2009)(Ezzet et al., 1998).

Lumf is an aryl-amino alcohol related to quinine, mefloquine, and halofantrine as depicted in **Scheme 4.1** (Souto, 2012). It is used in combination with artemether and marketed as coartem[®] (Makanga and Krudsood, 2009). Lumf has a \log_p (octanol-water partition coefficient) of 8.34 (Huang et al. 2012.), and is classified as a class II compound in the Biopharmaceutical Classification System (BCS) (Lindenberg et al., 2004), denoting that it has low solubility and high permeability. It is metabolized by cytochrome P450 3A4 (CYP450 3A4) to desbutyl lumefantrine (Kloprogge et al., 2015)(Wong et al., 2011)(White et al., 1999). Owing to its long half-life of 3 to 6 days (Makanga and Krudsood, 2009)(White et al., 1999)(Ezzet et al., 1998), Lumf is responsible for eliminating residual parasites that may have remained after dihydroartemisinin (DHA, active metabolite of artemether) has cleared from the body (Makanga and Krudsood, 2009).

Table 4.1: Antimalarial drugs based on chemical structure.

Chemical family	Drugs
4-Aminoquinolines	Chloroquine, amodiaquine, piperaquine
Amino-alcohols	Quinine, quinidine, mefloquine, halofantrine, lumefantrine
Sulfonamides and sulfones	Sulfadoxine, sulfalene, dapson
Biguanides	Proguanil, chlorproguanil
Diaminopyrimidine	Pyrimethamine
8-Aminoquinoline	Primaquine
Sesquiterpene lactones	Artemisinin, arteether, artemether, artesunate, dihydroartemisinin
Naphthoquinone	Atovaquone
Antibiotics	Azythromycin, clindamycin, doxycycline, tetracycline



Scheme 4.1: Chemical structure of (A) Lumefantrine, (B) Halofantrine, (C) Quinine and (D) Mefloquine

Complicated malaria, or instances where the patient is incapable of orally ingesting the ACT drugs, is first treated with an injectable form of artemisinin (WHO 2015)(WHO 2005)(Li and Weina, 2010). Artesunate, the hemisuccinate derivative form of DHA, is injected intravenously (I.V). This treatment is accompanied by a full oral ACT course (WHO 2015). The use of a combination with Lumf as an I.V.-administered treatment is precluded because Lumf is virtually insoluble in water.

Insolubility of drugs is often tackled by introducing chemical functionalities onto the compound structure (Zhao et al., 2012)(Yogeeswari and Sriram, 2005). While the desired solubility may be achieved by this method it also is highly vulnerable to destroying the attractive pharmacological and therapeutic properties of the parent compound. Toxicity might increase, potency might be lost or dosages might change.

Nanomedicinal drug delivery technology using polymers offers an alternative route to increase solubility which ensures that the parent compound is not irreversibly altered (Duncan, 2017)(Duncan & Gaspar 2011)(Duncan, 2003). Drugs with conjugable functional groups like

hydroxyls (-OH), amino (-NH₂), carboxylic (-COOH), and thiols (-SH) offer facile conjugating points to polymers. Lumf has a single hydroxyl group which can reversibly be linked via an ester linker to a polymer functionalized with a carboxylic group. In this chapter, Lumf was thus linked to hydrophilic polymers.

4.2 Results and Discussion

4.2.1 Synthesis and characterization of novel lumefantrine conjugates

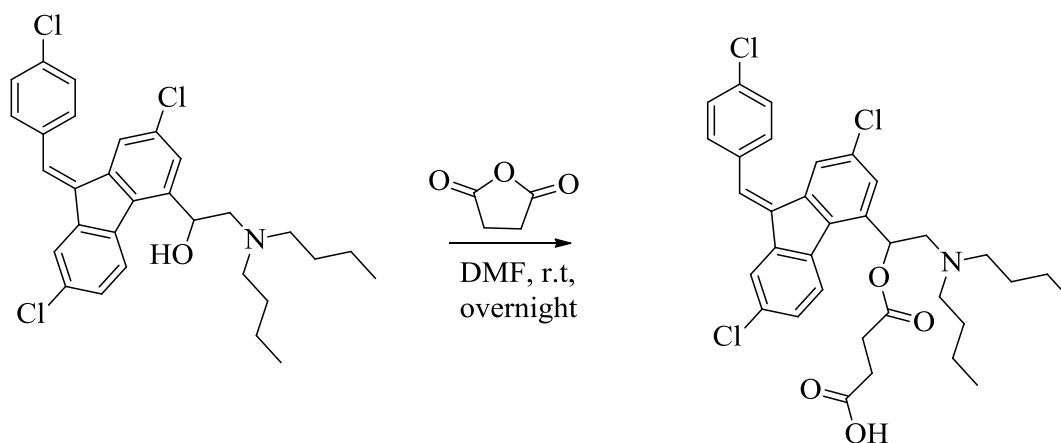
The solubility and chemical nature of a drug plays a major role in the development of polymer-drug conjugates (Larson and Ghandehari, 2012). Polymer-drug conjugation approaches consist of transient alteration of the physicochemical properties of a given drug through chemical modification. Such impermanent chemical derivatization is usually intended to change biodistribution and aqueous solubility whereas the intrinsic pharmacological properties of the parent drug remain intact (Kopeček, 2013)(Duncan and Vicent, 2013) (Markovsky et al., 2012). Lumf is insoluble in water with log_p of 8.34. As a result a series of Lumf prodrug conjugates namely PEG-O-Succ-Lumf, PEG-NH-Succ-Lumf and p-NAM-stat-p-AA-Lumf were synthesized using three different polymers (PEG-OH, PEG-NH₂ and p-NAM-stat-p-AA) and characterized. In all of the synthesized prodrug conjugates, the polymer was covalently conjugated to the Lumf directly or via pH-responsive linker i.e. succinic acid. Succinic acid is non-toxic and most importantly it is FDA approved and is known to hydrolyze easily under normal physiological conditions (Lee et al., 2008)(Safavy et al., 2004).

Lumf hydroxyl group was initially reacted with succinic anhydride to produce succinate ester conjugates [**Scheme 4.2**]. Succinic anhydride is extremely reactive towards nucleophiles (Hermanson, 2008). Nucleophilic attack at one of the carbonyl groups releases the anhydride ring, forming a releasable ester bond with Lumf and opening the other to create a free carboxylic acid. Because of the free carboxylic acid group, the reaction medium becomes acidic (Hermanson, 2008). As compared to the published data related to conjugation of small molecules, Lumf is an aryl-amino alcohol suggesting that the drug might activate the carboxyl group of succinic acid, and also maintain the environment at basic pH. As a result, two reactions were carried out, a) Lumf was reacted with succinic anhydride only, b) Lumf was reacted with succinic anhydride and a drop of trimethylamine (TEA) was added to the reaction. In all reactions anhydrous DMF and 4-(dimethylamino)-pyridine (DMAP) were used as solvent and

base catalyst or acyl transfer agent; respectively. The free carboxylic acid group on a newly formed prodrug of Lumf was used to attach to PEG-OH and PEG-NH₂.

4.2.1.1 Lumf-Succ conjugate

The proton NMR spectrum of Lumf is displayed in **Figure 4.1**. The characteristic proton peaks CH of the aromatic group were between 7.28-7.69 ppm and the oxymethine or chiral proton appeared at 5.37-5.34 ppm as a doublet of doublet. At 2.88-2.84 ppm another doublet of doublets was observed, related to diastereotopic protons (i). A series of multiplets were observed at 2.72-2.66 ppm, 2.56-2.42 ppm, 1.53-1.45 ppm and 1.40-1.28 ppm due to methylene protons of alkyl chain. A triplet was observed at 0.966-0.930 ppm associated with methyl protons of alkyl chain, thus confirming the identity of Lumf.



Scheme 4.2: Synthesis of Lumf-Succ conjugate.

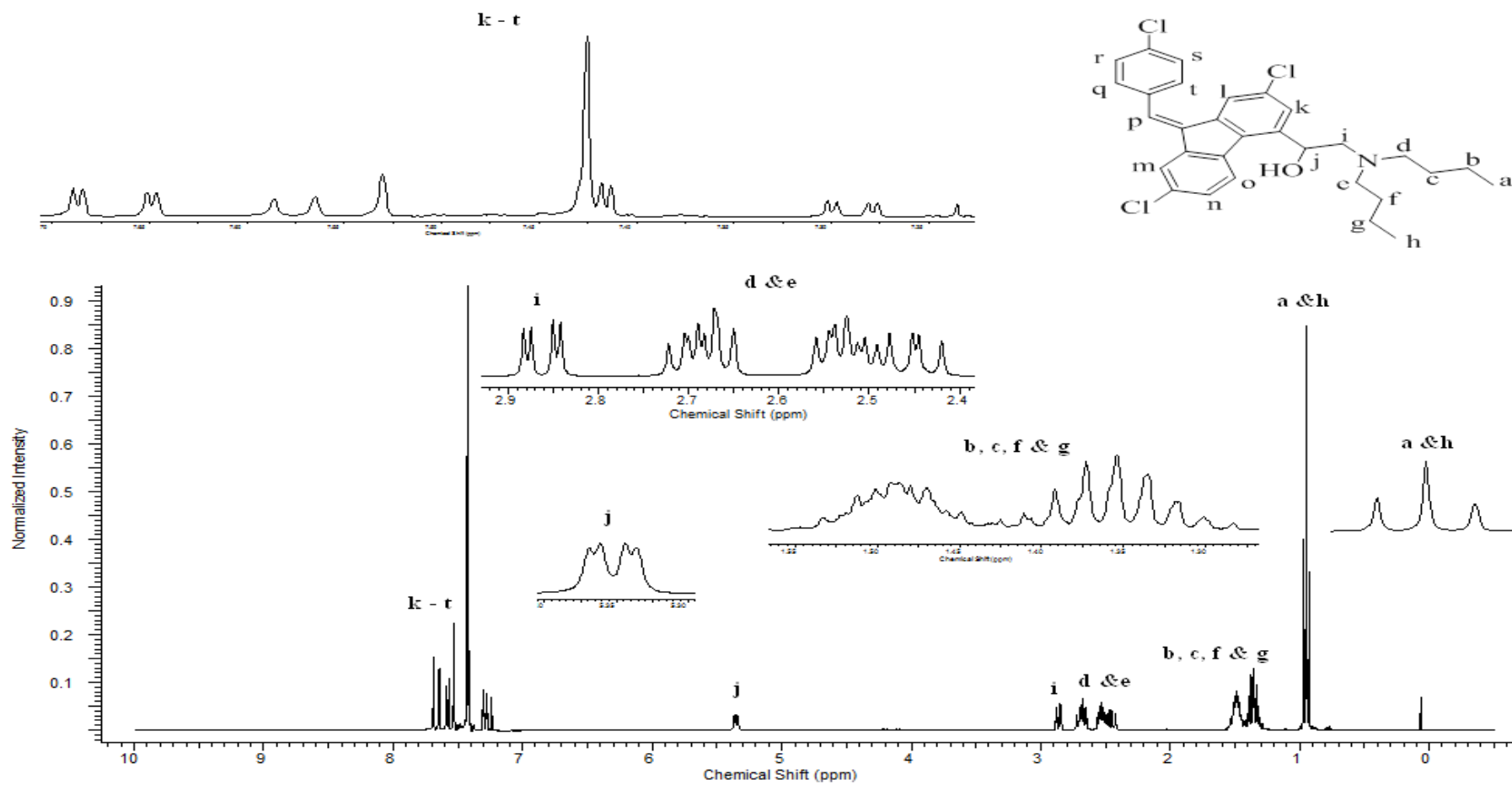


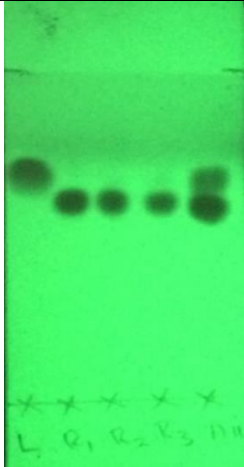

Figure 4.1: Proton NMR of Lumf (500 MHz, CDCl₃)

Successful *O*-succinylation of Lumf was confirmed by TLC, ^1H NMR analysis, ATR-FTIR and mass spectrometry (MS). TLC showed a lower retention factor (R_f , 0.75, acetone: ethylacetate (1:1) compared to Lumf for Lumf-Succ conjugate corresponding to the increased polarity from the new carboxylic acid group. Regardless of the reaction conditions, R_f was the same for the studied synthetic routes [Table 4.2]. The Lumf-Succ conjugate was purified by silica column chromatography and the pure product obtained as a yellow powder after solvent evaporation [Table 4.2]. ^1H NMR spectrum was almost identical to Lumf [Figure 1.2]. Esterification of the alcohol resulted in the downfield shift of the chiral proton to 5.73-5.67 ppm from 5.37-5.34 ppm. Long range coupling to a multiplet was displayed probably due to protons related to succinic acid. The characteristic shifts of the other functional groups of the Lumf structure confirmed the integrity of Lumf-Succ conjugate.

ATR/FTIR spectra of Lumf-Succ conjugate presented the characteristic peaks of raw Lumf at 3396.8 cm^{-1} (OH), 2953.28 cm^{-1} (aliphatic and aromatic CH), 1635.2 cm^{-1} (-C=C-), 933 cm^{-1} (alkanes) and $696.37\text{-}373.22\text{ cm}^{-1}$ (Cl). The new peak confirming esterification of the hydroxyl of Lumf after silica gel purification was formed at 1734.3 cm^{-1} [Figure 4.3].

The MS of pure Lumf showed a sharp molecular ion peak at 528.2 m/z ratio (observed to be the most abundant peak), confirming the molecular weight of the drug [Figure 4.4]. However in the spectrum of Lumf-Succ conjugate, 628.3 m/z was observed to be the most abundant m/z. The results confirm the molecular weight of Lumf-Succ conjugate.

Table 4.2: TLC of Lumf-Succ prodrugs and Lumf-succinic acid conjugate after silica gel purification

	
<p>TLC of crude reaction samples of Lumf-Succ prodrugs. L = Lumf, R1 = Lumf reacted with succinic anhydride only, R2 = Lumf reacted with succinic anhydride and a drop of TEA added to the reaction, R3 = R1 + R2. The last spot is co-spot of L, R1, R2 and R3. Solvent system = acetone: ethylacetate (1 : 1), $R_f = 0.75$.</p>	<p>Lumf-succinic acid conjugate</p>

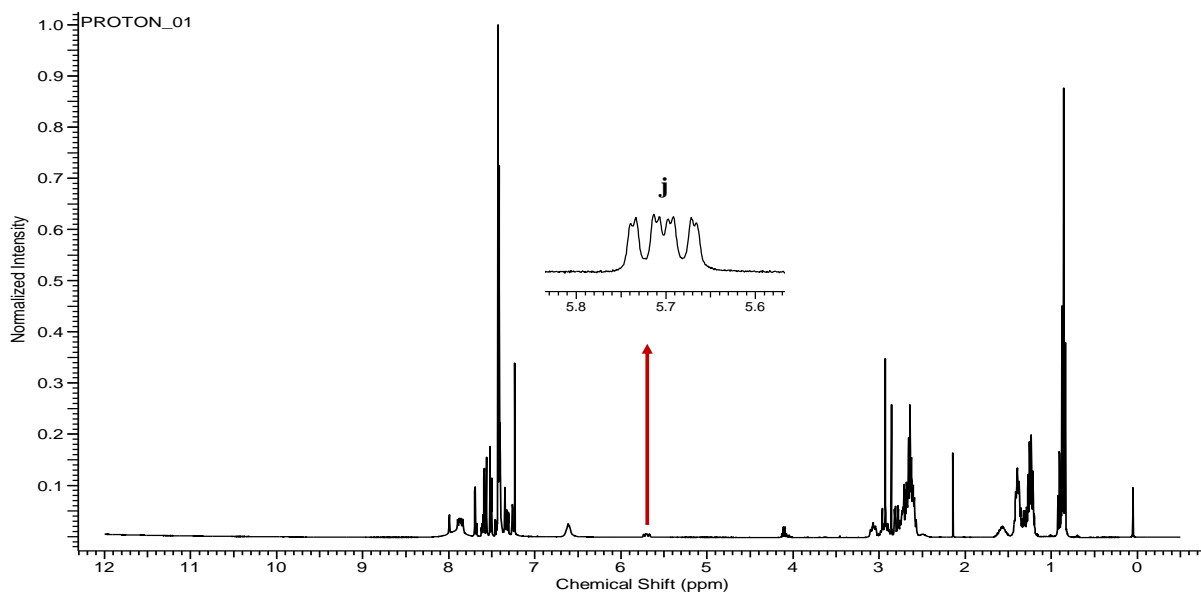


Figure 4.2: Proton NMR of Lumf-Succ conjugates (500 MHz, CDCl_3).

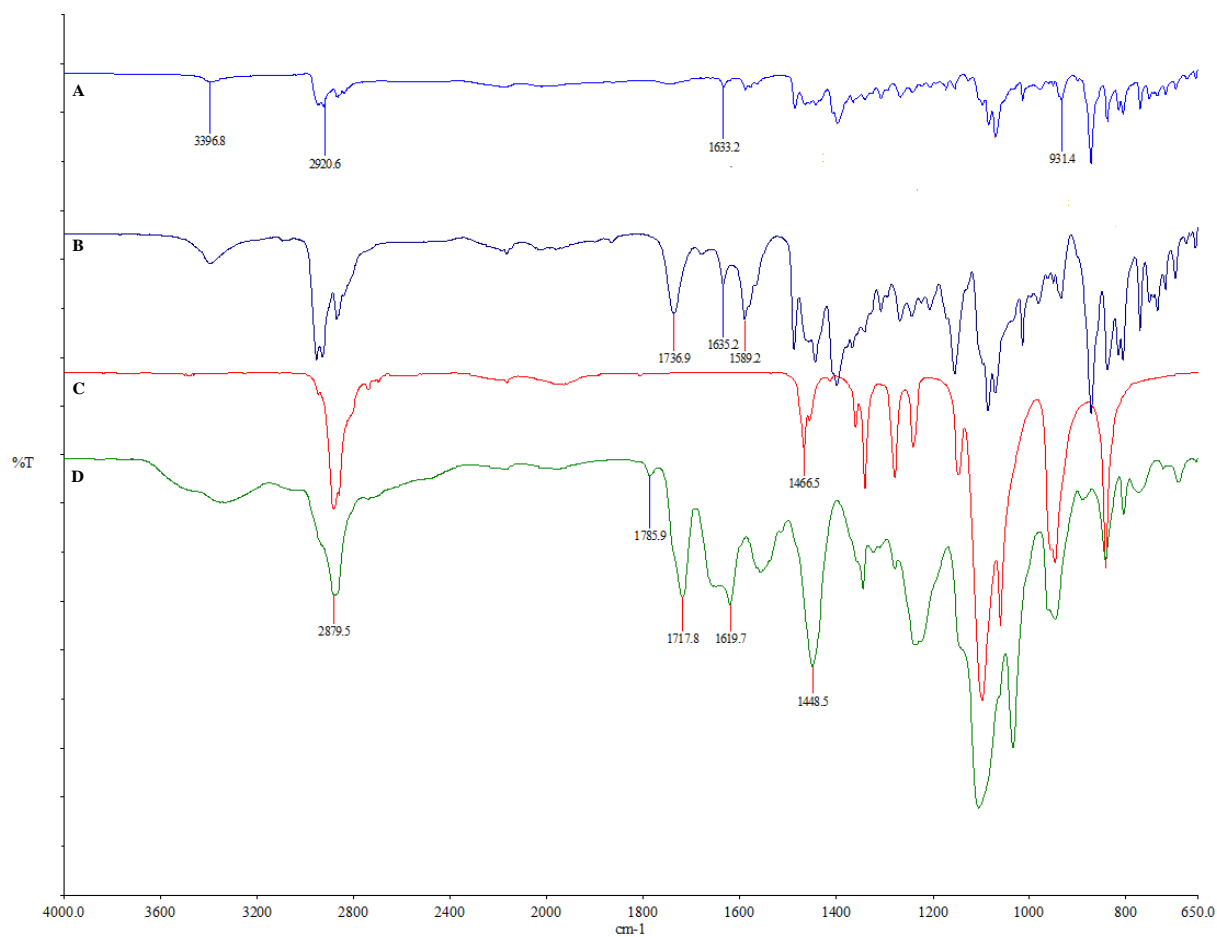


Figure 4.3: FTIR of A) Lumf, B) Lumf-Succ, C) PEG- OH and D) PEG- o -Succ-Lumf

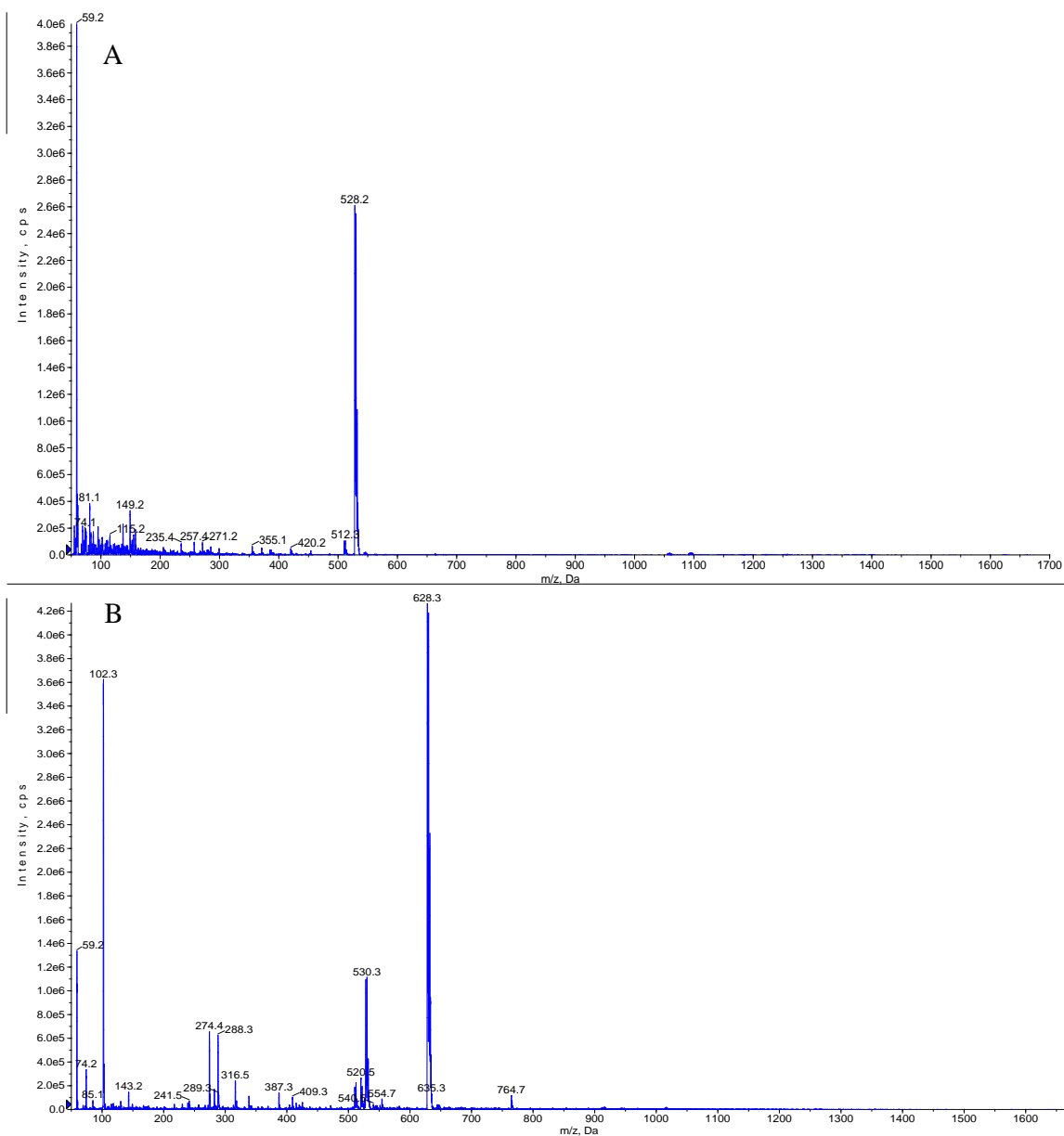


Figure 4.4: Mass spectrometry A) Lumf and B) Lumf-Succ conjugate.

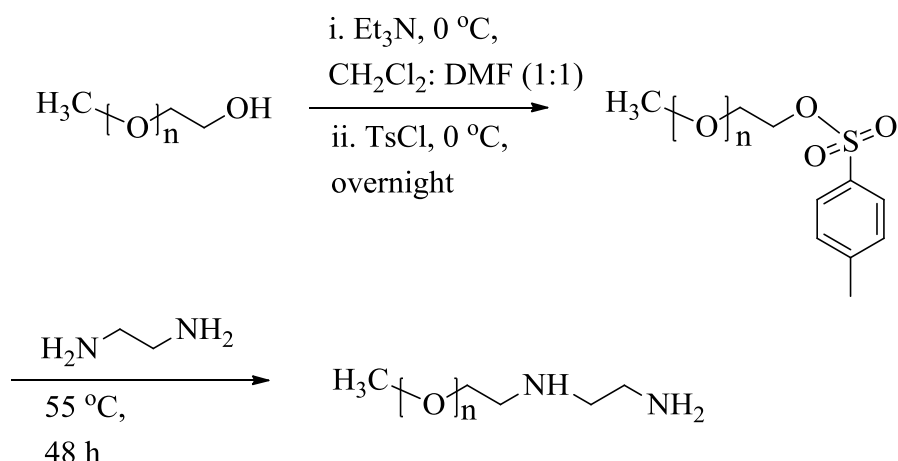
4.2.1.2 Synthesis and characterisation of PEG-NH₂

m-PEG has hydroxyl groups which can be conveniently converted into amines via a more reactive intermediate (Casettari et al., 2012)(Harris et al., 1984). The hydroxyl group itself is a poor leaving group [Table 4.3], since hydroxide ions are strong bases (Bauld, 2001). The

primary alcohol of m-PEG was converted to a more powerful leaving group namely the tosylate using 4-Toluenesulfonyl chloride (TsCl). Tosylates are much more reactive than the halides and amination via a tosylate was attempted in this project (Smith and March, 2006). The sulfonyl group increases significantly the electrophilicity of the alkyl group [Scheme 4.3].

Table 4.3: Functional groups reactivity organized approximately in decreasing ability to leave (Smith and March, 2006)

R-N ₂ ⁺	dinitrogen
R-OR' ₂ ⁺	dialkyl ether
R-OSO ₂ R ^F	perfluoroalkylsulfonates (e.g. triflate)
R-OTs, R-OMs, etc	tosylates, mesylates, and similar
R-I	iodide
R-Br	bromide
R-OH ₂ ⁺ , R-OHR' ²	Water, alcohols
R-Cl	chloride
R-ONO ₂ , R-OPO(OH) ₂	nitrate, phosphate, and other inorganic esters
R-SR' ₂ ⁺	thioether
R-NR' ₃ ⁺ , R-NH ₃ ⁺	amines, ammonia
R-F	fluoride
R-OCOR	carboxylate
R-OAr	phenoxides
R-OH, R-OR	hydroxide, alkoxides
R-NR ₂	amides



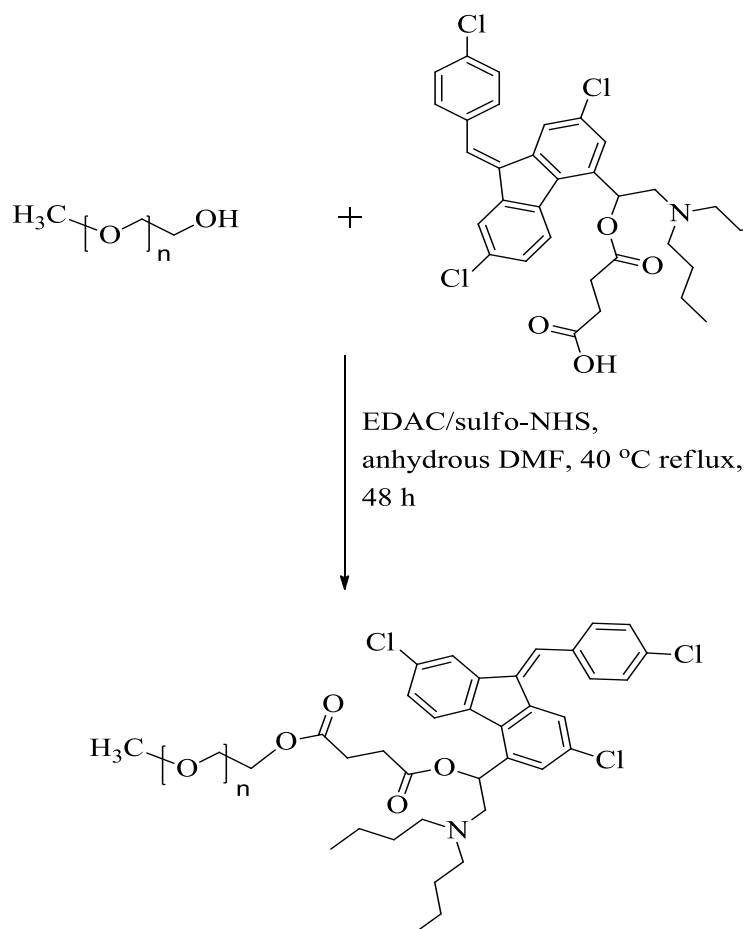
Scheme 4.3: Synthesis route of PEG-NH₂ (n = 5000 Da).

Tosylation of the PEG-OH was done for 3 h at 0 °C. The product was observed at $R_f = 0.00$ (acetone: ethylacetate, 1:1) on TLC by its UV visibility. The ¹H NMR spectrum clearly displayed a pair of doublets at 7.3 ppm and 7.8 ppm for the phenyl ring protons of the tosylate. The distinctive methylene protons of PEG backbone were observed at 3.61 ppm and methoxy protons at 3.29 ppm (results not shown). The more reactive intermediate i.e. tosylate permitted a facile introduction of the amino group at 40 °C by a S_N2 reaction. An excess of ethylenediamine was required [Scheme 4.3]. The product (PEG-NH₂) was readily purified by precipitating with cold diethyl ether and further filtered by repeated centrifugation in a Vivaspin™ ultrafiltration tube at 13 000 rpm and 25 °C to remove unreacted tosylate and ethylenediamine.

4.2.1.3 Conjugation of Lumf-Succ to PEG

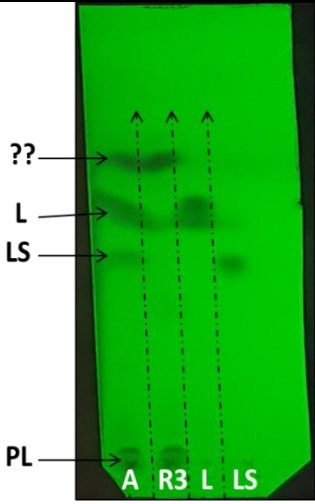
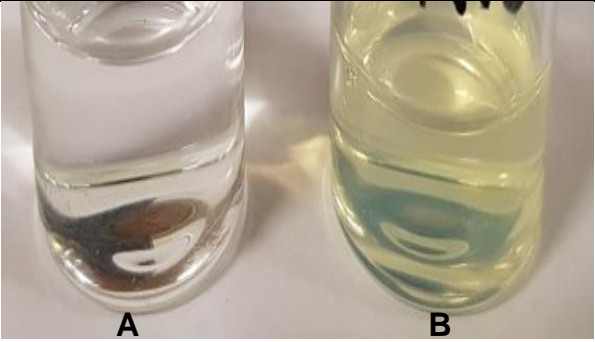
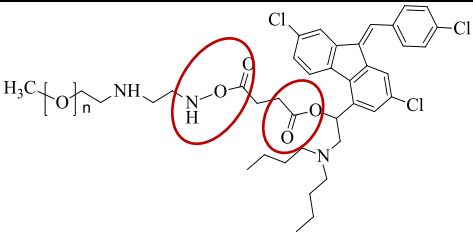
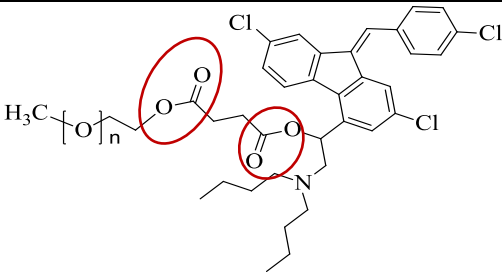
The general synthetic route to accomplish PEG-O-Succ-Lumf and PEG-NH-Succ-Lumf conjugate is shown in Scheme 4.4 and Scheme 4.5; respectively. In all reactions the coupling to the Lumf was achieved using EDAC/sulfo-NHS with succinic acid as a linker. The ester linker is generally hydrolytically labile under normal physiological conditions (Almudena Prudencio, Robert C. Schmeltzer, 2013). The formation of a PEG-O-Succ-Lumf conjugate was first indicated by the appearance of a UV-active spot on the baseline of the TLC [Table 4.4, $R_f = 0.00$ (acetone: ethylacetate, 1:1)] at the end of the reaction. PEG is not UV active, thus PEG-

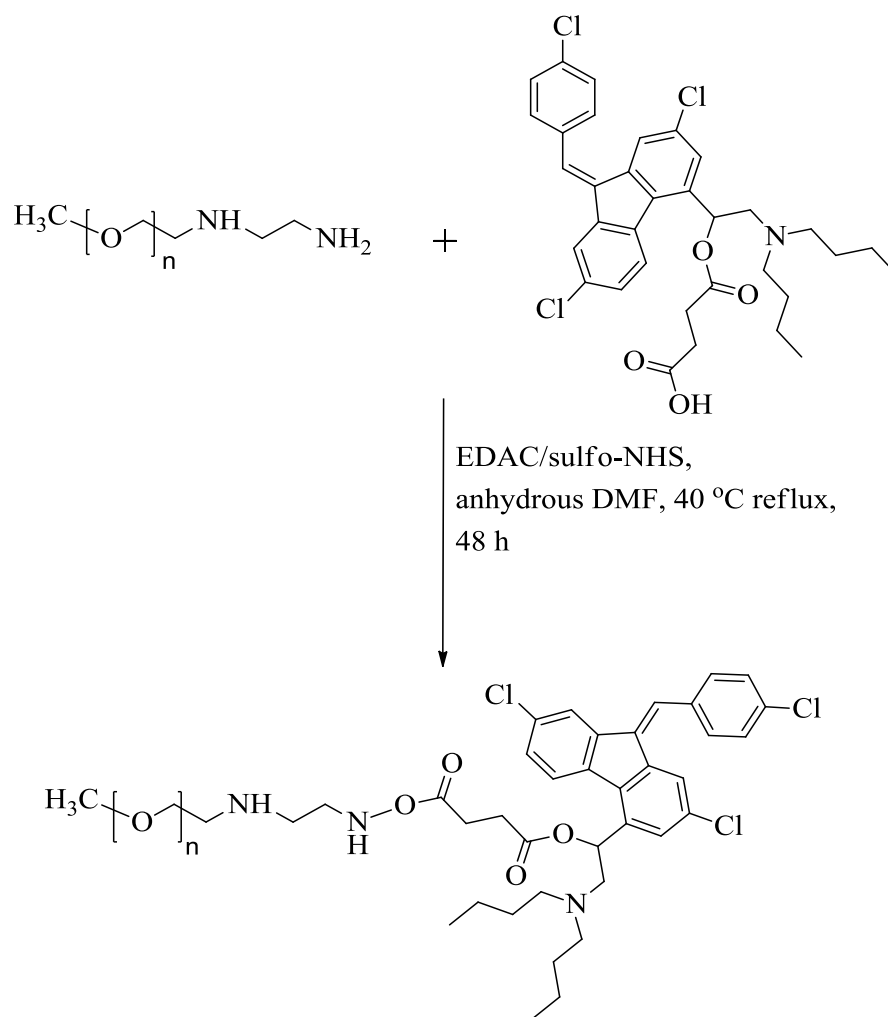
o-Succ-Lumf was expected to be UV visible on the TLC plate due to the Lumf chromophore. This assumption was further supported by the disappearance of the Lumf-Succ spot on the TLC attributed to the consumption of the Lumf-Succ in the reaction process. Further, the work-up of the reaction yielded an intensely yellow aqueous solution which remained so even after centrifugation at 20 000 rpm [Table 4.4]. It is worth mentioning that without adding carbodiimide reagents to the reaction media i.e PEG reacted with Lumf-Succ; conjugation of Lumf to PEG was not successful. The work-up of the reaction displayed a clear aqueous solution [Table 4.4]. Confirmation of the formation of a covalent ester linkage was carried with ^1H NMR and ATR-FTIR spectroscopies. ^1H NMR of PEG-o-Succ-Lumf conjugate depicted corresponding peaks of both Lumf and PEG-OH. The typical methylene protons of PEG backbone were observed at 3.61 ppm and characteristic proton peaks CH of the aromatic group of Lumf were between 7.276-7.689 ppm [Figure 4.5]. FTIR showed the formation of an ester bond at 1785.9 cm^{-1} [Figure 4.3]



Scheme 4.4: Synthesis route of PEG-o-Suc-Lumf (n = 5000 Da).

Table 4.4: TLC analysis and purified PEG-Succ-Lumf conjugate in aqueous solution.

 <p>PEG-Succ-Lumf</p> <p>TLC of crude reaction samples of A= all spots, R3 = PEG-O-Suc-Lumf crude, L = Lumf, LS =Lumf-Succ. Solvent system acetone : ethylacetate (1 : 1). $R_f = 0.00$</p>	 <p>A = PEG reacted with Lumf-Succ without adding carbodiimide reagent. The work-up of the reaction yielded clear solution after centrifugation at 20 000 rpm.</p> <p>B = PEG-Succ-Lumf conjugate. The work-up of the reaction yielded an intensely yellow aqueous solution which remained so even after centrifugation at 20 000 rpm.</p>
 <p>PEG-NH-Suc-Lumf</p> <p>Release Products</p> <ul style="list-style-type: none"> • Lumf-hemisuccinate + PEG-NH₂ 	 <p>PEG-O-Suc-Lumf</p> <p>Release Products</p> <ul style="list-style-type: none"> • Lumf + PEG-OH • Lumf + PEG-hemisuccinate



Scheme 4.5: Synthesis route of PEG-NH-Suc-Lumf ($n = 5000$ Da).

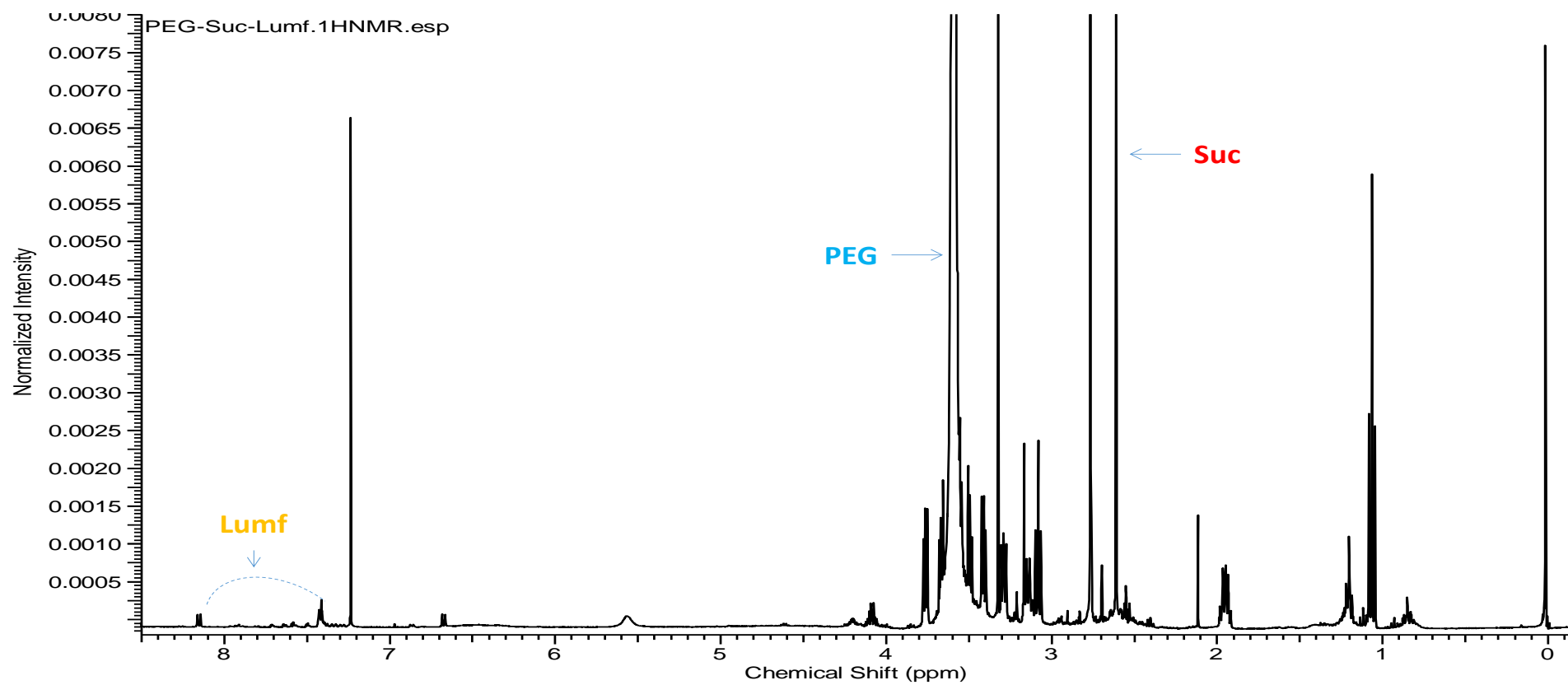


Figure 4.5 Proton NMR of PEG-Succ-Lumf conjugate (600 MHz, CDCl_3).

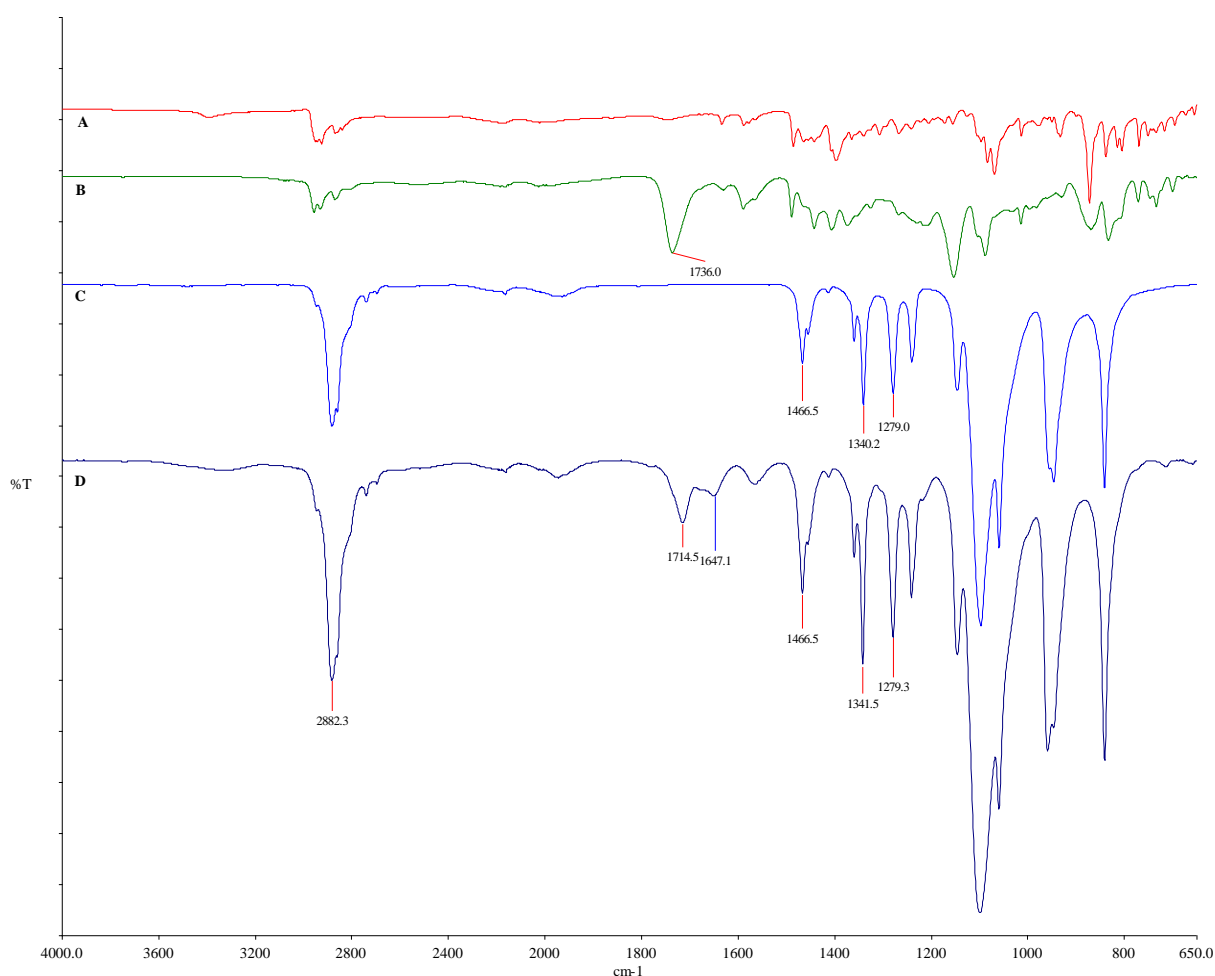


Figure 4.6: FTIR of A) Lumf, B) Lumf-Succ, C) PEG-OH and D) PEG-NH-Succ-Lumf

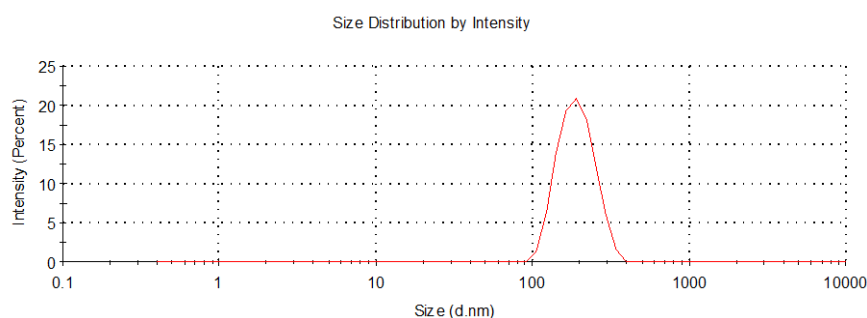
We postulated (as presented in the **Table 4.4**) that the release kinetics of PEG-o-Suc-Lumf will not result in a homogenous release of Lumf due to the diester linkage of the succinate linker. Conejos-Sánchez and co-workers synthesized poly-L-glutamic acid (PGA)-doxycycline (doxy) conjugate using biodegradable (ester) and a non-biodegradable bond (amide) as linkers (Conejos-Sánchez et al., 2015). The two linkages were incubated in PBS (pH 7.4, 37 °C) and scrutinized to check if drug release was a prerequisite for therapeutic response. Findings showed that an amide conjugate released doxy after 16 days of incubation while a clear release was observed from the ester counterpart. It was then decided to synthesize a conjugate in which the succinate is linked to the PEG via a more stable amide bond. To do this PEG-NH₂ would have to be used instead of the PEG-OH. We synthesised the PEG-NH₂ by tosylation as shown in

Scheme 4.3. Lumf-Succ was successfully linked to PEG-NH₂ in a reaction similar to that described for PEG-OH. The product obtained was identical in character to the PEG-O-Suc-Lumf. FTIR clearly showed the formation of an amide bond at 1647.1 cm⁻¹ [Figure 4.6]. It is worth mentioning that PEG-O-Suc-Lumf conjugate was only formed at reaction equivalence of more than 1:5 (Lumf-Succ: PEG-OH) whereas PEG-NH-Suc-Lumf was successful at 1:1.2 (Lumf-Succ: PEG-NH₂). The synthesized PEG-O-Suc-Lumf and PEG-NH-Suc-Lumf had a drug loading of less than 1% and 3%; respectively. The %loading was calculated by dividing Lumf mass by the whole molecule mass according to the ratio of Lumf substitution calculated from the integration of Lumf, succinic acid and PEG peaks in the ¹H NMR spectrum. An average particle size below 200 nm was obtained for PEG-Succ-Lumf conjugate irrespective of the type of linkage [Table 4.5] [Figure 4.7]. PDI values were always below 0.2, which is an indication of the relatively homogeneous size distribution achieved with carbodiimide chemistry. The free drug content was always less than 2% (calculated using the last wash on the UV/Vis spectrophotometer).

Table 4.5: Mean particle size, PDI, zeta potential (ZP, mV) and drug loading of the conjugates (data represent mean± SD, n = 3).

Material	Particle size (nm)	PDI	ZP (mV)	Drug loading (%)
PEG-Succ-Lumf	191±6	0.17±0.02		>1 and 3
P-NAM-stat-p-AA-Lumf	93±1	0.20±0.01	-29±2	8

A)



B)

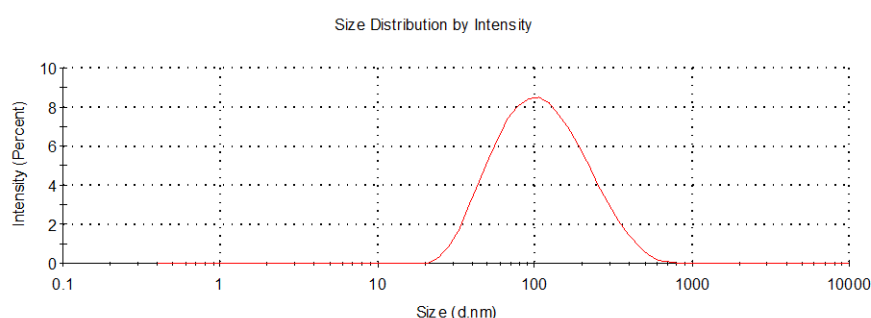


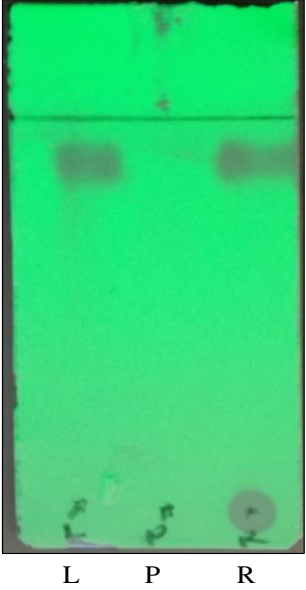
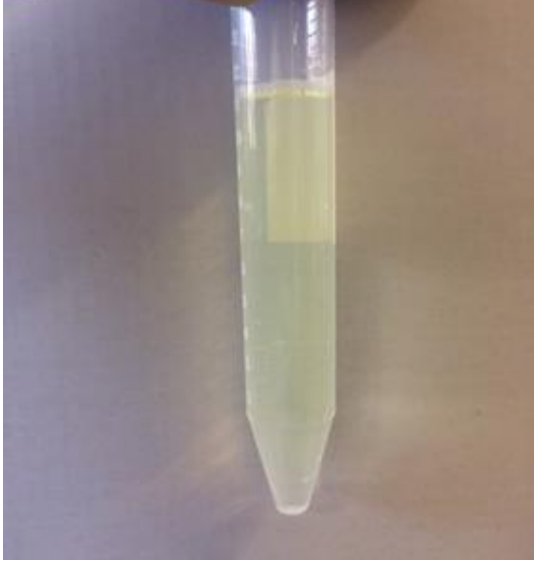
Figure 4.7: Average particle size distribution of PEG-Succ-conjugate (A) and p-NAM-*stat*-p-AA-Lumf conjugate (B).

4.2.1.4 Conjugation of Lumf to p-NAM-*stat*-p-AA

The polymer, p-NAM-*stat*-p-AA, polyacrylamide derivative was used to conjugate Lumf directly using EDAC/sulfo-NHS through the Lumf hydroxyl group [Scheme 4.6]. Unlike m-PEG containing only one attachment point, the polymer; p-NAM-*stat*-p-AA, is a multivalent polymer containing carboxylic acid (10%) in its backbone. After 48 h, a successful reaction was indicated by TLC analysis [Table 4.6] [$R_f = 0.00$ (acetone: ethylacetate, 1:1)]. PBS (pH 7.4) was poured into the crude mixture and centrifuged at 13 000 rpm and 25 °C to obtain a yellowish supernatant containing the product and a yellow pellet of by-products. The aqueous supernatant was further purified by repeated centrifugation in a Vivaspin™ ultrafiltration tube (PES membrane, MwCO 3kDa) at 13 000 rpm and 25 °C. The final concentrate was freeze-dried to yield the p-NAM-*stat*-p-AA-Lumf conjugate as a yellowish powder. The last wash was used to determine the free drug content using UV analysis.

The synthesized p-NAM-*stat*-p-AA-Lumf conjugate had a purity of >99% with a degree of substitution of ~8 wt%. The drug loading in the p-NAM-*stat*-p-AA-Lumf conjugate was calculated by dividing Lumf mass by the whole molecule mass according to the ratio of Lumf substitution calculated from the integration of Lumf and p-NAM-*stat*-p-AA peaks in the ¹H NMR spectrum. ATR-FTIR analysis also confirmed the formation of the ester bond at 1777.9 cm⁻¹. The p-NAM-*stat*-p-AA-Lumf conjugate, has amphiphilic characteristics due the hydrophilicity of polymeric material used and the hydrophobic nature of Lumf. An average particle size below 100 nm was achieved [Table 4.5] [Figure 4.7]; PDI values were always below 0.2, which is an indication of the relatively homogeneous size distribution achieved with carbodiimide chemistry. The free drug content was always less than 2%.

Table 4.6: TLC analysis and purified p-NAM-*stat*-p-AA-Lumf in aqueous solution

 <p style="text-align: center;">L P R</p> <p>TLC of crude reaction of p-NAM-<i>stat</i>-p-AA-Lumf conjugate. L = Lumf, P = p-NAM-<i>stat</i>-p-AA, R = p-NAM-<i>stat</i>-p-AA-Lumf conjugate (Crude reaction). Solvent system = acetone: ethylacetate (1 : 1)</p>	 <p>p-NAM-<i>stat</i>-p-AA-Lumf conjugate in aqueous solution (PBS [7.4])</p>
---	--

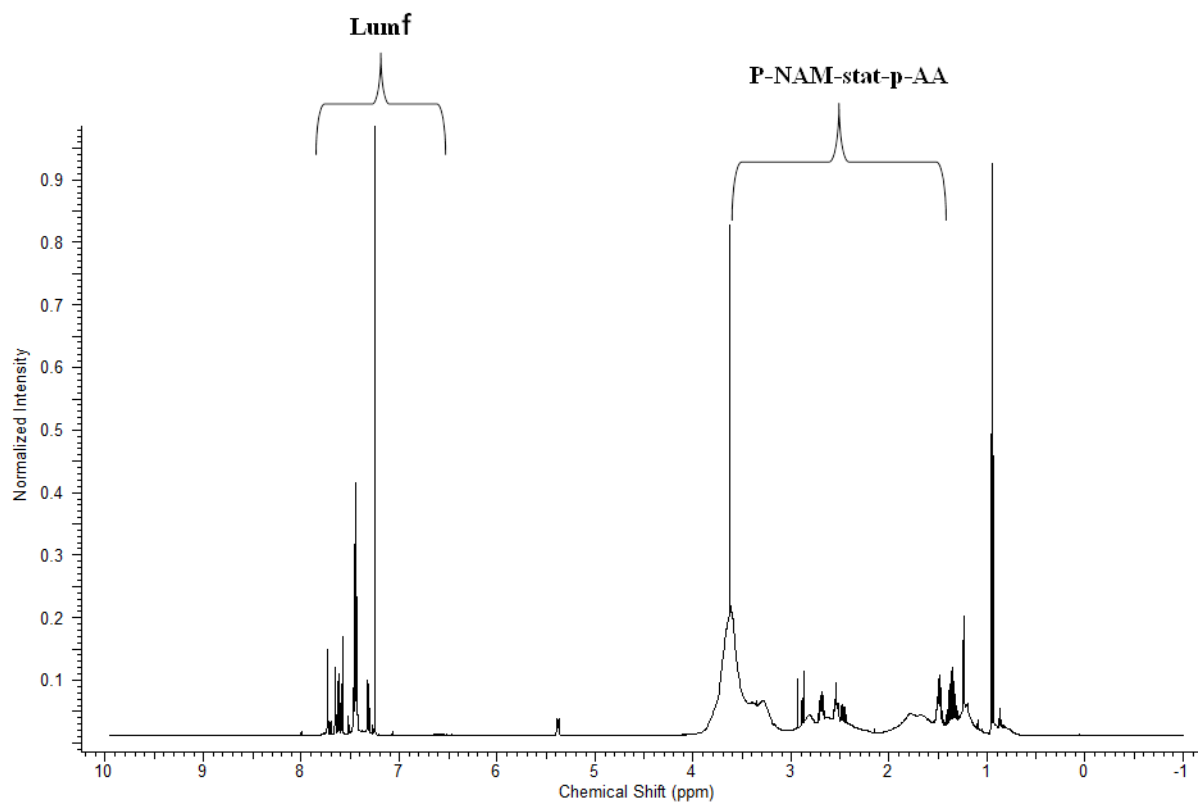
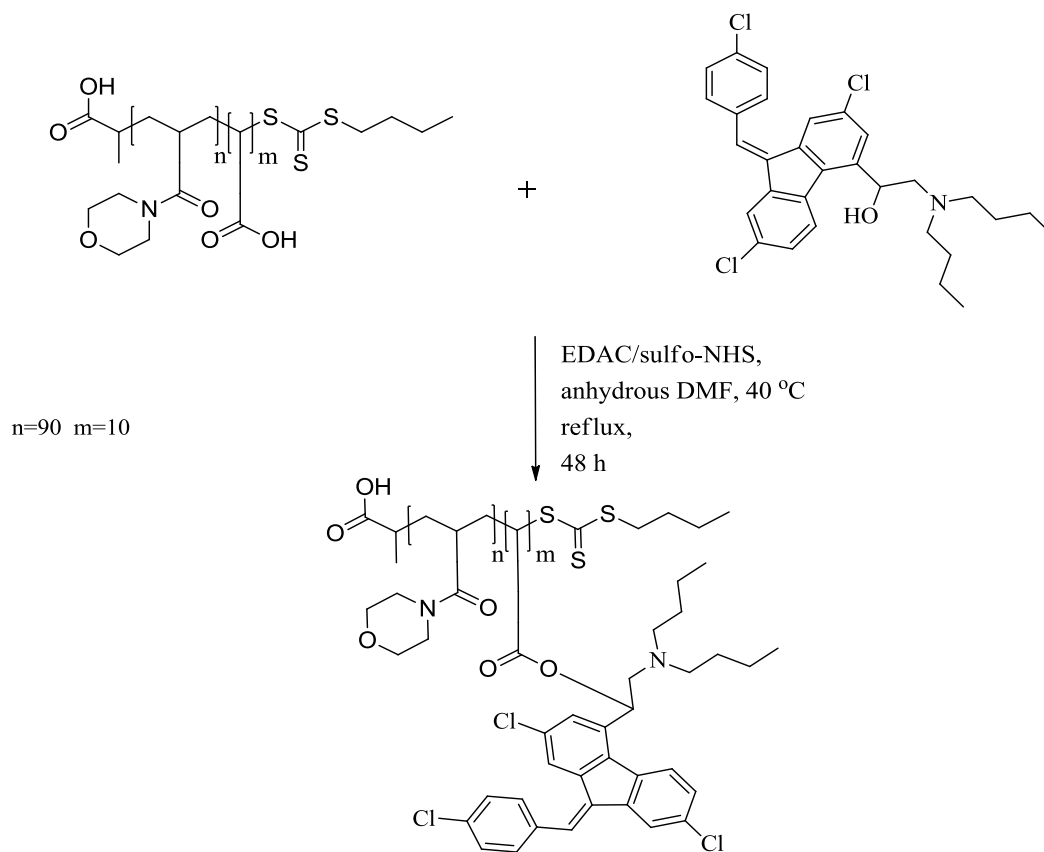


Figure 4.8: ^1H NMR of p-NAM-stat-p-AA-Lumf conjugate showing corresponding peaks to both Lumf and p-NAM-stat-p-AA (500 MHz, CDCl_3).



Scheme 4.6: Synthesis route of p-NAM-stat-p-AA-Lumf conjugate.

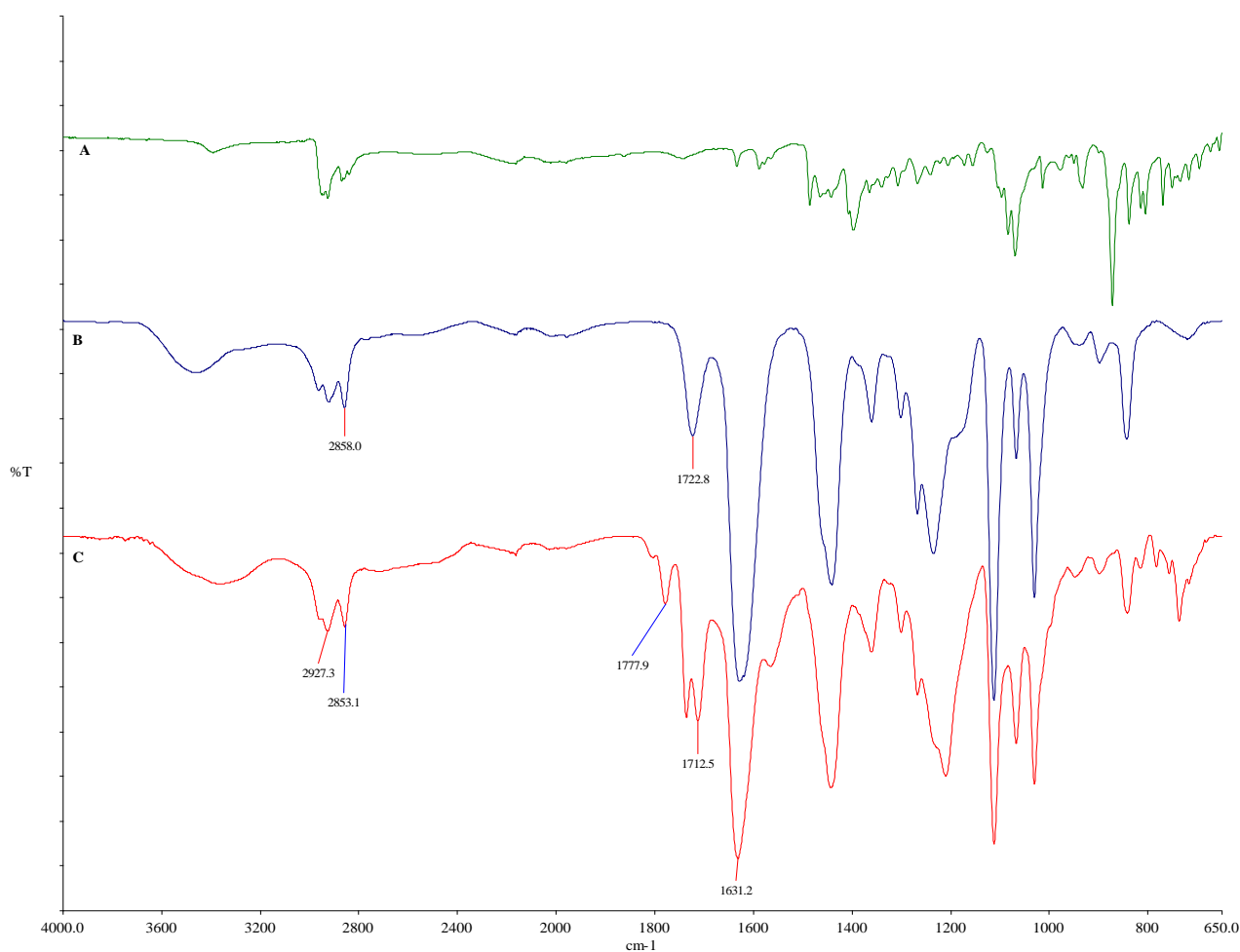


Figure 4.9: FTIR of A) Lumf, B) p-NAM-stat-p-AA, C) p-NAM-stat-p-AA-Lumf conjugate.

4.2.2 Solubility studies

The PEG-NH-Succ-Lumf and p-NAM-*stat*-p-AA-Lumf conjugates were dissolved in PBS (pH 7.4) and the concentration was increased gradually from 1 mg/mL to 4 mg/mL [Figure 4.10]. After 30 min incubation with shaking at room temperature, the conjugates were sonicated followed by centrifugation at 13 000 rpm and 25 °C for 5 min. As shown in Figure 4.10, the p-NAM-*stat*-p-AA-Lumf conjugate [Figure 4.10 (B)] appears yellow in colour for all concentrations as compared to the PEG-NH-Succ-Lumf conjugate [Figure 4.10 (A)], which is much clearer, an observation attributed to their drug loading capacity, 8% and 3% for p-NAM-*stat*-p-AA-Lumf and PEG-NH-Succ-Lumf conjugate; respectively. Table 4.7 shows the concentration of the conjugates PEG-NH-Succ-Lumf and p-NAM-*stat*-p-AA-Lumf versus the concentration of the drug in PBS. At 1mg/mL, the PEG-NH-Succ-Lumf conjugate constitutes

30 $\mu\text{g/mL}$ of the drug whilst the p-NAM-*stat*-p-AA-Lumf conjugate contains 266 $\mu\text{g/mL}$ of the drug at this concentration. This study confirms an improvement on the solubility of Lumf since free Lumf (unconjugated drug) is completely insoluble in water.

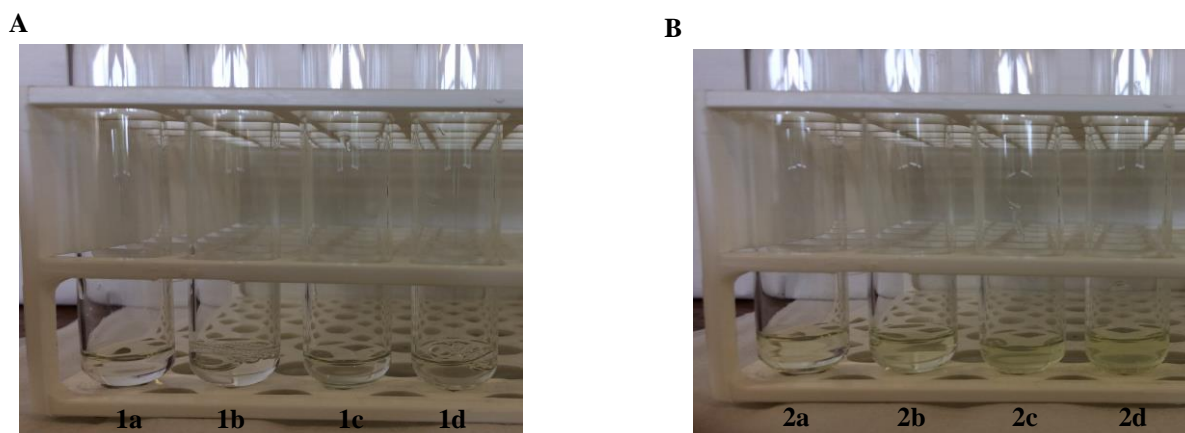


Figure 4.10: Solubility studies of the polymer-Lumf conjugate in PBS buffer (pH 7.5) (A) PEG-NH-Succ-Lumf. 1a = 1 mg/mL, 1b = 2 mg/mL, 1c = 3 mg/mL, 1d = 4 mg/mL and (B) p-NAM-*stat*-p-AA-Lumf: 2a = 1 mg/mL, 2b = 2 mg/mL, 2c = 3 mg/mL, 2d = 4 mg/mL.

Table 4.7: Solubility studies of the polymer-Lumf conjugate in PBS buffer.

PEG-NH-Succ-Lumf	Drug concentration (ug/mL)	p-NAM- <i>stat</i> -p-AA-Lumf	Drug concentration (ug/mL)
1 mg/mL	30.3	1 mg/mL	266
2 mg/mL	36.7	2 mg/mL	346
3 mg/mL	51.8	3 mg/mL	415.8
4 mg/mL	51.1	4 mg/mL	580

4.3 Conclusion

The anti-malarial drug, Lumf was successfully conjugated into water-soluble polymers using carbodiimide chemistry. The conjugation was via a releasable ester bond. Succinic acid was used as a linker. PEG-NH₂ showed better drug loading than PEG-OH. The weight percentage (wt %) of lumf in the PEG-NH-Succ-Lumf was analyzed using proton NMR and UV spectrophotometer resulting in ~3 wt%. The loading was further increased when a multivalent

polymer namely p-NAM-*stat*-p-AA was used. Lumf was conjugated directly into the p-NAM-*stat*-p-AA via a releasable ester bond. The weight percentage of lumf in the p-NAM-*stat*-p-AA-lumf conjugate was ~8 wt%. The synthesised conjugates have an amphiphilic characteristic due the hydrophilicity of polymeric material used and the hydrophobic nature of Lumf. Average particle size below 200 nm was archived and PDI values were always below 0.2, which is an indication of the relatively homogeneous size distribution achieved with carbodiimide chemistry. Solubility studies followed the same array. At 1 mg/mL, the PEG-Lumf conjugate constitutes 30 µg/mL of the drug whilst the p-NAM-*stat*-p-AA-Lumf conjugate contains 266 µg/mL of the drug at this concentration. We have for the first time, by applying the polymer therapeutics techniques, synthesized a polymer-drug conjugate of Lumf which has increased the solubility of the drug more than 10³ times.

5 Chapter Five: Conclusion

The three major infectious diseases HIV, malaria and TB still pose a global health threat. These poverty-related diseases have existed through periods of virtual latency and periods of disastrous epidemics. Although treatment options are available and much effort has been made to reduce the required daily dosage and number of individual medications, there is still the intrinsic therapeutic challenge of the drugs due to poor pharmacokinetics. Solubility is still a problem and most of the drugs possess harmful toxicities and unpleasant side-effects which lead to non-adherence to the treatment regimens. Nanomedicine using polymer therapeutics offers a powerful technological solution to the high toxicity and poor pharmacokinetics of drugs. However, this approach has not been extensively explored for infectious diseases. Reversibly conjugating the active ingredients to water-soluble polymeric carriers will favourably alter their pharmacokinetics and significantly reduce toxicity to patients. Combining this technology with traditional nanoencapsulation techniques will produce optimized formulations or treatments for infectious diseases.

The first part of this project successfully synthesized PEGylated RNA aptamers using carbodiimide chemistry to build a phosphoramidate link. Urea gel electrophoresis confirmed the conjugation and *in vitro* stability studies in human breast milk showed that PEGylated RNA aptamers were more stable than the parent aptamers. The TZM-bl neutralization assay also showed that PEGylated RNA aptamers maintained their binding integrity *in vitro* after pegylation. Double emulsion methods were employed to coat PCL nanoparticles with PEGylated RNA aptamers. Under the optimized conditions nanoparticles of less than 150 nm were produced with a higher surface charge, showing that the nanoparticles were stable. The CV and EIS experiments showed that the mercaptoacetic acid (MACA) SAM was stable when subjected to an electrical potential. The strong attraction of gold for thiol makes the functionalization of MACA convenient for immobilization of the gp 120 protein on MACA

SAM. Contrary to other forms of solid substrates like carbon and silver (which both have strong attraction to other functional groups); the thiolate-Au bond is of significance, since the formation of the SAMs can be unfailingly anticipated because the MACA will be linked to the Au surface only via the –SH, not any other functional group. The *in vitro* binding assay using electrochemical methods showed that the nanoparticles coated with PEGylated RNA aptamers had higher affinity and specificity to HIV-1 gp 120. HIV primarily resides in the anatomical and cellular reservoirs of the human body, which is the main problem as the ARVs cannot reach these places in therapeutic concentrations. Poor targeting ability of ARVs to latent sites of infection is the main reason for the relapse. Thus these nanoparticles coated with PEGylated RNA aptamers could be used to increase delivery of ARV drugs in latent sites of infections; as aptamers have higher affinity constant (K_d) values compared to antibodies.

The second part of this project was to conjugate Mox into PEG via a releasable amide bond. The PEG-Mox conjugate was further nano-encapsulated into PCL nanoparticles using double emulsion spray-drying technique. Spherical and amorphous nanoparticles with average particles size of less than 300 nm were obtained. Encapsulation efficiency (%EE) was found to be 60%. PCL-Mox nanoparticles and PEG-Mox conjugate were found to be significantly more hemocompatible than the free Mox drug. PCL nanoparticles were hemocompatible across the tested concentrations, showing that the polymer is biocompatible, biodegradable and non-toxic. *In vitro* stability in human plasma showed that PCL-Mox nanoparticles were stable for over 72 hrs. Results obtained showed that PCL nanoparticles could be used as a drug delivery system to minimize the high toxicity of TB drugs.

The third part of this project was to conjugate anti-malarial drug, Lumf to water-soluble polymers. Lumf is completely insoluble in water and it suffers from biocompatibility issues. Two biocompatible polymers namely PEG and p-NAM-*stat*-p-AA (polyacrylamide derivative) were used in effort to increase the solubility. The conjugation was via a releasable ester bond. The formation of a PEG-Lumf and p-NAM-*stat*-p-AA-Lumf conjugates were first indicated by the appearance of a UV-active spot on the baseline of the TLC. The conjugates were further characterized by proton NMR, showing corresponding peaks to both

Lumf and the polymers i.e PEG and p-NAM-*stat*-p-AA. ATR-FTIR also showed the esterification of Lumf. The synthesised PEG-Lumf and p-NAM-*stat*-p-AA-Lumf conjugates, have an amphiphilic characteristic due the hydrophilicity of polymeric material used and the hydrophobic nature of Lumf. Average particle size below 200 nm was archived and PDI values were always below 0.2, which is an indication of the relatively homogeneous size distribution achieved with carbodiimide chemistry. The weight percentage (wt %) of lumf in the p-NAM-*stat*-p-AA-lumf conjugate was analyzed using proton NMR and UV spectrophotometer, resulting in ~8 wt%. On the contrary, drug loading was found to be 3% when PEG was used. This was due to the fact that PEG has only one attachment point hence low loading as compared to p-NAM-*stat*-p-AA which has 10 attachment points. Solubility studies followed the same array. At 1 mg/mL, the PEG-Lumf conjugate constitutes 30 µg/mL of the drug whilst the p-NAM-*stat*-p-AA-Lumf conjugate contains 266 µg/mL of the drug at this concentration. We have for the first time, by applying the polymer therapeutics techniques, synthesized a polymer-drug conjugate of Lumf which has increased the solubility of the drug more than 10^3 times

The studies presented in these project have primarily focused on the development of nanomedicinal materials for infectious diseases. We have demonstrated the synthesis of polymeric conjugates using carbodiimide chemistry. Carbodiimide chemistry was applied to conjugate different active ingredients i.e RNA aptamers, moxifloxacin and lumefantrine to polymers via phosphoramidate, amide and ester bonds. These structures have been characterized by a range of techniques to demonstrate that covalent links have been formed. For two of the polymer conjugates; namely PEGylated RNA aptamers and PEG-Mox conjugates; we have demonstrated that these polymer conjugates can be coated onto or encapsulated in PCL nanoparticles of defined size and stability. Through the three different experimental chapters, we have demonstrated that polymer based drug conjugates can be used to address different issues: (1) drug delivery through coating nanoparticles with appropriate aptamers, (2) drug toxicity through encapsulation of a toxic drug in a heamocompatible nanoparticle and (3) greatly improved aqueous solubility of a hydrophobic drug. Furthermore, while there has been much excellent work using polymer based drug

Conclusion

conjugates in cancer, we have explored the approach to tackle different problems related to three different infectious diseases of poverty, namely HIV, TB and malaria.

6 Chapter Six: Experimental

6.1 Experimental for Chapters Two

Chemical Data

PCL (10 KDa), poly(vinylalcohol) (PVA, 13-23 KDa, 87-89% hydrolyzed), O-(2-Aminoethyl) PEG (PEG, 3 KDa), succinic anhydride, N-(ethylcarbonimidoyl)-N,N-dimethylpropane-1,3-diamine monohydrochloride (EDAC), imidazole, N-hydroxysulfosuccinimide (sulfo-NHS), dulbecco's modified eagle medium (DMEM), ethidium bromide, 40% bis-acrylamide, ammonium persulfate (APS) were obtained from Sigma-Aldrich (South Africa). JC53 bl (TZM-bl) cells line was provided by Professor Lynn Morris, National Institute of Communicable Diseases (NICD), South Africa. Potassium hexacyanoferrate (II) was purchased from B. Jones Ltd., South Africa, while potassium hexacyanoferric (III) was purchased from Bio-Zone Chemicals, South Africa. Polycrystalline gold electrode (BAS, r = 0.8 mm) was obtained from Metrohm, South Africa. VivaSpin 20 (3000 MWCO polyethersulfone membrane) were purchased from National Separation (Pty) Ltd (South Africa). The SELEX procedure was applied to carry out the rounds of selections of the RNA aptamers against the target protein at CSIR-Bioscience (South Africa). The following primers were used to amplify the library listed from 50 to 30: AAT TAA CCC TCA CTA AAG GGA ACT GTT GTG AGT CTC ATG TCG AA and TAA TAC GAC TCA CTA TAG GG AGA CAA GAC TAG ACG CTC AA (T7 promoter region is underlined). The recombinant HIV-1 gp120 protein was purchased from Biocom Biotech (Pty) Ltd (South Africa). All other chemicals were of analytical grade and purchased from Sigma-Aldrich (South Africa).

Conjugation of O-(2-Aminoethyl) PEG to 5' RNA aptamers

PEGylated RNA aptamers were synthesised using the modified EDAC/imidazole technique described by Ghosh et al. 1990. To a 7.5 μ L solution of RNA aptamer, EDAC (1.25 mg) and 5 μ L of 0.25 M O-(2-Aminoethyl)-PEG in 0.1 M imidazole (pH 6.0) were added. The reaction solution was mixed thoroughly by vortexing and then centrifuged for 5 min. Twenty microliters

(20 μ L) of 0.1 M imidazole (pH 6.0) was added to the solution and mixed for 48 h at room temperature. The resulting solution was subjected to centrifugation using Vivaspin[®] tubes to remove the by-product of EDAC and excess imidazole. The solution was lyophilized to obtain white powder.

Analysis of PEGylated and non-PEGylated RNA aptamers by urea gel

The integrity and size of PEGylated and non-PEGylated RNA aptamers were analysed on 8 M urea gel. The gel was prepared using 8-12% acrylamide (40% acrylamide/Bis-acrylamide, BioRad Laboratories GmbH, München), 8 M Urea (Thermo Fischer scientific, Inc MA, USA), 0.05% APS, 0.1% tetramethylethylenediamine (TEMED, Merck, South Africa) and 1 \times tris base, boric acid and EDTA buffer (TBE). RNA aptamers were mixed with 2 \times RNA loading dye (95% formamide, 0.025% SDS, 0.025% bromophenol blue, 0.025% xylene cyanol FF; 0.025% ethidium bromide; 0.5 mM EDTA) and denatured at 70 °C for 15 min. The gel was pre-run in 1 \times TBE buffer at 100 V for 30 min. Samples were loaded alongside a molecular weight marker (low range DNA marker) and the gel was electrophoresed at 200 V. Thereafter, the gel was stained with ethidium bromide and RNA bands were visualized on a molecular imager ChemiDoc XRS Imaging System (BioRad, USA).

Stability of PEGylated and non-PEGylated RNA aptamers in breast milk

The *in vitro* stability tests were carried out on PEGylated and non-PEGylated RNA aptamers. Briefly, to a 2 to 5 μ g of breast milk was added 10 μ g of PEGylated or non-PEGylated RNA aptamers separately at 37 °C placed in a water bath. At predetermined time intervals, a tube was withdrawn and ethidium bromide (10 μ l) was added to stop the reaction and denatured at 70 °C for 15 min. Then the electrophoresis was performed at 200 V and visualized on a molecular imager ChemiDoc XRS Imaging System (BioRad, USA).

HIV-1 neutralization assay

Single cycle pseudovirus neutralization assay was performed as described previously (London et al., 2015). Briefly, in the neutralization assay, threefold serial dilutions of aptamers (inhibitors) prepared in 25 μ L of DMEM was incubated with 25 μ L of 200 50% tissue culture infectious dose (TCID₅₀) of HIV-1 Du151 Env pseudovirions in a 96-well plate for 1 h at 37

°C, 5% CO₂. This was followed by the addition of 10⁴ TZM-bl cells/well and the plate was incubated at 37 °C, 5% CO₂ for an additional 48 h. After the incubation, 75 µL of supernatant was removed and 50 µL of Bright-Glo Luciferase assay substrate (Promega; Madison, WI, USA) was added to the cells. The plate was incubated for 2 min followed by the transfer of 75 µL of cell lysates to a solid black 96-well plate (Nunclon, Nunc, Thermo scientific) and luminescence was measured using Tecan-i-control, Infinite F500 (Männendof, Switzerland). The IC₅₀ values were calculated as the aptamer concentrations that caused 50% reduction of virus infection compared to virus control wells after subtraction of the background.

Preparation of PEGylated aptamer nanoparticles

PEGylated aptamer nanoparticles were produced using a modified double emulsion method (L. Tshweu et al. 2013). Briefly, PVA (1 mL, 1%) in water and Pluronic F127 (1 mL, 1%) containing PEGylated aptamer (1 mg, 930.9 ng/µL) in water were emulsified for 2 min with a solution of PCL (100 mg) in ethyl acetate (10 ml) using a high speed homogeniser at 5 000 rpm to form the primary water-in-oil emulsion (w₁/o). This emulsion was decanted into an aqueous solution (w₂) which consisted of 1% Pluronic F127 and the mixture was homogenised for 5 min at 8 000 rpm to form the water-in-oil-in-water (w₁/o/w₂) emulsion. The ethyl acetate was removed by high vacuum pump and the water was removed by lyophilization to obtain the PEGylated aptamer nanoparticles as a white powder.

Preparation of poly(epsilon-caprolactone) nanoparticles

PCL nanoparticles were produced using a modified double emulsion method. Briefly, PVA (1 mL, 1%) in water and Pluronic F127 (1 mL, 1%) in water were emulsified (2 min) with a solution of PCL (100 mg) in ethyl acetate (10 ml) using a high speed homogeniser (5 000 rpm) to form the w₁/o. This emulsion was decanted into an aqueous solution (w₂) comprised of 1 % Pluronic F127 and, the mixture was homogenised for 5 min (8 000 rpm) to form w₁/o/w₂ emulsion. After completion, the w₁/o/w₂ emulsion was directly subjected into high vacuum pump to remove the solvent and lyophilized to obtain white powder.

Particle size, particle size distribution and surface charge

The mean particle size and particle size distribution (polydispersity index, PDI) of the nanoparticles was determined by means of dynamic light scattering (DLS, Malvern Zetasizer Nano ZS, Malvern Instruments) at 25 °C. Samples were prepared by dispersing a small amount of the nanoparticles in deionised water and sonicated to ensure appropriate diffusion before measurement. Zeta potential (surface charge) of the nanoparticles was also measured using the same instrument. All results are expressed as mean \pm standard deviation (SD).

Electrochemical investigation of binding ability of PEGylated aptamer nanoparticles

Electrochemical impedance spectroscopy (EIS) was used to investigate the binding ability of the PEGylated aptamer and PEGylated aptamer nanoparticles. All solvents were purged of air by bubbling nitrogen gas prior to each characterisation experiment. Cyclic voltammetry (CV) and electrochemical impedance spectroscopy (EIS) characterizations were done immediately after each immobilization.

Prior to modification, the gold electrode was cleaned following the protocol reported elsewhere (Mathebula et al., 2009). Briefly, the gold electrode was firstly polished using an aqueous slurry of alumina to a mirror finish on Buehler felt pad. The electrode was rinsed with excess of distilled water and then subjected to ultrasonic vibration (Optima Scientific CC, Model: DC150H) in acetone to remove residual alumina particles at the surface. The electrode was again rinsed with distilled water and then dipped into freshly prepared Piranha solution ($\text{H}_2\text{O}_2:\text{H}_2\text{SO}_4$, 1:3) for about 2 min, followed by copious rinsing once again with distilled water. Finally, to confirm that the electrode surface was clean, cyclic voltammetry (CV) experiments were carried out with the electrode in H_2SO_4 (0.5 M) at a scan rate of 50 mV/s and a potential window of -0.2 V and -1.2 V.

A self-assembled monolayer (SAM) of mercaptoacetic acid (MACA) was formed on the cleaned gold electrode by incubating it in a N_2 -purged absolute ethanol solution of the acid (2%, 2 mL) for 24 h at 25 °C. The free carboxylic acid of the MACA was activated in a PBS buffer solution (pH 7.4) of EDAC (0.2 M) and sulfo-NHS (0.4 M) for 1 h to the active NHS esters. The Au-MACA electrode was rinsed with PBS buffer (pH 7.4) to remove by-products of EDAC/sulfo-NHS. Gp 120 protein was covalently linked into the activated Au-MACA by

immersing the electrode in PBS solution of gp 120 (100 ug/1 ml) for 48 h at 4 °C. The Au-MACA-gp 120 electrode was rinsed several times with PBS buffer to remove unbound proteins. The electrode was then immersed in 2.0 mg/mL PBS solution of ethanolamine for 3 h to block the unreacted and nonspecific binding sites.

The Au-MACA-gp 120 was incubated with PEGylated aptamer nanoparticles at 4 °C for 24 h. After the immobilization of the PEGylated aptamer nanoparticles, the electrode was cleaned with PBS solution to remove physically bound PEGylated aptamer nanoparticles.

Investigation of Bare Gold Electrode Surface by cyclic voltammetry and electrochemical impedance spectroscopy

Electrochemical measurements were carried out in triplicates in a solution of $K_3[Fe(CN)_6]/K_4[Fe(CN)_6]$ (40 mL, 1.0 mM) containing KCl (1.0 M). Cyclic voltammetry experiments were run at a scan rate of 20 mV/s and potential window of -0.1 to 0.5 V at room temperature. The impedance measurements were taken at a formal potential of 209 mV, which is equal to $E_{1/2}$ of the electrode. The electrochemical experiments, cyclic voltammetry (CV) and electrochemical impedance spectroscopy (EIS), were done on an Autolab Potentiostat PGSTAT 302 from Eco Chemie, Utrecht, Netherlands. Data was acquired and processed with General Purpose Electrochemical Systems (GPES) and Frequency Response Analyser (FRA) software version 4.9. For control experiments, the protocol described above was repeated with empty PCL nanoparticles.

Preparation of Solutions

a. Preparation of Phosphate-Buffered Saline Containing Sodium Azide and EDTA (PBS/AE, pH 7.4)

Phosphate buffered saline (PBS) azide EDTA buffer (PBS/AE) with the following: NaCl (8.0 g), KCl (0.2 g), KH_2PO_4 (0.2 g) and Na_2HPO_4 (1.05 g) dissolved in ddd H_2O (1.0 L) with 1 mM EDTA and sodium azide 0.025% (m/v). The solution was adjusted to pH 7.4.

b. Preparation of Ferricyanide/Ferrocyanide Redox Probe Solution (1.0 mM)

In PBS/AE buffer (250 ml) was dissolved $K_3[Fe(CN)_6]$ (82.3 mg, 0.25 mmol), $K_4[Fe(CN)_6]$ (105.6 mg, 0.25 mmol), and KCl (1.86 g, 25 mmol). The solution was prepared a few days

before use and purged of air by bubbling an inert gas through it for at least 30 min immediately before every electrochemistry experiment.

c. Preparation of tris base, boric acid and EDTA (TBE) Buffer

Tris base, boric acid and EDTA (TBE) Buffer with the following: tris base (108 g boric acid (55 g) and EDTA (7.44 g) dissolved in ddd H₂O (1.0 L) with 1 mM EDTA and sodium azide 0.025% (m/v). To make 1 × TBE buffer: 1.0 L TBE buffer was mixed with 9.0 L ddd H₂O.

6.2 Experimental for Chapter Three

Chemical Data

Poly(ethylene glycol) bis(amine) (PEG, MW 1.5 KDa), PCL (10 KDa), poly(vinylalcohol) (PVA, 13-23 KDa, 87-89% hydrolyzed), N-(ethylcarbonimidoyl)-N,N-dimethylpropane-1,3-diamine monohydrochloride (EDAC), N-hydroxysulfosuccinimide (sulfo-NHS), Madin-Darby bovine kidney (MDBK), MEM, foetal bovine serum (FBS), penicillin/streptomycin, 4-(2-hydroxyethyl)-1-piperazineethanesulfonic acid (HEPES) buffer and 3-(4, 5-dimethylthiazol-2-yl)-2, 5-diphenyl tetrazolium bromide [MTT] were obtained from Sigma-Aldrich (South Africa). N,N-dimethylformamide (DMF), ethyl acetate and drying-aid excipient lactose monohydrate were obtained from Sigma-Aldrich (South Africa). With the exception of Moxifloxacin hydrochloride (Mox) purchased from DB Fine Chemicals (South Africa). All other chemicals were of analytical grade and purchased from Sigma-Aldrich (South Africa).

Synthesis of PEG-Mox conjugate

To a stirred solution of Mox.HCl (64 mg, 0.15 mmol) in anhydrous DMF (3 mL) was added EDAC (93.12 mg, 0.6 mmol) and sulfo-NHS (116.5 mg, 0.6 mmol). The reaction was allowed to run in the dark at room temperature. After 3 h the crude solution was added dropwise to PEG (200 mg, 0.13 mmol) [dissolved in anhydrous DMF (2 mL)] and the reaction was allowed to run overnight in the dark at room temperature. At the end of the reaction period the DMF was removed under reduced pressure. Cold diethyl ether/ethanol solution (50 mL, 4:1 v/v) was added to the crude product and vortexed. The precipitate was collected by centrifugation (6000 rpm), washed twice again with the same solution, dissolved in PBS buffer (pH 7.4) and finally lyophilized to obtain the PEG-Mox conjugate.

Synthesis of PCL-Mox nanoparticles

PCL-Mox nanoparticles were prepared using a modified double emulsion spray-dried method (Tshweu et al. 2013). An aqueous solution of PVA (2%, 2 mL) containing PEG-Mox conjugate (the conjugate contains 100 mg Mox) was emulsified for 3 min with a solution of PCL (100 mg, 8 mL), dissolved in ethyl acetate by means of a high-speed homogeniser (Silverson L4R GX-10 model, Silverson Machines Limited, United Kingdom) rotating at 5000 rpm to form a water-in-oil (w_1/o) emulsion. The resulting emulsion was transferred into an aqueous solution (20 mL) containing PVA (2%) and lactose (5%). The mixture was homogenised for 5 min at 8000 rpm to form water-in-oil-in-water ($w_1/o/w_2$) emulsion. The nanoemulsion was immediately spray-dried (model B-290, BuchiLabortechnik AG, Switzerland) to produce a powder of PCL-Mox nanoparticles. Empty PCL nanoparticles were prepared without adding the PEG-Mox conjugate to the formulation.

Particle size, particle size distribution and zeta potential

Dynamic light scattering (DLS, Malvern Zetasizer Nano ZS, Malvern Instruments) was used to determine average particle size and particle size distribution (expressed as polydispersity index, PDI) at 25°C. Typically, PEG-Mox (1 mg) conjugate and PCL-Mox nanoparticles (1 mg) were dissolved and suspended, respectively, in filtered deionised water (0.2 μm , 2 mL) and sonicated for 10 s to ensure uniform dispersion before measurement. Surface charge densities, i.e. the zeta potential, of the PEG-Mox conjugate and PCL-Mox nanoparticles were measured using the same instrument.

Morphology

Scanning electron microscopy (SEM, Field Emission Electron Microscope, JEOL JSM-7500F, Japan) was used for morphology studies. Nanoparticles were mounted onto carbon stubs using a double-sided carbon adhesive tape and sputter-coated with conductive gold prior to SEM examination.

Encapsulation efficiency

The PEG-Mox conjugate encapsulation efficiency (EE) was calculated as the percentage of drug entrapped in PCL nanoparticles compared with the initial amount of PEG-Mox conjugate. This was done using UV-visible spectrophotometer (Perkin Elmer, Lambda 35, Singapore). Briefly, PCL-Mox nanoparticles (20 mg, 10 mL) were dispersed in deionised water and sonicated to obtain a homogenous particle distribution. The sample was centrifuged (10 °C, 15000 rpm) and the supernatant was analyzed by UV. The EE was calculated using the following equation:

$$\% EE = \frac{Mox_0 - Mox_{supernatant}}{Mox_0};$$

and is defined by the ratio of measured and initial amount of the Mox encapsulated in the nanoparticles. Where PEG-Mox₀ and PEG-Mox_{supernatant} are the initial amount of drug used in the production of the nanoparticles (100 mg) and in the Mox concentration in the supernatant after the centrifugation.

X-ray diffraction

X-ray diffraction (XRD) measurements of pure polymers, i.e. PCL, Mox, PCL nanoparticles and PCL-Mox nanoparticles were carried out using Phillips X'Pert PRO diffractometer from PANalytical (Netherlands) under reflection–transmission mode. Samples were placed in glass sample holders and scanned from $2\theta = 5^\circ$ to 60° , using a beam of Cu K α radiation of $\lambda = 0.1542$ nm, operated at 45 kV, 40 mA. The scan speed and exposure time were 0.109419°/s and 17 min 27 s, respectively.

Thermogravimetric analysis

Thermogravimetric analysis (TGA) of pure polymers, i.e. PEG and PCL, Mox, PCL nanoparticles and PCL-Mox nanoparticles were characterized using a thermal analysis (TA) Instrument (TGA Q 500, USA), using balance and sample purge nitrogen gas of 30 and 60 mL/min, respectively. Sample weights between 5 and 12 mg were used and placed into open aluminium pans. A heating rate of 10 °C/min was implemented, with a heating ramp from room temperature to 700 °C.

² Hemolysis studies

Preparation of erythrocyte suspensions

Blood was collected from healthy human donors in BD Vacutainer® Venous Blood Collection Tubes already prepared with 10-30 USP units of heparin/mL of blood in order to prevent clotting. 10 mL of blood was centrifuged at 500xg for 10 min at 4 °C to separate plasma and erythrocytes. The retrieved erythrocytes were washed three times with six volumes of the PBS (pH 7.4) buffer. The buffy coat was carefully removed with each wash. After the last washing, the packed cells were re-suspended in PBS and the haematocrit was determined.

Erythrocytes (RBCs) Lysis Reaction

Mox, PEG-Mox conjugate, PCL-Mox nanoparticles and PCL nanoparticles were dissolved or suspended in PBS (1 mL, pH 7.4) and serially diluted from 1 mg/mL to 0.98 ng/mL. After overnight incubation with shaking at 37 °C for all samples, 400 µL of each sample was added to 100 µL RBC solution (1 mL RBC in 10 mL PBS). After 4 hours of incubation at 37 °C, all tubes were centrifuged for 10 min at 2000 rpm and the supernatant was withdrawn and haemolysis was estimated from the 540 nm absorbance of haemoglobin released into the supernatant using Abbotta Kinetic Spectrophotometer. The results were expressed as percent haemolysis. Zero haemolysis was taken as the absorbance of the supernatant of only the RBC in PBS solution while 100% haemolysis was taken as the absorbance of the supernatant when buffer was replaced by 1% w/v solution of Triton X100. These were the negative and positive controls, respectively. Percent haemolysis was calculated according to the equation:

² Mohamed Shamies, Aya Abdelghany, Abdullah Gouda

Biochemistry & Molecular Biology Department, Theodor Bilharz Research Institute, Warak El-Hadar, Kornish El-Nile, P.O. Box 30, Imbaba, 12411-Giza, Egypt.

$$\% \text{Haemolysis} = \left[\frac{(\text{Average absorbance of the sample}) - (\text{Average absorbance of the negative control})}{(\text{Maximum absorbance of positive control})} \right] \times 100$$

MTT 3-[(4, 5-dimethylthiazol-2-yl)-2, 5-diphenyl tetrazolium bromide] Assay

Sample preparation:

Mox, PEG-Mox conjugate and PCL-Mox nanoparticles were dissolved or suspended in PBS (pH 7.4). Serial dilution of each element with drug content ranging from 1 mg/ml to 3.9 ng/ml was prepared using maintenance media (MEM growth media containing 2% foetal bovine serum (FBS), 1% penicillin/streptomycin and 1% HEPES buffer) to produce standard solutions that are further used in the MTT assay.

Cell line Preparation:

Madin-Darby bovine kidney (MDBK) cells were grown in MEM growth medium containing 10% foetal bovine serum (FBS), 1% penicillin/streptomycin and 1% HEPES buffer. 100 μL of cell solution was plated in a 96-well culture plate and made up to 200 μL using maintenance media to produce cell count of 40 000. The culture was incubated for 24 h at 37 $^{\circ}\text{C}$ to reach 70% confluency and 100 μL of each drug at the concentration to be tested was added to the wells. Two wells of only media for negative control and blank were also prepared. The plate was incubated for 48 h at 37 $^{\circ}\text{C}$ after which the medium was replaced with 200 μL of fresh medium. 50 μL of 5 mg/ml of MTT (3-[(4, 5-dimethylthiazol-2-yl)-2, 5-diphenyl tetrazolium bromide) dye was added to each well. The plate was covered with aluminium foil and incubated for 4 h at 37 $^{\circ}\text{C}$. The medium containing MTT was removed and 200 μL DMSO added to solubilize the formazan crystals. The absorbance was measured at 490 nm with a ELX-50 plate reader (Bioteck instrument, US) using reference wavelength of 655 nm. The percent cytotoxicity was calculated using the formula:

$$\% \text{Cytotoxicity} = \left[\frac{A \text{ sample} - A \text{ blank}}{A \text{ medium control} - A \text{ blank}} \right] \times 100$$

***In vitro* stability in plasma**

The *in vitro* stability of the PCL-Mox nanoparticles was studied in human plasma. Fresh whole blood was collected from human donors in EDTA tubes to inhibit blood clotting. The blood samples were centrifuged (2200 rpm) to pellet the erythrocytes and collect the plasma. The PCL-Mox nanoparticles were suspended in PBS buffer (1mg/mL, pH 7.4). Different concentrations of each element were prepared to produce standard solutions that were further used in HPLC analysis.

The reactions were initiated by addition of the nanoparticle suspension (400 μ L) to 1 mL of plasma and incubated at 37 °C with mild shaking. At regular time intervals (6, 12, 24, 48, 72, and 96 h), 100 μ L of PCL-Mox nanoparticles were withdrawn and immediately placed on ice to stop plasma protein reaction. HPLC grade acetonitrile (135 μ L) was added to precipitate the plasma proteins followed by supernatant withdrawal for HPLC analysis. The same procedure was applied to plasma alone to determine its correspondent chromatogram to correct for matrix interference.

6.3 Experimental for Chapter Four

General

Lumefantrine (Lumf) was supplied by Novartis (Switzerland). Polyethylene glycol (PEG, 5 KDa), N-(ethylcarboimidoyl)-N,N-dimethylpropane-1,3-diamine monohydrochloride (EDAC), N-hydroxysulfosuccinimide (sulfo-NHS), diisopropyl carbodiimide (DIC), 4-Dimethylaminopyridine (DMAP), N,N-Diisopropylethylamine (DIEA) and Hydroxybenzotriazole (HOBt) were obtained from Sigma-Aldrich (South Africa). p-NAM-*stat*-p-AA was received as a gifts (Cheng Sang, Monash University, Australia). Thin layer chromatography (TLC) was obtained on a commercially available silica plates (Merck Kieselgel 60 0.25 mm F254) purchased from Merck chemicals (South Africa).

All moisture sensitive reactions were carried out using anhydrous solvents under dry conditions and purging with nitrogen gas. Glassware was washed and dried in an oven at 90 °C before use. For experiments requiring strictly dry conditions all non-melting equipment was further dried at 120 °C for a minimum of 12 h before use. Solvents used in such reactions were appropriately dried also for a minimum of 12 h and where necessary distilled immediately before use. Reactions were monitored by TLC using silica gel plates. The plates were viewed under with ethanolic solution of phosphomolybdic acid (PMA) and charred with an electric heat gun. Column chromatography was done with Merck silica gel 60 (0.063-0.200 mm). All other chemicals were of analytical grade and purchased from Sigma-Aldrich (South Africa).

The ^1H and ^{13}C nuclear magnetic resonance (NMR) spectra were recorded on a 600MHz Varian INOVA or 400MHz Varian INOVA spectrometers. Chemical shifts (δ) are reported in parts per million (ppm) downfield with deuteriated chloroform (CDCl_3) as a solvent and an internal reference. For polymer-drug conjugates only chemical shifts of clearly resolved peaks are reported as spectra contains many overlapping multiplets. ATR/FTIR was carried out using Perkin Elmer spectrum 100 FTIR spectrophotometer between 4000 and 650 cm^{-1} . Particle size, particle size distribution and zeta potential were obtained on Dynamic light scattering (DLS, Malvern Zetasizer Nano ZS, Malvern Instruments). Mass spectra were recorded on a Bruker Microtof ESI instrument

Lumf-Succinic acid conjugate (Lumf-Succ conjugate)

To a stirred solution of the alcohol (1.0 g, 1.9 mmol) in anhydrous DMF (10.0 ml) was added succinic anhydride (0.57 g, 5.7 mmol) and DMAP (0.023 g, 0.19 mmol). The reaction was allowed to run in the dark for 18 hours when TLC showed all the alcohol had been consumed. To quench, the reaction mixture was concentrated *in vacuo* and subjected to silica gel column chromatography for purification. $R_f = 0.75$ (acetone:ethylacetate, 1:1, containing trimethylamine) (0.82 g, 90%). ^1H NMR (400); δ_{H} (600 MHz, CDCl_3):

Synthesis of PEG-NH₂

To a stirred solution of alcohol (5.0 g, 1.0 mmol) in dry CH_2Cl_2 (15 ml) was added triethylamine (303.5 mg). The solution was cooled to 0 °C in an ice-bath and stirred for 30 min under nitrogen. Toluene sulfonylchloride (953.25 mg, 5 mmol) was added and the reaction was

continued at 0 °C for 3 hours. The solvent was evaporated and the crude product was purified by precipitating with diethyl ether. The pellet was washed several times with diethyl ether (4 x 100 ml) and dried under *vacuo*.

To a stirred solution of the tosylate (5 g, 1 mmol) in dry CH₂Cl₂:DMF (1:3) (15 ml) was added ethylene diamine (180,03 mg, 3 mmol) and the reaction was stirred for 48 h at 40 °C. The solvent was then evaporated and the crude product was purified by precipitating with diethyl ether. The pellet was washed several times with diethyl ether (4 x 100 ml) and dried under *vacuo*.

Conjugation of Lumf-Succ to PEG-OH

To a stirred solution of acid, Lum-Succ conjugate (0.10 g, 0.16 mmol) in anhydrous DMF (5.0 ml) was added the alcohol, PEG-OH (1.59 g, 0.32 mmol), EDAC (0.1 g, 0.52 mmol) and Sulfo-NHS (0.075 g, 0.35 mmol). The reaction was allowed to proceed at 40 °C under a condenser for 48 hours. The reaction was terminated when TLC showed complete consumption of the starting acid and appearance of a UV active spot on the baseline. To quench, the reaction mixture was allowed to cool to room temperature and concentrated *in vacuo*. PBS buffer (30.0 mL, pH 7.4) was poured into the crude mixture and stirred at 40 °C for 18 hours. After this, the mixture was centrifuged in a normal 50 mL centrifuge tube at 13 000 rpm and 25 °C for three periods of 1 h each to obtain a yellowish supernatant containing the product and a yellow pellet of by-products. The aqueous supernatant was further purified by repeated centrifugation in a Vivaspin™ ultrafiltration tube (PES membrane, MWCO 3kDa) at 13 000 rpm and 25 °C. The final concentrate was freeze-dried to yield the product; PEG-o-Succ-Lumf conjugate, as a yellowish powder. $R_f = 0.00$ (acetone : ethylacetate, 1:1); (600MHz, CDCl₃):

Conjugation of Lumf-Succ to PEG-NH₂

To a stirred solution of acid; Lum-Succ (0.063 g, 0.10 mmol) in anhydrous DMF (2.5 ml) was added the amine; PEG-NH₂ (0.40 g, 0.08 mmol), EDAC (0.094 g, 0.60 mmol) and Sulfo-NHS (0.046 g, 0.40 mmol). The reaction was allowed to proceed at 40 °C under a condenser for 48 h. The reaction was terminated when TLC showed complete consumption of the starting acid and appearance of a UV active spot on the baseline. To quench, the reaction mixture was allowed to cool to room temperature and concentrated *in vacuo*. PBS buffer (30.0 mL, pH 7.4)

was poured into the crude mixture and stirred at 40 °C for 18 hours. After this, the mixture was centrifuged in a normal 50 mL centrifuge tube at 13 000 rpm and 25 °C for three periods of 1 h each to obtain a yellowish supernatant containing the product and a yellow pellet of by-products. The aqueous supernatant was further purified by repeated centrifugation in a Vivaspin™ ultrafiltration tube (PES membrane, MWCO 3kDa) at 13 000 rpm and 25 °C. The final concentrate was freeze-dried to yield the product; PEG-NH-Succ-Lumf conjugate; as a yellowish powder. $R_f = 0.00$ (acetone : ethylacetate, 1 : 1); δ_H (600MHz, $CDCl_3$):

Conjugation of Lumf to p-NAM-stat-p-AA

To a stirred solution of acid; p-NAM-stat-p-AA (0.200 g, 0.015 mmol) in anhydrous DMF (5.0 ml) was added the alcohol Lumf (0.118 g, 0.224 mmol), EDAC (0.009 g, 0.045 mmol) and Sulfo-NHS (0.0097 g, 0.045 mmol). The reaction was allowed to proceed at 40 °C under a condenser for 48 hours. The reaction was terminated when TLC showed complete consumption of the starting acid and appearance of a UV active spot on the baseline. To quench, the reaction mixture was allowed to cool to room temperature and concentrated *in vacuo*. PBS (30.0 ml, pH 7.4) was poured into the crude mixture and stirred at 40 °C for 18 hours. After this, the mixture was centrifuged in a normal 50 ml centrifuge tube at 13 000 rpm and 25 °C for three periods of 1 hour each to obtain a yellowish supernatant containing the product and a yellow pellet of by-products. The aqueous supernatant was further purified by repeated centrifugation in a Vivaspin™ ultrafiltration tube (PES membrane, MWCO 3kDa) at 13 000 rpm and 25 °C. The final concentrate was freeze-dried to yield the product as a yellowish powder. $R_f = 0.00$ (acetone : ethylacetate, 1 : 1); δ_H (600MHz, $CDCl_3$)

Solubility and Partition Coefficients of the synthesized polymer-drug conjugates

The solubility was determined by dissolving the polymer-drug conjugates in PBS (pH 7.4) and the concentration was increased gradually from 1 mg/mL to 4 mg/mL. After 30 min incubation with shaking at room temperature, the conjugates were sonicated followed by centrifugation at 13 000 rpm and 25 °C for 5 min. The supernatants were then analyzed by UV-Vis spectrophotometry using the following equation $y = 18.879x + 0.1365$ ($R^2 = 0.9942$)

The partition coefficients was determined by dissolving 1 mg/mL (drug equivalent in the conjugate) in PBS solution (ph 7.4) followed by 1 mL of DCM. The mixture was vortexed for

24 h and the concentration in each layer was calculated by UV-Vis spectrophotometry. The LogP was obtained by $[c]_{\text{DCM}}/[c]_{\text{water}}$.

References

- Adamson, N.J., Reynolds, E.C., 1997. Rules relating electrophoretic mobility, charge and molecular size of peptides and proteins. *J. Chromatogr. B Biomed. Appl.* 699, 133–147. [https://doi.org/10.1016/S0378-4347\(97\)00202-8](https://doi.org/10.1016/S0378-4347(97)00202-8)
- Al-Huniti, N., Chapel, S., Xu, H., Bui, K.H., Sostek, M., 2016. Population pharmacokinetics of naloxegol in a population of 1247 healthy subjects and patients. *Br. J. Clin. Pharmacol.* 81, 89–100. <https://doi.org/10.1111/bcp.12756>
- Alessandro, U.D., 2009. Existing antimalarial agents and malaria-treatment strategies 1291–1306.
- Alexandre, K.B., Mufhandu, H.T., London, G.M., Chakauya, E., Khati, M., 2016. Progress and Perspectives on HIV-1 microbicide development. *Virology* 497, 69–80. <https://doi.org/10.1016/j.virol.2016.07.004>
- Almudena Prudencio, Robert C. Schmeltzer, K.E.U., 2013. Effect of Linker Structure on Salicylic Acid-Derived Poly(anhydride-esters). *Macromolecules* 31, 1713–1723. <https://doi.org/10.1109/TMI.2012.2196707>. Separate
- Aly, A.S.I., Vaughan, A.M., Kappe, S.H.I., 2010. Malaria Parasite Development in the Mosquito and Infection of the Mammalian Host. *Annu Rev Microbiol* 63, 195–221. <https://doi.org/10.1146/annurev.micro.091208.073403>. Malaria
- Anderson, P.L., Kakuda, T.N., Lichtenstein, K. a, 2004. The cellular pharmacology of nucleoside- and nucleotide-analogue reverse-transcriptase inhibitors and its relationship to clinical toxicities. *Clin. Infect. Dis.* 38, 743–753. <https://doi.org/10.1086/381678>
- Apetrei, C., Gormus, B., Pandrea, I., Metzger, M., ten Haaft, P., Martin, L.N., Bohm, R., Alvarez, X., Koopman, G., Murphey-Corb, M., Veazey, R.S., Lackner, A. a, Baskin, G., Heeney, J., Marx, P. a, 2004. Direct inoculation of simian immunodeficiency virus from sooty mangabeys in black mangabeys (*Lophocebus aterrimus*): first evidence of AIDS in

- a heterologous African species and different pathologic outcomes of experimental infection. *J. Virol.* 78, 11506–11518. <https://doi.org/10.1128/JVI.78.21.11506-11518.2004>
- Arpagaus, C., Schafroth, N., Meuri, M., 2010. Laboratory Scale Spray Drying of Lactose: A Review. *Inf. Bull. Büchi Switz.* 1–12.
- Arts, E.J., Hazuda, D.J., 2012. HIV-1 antiretroviral drug therapy. *Cold Spring Harb. Perspect. Med.* 2. <https://doi.org/10.1101/cshperspect.a007161>
- Babina, S.E., Semenov, D. V., Buneva, V.N., Nevinsky, G.A., 2005. Human milk lactoferrin hydrolyzes ribonucleoside 5'-triphosphates. *Mol. Biol.* 39, 452–458. <https://doi.org/10.1007/s11008-005-0061-5>
- Bailon, P., Berthold, W., Bailon, P., Berthold, W., 1998. Polyethylene glycol-conjugated pharmaceutical proteins 1, 352–356.
- Bajaj, I., Singhal, R., 2011. Poly (glutamic acid) - An emerging biopolymer of commercial interest. *Bioresour. Technol.* <https://doi.org/10.1016/j.biortech.2011.02.047>
- Baker, O., Lee, O.Y.C., Wu, H.H.T., Besra, G.S., Minnikin, D.E., Llewellyn, G., Williams, C.M., Maixner, F., O'Sullivan, N., Zink, A., Chamel, B., Khawam, R., Coqueugniot, E., Helmer, D., Le Mort, F., Perrin, P., Gourichon, L., Dutailly, B., Pálfi, G., Coqueugniot, H., Dutour, O., 2015. Human tuberculosis predates domestication in ancient Syria. *Tuberculosis* 95, S4–S12. <https://doi.org/10.1016/j.tube.2015.02.001>
- Balint, G.A., 2001. Antiretroviral therapeutic possibilities for human immunodeficiency virus/acquired immunodeficiency syndrome. *Pharmacol. Ther.* 89, 17–27. [https://doi.org/10.1016/S0163-7258\(00\)00101-7](https://doi.org/10.1016/S0163-7258(00)00101-7)
- Banerjee, S.S., Aher, N., Patil, R., Khandare, J., 2012. Poly(ethylene glycol)-Prodrug Conjugates: Concept, Design, and Applications. *J. Drug Deliv.* 2012, 1–17. <https://doi.org/10.1155/2012/103973>
- Barbas, A.S., Mi, J., Clary, B.M., White, R.R., 2010. Aptamer applications for targeted cancer therapy. *Future Oncol.* 6, 1117–1126. <https://doi.org/10.2217/fon.10.67>

- Barril, P., Nates, S., 2012. Introduction to Agarose and Polyacrylamide Gel Electrophoresis Matrices with Respect to Their Detection Sensitivities. *Gel Electrophor. - Princ. Basics*. <https://doi.org/10.5772/38573>
- Barry 3rd, C.E., Lee, R.E., Mdluli, K., Sampson, A.E., Schroeder, B.G., Slayden, R.A., Yuan, Y., 1998. Mycolic acids: structure, biosynthesis and physiological functions. *Prog. Lipid. Res.* 37, 143–179. [https://doi.org/S0163-7827\(98\)00008-3](https://doi.org/S0163-7827(98)00008-3) [pii]
- Bauld, N.L., 2001. Chapter 21: Amines.
- Beaumier, C.M., Gomez-Rubio, A.M., Hotez, P.J., Weina, P.J., 2013. United States Military Tropical Medicine: Extraordinary Legacy, Uncertain Future. *PLoS Negl. Trop. Dis.* 7. <https://doi.org/10.1371/journal.pntd.0002448>
- Bertrand, N., Wu, J., Xu, X., Kamaly, N., Farokhzad, O.C., 2015. HHS Public Access 2–25. <https://doi.org/10.1016/j.addr.2013.11.009.Cancer>
- Besra, G.S., Brennan, P.J., 1997. The mycobacterial cell envelope: A target for novel drugs against tuberculosis. *J. Pharm. Pharmacol.* 49, 25–30. <https://doi.org/10.1111/j.2042-7158.1997.tb06146.x>
- BiscevicTokic, J., Tokic, N., Musanovic, A., 2013. Pneumonia as the Most Common Lower Respiratory Tract Infection. *Med. Arch.* 67, 442. <https://doi.org/10.5455/medarh.2013.67.442-445>
- Bobo, D., Robinson, K.J., Islam, J., Thurecht, K.J., Corrie, S.R., Corrie, S.R., 2016. Nanoparticle-Based Medicines: A Review of FDA-Approved Materials and Clinical Trials to Date. *Pharm. Res.* 2373–2387. <https://doi.org/10.1007/s11095-016-1958-5>
- Bouchard, P.R., Hutabarat, R.M., Thompson, K.M., 2010. Discovery and Development of Therapeutic Aptamers. *Annu. Rev. Pharmacol. Toxicol.* 50, 237–257. <https://doi.org/10.1146/annurev.pharmtox.010909.105547>
- Bousema, T., Drakeley, C., 2011. Epidemiology and infectivity of *Plasmodium falciparum* and *Plasmodium vivax* gametocytes in relation to malaria control and elimination. *Clin. Microbiol. Rev.* 24, 377–410. <https://doi.org/10.1128/CMR.00051-10>

- Brennan, P.J., 2003. Structure, function, and biogenesis of the cell wall of *Mycobacterium tuberculosis*. *Tuberculosis* 83, 91–97. [https://doi.org/10.1016/S1472-9792\(02\)00089-6](https://doi.org/10.1016/S1472-9792(02)00089-6)
- Brennan, P.J., Crick, D.C., 2007. The cell-wall core of *Mycobacterium tuberculosis* in the context of drug discovery. *Curr. Top. Med. Chem.* 7, 475–488. <https://doi.org/10.2174/156802607780059763>
- Broder, S., 2010. The development of antiretroviral therapy and its impact on the HIV-1/AIDS pandemic. *Antiviral Res.* 85, 1–18. <https://doi.org/10.1016/j.antiviral.2009.10.002>
- Büchi Labortechnik AG, 2002. Training Papers Spray Drying. *Train. Pap.* 1–19.
- Bunaciu, A.A., Udriștioiu, E. gabriela, Aboul-Enein, H.Y., 2015. X-Ray Diffraction: Instrumentation and Applications. *Crit. Rev. Anal. Chem.* 45, 289–299. <https://doi.org/10.1080/10408347.2014.949616>
- Buss, N., Snell, P., Bock, J., Hsu, A., Jorga, K., 2001. Saquinavir and ritonavir pharmacokinetics following combined ritonavir and saquinavir (soft gelatin capsules) administration. *Br. J. Clin. Pharmacol. Suppl.* 52, 255–264. <https://doi.org/10.1046/j.0306-5251.2001.01452.x>
- Byerly, C.R., 2017. Review : Of Smallpox and Empire Reviewed Work (s): *Pox Americana : The Great Smallpox Epidemic of 1775-82* by Elizabeth Anne Fenn Review by : Carol R . Byerly and Carol Byerly Source : *Reviews in American History* , Vol . 30 , No . 2 (Jun . , 2002) , pp . 30, 204–211.
- Caminero, J. a, 2006. Treatment of multidrug-resistant tuberculosis : *Int. J. Tuberc. Lung Dis.* 10, 829–837.
- Casettari, L., Villasaliu, D., Castagnino, E., Stolnik, S., Howdle, S., Illum, L., 2012. Progress in Polymer Science PEGylated chitosan derivatives : Synthesis , characterizations and pharmaceutical applications. *Prog. Polym. Sci.* 37, 659–685. <https://doi.org/10.1016/j.progpolymsci.2011.10.001>
- Chae, S.Y., Jang, M., Nah, J., 2005. Influence of molecular weight on oral absorption of water soluble chitosans 102, 383–394. <https://doi.org/10.1016/j.jconrel.2004.10.012>

- Chatterjee, D., 1997. The mycobacterial cell wall: structure, biosynthesis and sites of drug action. *Curr. Opin. Chem. Biol.* 1, 579–588. [https://doi.org/10.1016/S1367-5931\(97\)80055-5](https://doi.org/10.1016/S1367-5931(97)80055-5)
- Cheng, J., Teply, B.A., Sherifi, I., Sung, J., Luther, G., Gu, F.X., Levy-nissenbaum, E., Radovic-moreno, A.F., Langer, R., Farokhzad, O.C., 2007. Formulation of functionalized PLGA – PEG nanoparticles for in vivo targeted drug delivery 28, 869–876. <https://doi.org/10.1016/j.biomaterials.2006.09.047>
- Cheung, R.C.F., Ng, T.B., Wong, J.H., Chan, W.Y., 2015. Chitosan: An update on potential biomedical and pharmaceutical applications, *Marine Drugs*. <https://doi.org/10.3390/md13085156>
- Chimalakonda, K.C., Agarwal, H.K., Kumar, A., Parang, K., Mehvar, R., 2007. Synthesis, analysis, in vitro characterization, and in vivo disposition of a lamivudine-dextran conjugate for selective antiviral delivery to the liver. *Bioconjug. Chem.* 18, 2097–2108. <https://doi.org/10.1021/bc700193d>
- Choi, H.S., Liu, W., Misra, P., Tanaka, E., Zimmer, J.P., Itty Ipe, B., Bawendi, M.G., Frangioni, J. V, 2007. Renal clearance of nanoparticles. *Nat. Biotechnol.* 25, 1165–1170. <https://doi.org/10.1038/nbt1340.Renal>
- Chu, B.C.F., Kramer, F.R., Orgel, L.E., 1986. Synthesis of an amplifiable reporter RNA for bioassays. *Nucleic Acids Res.* 14, 5591–5603. <https://doi.org/10.1093/nar/14.14.5591>
- Chu, B.C.F., Wahl, G.M., Orgel, L.E., 1983. Derivatization of unprotected polynucleotides. *Nucleic Acids Res.* 11, 6513–6529. <https://doi.org/10.1093/nar/11.18.6513>
- Chytil, P., Koziolová, E., Etrych, T., Ulbrich, K., 2018. HPMA Copolymer–Drug Conjugates with Controlled Tumor-Specific Drug Release. *Macromol. Biosci.* 18, 1–15. <https://doi.org/10.1002/mabi.201700209>
- Clapham, P.R., McKnight, Á., 2002. Cell surface receptors, virus entry and tropism of primate lentiviruses. *J. Gen. Virol.* 83, 1809–1829. <https://doi.org/10.1099/0022-1317-83-8-1809>
- Cohen, M.S., Hellmann, N., Levy, J.A., Decock, K., Lange, J., Hill, C., Hill, C., Carolina, N.,

- Foundation, M.G., 2008. The spread, treatment, and prevention of HIV-: evolution of a global pandemic. *J. Clin. Invest.* 118, 1244–54. <https://doi.org/10.1172/JCI34706.1244>
- Conejos-Sánchez, I., Cardoso, I., Oteo-Vives, M., Romero-Sanz, E., Paul, A., Sauri, A.R., Morcillo, M.A., Saraiva, M.J., Vicent, M.J., 2015. Polymer-doxycycline conjugates as fibril disrupters: An approach towards the treatment of a rare amyloidotic disease. *J. Control. Release* 198, 80–90. <https://doi.org/10.1016/j.jconrel.2014.12.003>
- Coovadia, H.M., Rollins, N.C., 1999. Current controversies in the perinatal transmission of HIV in developing countries. *Semin. Neonatol.* 4, 193–200. [https://doi.org/10.1016/S1084-2756\(99\)90070-2](https://doi.org/10.1016/S1084-2756(99)90070-2)
- Cui, L., Mharakurwa, S., Ndiaye, D., Rathod, P.K., Rosenthal, P.J., 2015. Antimalarial drug resistance: Literature review and activities and findings of the ICEMR network. *Am. J. Trop. Med. Hyg.* 93, 57–68. <https://doi.org/10.4269/ajtmh.15-0007>
- Cui, L., Su, X.-Z., n.d. Discovery, mechanisms of action and combination therapy of artemisinin. <https://doi.org/10.1586/eri.09.68>
- Dakwar, G.R., Shariati, M., Willaert, W., Ceelen, W., De Smedt, S.C., Remaut, K., 2017. Nanomedicine-based intraperitoneal therapy for the treatment of peritoneal carcinomatosis — Mission possible? *Adv. Drug Deliv. Rev.* 108, 13–24. <https://doi.org/10.1016/j.addr.2016.07.001>
- Daniel Elieh-Ali-Komi, M.R.H., 2017. Chitin and Chitosan: Production and Application of Versatile Biomedical Nanomaterials. *Int J Adv Res* 4, 411–427. <https://doi.org/10.5588/ijtdl.16.0716.Isoniazid>
- das Neves, J., Amiji, M.M., Bahia, M.F., Sarmiento, B., 2010. Nanotechnology-based systems for the treatment and prevention of HIV/AIDS. *Adv. Drug Deliv. Rev.* 62, 458–477. <https://doi.org/10.1016/j.addr.2009.11.017>
- Das, S., Ng, W.K., Kanaujia, P., Kim, S., Tan, R.B.H., 2011. Formulation design, preparation and physicochemical characterizations of solid lipid nanoparticles containing a hydrophobic drug: Effects of process variables. *Colloids Surfaces B Biointerfaces* 88, 483–489. <https://doi.org/10.1016/j.colsurfb.2011.07.036>

- De Clercq, E., 2010. Antiretroviral drugs. *Curr. Opin. Pharmacol.* 10, 507–515.
<https://doi.org/10.1016/j.coph.2010.04.011>
- De Clercq, E., 2009. Anti-HIV drugs: 25 compounds approved within 25 years after the discovery of HIV. *Int. J. Antimicrob. Agents* 33, 307–320.
<https://doi.org/10.1016/j.ijantimicag.2008.10.010>
- de Silva, T.I., Cotten, M., Rowland-Jones, S.L., 2008. HIV-2: the forgotten AIDS virus. *Trends Microbiol.* 16, 588–595. <https://doi.org/10.1016/j.tim.2008.09.003>
- Deffur, A., Mulder, N.J., Wilkinson, R.J., 2013. Co-infection with *Mycobacterium tuberculosis* and human immunodeficiency virus: An overview and motivation for systems approaches. *Pathog. Dis.* 69, 101–113. <https://doi.org/10.1111/2049-632X.12060>
- Delaney, M., 2006. History of HAART – the true story of how effective multi-drug therapy was developed for treatment of HIV disease. *Retrovirology* 3, S6.
<https://doi.org/10.1186/1742-4690-3-S1-S6>
- Desai, M.P., Labhsetwar, V., Walter, E., Levy, R.J., Amidon, G.L., 1997. The mechanism of uptake of biodegradable microparticles in Caco-2 cells is size dependent. *Pharm. Res.*
<https://doi.org/10.1023/A:1012126301290>
- Dey, A.K., Griffiths, C., Lea, S.M., James, W., 2005. Structural characterization of an anti-gp120 RNA aptamer that neutralizes R5 strains of HIV-1. *RNA* 11, 873–84.
<https://doi.org/10.1261/rna.7205405>
- Diao, P., Guo, M., Jiang, D., Jia, Z., Cui, X., Gu, D., 2000. Fractional coverage of defects in self-assembled thiol monolayers on gold 480, 59–63.
- Diedrich, C.R., Flynn, J.A.L., 2011. HIV-1/*Mycobacterium tuberculosis* coinfection immunology: How does HIV-1 exacerbate tuberculosis? *Infect. Immun.* 79, 1407–1417.
<https://doi.org/10.1128/IAI.01126-10>
- Diedrich, C.R., O’Hern, J., Wilkinson, R.J., 2016. HIV-1 and the *Mycobacterium tuberculosis* granuloma: A systematic review and meta-analysis. *Tuberculosis* 98, 62–76.
<https://doi.org/10.1016/j.tube.2016.02.010>

- Duncan, R., 2017. Polymer therapeutics at a crossroads? Finding the path for improved translation in the twenty-first century. *J. Drug Target.* 25, 759–780. <https://doi.org/10.1080/1061186X.2017.1358729>
- Duncan, R., 2009. Development of HPMA copolymer-anticancer conjugates: Clinical experience and lessons learnt. *Adv. Drug Deliv. Rev.* <https://doi.org/10.1016/j.addr.2009.05.007>
- Duncan, R., 2005. Nanomedicine gets clinical. *Mater. Today* 8, 16–17. [https://doi.org/10.1016/S1369-7021\(05\)71032-4](https://doi.org/10.1016/S1369-7021(05)71032-4)
- Duncan, R., 2003. The dawning era of polymer therapeutics. *Nat. Rev. Drug Discov.* 2, 347–60. <https://doi.org/10.1038/nrd1088>
- Duncan, R., Gac-Breton, S., Keane, R., Musila, R., Sat, Y.N., Satchi, R., Searle, F., 2001. Polymer-drug conjugates, PDEPT and PELT: Basic principles for design and transfer from the laboratory to clinic. *J. Control. Release* 74, 135–146. [https://doi.org/10.1016/S0168-3659\(01\)00328-5](https://doi.org/10.1016/S0168-3659(01)00328-5)
- Duncan, R., Gaspar, R., 2011a. Nanomedicine(s) under the microscope. *Mol. Pharm.* <https://doi.org/10.1021/mp200394t>
- Duncan, R., Gaspar, R., 2011b. Nanomedicine (s) under the Microscope 2101–2141.
- Duncan, R., Ringsdorf, H., Satchi-fainaro, R., 2006. Polymer therapeutics — polymers as drugs , drug and protein conjugates and gene delivery systems : Past , present and future opportunities * 14, 337–341. <https://doi.org/10.1080/10611860600833856>
- Duncan, R., Seymour, L.W., O'Hare, K.B., Flanagan, P.A., Wedge, S., Hume, I.C., Ulbrich, K., Strohal, J., Subr, V., Spreafico, F., Grandi, M., Ripamonti, M., Farao, M., Suarato, A., 1992. Preclinical evaluation of polymer-bound doxorubicin. *J. Control. Release* 19, 331–346. [https://doi.org/10.1016/0168-3659\(92\)90088-9](https://doi.org/10.1016/0168-3659(92)90088-9)
- Duncan, R., Vicent, M.J., 2013. Polymer therapeutics-prospects for 21st century: The end of the beginning. *Adv. Drug Deliv. Rev.* 65, 60–70. <https://doi.org/10.1016/j.addr.2012.08.012>

- Duncan, R., Vicent, M.J., 2010. Do HPMA copolymer conjugates have a future as clinically useful nanomedicines? A critical overview of current status and future opportunities. *Adv. Drug Deliv. Rev.* 62, 272–282. <https://doi.org/10.1016/j.addr.2009.12.005>
- Ehrt, S., Schnappinger, D., 2009. Mycobacterial survival strategies in the phagosome: Defence against host stresses. *Cell. Microbiol.* 11, 1170–1178. <https://doi.org/10.1111/j.1462-5822.2009.01335.x>
- Eldar-Boock, A., Blau, R., Ryppa, C., Baabur-Cohen, H., Many, A., Vicent, M.J., Kratz, F., Sanchis, J., Satchi-Fainaro, R., 2017. Integrin-targeted nano-sized polymeric systems for paclitaxel conjugation: a comparative study. *J. Drug Target.* 25, 829–844. <https://doi.org/10.1080/1061186X.2017.1358727>
- Eldar-Boock, A., Miller, K., Sanchis, J., Lupu, R., Vicent, M.J., Satchi-Fainaro, R., 2011. Integrin-assisted drug delivery of nano-scaled polymer therapeutics bearing paclitaxel. *Biomaterials* 32, 3862–3874. <https://doi.org/10.1016/j.biomaterials.2011.01.073>
- Espinal, M.A., 2003. The global situation of MDR-TB. *Tuberculosis* 83, 44–51. [https://doi.org/10.1016/S1472-9792\(02\)00058-6](https://doi.org/10.1016/S1472-9792(02)00058-6)
- Esté, J.A., Cihlar, T., 2010. Current status and challenges of antiretroviral research and therapy. *Antiviral Res.* 85, 25–33. <https://doi.org/10.1016/j.antiviral.2009.10.007>
- Et, B., Acta, B., 1969. *Bba biochimica et biophysica acta* 26344 6, 444–451.
- Everaerts, F., Torrianni, M., Hendriks, M., Feijen, J., 2008. Biomechanical properties of carbodiimide crosslinked collagen: Influence of the formation of ester crosslinks. *J. Biomed. Mater. Res. - Part A* 85, 547–555. <https://doi.org/10.1002/jbm.a.31524>
- Ezzet, F., Mull, R., Karbwang, J., 1998. Population pharmacokinetics and therapeutic response of CGP 56697(artemether +benflumetol) in malaria patients. *Br J Clin Pharmacol* 46, 553–561.
- Farnaud, S., Evans, R.W., 2003. Lactoferrin - A multifunctional protein with antimicrobial properties. *Mol. Immunol.* 40, 395–405. [https://doi.org/10.1016/S0161-5890\(03\)00152-4](https://doi.org/10.1016/S0161-5890(03)00152-4)
- Farokhzad, O.C., Cheng, J., Teply, B.A., Sherifi, I., Jon, S., Kantoff, P.W., Richie, J.P., Langer,

- R., 2006. Targeted nanoparticle-aptamer bioconjugates for cancer chemotherapy in vivo. *Proc. Natl. Acad. Sci.* 103, 6315–6320. <https://doi.org/10.1073/pnas.0601755103>
- Fogel, N., 2015. Tuberculosis: A disease without boundaries. *Tuberculosis* 95, 527–531. <https://doi.org/10.1016/j.tube.2015.05.017>
- Folkers, J.P., Laibinis, P.E., Whitesides, G.M., 1992. Self-assembled monolayers of alkanethiols on gold: the adsorption and wetting properties of monolayers derived from two components with alkane chains of different lengths. *J. Adhes. Sci. Technol.* 6, 1397–1410. <https://doi.org/10.1163/156856192X00700>
- Fuertges, F., Abuchowski, A., 1990. The clinical efficacy of poly(ethylene glycol)-modified proteins. *J. Control. Release* 11, 139–148. [https://doi.org/10.1016/0168-3659\(90\)90127-F](https://doi.org/10.1016/0168-3659(90)90127-F)
- Gallo, S.A., Finnegan, C.M., Viard, M., Raviv, Y., Dimitrov, A., Rawat, S.S., Puri, A., Durell, S., Blumenthal, R., 2003. The HIV Env-mediated fusion reaction. *Biochim. Biophys. Acta - Biomembr.* 1614, 36–50. [https://doi.org/10.1016/S0005-2736\(03\)00161-5](https://doi.org/10.1016/S0005-2736(03)00161-5)
- Gazzinelli, R.T., Kalantari, P., Fitzgerald, K.A., 2014. Innate sensing of malaria parasites. *Nat. Publ. Gr.* 1–14. <https://doi.org/10.1038/nri3742>
- Geng, P., Zhang, X., Meng, W., Wang, Q., Zhang, W., Jin, L., Feng, Z., Wu, Z., 2008. Self-assembled monolayers-based immunosensor for detection of *Escherichia coli* using electrochemical impedance spectroscopy. *Electrochim. Acta* 53, 4663–4668. <https://doi.org/10.1016/j.electacta.2008.01.037>
- Ghosh, S.K., 2006. Functional Coatings and Microencapsulation: A General Perspective. *Funct. Coatings By Polym. Microencapsul.* 1–28. <https://doi.org/10.1002/3527608478.ch1>
- Ghosh, S.S., Kao, P.M., Kwoh, D.Y., 1989. Synthesis of 5'-oligonucleotide hydrazide derivatives and their use in preparation of enzyme-nucleic acid hybridization probes. *Anal. Biochem.* 178, 43–51. [https://doi.org/10.1016/0003-2697\(89\)90354-0](https://doi.org/10.1016/0003-2697(89)90354-0)
- Ghosh, S.S., Kao, P.M., McCue, A.W., Chappelle, H.L., 1990. Use of Maleimide-Thiol

- Coupling Chemistry for Efficient Syntheses of Oligonucleotide-Enzyme Conjugate Hybridization Probes. *Bioconjug. Chem.* 1, 71–76. <https://doi.org/10.1021/bc00001a009>
- Giacalone, G., Hillaireau, H., Fattal, E., 2015. Improving bioavailability and biodistribution of anti-HIV chemotherapy. *Eur. J. Pharm. Sci.* 75, 40–53. <https://doi.org/10.1016/j.ejps.2015.04.011>
- GLOBAL BURDEN OF DISEASE, WHO, 2014, 2014. WHO | The top 10 causes of death. Fact sheet N°310 (Updated May 2014). <https://doi.org/entity/mediacentre/factsheets/fs310/en/index.html>
- González-Chávez, S.A., Arévalo-Gallegos, S., Rascón-Cruz, Q., 2009. Lactoferrin: structure, function and applications. *Int. J. Antimicrob. Agents* 33. <https://doi.org/10.1016/j.ijantimicag.2008.07.020>
- Goy, R.C., Britto, D. de, Assis, O.B.G., 2009. A review of the antimicrobial activity of chitosan. *Polímeros* 19, 241–247. <https://doi.org/10.1093/jac/dkg286>
- Grumezescu, A.M., Fangueiro, J.F., Souto, E.B., Silva, A.M., 2016. 9 – Encapsulation of nutraceuticals in novel delivery systems, *Nutraceuticals*. Elsevier Inc. <https://doi.org/10.1016/B978-0-12-804305-9.00009-9>
- Guan, N., Xu, J., Wang, L., Sun, D., 2009. One-step synthesis of amine-functionalized thermo-responsive magnetite nanoparticles and single-crystal hollow structures. *Colloids Surfaces A Physicochem. Eng. Asp.* 346, 221–228. <https://doi.org/10.1016/j.colsurfa.2009.06.022>
- Gunaseelan, S., Debrah, O., Wan, L., Leibowitz, M.J., Rabson, A.B., Stein, S., Sinko, P.J., 2004. Synthesis of poly(ethylene glycol)-based saquinavir prodrug conjugates and assessment of release and anti-HIV-1 bioactivity using a novel protease inhibition assay. *Bioconjug. Chem.* 15, 1322–1333. <https://doi.org/10.1021/bc0498875>
- Guo, J., Gao, X., Su, L., Xia, H., Gu, G., Pang, Z., Jiang, X., Yao, L., Chen, J., Chen, H., 2011. Aptamer-functionalized PEG-PLGA nanoparticles for enhanced anti-glioma drug delivery. *Biomaterials* 32, 8010–8020. <https://doi.org/10.1016/j.biomaterials.2011.07.004>

- Gupta, U., Jain, N.K., 2010. Non-polymeric nano-carriers in HIV/AIDS drug delivery and targeting. *Adv. Drug Deliv. Rev.* 62, 478–490. <https://doi.org/10.1016/j.addr.2009.11.018>
- Gursahani, H., Wong, S., Pfeiffer, J., Allums, S., Zhang, W., Deng, B., Trincherro, P., Quach, P., Brew, C., Evans, J., Harrison, S., Doberstein, S., Riley, T.A., Fishburn, C.S., Therapeutics, N., Carlos, S., 2010. Controlling the rate of entry to the CNS by polymer conjugation 2010.
- Guterres, S.S., Beck, R.C.R., Pohlmann, a R., 2009. Spray-drying technique to prepare innovative nanoparticulated formulations for drug administration: a brief overview. *Brazilian J. Phys.* 39, 205–209. <https://doi.org/10.1590/S0103-97332009000200013>
- Hare, J.I., Lammers, T., Ashford, M.B., Puri, S., Storm, G., Barry, S.T., 2017. Challenges and strategies in anti-cancer nanomedicine development: An industry perspective. *Adv. Drug Deliv. Rev.* 108, 25–38. <https://doi.org/10.1016/j.addr.2016.04.025>
- Harris, J.M., Struck, E.C., Case, M.G., Al, H.E.T., 1984. Synthesis and Characterization of Poly(ethylene Glycol) Derivatives. *J. Polym. Sci.* 22, 341–352.
- Hartman, D.A., 2003. Determination of the Stability of Drugs in Plasma. *Curr. Protoc. Pharmacol.* 1–8. <https://doi.org/10.1002/0471141755.ph0706s19>
- Heiati, H., Tawashi, R., Phillips, N.C., 1998. Solid lipid nanoparticles as drug carriers. *Int. J. Pharm.* 174, 71–80. [https://doi.org/10.1016/S0378-5173\(98\)00236-1](https://doi.org/10.1016/S0378-5173(98)00236-1)
- Hellman, L., Fried, M., 2007. Electrophoretic Mobility Shift Assay (EMSA) for Detecting Protein- Nucleic Acid Interactions. *Nat. Protoc.* 2, 1849–1861. <https://doi.org/10.1038/nprot.2007.249>.Electrophoretic
- Hermanson, G.T., 2008. Bioconjugate echniques, 2nd Editio. ed. Academic Press.
- Herskovitz, I., Donoghue, H.D., Minnikin, D.E., Besra, G.S., Lee, O.Y.C., Gernaey, A.M., Galili, E., Eshed, V., Greenblatt, C.L., Lemma, E., Bar-Gal, G.K., Spigelman, M., 2008. Detection and molecular characterization of 9000-year-old Mycobacterium tuberculosis from a neolithic settlement in the Eastern mediterranean. *PLoS One* 3, 1–6. <https://doi.org/10.1371/journal.pone.0003426>

- Hirsh, A.E., Tsolaki, A.G., DeRiemer, K., Feldman, M.W., Small, P.M., 2004. Stable association between strains of *Mycobacterium tuberculosis* and their human host populations. *Proc. Natl. Acad. Sci. U. S. A.* 101, 4871–6. <https://doi.org/10.1073/pnas.0305627101>
- Hovanessian, A.G., Soundaramourty, C., El Khoury, D., Nondier, I., Svab, J., Krust, B., 2010. Surface expressed nucleolin is constantly induced in tumor cells to mediate calcium-dependent ligand internalization. *PLoS One* 5. <https://doi.org/10.1371/journal.pone.0015787>
- Hu, C.-M.J., Zhang, L., Aryal, S., Cheung, C., Fang, R.H., Zhang, L., 2011. Erythrocyte membrane-camouflaged polymeric nanoparticles as a biomimetic delivery platform. *Proc. Natl. Acad. Sci.* 108, 10980–10985. <https://doi.org/10.1073/pnas.1106634108>
- Huang, L., Li, X., Marzan, F., Lizak, P.S., Aweeka, F.T., n.d. Determination of lumefantrine in small-volume human plasma by LC–MS/MS: using a deuterated lumefantrine to overcome matrix effect and ionization saturation.
- Iacob, S.A., Iacob, D.G., Jugulete, G., 2017. Improving the adherence to antiretroviral therapy, a difficult but essential task for a successful HIV treatment-clinical points of view and practical considerations. *Front. Pharmacol.* 8. <https://doi.org/10.3389/fphar.2017.00831>
- Instruments, M., 2011. Dynamic Light Scattering: An Introduction in 30 Minutes. Tech. Note MRK656-01 1–8.
- Jain, R.A., 2000. The manufacturing techniques of various drug loaded biodegradable poly(lactide-co-glycolide) (PLGA) devices. *Biomaterials* 21, 2475–2490. [https://doi.org/10.1016/S0142-9612\(00\)00115-0](https://doi.org/10.1016/S0142-9612(00)00115-0)
- Jarlier, V., Gutmann, L., Nikaido, H., 1991. Interplay of cell wall barrier and beta-lactamase activity determines high resistance to beta-lactam antibiotics in *Mycobacterium chelonae*. *Antimicrob. Agents Chemother.* 35, 1937–9. <https://doi.org/10.1128/AAC.35.9.1937>
- Jayakumar, R., Prabakaran, M., Nair, S. V., Tamura, H., 2010. Novel chitin and chitosan nanofibers in biomedical applications. *Biotechnol. Adv.* 28, 142–150. <https://doi.org/10.1016/j.biotechadv.2009.11.001>

- Jyothi, N.V.N., Prasanna, P.M., Sakarkar, S.N., Prabha, K.S., Ramaiah, P.S., Srawan, G.Y., 2010. Microencapsulation techniques, factors influencing encapsulation efficiency. *J. Microencapsul.* 27, 187–197. <https://doi.org/10.3109/02652040903131301>
- K Sollohub, K.C., 2010. Spray Drying Technique: II. Current Applications in Pharmaceutical Technology. *J. Pharm. Sci.* 99, 587–597. <https://doi.org/10.1002/jps>
- Kalepu, S., Nekkanti, V., 2015. Insoluble drug delivery strategies: Review of recent advances and business prospects. *Acta Pharm. Sin. B* 5, 442–453. <https://doi.org/10.1016/j.apsb.2015.07.003>
- Kallianpur, A.R., Hulgan, T., 209AD. Pharmacogenetics of nucleoside reverse-transcriptase inhibitor- associated peripheral neuropathy. *Pharmacogenomics* 10, 623–637. <https://doi.org/10.2217/pgs.09.14.Pharmacogenetics>
- Katata, L., Tshweu, L., Naidoo, S., Kalombo, L., Swai, H., 2012. Design and formulation of nano-sized spray dried efavirenz-part I: Influence of formulation parameters. *J. Nanoparticle Res.* 14. <https://doi.org/10.1007/s11051-012-1247-0>
- Keusch, G.T., Fontaine, O., Bhargava, A., Boschi-, C., Bhutta, Z. a., Gotuzzo, E., Rivera, J., Chow, J., Shahid-Salles, S., Laxminarayan, R., 2006. Diarrheal Diseases. *Dis. Control Priorities Dev. Ctries.* 371–87. <https://doi.org/NBK11764> [bookaccession]
- Khalil, I.R., Burns, A.T.H., Radecka, I., Kowalczyk, M., Khalaf, T., Adamus, G., Johnston, B., Khechara, M.P., 2017. Bacterial-derived polymer poly- γ -glutamic acid (γ -PGA)-based micro/nanoparticles as a delivery system for antimicrobials and other biomedical applications. *Int. J. Mol. Sci.* 18, 1–18. <https://doi.org/10.3390/ijms18020313>
- Khandare, J., Minko, T., 2006. Polymer-drug conjugates: Progress in polymeric prodrugs. *Prog. Polym. Sci.* <https://doi.org/10.1016/j.progpolymsci.2005.09.004>
- Khati, M., Schüman, M., Ibrahim, J., Sattentau, Q., Gordon, S., James, W., Aptamers, J.F., Schu, M., 2003. Neutralization of Infectivity of Diverse R5 Clinical Isolates of Human Immunodeficiency Virus Type 1 by gp120-Binding 2 'F-RNA Aptamers. *J. Virol.* 77, 12692–12698. <https://doi.org/10.1128/JVI.77.23.12692>

- Kirby, A.J., Younas, M., 1970. The reactivity of phosphate esters. Reactions of diesters with nucleophiles. *J. Chem. Soc. B Phys. Org.* 1165–1172. <https://doi.org/10.1039/j29700001165>
- Kloprogge, F., McGready, R., Hanpithakpong, W., Blessborn, D., Day, N.P.J., White, N.J., Nosten, F., Tarninga, J., 2015. Lumefantrine and desbutyl-lumefantrine population pharmacokinetic-pharmacodynamic relationships in pregnant women with uncomplicated *Plasmodium falciparum* malaria on the Thailand-Myanmar border. *Antimicrob. Agents Chemother.* 59, 6375–6384. <https://doi.org/10.1128/AAC.00267-15>
- Kobayashi, H., Watanabe, R., Choyke, P.L., 2014. Improving conventional enhanced permeability and retention (EPR) effects; What is the appropriate target? *Theranostics* 4, 81–89. <https://doi.org/10.7150/thno.7193>
- Kong, H.Y., Byun, J., 2013. Nucleic acid aptamers: New methods for selection, stabilization, and application in biomedical science. *Biomol. Ther.* 21, 423–434. <https://doi.org/10.4062/biomolther.2013.085>
- Kopeček, J., 2013. Polymer-drug conjugates: Origins, progress to date and future directions. *Adv. Drug Deliv. Rev.* <https://doi.org/10.1016/j.addr.2012.10.014>
- Kopeček, J., Kopečková, P., 2010. HPMA copolymers: Origins, early developments, present, and future. *Adv. Drug Deliv. Rev.* 62, 122–149. <https://doi.org/10.1016/j.addr.2009.10.004>
- Koram, K.A., Abuaku, B., Duah, N., Quashie, N., 2005. Comparative efficacy of antimalarial drugs including ACTs in the treatment of uncomplicated malaria among children under 5 years in Ghana. *Acta Trop.* 95, 194–203. <https://doi.org/10.1016/j.actatropica.2005.06.018>
- Krettli, A.U., Miller, L.H., 2001. Malaria: A sporozoite runs through it. *Curr. Biol.* [https://doi.org/10.1016/S0960-9822\(01\)00221-4](https://doi.org/10.1016/S0960-9822(01)00221-4)
- Krettli, A.U., Miller, L.H., 2001. Malaria : A sporozoite runs through it 409–412.
- Krudsood, S., Chalermrut, K., Pengruksa, C., Srivilairit, S., Silachamroon, U., Treeprasertsuk,

- S., Kano, S., Brittenham, G.M., Looareesuwan, S., 2003. Comparative clinical trial of two-fixed combinations dihydroartemisinin-naphthoquine-trimethoprim (DNP®) and artemether-lumefantrine (Coartem®/Riamet®) in the treatment of acute uncomplicated falciparum malaria in Thailand. *Southeast Asian J. Trop. Med. Public Health* 34, 316–321.
- Kumar, H., Sattler, J.M., Singer, M., Heiss, K., Reinig, M., Hammerschmidt-Kamper, C., Heussler, V., Mueller, A.K., Frischknecht, F., 2016. Protective efficacy and safety of liver stage attenuated malaria parasites. *Sci. Rep.* 6, 1–9. <https://doi.org/10.1038/srep26824>
- Kumar Pandey, P., Kumar Sharma, A., Gupta, U., 2016. Blood brain barrier: An overview on strategies in drug delivery, realistic in vitro modeling and in vivo live tracking Blood brain barrier: An overview on strategies in drug delivery, realistic in vitro modeling and in vivo live tracking. *Tissue Barriers* 1–14. <https://doi.org/10.1080/21688370.2015.1129476>
- Kurita, K., 2006. Chitin and chitosan: Functional biopolymers from marine crustaceans. *Mar. Biotechnol.* 8, 203–226. <https://doi.org/10.1007/s10126-005-0097-5>
- Lai, Y., Chiang, P.C., Blom, J.D., Li, N., Shevlin, K., Brayman, T.G., Hu, Y., Selbo, J.G., Hu, L.G., 2008. Comparison of in vitro nanoparticles uptake in various cell lines and in vivo pulmonary cellular transport in intratracheally dosed rat model. *Nanoscale Res. Lett.* 3, 321–329. <https://doi.org/10.1007/s11671-008-9160-2>
- Larson, N., Ghandehari, H., 2012. Polymeric conjugates for drug delivery. *Chem. Mater.* <https://doi.org/10.1021/cm2031569>
- Lawrence, P.B., Gavrillov, Y., Matthews, S.S., Langlois, M.I., Shental-Bechor, D., Greenblatt, H.M., Pandey, B.K., Smith, M.S., Paxman, R., Torgerson, C.D., Merrell, J.P., Ritz, C.C., Prigozhin, M.B., Levy, Y., Price, J.L., 2014. Criteria for selecting PEGylation sites on proteins for higher thermodynamic and proteolytic stability. *J. Am. Chem. Soc.* 136, 17547–17560. <https://doi.org/10.1021/ja5095183>
- Lee, A.L.Z., Wang, Y., Cheng, H.Y., Pervaiz, S., Yang, Y.Y., 2009. The co-delivery of paclitaxel and Herceptin using cationic micellar nanoparticles. *Biomaterials* 30, 919–927.

<https://doi.org/10.1016/j.biomaterials.2008.10.062>

Lee, E., Kim, H., Lee, I.H., Jon, S., 2009. In vivo antitumor effects of chitosan-conjugated docetaxel after oral administration. *J. Control. Release.*
<https://doi.org/10.1016/j.jconrel.2009.08.014>

Lee, E., Lee, J., Lee, I., Yu, M., Kim, H., Chae, S.Y., Jon, S., 2008. Conjugated Chitosan as a Novel Platform for Oral Delivery of Paclitaxel 6442–6449.

Lee, J.-H., Canny, M.D., De Erkenez, A., Krilleke, D., Ng, Y.-S., Shima, D.T., Pardi, A., Jucker, F., 2005. A therapeutic aptamer inhibits angiogenesis by specifically targeting the heparin binding domain of VEGF165. *Proc. Natl. Acad. Sci. U. S. A.* 102, 18902–7.
<https://doi.org/10.1073/pnas.0509069102>

Leriche, G., Chisholm, L., Wagner, A., 2012. Cleavable linkers in chemical biology. *Bioorganic Med. Chem.* 20, 571–582. <https://doi.org/10.1016/j.bmc.2011.07.048>

Letchford, K., Liggins, R., Wasan, K.M., Burt, H., 2009. In vitro human plasma distribution of nanoparticulate paclitaxel is dependent on the physicochemical properties of poly(ethylene glycol)-block-poly(caprolactone) nanoparticles. *Eur. J. Pharm. Biopharm.* 71, 196–206. <https://doi.org/10.1016/j.ejpb.2008.08.003>

Levy-Nissenbaum, E., Radovic-Moreno, A.F., Wang, A.Z., Langer, R., Farokhzad, O.C., 2008. Nanotechnology and aptamers: applications in drug delivery. *Trends Biotechnol.* 26, 442–449. <https://doi.org/10.1016/j.tibtech.2008.04.006>

Li Di , Edward H. Kerns, Yan Hong, H.C., 2005. Development and Application of High throughput plasma stability assay for drug discovery.

Li, F., Mahato, R.I., 2017. Bioconjugate Therapeutics: Current Progress and Future Perspective. *Mol. Pharm.* 14, 1321–1324.
<https://doi.org/10.1021/acs.molpharmaceut.7b00263>

Li, P., Dai, Y., Zhang, J., Wang, A., Wei, Q., 2008. Chitosan-Alginate Nanoparticles as a Novel Drug Delivery System for Nifedipine 4, 221–228.

Li, Q., Weina, P., 2010. Artesunate: The best drug in the treatment of severe and complicated

- malaria. *Pharmaceuticals* 3, 2322–2332. <https://doi.org/10.3390/ph3072322>
- Li, W., Wu, J., Zhan, P., Chang, Y., Pannecouque, C., De Clercq, E., Liu, X., 2012. Synthesis, drug release and anti-HIV activity of a series of PEGylated zidovudine conjugates. *Int. J. Biol. Macromol.* <https://doi.org/10.1016/j.ijbiomac.2012.02.019>
- Li, W., Zhan, P., De Clercq, E., Lou, H., Liu, X., 2013. Current drug research on PEGylation with small molecular agents. *Prog. Polym. Sci.* 38, 421–444. <https://doi.org/10.1016/j.progpolymsci.2012.07.006>
- Li, X., Anton, N., Arpagaus, C., Belleiteix, F., Vandamme, T.F., 2010. Nanoparticles by spray drying using innovative new technology: The Büchi Nano Spray Dryer B-90. *J. Control. Release* 147, 304–310. <https://doi.org/10.1016/j.jconrel.2010.07.113>
- Li, X., Yu, Y., Ji, Q., Qiu, L., 2015. Targeted delivery of anticancer drugs by aptamer AS1411 mediated Pluronic F127/cyclodextrin-linked polymer composite micelles. *Nanomedicine Nanotechnology, Biol. Med.* <https://doi.org/10.1016/j.nano.2014.08.013>
- Liechty, W.B., Kryscio, D.R., Slaughter, B. V, Peppas, N.A., n.d. *Polymers for Drug Delivery Systems.* <https://doi.org/10.1146/annurev-chembioeng-073009-100847>
- Lindenberg, M., Kopp, S., Dressman, J.B., 2004. Classification of orally administered drugs on the World Health Organization Model list of Essential Medicines according to the biopharmaceutics classification system. *Eur. J. Pharm. Biopharm.* 58, 265–278. <https://doi.org/10.1016/j.ejpb.2004.03.001>
- Liu, L., Gao, Q., Lu, X., Zhou, H., 2016. In situ forming hydrogels based on chitosan for drug delivery and tissue regeneration. *Asian J. Pharm. Sci.* 11, 673–683. <https://doi.org/10.1016/j.ajps.2016.07.001>
- London, G.M., Mayosi, B.M., Khati, M., 2015. Isolation and characterization of 2'-F-RNA aptamers against whole HIV-1 subtype C envelope pseudovirus. *Biochem. Biophys. Res. Commun.* 456, 428–433. <https://doi.org/10.1016/j.bbrc.2014.11.101>
- Longmire, M., Choyke, P.L., Kobayashi, H., 2008. Clearance properties of nano-sized particles and molecules as imaging agents: consideration and caveats. *Nanomedicine (Lond)* 3, 703–

717. <https://doi.org/10.2217/17435889.3.5.703>. Clearance
- Luo, Z., Guo, Y., Liu, J., Qiu, H., Zhao, M., Zou, W., Li, S., 2016. Biotechnology for Biofuels
Microbial synthesis of poly - γ - glutamic acid : current progress , challenges , and future
perspectives. *Biotechnol. Biofuels* 1–12. <https://doi.org/10.1186/s13068-016-0537-7>
- Lv, Z., Chu, Y., Wang, Y., 2015. HIV protease inhibitors: a review of molecular selectivity
and toxicity. *HIV. AIDS. (Auckl)*. 7, 95–104. <https://doi.org/10.2147/HIV.S79956>
- Ma, P., Mumper, R.J., 2013. NIH Public Access. *J Nanomed Nanotecghnology* 4, 1–35.
<https://doi.org/10.4172/2157-7439.1000164>. Paclitaxel
- Mackie, T.T., 1946. Tropical Disease Problems Among Veterans of World War II. Preliminary
Report [WWW Document]. *Trans Am Clin Clim. Assoc.*
- Maeda, H., 2001. SMANCS and polymer-conjugated macromolecular drugs: Advantages in
cancer chemotherapy. *Adv. Drug Deliv. Rev.* 46, 169–185.
[https://doi.org/10.1016/S0169-409X\(00\)00134-4](https://doi.org/10.1016/S0169-409X(00)00134-4)
- Maeda, H., Nakamura, H., Fang, J., 2013. The EPR effect for macromolecular drug delivery to
solid tumors: Improvement of tumor uptake, lowering of systemic toxicity, and distinct
tumor imaging in vivo. *Adv. Drug Deliv. Rev.* 65, 71–79.
<https://doi.org/10.1016/j.addr.2012.10.002>
- Mahor, A., Prajapati, S.K., Verma, A., Gupta, R., Iyer, A.K., Kesharwani, P., 2016.
Moxifloxacin loaded gelatin nanoparticles for ocular delivery: Formulation and in-vitro,
in-vivo evaluation. *J. Colloid Interface Sci.* 483, 132–138.
<https://doi.org/10.1016/j.jcis.2016.08.018>
- Mainardes, R.M., Gremião, M.P.D., Evangelista, R.C., 2006. Thermoanalytical study of
praziquantel-loaded PLGA nanoparticles. *Rev. Bras. Ciências Farm.* 42, 523–530.
<https://doi.org/10.1590/S1516-93322006000400007>
- Makanga, M., Krudsood, S., 2009. The clinical efficacy of artemether / lumefantrine (Coartem
®) 12, 1–12. <https://doi.org/10.1186/1475-2875-8-S1-S5>
- MALARIA CONTROL TODAY, 2005.

- Mallipeddi, R., Rohan, L.C., 2010. Progress in antiretroviral drug delivery using nanotechnology. *Int. J. Nanomedicine* 5, 533–547.
- Mamo, T., Moseman, E.A., Kolishetti, N., Salvador-, C., Shi, J., Kuritzkes, D.R., Langer, R., Andrian, U. Von, Farokhzad, O.C., 2010. Emerging nanotechnology approaches for HIV/AIDS treatment and Prevention. *Nanomedicine* . 5, 269–285. <https://doi.org/10.2217/nnm.10.1.Emerging>
- Manaia, E.B., Abuçafy, M.P., Chiari-Andréo, B.G., Silva, B.L., Oshiro Junior, J.A., Chiavacci, L.A., 2017. Physicochemical characterization of drug nanocarriers. *Int. J. Nanomedicine* 12, 4991–5011. <https://doi.org/10.2147/IJN.S133832>
- Manjelievskaja, J., Erck, D., Piracha, S., Schragger, L., 2015. Drug-resistant TB: Deadly, costly and in need of a vaccine. *Trans. R. Soc. Trop. Med. Hyg.* 110, 186–191. <https://doi.org/10.1093/trstmh/trw006>
- Manu, J., Ganesh, L., Manoj, B., Randhir, C., Shashikant, B., Chirag, S., 2012. Spray Drying in Pharmaceutical Industry: A Review. *Res. J. Pharma* 4, 74–79.
- Manuscript, A., Stability, P., Histone, M., Inhibitors, D., 2009. NIH Public Access. *Int. J.* 361, 19–25. <https://doi.org/10.1016/j.ijpharm.2008.05.001>.In
- Markovsky, E., Baabur-Cohen, H., Eldar-Boock, A., Omer, L., Tiram, G., Ferber, S., Ofek, P., Polyak, D., Scomparin, A., Satchi-Fainaro, R., 2012. Administration, distribution, metabolism and elimination of polymer therapeutics. *J. Control. Release* 161, 446–460. <https://doi.org/10.1016/j.jconrel.2011.12.021>
- Mathebula, N.S., Pillay, J., Toschi, G., Verschoor, J. a, Ozoemena, K.I., 2009. Recognition of anti-mycolic acid antibody at self-assembled mycolic acid antigens on a gold electrode: a potential impedimetric immunosensing platform for active tuberculosis. *Chem. Commun. (Camb)*. 3345–3347. <https://doi.org/10.1039/b905192a>
- Matteelli, A., Roggi, A., Carvalho, A.C.C., 2014. Extensively drug-resistant tuberculosis: Epidemiology and management. *Clin. Epidemiol.* 6, 111–118. <https://doi.org/10.2147/CLEP.S35839>

- Matteelli, A., Sulis, G., Capone, S., D'Ambrosio, L., Migliori, G.B., Getahun, H., 2017. Tuberculosis elimination and the challenge of latent tuberculosis. *Press. Medica* 46, e13–e21. <https://doi.org/10.1016/j.lpm.2017.01.015>
- Mclean, A.R., 1998. Vaccines and their impact on the control of disease. *Br. Med. Bull.* 54, 545–556. <https://doi.org/10.1093/oxfordjournals.bmb.a011709>
- McNeil, M., Daffe, M., Brennan, P.J., 1990. Evidence for the nature of the link between the arabinogalactan and peptidoglycan of mycobacterial cell walls. *J. Biol. Chem.* 265, 18200–18206.
- Mehvar, R., 2000. Dextrans for targeted and sustained delivery of therapeutic and imaging agents. *J. Control. Release.* [https://doi.org/10.1016/S0168-3659\(00\)00302-3](https://doi.org/10.1016/S0168-3659(00)00302-3)
- Mehvar, R., Robinson, A., Reynolds, M., 1994. Molecular Weight Dependent Tissue Accumulation of Dextrans : In Vivo Studies in Rats 83, 1495–1499.
- Mercier, M.C., Dontenwill, M., Choulier, L., 2017. Selection of nucleic acid aptamers targeting tumor cell-surface protein biomarkers. *Cancers (Basel)*. 9. <https://doi.org/10.3390/cancers9060069>
- Miele, E., Spinelli, G.P., Miele, E., Tomao, F., Tomao, S., 2009. Albumin-bound formulation of paclitaxel (Abraxane®; ABI-007) in the treatment of breast cancer. *Int. J. Nanomedicine* 4, 99–105. <https://doi.org/10.2147/IJN.S3061>
- Mischlinger, J., Agnandji, S.T., Ramharter, M., 2016. Single dose treatment of malaria - current status and perspectives. *Expert Rev. Anti. Infect. Ther.* 14, 669–678. <https://doi.org/10.1080/14787210.2016.1192462>
- Mishra, B., Patel, B.B., Tiwari, S., 2010. Colloidal nanocarriers: a review on formulation technology, types and applications toward targeted drug delivery. *Nanomedicine Nanotechnology, Biol. Med.* 6, 9–24. <https://doi.org/10.1016/j.nano.2009.04.008>
- Mizgerd, J., 2008. Acute lower respiratory tract infection. *N. Engl. J. Med.* 358, 716–727. <https://doi.org/10.1056/NEJMra074111.Acute>
- Mokhtarzadeh, A., Tabarzad, M., Ranjbari, J., de la Guardia, M., Hejazi, M., Ramezani, M.,

2016. Aptamers as smart ligands for nano-carriers targeting. *TrAC - Trends Anal. Chem.* 82, 316–327. <https://doi.org/10.1016/j.trac.2016.06.018>
- Montefiori, D., Sattentau, Q., Flores, J., Esparza, J., Mascola, J., 2007. Antibody-Based HIV-1 Vaccines: Recent Developments and Future Directions. *PLoS Med.* 4, e348. <https://doi.org/10.1371/journal.pmed.0040348>
- Montefiori, D.C., 2005. Evaluating neutralizing antibodies against HIV, SIV, and SHIV in luciferase reporter gene assays. *Curr. Protoc. Immunol.* Chapter 12, Unit 12.11. <https://doi.org/10.1002/0471142735.im1211s64>
- Mpagama, S.G., Houpt, E.R., Stroup, S., Kumburu, H., Gratz, J., Kibiki, G.S., Heysell, S.K., 2013. Application of quantitative second-line drug susceptibility testing at a multidrug-resistant tuberculosis hospital in Tanzania. *BMC Infect. Dis.* 13, 1. <https://doi.org/10.1186/1471-2334-13-432>
- Mufhandu, H.T., Alexandre, K.B., Gray, E.S., Morris, L., Khati, M., 2012. HIV-1 subtype C primary isolates exhibit high sensitivity to an anti-gp120 RNA aptamer. *Retrovirology* 9, P215. <https://doi.org/10.1186/1742-4690-9-s2-p215>
- Mukherjee, J.S., Rich, M.L., Socci, A.R., Joseph, J.K., Virú, F.A., Shin, S.S., Furin, J.J., Becerra, M.C., Barry, D.J., Kim, J.Y., Bayona, J., Farmer, P., Fawzi, M.C.S., Seung, K.J., 2004. Programmes and principles in treatment of multidrug-resistant tuberculosis. *Lancet* 363, 474–481. [https://doi.org/10.1016/S0140-6736\(04\)15496-2](https://doi.org/10.1016/S0140-6736(04)15496-2)
- Muzykantov, V.R., 2011. Drug delivery by red blood cells: vascular carriers designed by Mother Nature, Expert Opinion on Drug Delivery. <https://doi.org/10.1517/17425241003610633.Drug>
- Nakajima, N., Ikada, Y., 1995. Mechanism of amide formation by carbodiimide for bioconjugation in aqueous media. *Bioconjug. Chem.* 6, 123–130. <https://doi.org/10.1021/Bc00031a015>
- Nermut, M. V, Fassati, A., 2003. Structural analyses of purified human immunodeficiency virus type 1 intracellular reverse transcription complexes. *J. Virol.* 77, 8196–206. <https://doi.org/10.1128/JVI.77.15.8196>

- Ng, E.W.M., Shima, D.T., Calias, P., Cunningham, E.T., Guyer, D.R., Adamis, A.P., 2006. Pegaptanib, a targeted anti-VEGF aptamer for ocular vascular disease. *Nat. Rev. Drug Discov.* 5, 123–132. <https://doi.org/10.1038/nrd1955>
- Nobbmann, U., Connah, M., Fish, B., Varley, P., Gee, C., Mulot, S., Chen, J., Zhou, L., Lu, Y., Sheng, F., Yi, J., Harding, S.E., 2007. Dynamic light scattering as a relative tool for assessing the molecular integrity and stability of monoclonal antibodies. *Biotechnol. Genet. Eng. Rev.* 24, 117–128. <https://doi.org/10.1080/02648725.2007.10648095>
- Nosten, F., White, N.J., 2007. Artemisinin-based combination treatment of falciparum malaria. *Am. J. Trop. Med. Hyg.* 77, 181–192. https://doi.org/77/6_Suppl/181 [pii]
- Nwe, N., Furuike, T., Tamura, H., 2009. The mechanical and biological properties of chitosan scaffolds for tissue regeneration templates are significantly enhanced by chitosan from *Gongronella butleri*. *Materials (Basel)*. 2, 374–398. <https://doi.org/10.3390/ma2020374>
- Ogunleye, A., Bhat, A., Irorere, V.U., Hill, D., Williams, C., Radecka, I., 2015. Poly- γ -glutamic acid: production, properties and applications. *Microbiology* 161, 1–17. <https://doi.org/10.1099/mic.0.081448-0>
- Orfano, A.S., Nacif-Pimenta, R., Duarte, A.P.M., Villegas, L.M., Rodrigues, N.B., Pinto, L.C., Campos, K.M.M., Pinilla, Y.T., Chaves, B., Barbosa Guerra, M.G.V., Monteiro, W.M., Smith, R.C., Molina-Cruz, A., Lacerda, M.V.G., Secundino, N.F.C., Jacobs-Lorena, M., Barillas-Mury, C., Pimenta, P.F.P., 2016. Species-specific escape of *Plasmodium* sporozoites from oocysts of avian, rodent, and human malarial parasites. *Malar. J.* 15, 1–13. <https://doi.org/10.1186/s12936-016-1451-y>
- Osada, K., Christie, R.J., Kataoka, K., 2009. Polymeric micelles from poly(ethylene glycol)-poly(amino acid) block copolymer for drug and gene delivery. *J. R. Soc. Interface* 6. <https://doi.org/10.1098/rsif.2008.0547.focus>
- Pan, D., Vargas-Morales, O., Zern, B., Anselmo, A.C., Gupta, V., Zakrewsky, M., Mitragotri, S., Muzykantov, V., 2016. The effect of polymeric nanoparticles on biocompatibility of carrier red blood cells. *PLoS One* 11, 1–17. <https://doi.org/10.1371/journal.pone.0152074>
- Pasut, G., Veronese, F.M., 2009. PEG conjugates in clinical development or use as anticancer

- agents : An overview ☆. *Adv. Drug Deliv. Rev.* 61, 1177–1188.
<https://doi.org/10.1016/j.addr.2009.02.010>
- Pasut, G., Veronese, F.M., 2007. Polymer-drug conjugation, recent achievements and general strategies. *Prog. Polym. Sci.* 32, 933–961.
<https://doi.org/10.1016/j.progpolymsci.2007.05.008>
- Patel, A., Patel, M., Yang, X., Mitra, A., 2014. Recent Advances in Protein and Peptide Drug Delivery: A Special Emphasis on Polymeric Nanoparticles. *Protein Pept. Lett.* 21, 1102–1120. <https://doi.org/10.2174/0929866521666140807114240>
- Patel, B.B., Patel, J.K., Chakraborty, S., Shukla, D., 2015. Revealing facts behind spray dried solid dispersion technology used for solubility enhancement. *Saudi Pharm. J.* 23, 352–365. <https://doi.org/10.1016/j.jsps.2013.12.013>
- Pawar, S.N., Edgar, K.J., 2012. Alginate derivatization: A review of chemistry, properties and applications. *Biomaterials* 33, 3279–3305.
<https://doi.org/10.1016/j.biomaterials.2012.01.007>
- PerkinElmer, 2010. Thermogravimetric Analysis (TGA) A Beginner ’ s Guide. Analysis 1–19.
- Persenaire, O., Alexandre, M., Degée, P., Dubois, P., 2001. Mechanisms and kinetics of thermal degradation of poly(epsilon-caprolactone). *Biomacromolecules* 2, 288–294.
<https://doi.org/10.1021/bm0056310>
- Pietrucha, F., 2015. 4 Tips From America’s Top Doc_ Dr.
- Pillai, G., Ceballos-Coronel, M.L., 2013. Science and technology of the emerging nanomedicines in cancer therapy: A primer for physicians and pharmacists. *SAGE Open Med.* 1, 205031211351375. <https://doi.org/10.1177/2050312113513759>
- Pinto Reis, C., Neufeld, R.J., Ribeiro, A.J., Veiga, F., 2006. Nanoencapsulation I. Methods for preparation of drug-loaded polymeric nanoparticles. *Nanomedicine Nanotechnology, Biol. Med.* 2, 8–21. <https://doi.org/10.1016/j.nano.2005.12.003>

- Platt, E.J., Wehrly, K., Kuhmann, S.E., Chesebro, B., Kabat, D., 1998. Effects of CCR5 and CD4 Cell Surface Concentrations on Infections by Macrophagetropic Isolates of Human Immunodeficiency Virus Type 1. *J. Virol.* 72, 2855–2864.
- Pm, G., Choi, L., Gelband, H., Garner, P., 2018. Primaquine or other 8-aminoquinolines for reducing *Plasmodium falciparum* transmission (Review). *Cochrane Database Syst. Rev.* <https://doi.org/10.1002/14651858.CD008152.pub5>. www.cochranelibrary.com
- Poshadri, a, Kuna, A., 2010. Microencapsulation technology: A review. *J. Res. ANGRAU* 38, 86–102.
- Queval, C.J., Brosch, R., Simeone, R., 2017. The macrophage: A disputed fortress in the battle against *Mycobacterium tuberculosis*. *Front. Microbiol.* 8, 1–11. <https://doi.org/10.3389/fmicb.2017.02284>
- Ramharter, M., Kurth, F., Schreier, A.C., Nemeth, J., Glasenapp, I. von, B elard, S., Schlie, M., Kammer, J., Koumba, P.K., Cisse, B., Mordm uller, B., Lell, B., Issifou, S., Oeuvray, C., Fleckenstein, L., Kremsner, P.G., 2008. Fixed-Dose Pyronaridine-Artesunate Combination for Treatment of Uncomplicated *Falciparum* Malaria in Pediatric Patients in Gabon. *J. Infect. Dis.* 198, 911–919. <https://doi.org/10.1086/591096>
- Rao, J.P., Geckeler, K.E., 2011. Polymer nanoparticles: Preparation techniques and size-control parameters. *Prog. Polym. Sci.* 36, 887–913. <https://doi.org/10.1016/j.progpolymsci.2011.01.001>
- Rao, K.S., Ghorpade, A., Labhasetwar, V., 2009. Targeting anti-HIV drugs to the CNS. *Expert Opin. Drug Deliv.* 6, 771–84. <https://doi.org/10.1517/17425240903081705>
- Reddy, P.R., Raju, N., 2012. Gel-Electrophoresis and Its Applications 346.
- Rehman, S.U., Kim, I.S., Choi, M.S., Luo, Z., Yao, G., Xue, Y., Zhang, Y., Yoo, H.H., 2016. Development of a hydrophilic interaction liquid chromatography–tandem mass spectrometric method for the determination of kinsenoside, an antihyperlipidemic candidate, in rat plasma and its application to pharmacokinetic studies. *J. Pharm. Biomed. Anal.* 120, 19–24. <https://doi.org/10.1016/j.jpba.2015.12.003>

- Retna Raj, C., Ohsaka, T., 2002. Analytical applications of functionalized self-assembled monolayers on gold electrode: Voltammetric sensing of DOPAC at the physiological level. *Electroanalysis* 14, 679–684. [https://doi.org/10.1002/1521-4109\(200205\)14:10<679::AID-ELAN679>3.0.CO;2-T](https://doi.org/10.1002/1521-4109(200205)14:10<679::AID-ELAN679>3.0.CO;2-T)
- Richman, D.D., Margolis, D.M., Delaney, M., Greene, W.C., Hazuda, D., Pomerantz, R.J., 2009. The challenge of finding a cure for HIV infection. *Science* (80-.). 323, 1304–1307.
- Riehemann, K., Schneider, S.W., Luger, T.A., Godin, B., Ferrari, M., Fuchs, H., 2009. Nanomedicine--challenge and perspectives. *Angew. Chem. Int. Ed. Engl.* 48, 872–97. <https://doi.org/10.1002/anie.200802585>
- Rinaudo, M., 2006. Chitin and chitosan : Properties and applications. *Prog. Polym. Sci.* 31, 603–632. <https://doi.org/10.1016/j.progpolymsci.2006.06.001>
- Ringsdorf, H., 1975. Structure and properties of pharmacologically active polymers. *J. Polym. Sci. Polym. Symp.* 51, 135–153. <https://doi.org/10.1002/polc.5070510111>
- Roberts, M.J., Bentley, M.D., Harris, J.M., 2002. Chemistry for peptide and protein PEGylation.pdf. *Adv. Drug Deliv. Rev.* 54, 459–476.
- Rodgers, P.J., Amemiya, S., 2007. Cyclic voltammetry at micropipet electrodes for the study of ion-transfer kinetics at liquid/liquid interfaces. *Anal. Chem.* 79, 9276–9285. <https://doi.org/10.1021/ac0711642>
- Rodrigues, S., Dionísio, M., López, C.R., Grenha, A., 2012. Biocompatibility of Chitosan Carriers with Application in Drug Delivery. *J. Funct. Biomater.* 3, 615–641. <https://doi.org/10.3390/jfb3030615>
- Roy, A., Shrivastava, S.L., Mandal, S.M., 2016. 5 – Self-assembled carbohydrate nanostructures: synthesis strategies to functional application in food, *Novel Approaches of Nanotechnology in Food*. Elsevier Inc. <https://doi.org/10.1016/B978-0-12-804308-0.00005-4>
- Ruscito, A., DeRosa, M.C., 2016. Small-Molecule Binding Aptamers: Selection Strategies, Characterization, and Applications. *Front. Chem.* 4, 1–14.

<https://doi.org/10.3389/fchem.2016.00014>

- Sadeek, S.A., El-Shwiniy, W.H., El-Attar, M.S., 2011a. Synthesis, characterization and antimicrobial investigation of some moxifloxacin metal complexes. *Spectrochim. Acta - Part A Mol. Biomol. Spectrosc.* 84, 99–110. <https://doi.org/10.1016/j.saa.2011.09.010>
- Sadeek, S.A., El-Shwiniy, W.H., Zordok, W.A., Kotb, E., 2011b. Spectroscopic studies, thermal analyses and biological evaluation of new V(IV), Zr(IV) and U(VI) moxifloxacin complexes. *J. Mol. Struct.* 1006, 192–209. <https://doi.org/10.1016/j.molstruc.2011.09.009>
- Safavy, A., Georg, G.I., Vander Velde, D., Raisch, K.P., Safavy, K., Carpenter, M., Wang, W., Bonner, J.A., Khazaeli, M.B., Buchsbaum, D.J., 2004. Site-specifically traced drug release and biodistribution of a paclitaxel-antibody conjugate toward improvement of the linker structure. *Bioconjug. Chem.* 15, 1264–1274. <https://doi.org/10.1021/bc049868v>
- Sahoo, S., Sasmal, A., Nanda, R., Phani, A.R., Nayak, P.L., 2010. Synthesis of chitosan-polycaprolactone blend for control delivery of ofloxacin drug. *Carbohydr. Polym.* 79, 106–113. <https://doi.org/10.1016/j.carbpol.2009.07.042>
- Sanchis, J., Canal, F., Lucas, R., 2010. Polymer – drug conjugates for novel molecular targets R review 5, 915–935.
- Santiago, M.L., Range, F., Keele, B.F., Li, Y., Bailes, E., Bibollet-ruche, F., Fruteau, C., Noe, R., Peeters, M., Brookfield, J.F.Y., Shaw, G.M., Sharp, P.M., Hahn, B.H., 2005. Simian Immunodeficiency virus infection in free-ranging Sooty Mangabeys (*Cercocebus atys atys*) from the Tai Forest, Cote d’Ivoire: implications for the origin of epidemic Human Immunodeficiency virus Type 2. *Society* 79, 12515–12527. <https://doi.org/10.1128/JVI.79.19.12515>
- Santos-Magalhães, N.S., Mosqueira, V.C.F., 2010. Nanotechnology applied to the treatment of malaria. *Adv. Drug Deliv. Rev.* <https://doi.org/10.1016/j.addr.2009.11.024>
- Santos, M., Teixeira, J., 2000. Production of dextransucrase, dextran and fructose from sucrose using *Leuconostoc mesenteroides* NRRL B512 (f) 4, 177–188.
- Sarmento, B., Mazzaglia, D., Bonferoni, M.C., Neto, A.P., Do Céu Monteiro, M., Seabra, V.,

2011. Effect of chitosan coating in overcoming the phagocytosis of insulin loaded solid lipid nanoparticles by mononuclear phagocyte system. *Carbohydr. Polym.* 84, 919–925. <https://doi.org/10.1016/j.carbpol.2010.12.042>
- Sasindran, S.J., Torrelles, J.B., 2011. Mycobacterium tuberculosis infection and inflammation: What is beneficial for the host and for the bacterium? *Front. Microbiol.* 2, 1–16. <https://doi.org/10.3389/fmicb.2011.00002>
- Sauter, D., Unterweger, D., Vogl, M., Usmani, S.M., Heigele, A., Kluge, S.F., Hermkes, E., Moll, M., Barker, E., Peeters, M., Learn, G.H., Bibollet-Ruche, F., Fritz, J. V., Fackler, O.T., Hahn, B.H., Kirchhoff, F., 2012. Human Tetherin Exerts Strong Selection Pressure on the HIV-1 Group N Vpu Protein. *PLoS Pathog.* 8. <https://doi.org/10.1371/journal.ppat.1003093>
- Schluger, N.W., 2005. The pathogenesis of tuberculosis: The first one hundred (and twenty-three) years. *Am. J. Respir. Cell Mol. Biol.* 32, 251–256. <https://doi.org/10.1165/rcmb.F293>
- Schmidt, M., Kusche, R., von Issendorff, B., Haberland, H., 1998. Irregular variations in the melting point of size- selected atomic clusters. *Nature* 393, 238–240.
- Seifert, M., Catanzaro, D., Catanzaro, A., Rodwell, T.C., 2015. Genetic mutations associated with isoniazid resistance in Mycobacterium tuberculosis: A systematic review. *PLoS One* 10, 1–13. <https://doi.org/10.1371/journal.pone.0119628>
- Seitz, R., 2016. Human Immunodeficiency Virus (HIV). *Transfus. Med. Hemotherapy* 43, 203–222. <https://doi.org/10.1159/000445852>
- Semete, B., Booyesen, L., Lemmer, Y., Kalombo, L., Katata, L., Verschoor, J., Swai, H.S., 2010. In vivo evaluation of the biodistribution and safety of PLGA nanoparticles as drug delivery systems. *Nanomedicine Nanotechnology, Biol. Med.* 6, 662–671. <https://doi.org/10.1016/j.nano.2010.02.002>
- Shah, C., 2007. Adherence to High Active Antiretroviral Therapy (HAART) in Pediatric Patients infected with HIV: Issues and Interventions. *Indian J. Pediatr.* 74, 55–60.

- Sharma, P., Garg, S., 2010. Pure drug and polymer based nanotechnologies for the improved solubility, stability, bioavailability and targeting of anti-HIV drugs. *Adv. Drug Deliv. Rev.* 62, 491–502. <https://doi.org/10.1016/j.addr.2009.11.019>
- Shi, J., Kantoff, P.W., Wooster, R., Farokhzad, O.C., Sloan, M., Cancer, K., Arabia, S., 2017. Cancer nanomedicine: progress, challenges and opportunities. *Nat Rev Cancer* 17, 20–37. <https://doi.org/10.1038/nrc.2016.108.Cancer>
- Shi, S., Nguyen, P.K., Cabral, H.J., Diez-Barroso, R., Derry, P.J., Kanahara, S.M., Kumar, V.A., 2016. Development of peptide inhibitors of HIV transmission. *Bioact. Mater.* 1, 109–121. <https://doi.org/10.1016/j.bioactmat.2016.09.004>
- Shin, H.J., Kwon, Y.S., 2015. Treatment of drug susceptible pulmonary tuberculosis. *Tuberc. Respir. Dis. (Seoul)*. 78, 161–167. <https://doi.org/10.4046/trd.2015.78.3.161>
- Simon, V., Ho, D., Karim, Q., 2010. HIV/AIDS epidemiology, pathogenesis, prevention and treatment. *Lancet* 368, 489–504. [https://doi.org/10.1016/S0140-6736\(06\)69157-5.HIV/AIDS](https://doi.org/10.1016/S0140-6736(06)69157-5.HIV/AIDS)
- Singer, J.W., 2005. Paclitaxel poliglumex (XYOTAX???, CT-2103): A macromolecular taxane, in: *Journal of Controlled Release*. <https://doi.org/10.1016/j.jconrel.2005.09.033>
- Singh, R., W., L.J., 2009. Nanoparticle-based targeted drug delivery. *Exp. Mol. Pathol.* 86, 215–223. <https://doi.org/10.1016/j.yexmp.2008.12.004.Nanoparticle-based>
- Smith, I., 2003. *Mycobacterium tuberculosis* pathogenesis and molecular determinants of virulence. *Clin. Microbiol. Rev.* 16, 463–496. <https://doi.org/10.1128/CMR.16.3.463>
- Smith, M.B., March, J., 2006. March's Advanced Organic Chemistry: Reactions, Mechanisms, and Structure: Sixth Edition, March's Advanced Organic Chemistry: Reactions, Mechanisms, and Structure: Sixth Edition. <https://doi.org/10.1002/9780470084960>
- Smolkova, B., Dusinska, M., Gabelova, A., 2017. Nanomedicine and epigenome. Possible health risks. *Food Chem. Toxicol.* 109, 780–796. <https://doi.org/10.1016/j.fct.2017.07.020>
- Song, K.M., Lee, S., Ban, C., 2012. Aptamers and their biological applications. *Sensors* 12, 186

- 612–631. <https://doi.org/10.3390/s120100612>
- Soppimath, K.S.K., Aminabhavi, T.M.T.M., Kulkarni, A.R.A.R., Rudzinski, W.E., 2001. Biodegradable polymeric nanoparticles as drug delivery devices. *J. Control. Release* 70, 1–20. [https://doi.org/10.1016/S0168-3659\(00\)00339-4](https://doi.org/10.1016/S0168-3659(00)00339-4)
- Sosnik, A., Carcaboso, Á.M., Glisoni, R.J., Moretton, M.A., Chiappetta, D.A., 2010. New old challenges in tuberculosis: Potentially effective nanotechnologies in drug delivery. *Adv. Drug Deliv. Rev.* <https://doi.org/10.1016/j.addr.2009.11.023>
- Sosnik, A., Chiappetta, D.A., Carcaboso, Á.M., 2009. Drug delivery systems in HIV pharmacotherapy: What has been done and the challenges standing ahead. *J. Control. Release* 138, 2–15. <https://doi.org/10.1016/j.jconrel.2009.05.007>
- Soulard, V., Bosson-Vanga, H., Lorthiois, A., Roucher, C., Franetich, J.F., Zanghi, G., Bordessoulles, M., Tefit, M., Thellier, M., Morosan, S., Le Naour, G., Capron, F., Suemizu, H., Snounou, G., Moreno-Sabater, A., Mazier, D., 2015. Plasmodium falciparum full life cycle and Plasmodium ovale liver stages in humanized mice. *Nat. Commun.* 6. <https://doi.org/10.1038/ncomms8690>
- Souto, E.B., 2012. Patenting nanomedicines: Legal aspects, intellectual property and grant opportunities, *Patenting Nanomedicines: Legal Aspects, Intellectual Property and Grant Opportunities.* <https://doi.org/10.1007/978-3-642-29265-1>
- Stellwagen, N.C., 2010. Electrophoresis of DNA in agarose gels, polyacrylamide gels and in free solution. *Electrophoresis* 30, 1–14. <https://doi.org/10.1002/elps.200900052>.Electrophoresis
- Stetefeld, J., McKenna, S.A., Patel, T.R., 2016. Dynamic light scattering: a practical guide and applications in biomedical sciences. *Biophys. Rev.* 8, 409–427. <https://doi.org/10.1007/s12551-016-0218-6>
- Stevens, P., 2004. Diseases of poverty and the 90/10 gap. *Int. Policy Netw.* 16.
- Storm, G., Belliot, S.O., Daemen, T., Lasic, D.D., 1995. Surface modification of nanoparticles to oppose uptake by the mononuclear phagocyte system. *Adv. Drug Deliv. Rev.* 17, 31–

48. [https://doi.org/10.1016/0169-409X\(95\)00039-A](https://doi.org/10.1016/0169-409X(95)00039-A)
- Su, X.L., Li, Y., 2004. A self-assembled monolayer-based piezoelectric immunosensor for rapid detection of *Escherichia coli* O157:H7. *Biosens. Bioelectron.* 19, 563–574. [https://doi.org/10.1016/S0956-5663\(03\)00254-9](https://doi.org/10.1016/S0956-5663(03)00254-9)
- Sun, H., Zhu, X., Lu, P.Y., Rosato, R.R., Tan, W., Zu, Y., 2014. Oligonucleotide aptamers: New tools for targeted cancer therapy. *Mol. Ther. - Nucleic Acids* 3, e182. <https://doi.org/10.1038/mtna.2014.32>
- Sung, H.W., Sonaje, K., Liao, Z.X., Hsu, L.W., Chuang, E.Y., 2012. PH-responsive nanoparticles shelled with chitosan for oral delivery of insulin: From mechanism to therapeutic applications. *Acc. Chem. Res.* 45, 619–629. <https://doi.org/10.1021/ar200234q>
- Talisuna, A.O., Bloland, P., D'Alessandro, U., 2004. History, dynamics, and public health importance of malaria parasite resistance. *Clin.Microbiol.Rev.* 17, 235–254. <https://doi.org/10.1128/CMR.17.1.235>
- Tan, W., Wang, H., Chen, Y., Zhang, X., Zhu, H., Yang, C., Yang, R., Liu, C., 2011. Molecular aptamers for drug delivery. *Trends Biotechnol.* 29, 634–640. <https://doi.org/10.1016/j.tibtech.2011.06.009>
- Taubenberger, J.K., Morens, D.M., 2006. 1918 Influenza: The mother of all pandemics. *Emerg. Infect. Dis.* 12, 15–22. <https://doi.org/10.3201/eid1209.05-0979>
- Thanou, M., Verhoef, J.C., Junginger, H.E., 2001. Oral drug absorption enhancement by chitosan and its derivatives 52, 117–126.
- The, O.N., Sector, H., Hiv, R.T.O., 2014. Global update.
- Tian, L., Kim, M.-S., Li, H., Wang, J., Yang, W., 2018. Structure of HIV-1 reverse transcriptase cleaving RNA in an RNA/DNA hybrid. *Proc. Natl. Acad. Sci.* 201719746. <https://doi.org/10.1073/pnas.1719746115>
- Tiberi, S., Carvalho, A.C.C., Sulis, G., Vaghela, D., Rendon, A., Mello, F.C. d. Q., Rahman, A., Matin, N., Zumla, A., Pontali, E., 2017. The cursed duet today: Tuberculosis and HIV-

- coinfection. *Press. Medica* 46, e23–e39. <https://doi.org/10.1016/j.lpm.2017.01.017>
- Todar, K., 2009. *Todar's Online Textbook of Bacteriology*. *Todar's Online Textb. Bacteriol.* 1–580. <https://doi.org/http://textbookofbacteriology.net/pseudomonas.html>
- Tomiya, N., Jardim, J.G., Hou, J., Pastrana-Mena, R., Dinglasan, R.R., Lee, Y.C., 2013. Liver-targeting of primaquine-(poly- γ -glutamic acid) and its degradation in rat hepatocytes. *Bioorganic Med. Chem.* <https://doi.org/10.1016/j.bmc.2013.06.028>
- Tregoning, J.S., Schwarze, J., 2010. Respiratory viral infections in infants: Causes, clinical symptoms, virology, and immunology. *Clin. Microbiol. Rev.* 23, 74–98. <https://doi.org/10.1128/CMR.00032-09>
- Trif, M., Florian, P.E., Roseanu, A., Moisei, M., Craciunescu, O., Astete, C.E., Sabliov, C.M., 2015. Cytotoxicity and intracellular fate of PLGA and chitosan-coated PLGA nanoparticles in Madin-Darby bovine kidney (MDBK) and human colorectal adenocarcinoma (Colo 205) cells. *J. Biomed. Mater. Res. - Part A* 103, 3599–3611. <https://doi.org/10.1002/jbm.a.35498>
- Tshweu, L., Katata, L., Kalombo, L., Chiappetta, D., Hocht, C., Sosnik, A., Swai, H., 2013. Enhanced oral bioavailability of the antiretroviral efavirenz encapsulated in poly(ϵ -caprolactone) nanoparticles by a spray-drying method. *Nanomedicine* 0, 1–13.
- Tshweu, L., Katata, L., Kalombo, L., Swai, H., 2013. Nanoencapsulation of water-soluble drug, lamivudine, using a double emulsion spray-drying technique for improving HIV treatment. *J. Nanoparticle Res.* 15. <https://doi.org/10.1007/s11051-013-2040-4>
- Tukulula, M., Hayeshi, R., Fonteh, P., Meyer, D., Ndamase, A., Madziva, M.T., Khumalo, V., Labuschagne, P., Lubuschagne, P., Naicker, B., Swai, H., Dube, A., 2015. Curdlan-Conjugated PLGA Nanoparticles Possess Macrophage Stimulant Activity and Drug Delivery Capabilities. *Pharm. Res.* <https://doi.org/10.1007/s11095-015-1655-9>
- Ulbrich, K., Holá, K., Šubr, V., Bakandritsos, A., Tuček, J., Zbořil, R., 2016. Targeted Drug Delivery with Polymers and Magnetic Nanoparticles: Covalent and Noncovalent Approaches, Release Control, and Clinical Studies. *Chem. Rev.* 116, 5338–5431. <https://doi.org/10.1021/acs.chemrev.5b00589>

- Van der Strate, B.W.A., Beljaars, L., Molema, G., Harmsen, M.C., Meijer, D.K.F., 2001. Antiviral activities of lactoferrin. *Antiviral Res.* 52, 225–239. [https://doi.org/10.1016/S0166-3542\(01\)00195-4](https://doi.org/10.1016/S0166-3542(01)00195-4)
- Van Vugt, M., Wilairatana, P., Gemperli, B., Gathmann, I., Phaipun, L., Brockman, A., Luxemburger, C., White, N.J., Nosten, F., Looareesuwan, S., 1999. Efficacy of six doses of artemether-lumefantrine (benflumetol) in multidrug-resistant *Plasmodium falciparum* malaria. *Am. J. Trop. Med. Hyg.* 60, 936–942.
- Varatharajan, L., Thomas, S.A., 2009. The transport of anti-HIV drugs across blood-CNS interfaces: Summary of current knowledge and recommendations for further research. *Antiviral Res.* 82, 99–109. <https://doi.org/10.1016/j.antiviral.2008.12.013>
- Venditto, V.J., Szoka, F.C., 2013. Cancer nanomedicines: So many papers and so few drugs! *Adv. Drug Deliv. Rev.* 65, 80–88. <https://doi.org/10.1016/j.addr.2012.09.038>
- Vyas, T.K., Shahiwala, A., Amiji, M.M., 2008. Improved oral bioavailability and brain transport of Saquinavir upon administration in novel nanoemulsion formulations. *Int. J. Pharm.* 347, 93–101. <https://doi.org/10.1016/j.ijpharm.2007.06.016>
- Washington, C.B., Wiltshire, H.R., Man, M., Moy, T., Harris, S.R., Worth, E., Weigl, P., Liang, Z., Hall, D., Marriott, L., Blaschke, T.F., 2000. The disposition of saquinavir in normal and P-glycoprotein deficient mice, rats, and in cultured cells. *Drug Metab. Dispos.* 28, 1058–1062.
- Weiss, B.R.B., Donehower, R.C., Wiernik, P.H., Ohnuma, T., Gralla, R.J., Trump, D.L., Baker, J.R., Echo, D.A. Van, Hoff, D.D. Von, Leyland-jones, B., 1990. Hypersensitivity Reactions From Taxol. *J. Clin. Oncol.* 8, 1263–1268.
- White, N.J., 2004. Review series Antimalarial drug resistance. *Trends Parasitol.* 113, 1084–1092. <https://doi.org/10.1172/JCI200421682.1084>
- White, N.J., Van Vugt, M., Ezzet, F., 1999. Clinical pharmacokinetics and pharmacodynamics of artemether-lumefantrine. *Clin. Pharmacokinet.* 37, 105–125. <https://doi.org/10.2165/00003088-199937020-00002>

- WHO, 2017. WHO | Diarrhoeal disease. WHO Media Cent.
- WHO, 2016. World malaria report 2015: summary. Who.
- WHO, 2010. Global report on antimalarial drug efficacy and drug resistance: 2000-2010. Who 115. <https://doi.org/10.1371/journal.pmed.0050109>
- Williams, A., Ibrahim, I.T., 1981. Carbodiimide Chemistry: Recent Advances. Chem. Rev 81, 589–636.
- Williams, K.C., Burdo, T.H., 2009. HIV and SIV infection - the role of cellular restriction and immune responses in viral replication and pathogenesis. Apmis 117, 15. <https://doi.org/10.1111/j.1600-0463.2009.02450.x.HIV>
- Wong, H.L., Chattopadhyay, N., Wu, X.Y., Bendayan, R., 2010. Nanotechnology applications for improved delivery of antiretroviral drugs to the brain. Adv. Drug Deliv. Rev. 62, 503–517. <https://doi.org/10.1016/j.addr.2009.11.020>
- Wong, R.P.M., Salman, S., Ilett, K.F., Siba, P.M., Mueller, I., Davis, T.M.E., 2011. Desbutyl-lumefantrine is a metabolite of lumefantrine with potent in vitro antimalarial activity that may influence artemether-lumefantrine treatment outcome. Antimicrob. Agents Chemother. 55, 1194–1198. <https://doi.org/10.1128/AAC.01312-10>
- Woodruff, M.A., Hutmacher, D.W., 2010. The return of a forgotten polymer - Polycaprolactone in the 21st century. Prog. Polym. Sci. <https://doi.org/10.1016/j.progpolymsci.2010.04.002>
- World Health Organization, 2015. Treatment of Severe Malaria. Guidel. Treat. Malar. 71–88. [https://doi.org/10.1016/0035-9203\(91\)90261-V](https://doi.org/10.1016/0035-9203(91)90261-V)
- World Health Organization, W.H., Global Tuberculosis Programme, 2016. WHO treatment guidelines for drug-resistant tuberculosis: 2016 update. Who 56. <https://doi.org/WHO/HTM/TB/2016.04>
- World Malaria Report 2015, 2015.
- Wu, C.S., 2005. A comparison of the structure, thermal properties, and biodegradability of

- polycaprolactone/chitosan and acrylic acid grafted polycaprolactone/chitosan. *Polymer (Guildf)*. 46, 147–155. <https://doi.org/10.1016/j.polymer.2004.11.013>
- Yang, L., Chen, L., Zeng, R., Li, C., Qiao, R., Hu, L., Li, Z., 2010. Bioorganic & Medicinal Chemistry Synthesis , nanosizing and in vitro drug release of a novel anti-HIV polymeric prodrug : Chitosan- O -isopropyl-5' - O -d4T monophosphate conjugate. *Bioorg. Med. Chem.* 18, 117–123. <https://doi.org/10.1016/j.bmc.2009.11.013>
- Yogeeswari, P., Sriram, D., 2005. Betulinic Acid and Its Derivatives: A Review on their Biological Properties. *Curr. Med. Chem.* 12, 657–666. <https://doi.org/10.2174/0929867053202214>
- Yu, L., 2001. Amorphous pharmaceutical solids: Preparation, characterization and stabilization. *Adv. Drug Deliv. Rev.* 48, 27–42. [https://doi.org/10.1016/S0169-409X\(01\)00098-9](https://doi.org/10.1016/S0169-409X(01)00098-9)
- Yurkovetskiy, A. V., Fram, R.J., 2009. XMT-1001, a novel polymeric camptothecin pro-drug in clinical development for patients with advanced cancer. *Adv. Drug Deliv. Rev.* 61, 1193–1202. <https://doi.org/10.1016/j.addr.2009.01.007>
- Zhao, H., Holmes, S.S., Baker, G.A., Challa, S., Bose, H.S., Song, Z., 2012. Ionic derivatives of betulinic acid as novel HIV-1 protease inhibitors. *J. Enzyme Inhib. Med. Chem.* 27, 715–721. <https://doi.org/10.3109/14756366.2011.611134>
- Zhao, W., Xu, J.J., Chen, H.Y., 2006. Electrochemical biosensors based on layer-by-layer assemblies. *Electroanalysis* 18, 1737–1748. <https://doi.org/10.1002/elan.200603630>
- Zhou, J., Rossi, J.J., 2010. Aptamer-targeted cell-specific RNA interference. *Silence* 1, 4. <https://doi.org/10.1186/1758-907X-1-4>
- Zumla, A., Nahid, P., Cole, S.T., 2013. Advances in the development of new tuberculosis drugs and treatment regimens. *Nat. Rev. Drug Discov.* 12, 388–404. <https://doi.org/10.1038/nrd4001>